

wordt niet uitgeleend

G.J.J. Ruijgrok



ELEMENTS OF AVIATION ACOUSTICS



2034761

C. L. Mandelbaum

583930

**ELEMENTS OF
AVIATION
ACOUSTICS**

Bibliothek TU Delft



C 2267973

2402
552
0



ELEMENTS OF AVIATION ACOUSTICS

G.J.J. Ruijgrok



Delft University Press / 1993

Published and distributed by:

Delft University Press
Stevinweg 1
2628 CN Delft

tel. +31-15-783254
fax +31-15-781661

CIP-GEGEVENS KONINKLIJKE BIBLIOTHEEK, DEN HAAG

Ruijgrok, G.J.J.

Elements of aviation acoustics / G.J.J. Ruijgrok. - Delft : Delft University Press. - III.
Met index, lit. opg.

ISBN 90-6275-899-1

NUGI 834

Trefw.: akoestiek ; luchtvaarttechniek.

Copyright © 1993 by G.J.J. Ruijgrok

All rights reserved

No part of the material protected by this copyright notice may be reproduced or utilized in any form or by any means, electronic or mechanical, including photocopying, recording or by any information storage and retrieval system, without permission from the publisher: Delft University Press, Stevinweg 1, 2628 CN Delft, The Netherlands.

The Greek alphabet

NAME	SMALL LETTER	CAPITAL	NAME	SMALL LETTER	CAPITAL
alpha (a)	α	A	nu (n)	ν	N
beta (b)	β	B	xi (ks)	ξ	Ξ
gamma (g)	γ	Γ	omicron (o)	\circ	O
delta (d)	δ	Δ	pi (p)	π (ϖ)	Π
epsilon (e)	ε (ε)	E	rho (r)	ρ (ϱ)	P
zeta (z)	ζ	Z	sigma (s)	σ	Σ
eta (e)	η	H	tau (t)	τ	T
theta (th)	θ (ϑ)	Θ	upsilon (y)	υ	Y
iota (i)	ι	I	phi (ph)	ϕ (φ)	Φ
kappa (k)	κ (κ)	K	chi (ch)	χ	X
lambda (l)	λ	Λ	psi (ps)	ψ	Ψ
mu (m)	μ	M	omega (o)	ω	Ω

Standard multiples and decimal fractions

MULTIPLE / FRACTION	PREFIX	SYMBOL
10^{12}	tera	T
10^9	giga	G
10^6	mega	M
10^3	kilo	k
10^2	hecto	h
10	deca	da
10^{-1}	deci	d
10^{-2}	centi	c
10^{-3}	milli	m
10^{-6}	micro	μ
10^{-9}	nano	n
10^{-12}	pico	p
10^{-15}	femto	f
10^{-18}	atto	a

CONTENTS

PREFACE	xi
1 BASIC FACTS	1
1.1 Introduction	1
1.2 Sound and sound waves	2
1.3 Diffraction	7
1.4 Refraction	8
1.5 Sound fields	11
1.6 Acoustic power	11
1.7 Sound intensity	13
1.8 Sound pressure level	15
1.9 Addition of sound pressure levels	19
1.10 Directionality	21
1.11 Idealized directional patterns	22
1.12 Types of sound	24
1.13 Doppler effect	27
1.14 Limits of audibility	29
2 DYNAMICS OF SOUND WAVES	30
2.1 Introduction	30
2.2 The equation of continuity	30
2.3 Euler's equations	32
2.4 Poisson's relations	35
2.5 The wave equation	38
2.6 Velocity potential	39
2.7 Plane waves	40
2.8 Spherical waves	45
2.9 The Helmholtz equation	50
3 ELEMENTARY SOURCES	51
3.1 Monopole source	51
3.2 Dipole source	58
3.3 The quadrupole and the aerodynamic jet noise	63

4 PROPAGATION OF SOUND IN THE ATMOSPHERE	69
4.1 Spreading	69
4.2 Atmospheric attenuation of sound	71
4.3 Transmission of sound from one air layer to another	75
4.4 Effect of temperature gradients	80
4.5 Temperature inversion effects	84
4.6 Combined effect of wind and temperature	88
4.7 Convergence and divergence effects	92
5 SOUND IN ENCLOSURES	97
5.1 The sound field	97
5.2 Diffuse field	98
5.3 Absorption	100
5.4 Reverberation time	105
5.5 Normal transmission of sound through a rigid wall	107
5.6 The coincidence effect	109
5.7 Standing sound waves	113
5.8 Measurement of sound intensity	115
6 ATTENUATION OF SOUND IN DUCTS	118
6.1 Change in cross-sectional area	118
6.2 Single-expansion chamber	120
6.3 Closed side branch tube	124
6.4 Helmholtz resonator	126
6.5 Single resonator in a side branch	129
6.6 Higher order modes in ducts	133
7 FREQUENCY SPECTRA	136
7.1 General	136
7.2 Fourier transform	139
7.3 Bandwidth	145
7.4 Effect of bandwidth on measured spectra	150
7.5 Measured spectra from flyovers	153

8 GROUND REFLECTION	160
8.1 Observed sound pressure level	160
8.2 Effect of finite-width filters	167
8.3 Plane wave reflection coefficient	168
8.4 Surface impedance data	171
8.5 Validity of plane wave approximation	176
8.6 Acquisition of free-field noise levels	178
8.7 Excess ground attenuation	182
9 NOISE MEASURES	185
9.1 Loudness level	185
9.2 Perceived noise level	187
9.3 Measuring loudness levels	189
9.4 Effect of duration	193
9.5 Calculation of effective perceived noise level	197
9.6 Noise contours	203
9.7 Indices of total noise exposure	205
9.8 Noise induced sleep disturbance	210
9.9 Loss of hearing from noise exposure	211
10 NOISE CERTIFICATION	215
10.1 Introduction	215
10.2 Annex 16 / Volume I / Chapter 3	218
10.3 Annex 16 / Volume I / Chapter 6	224
10.4 Annex 16 / Volume I / Chapter 7	228
10.5 Annex 16 / Volume I / Chapter 10	229
10.6 Calculating the confidence interval	234
11 EFFECTS OF FORWARD MOTION	237
11.1 Introduction	237
11.2 Geometric acoustics (subsonic speeds)	237
11.3 Geometric acoustics (supersonic speeds)	239
11.4 Velocity potential	242
11.5 Sound pressure	245

X ELEMENTS OF AVIATION ACOUSTICS

11.6	Sound pressure level	248
11.7	Sonic boom	249
11.8	Microphone selection	254

12 AIRPLANE NOISE SOURCES 256

12.1	Introduction	256
12.2	Piston engine noise characteristics	260
12.3	propeller-driven airplane noise	263
12.4	Propeller noise prediction	267
12.5	Turbo-engine noise	269
12.6	Fan and exhaust jet noise	273
12.7	Airframe noise	276
12.8	Noise inside aircraft	279

REFERENCES 283

APPENDIX A NOY VALUES 288

APPENDIX B SI-UNITS 294

APPENDIX C GLOSSARY 296

INDEX 302

PREFACE

ABOUT THE CONTENTS

Quieting cabin and flight deck noise, and reducing the impact of noise on communities near airports are matters of great importance to aircraft manufacturers and airline operators for already more than four decades.

Undoubtedly, knowledge of both aeronautics and acoustics is essential for a clear understanding of any aviation noise problem. Such understanding is a necessary prerequisite to the control of interior and exterior noise.

In view of the importance of education in dealing with noise control, this book is devoted to the branch of aerospace engineering known as *aviation acoustics*. The book contains twelve chapters and three appendixes which originate from an annual course on airplane noise given by the author to aerospace engineering students at Delft University of Technology (DUT).

The book is intended to be useful to undergraduate students of aerospace engineering, and also to researchers and practicing engineers who wish to improve their understanding of the topic.

The text assumes little or no previous knowledge of acoustics. For this reason, the first chapter introduces basic facts and concepts about the generation, propagation, and specification of sound. The second chapter describes the dynamics of sound waves. Since acoustics can be seen as a fluid mechanics discipline, this chapter starts with deriving the three basic equations of classical aerodynamic theory. These equations are then linearized to obtain their acoustic equivalents and combined into a single wave equation. Also the solutions of plane and spherical wave propagation are presented.

The third chapter develops the free-field radiation properties of the three principal sources of sound, i.e., the acoustic monopole, dipole, and quadrupole. In Chapter four is considered the manner in which the propagation of sound away from the source is influenced by distance, atmospheric absorption losses, and refractive conditions due to vertical wind and temperature gradients. Also a procedure for the determination of atmospheric attenuation rate is included.

Chapter five outlines, in a concise form, the types of sound field occurring in enclosures and the absorption of sound energy by the walls. Chapter six briefly describes the attenuation of sound in ducts provided by cross-sectional area changes and wall cavities.

In Chapter seven are treated certain practical aspects of frequency analysis, and Chapter eight is concerned with the effects of ground reflection on observed noise levels.

Chapter nine deals with the subjective assessment of airplane noise. The chapter is supplemented by Appendix A, providing data for the calculation of the perceived noisiness of sounds.

A review of the international standards and recommended practices for civil aircraft as published in Annex 16 to the Chicago Convention on International Civil Aviation is given in Chapter ten.

The effects of forward motion on the radiation characteristics of a sound source is the subject of discussion in Chapter eleven. This chapter also includes sections on sonic boom and microphone selection.

The concluding chapter (12) examines the various noise sources found on the different types of airplane.

Experimental results throughout the book are presented in order to illustrate the basic theory enunciated in the text.

References to the literature are indicated in the text and listed at the end of the text.

In the book the International System of Units (Système International d'Unités) is used. Besides these metric units, in international civil aviation the use of certain English units is prescribed, such as foot for altitude, and so these are also cited in the text. In Appendix B information is given about the SI-units. Also are tabulated a number of factors with which English units can be converted into metric SI-units.

In bringing the book to a close, a glossary of terms that appear in the text are collected in Appendix C.

ACKNOWLEDGMENTS

The author wishes to express his deep appreciation to Mr. D.M. van Paassen of DUT for his cooperation in the preparation of the book. He especially deserves the author's sincere thanks for reading and commenting of the manuscript, and for supplying the experimental data.

The author is also grateful to Mr. W. Spee of DUT for preparing the illustrations with his characteristic skill and loyalty.

Delft, The Netherlands
15 July 1993

G.J.J. Ruijgrok

1 BASIC FACTS

1.1 INTRODUCTION

Sound is a physical disturbance in the air, produced by a sound source. If the disturbance reaches a listener, a sound is heard.

Mostly we appreciate sound. It enables conversation and many other forms of communication. Sound furnishes pleasant experiences such as listening to music. It also permits us to evaluate the condition of man and machine, and to make diagnoses.

On the contrary, sound can be undesired and annoying when it interferes with specific activities such as speech communication and recreation.

It also can induce stress and prevent sleep, it can produce irritation, disturb concentration, and it can cause a decrement in human performance. There are indications that exposure to intense sound may be a contributing factor to physical illness. Repeated exposure to very intense sound can even harm the human ear, leading to a temporary or permanent loss of hearing. In all these cases it is called *noise*, accepting the definition of noise as *sound that is unwanted by the observer*. This definition emphasizes the admitted fact that noise is a subjective phenomenon. In other words, the question or a given sound is experienced as noise and what its level of annoyance is, is influenced by personal feelings and depends also on our attitude toward the source.

Since the number of noise sources is continually increasing in our technological society, it has become necessary to control and reduce the noise levels to which we are subjected in every day life.

In aeronautical engineering, obviously, we are faced with two kinds of noise problems; (a) flight deck and cabin noise (*interior noise*) of which the control is required as an element in providing a safe and comfortable environment for crew and passengers, and (b) community noise impact as one of the most serious problems of aircraft operations (*exterior noise*).

Aviation noise introduces a complex problem that consists of three main parts; (1) the production of noise by the aircraft (*the source*), (2) the propagation of noise through the atmosphere and the influences of obstacles and/or ground surface on sound propagation (the transmission path), and (3) the effect of noise on man, the reactions of the occupants of the airplane and the people working at or living in the vicinity of civilian airports and military airfields (*the receivers of the noise*).

A clear appreciation of the nature of these component parts is a prerequisite to a sensible approach and subsequent process of finding an adequate answer to the various noise problems as related to aviation.

A complicating factor is that we are concerned with many types of aircraft which all have their own noise radiation characteristics, and which are heard under various atmospheric, meteorological and terrain conditions. We also have to consider the many kinds of people and the many kinds of reaction from each individual.

The aim of this book is to treat the most important theories, quantities and procedures necessary for describing the features of emission, propagation and reception of aviation noise. In preparing the text, emphasis has been placed on those noise problems that are related to the operations of airplanes. By definition, an airplane is a mechanically driven aircraft, heavier than air, which is supported chiefly by aerodynamic reaction forces on surfaces which remain fixed under given conditions of flight.

As little previous knowledge of the subject is assumed, some basic concepts of acoustics will be introduced subsequently in this first chapter.

1.2 SOUND AND SOUND WAVES

A sound source sets the nearest particles of air into vibration through which acoustic energy is transmitted from the source to the surrounding air. The movement gradually spreads to air particles further away from the source since energy is transferred from one vibrating particle to the next.

Thus sound is a form of energy which propagates through the air as progressive waves, as illustrated in Figure 1.2-1a.

Sound generally travels in longitudinal waves in which the particle displacements take place in the same direction as the movement of the wave. The region in

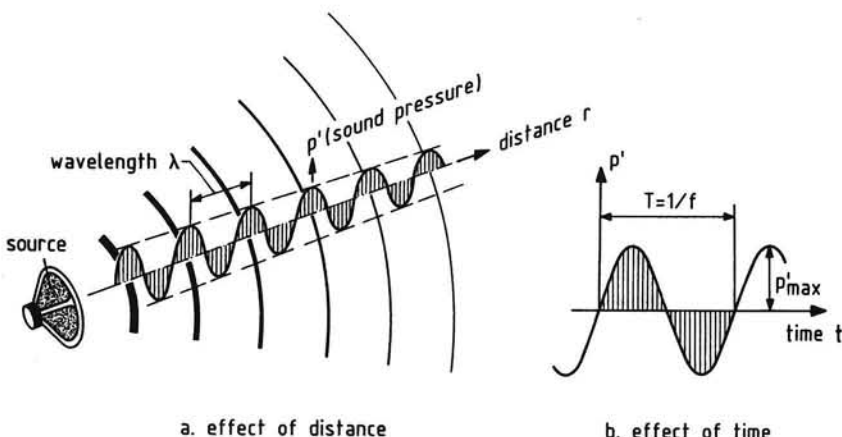


Figure 1.2-1. Progressive sound waves

which the wave travels is termed the *sound field*. In a space where the sound waves can propagate freely without reflection they are termed *free progressive waves* traveling in a *free field*.

The motion of the air particles about their equilibrium position produces a local compression followed by a local rarefaction and so on. The instantaneous value of the fluctuating pressure disturbance on the ambient pressure is called the *sound pressure* and is given the symbol p' .

The action of the pressure variations on the eardrum of a listener produces neural impulses in the inner ear, which are transmitted to the brain, where they are experienced as a hearing sensation.

The oscillating line in Figure 1.2-1b represents a periodic variation of the local sound pressure with time. The time history of the sound pressure repeats itself exactly. Each unique sequence of variations is a cycle. The time required to complete one cycle is the *period T*. In symbols:

$$p'(t) = p'(t+T)$$

The number of oscillations per second is the *frequency f* of the disturbance expressed in terms of cycles per second (cps) or more recently referred to as *Hertz*, abbreviated Hz.

Clearly the frequency is the reciprocal of the period,

$$f = \frac{1}{T} \quad . \quad (1.2-1)$$

At low frequencies the air particles oscillate slowly producing low or bass tones. At high frequencies the air particles vibrate quickly giving high tones (Figure 1.2-2).

The frequencies audible to the human ear may range from about 20 Hz to 20,000 Hz.

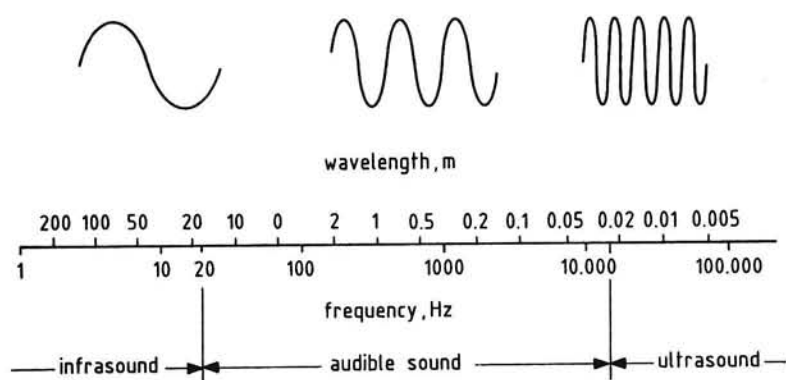


Figure 1.2-2. Frequency and wavelength (0 m I.S.A.)

The inaudible sound with frequencies under 20 Hz is named *infrasound*. Sound over 20,000 Hz which is also normally inaudible is termed *ultrasound*. Especially the highest perceptible frequency decays with age. However, it appears that, independent of age, frequencies higher than ca 11,000 Hz hardly contribute to the *loudness*, i.e., the way in which a listener reacts to a sound in terms of how quiet or how loud. Moreover, it is known that the great majority of sound sources radiate very little energy in the frequency range above 11,000 Hz.

The sound pressure variation in Figure 1.2-1b may have the form of a sinusoid. An oscillation that can be described by the sine function is called *simple harmonic motion*.

Generally, the sound pressure is a function of both time and distance from the source,

$$p' = p'(r, t) , \quad (1.2-2)$$

where r is the distance from the acoustic center of the source.

Returning to Figure 1.2-1a, we see that in the sound field around the source the acoustic energy spreads out in all directions through which the *peak value* or *amplitude* of the sound pressure decreases as the distance from the source increases.

Anticipating later derivations in Chapter 2, for simple harmonic motion of a point sound source, the variations of the sound pressure with time and distance can be expressed as

$$p'(r, t) = \frac{A}{r} \cos \omega(t - r/c) , \quad (1.2-3)$$

where A is the strength of the source and ω the angular frequency in radians per second, $\omega = 2\pi f$. The ratio A/r is the amplitude of the local sound pressure.

Since the pressure disturbance propagates with the speed c , the time r/c is taken for the sound wave to travel to a point at distance r from the source.

For this reason, the pressure variations reaching a distance r at time t are determined by a value of p' at an earlier time $(t - r/c)$.

Noting that $\cos x + i \sin x = e^{ix}$, alternatively, we can write

$$p'(r, t) = \operatorname{Re} \left[\frac{A}{r} e^{i\omega(t-r/c)} \right] , \quad (1.2-4)$$

where Re stands for the real part. Normally, however, this prefix is dropped. Using this complex notation for the sound pressure has the advantage that it is easier to manipulate mathematically than the trigonometric notation of Equation (1.2-3).

As depicted in Figure 1.2-1b, the magnitude of a sound signal can be expressed by the amplitude, p'_{\max} , of the instantaneous sound pressure. However, the most often used measure of amplitude is the *effective (sound) pressure*, which is the *root-mean-square* value of the instantaneous sound pressures over one period or an integral number of periods at the point under consideration,

$$p_e = \left[\frac{1}{T} \int_0^T [p'(t)]^2 dt \right]^{1/2} . \quad (1.2-5)$$

Using Equation (1.2-3) we find

$$p_e = \left[\frac{1}{T} \int_0^T \left[\frac{A}{r} \cos \omega(t - r/c) \right]^2 dt \right]^{1/2} = \frac{A}{r\sqrt{2}} . \quad (1.2-6)$$

Equation (1.2-6) shows that for a sinusoidally varying sound pressure the amplitude of the sound pressure and the effective pressure are simply related by the factor $\sqrt{2} = 1.414$. This ratio is known as the *crest factor* of a sound signal.

The rate at which the pressure disturbance travels through the medium is the *speed of sound* c . In air we have

$$c = \sqrt{\gamma R T} , \quad (1.2-7)$$

where $\gamma = c_p/c_v = 1.4$ is the *ratio of the specific heats of air*, $R = 287.05 \text{ m}^2/\text{s}^2\text{K}$ is the *specific gas constant* and T is the *ambient temperature* in kelvin. At a sea-level temperature of $15^\circ\text{C} = 288.15 \text{ K}$ the speed of sound is 340.29 m/s .

The *wavefronts* pictured in Figure 1.2-1a are imaginary surfaces around the source which are the loci of points having the same particle displacements at a given instant.

The perpendicular distance between two wavefronts is the *wavelength*, which is thus the distance that a sound wave travels in one period. Using the symbol λ to denote the wavelength, we can write

$$\lambda = cT = \frac{c}{f} . \quad (1.2-8)$$

The directions in which the wave propagates are given by the *sound rays*, which are the imaginary curves directed normally to the wavefronts. The

relationship between wavelength and frequency for the speed of sound under standard sea-level conditions is shown in the previous Figure 1.2-2.

Wavelength is a meaningful acoustic quantity. For example, sound having a wavelength much smaller than the size of an obstacle is strongly affected by the presence of the obstacle. The sound will be reflected or scattered in many directions and the obstacle will cast a so-called *shadow zone*. This is suggested in Figure 1.2-3a, where the dashed lines indicate sound reflected back from the obstacle. Thus barriers and screens are effective against high frequency (short-wavelength) sound. If the wavelength is large in comparison with the size of the obstacle the wave behaves almost as if the obstacle does not exist. As sketched in Figure 1.2-3b, the sound will be bent round the obstacle. Hence low frequency (large-wavelength) sound diffuses round obstacles and through holes without losing energy, so barriers and screens are not very effective against it unless they are very large. In this connection we have the requirement that, when measuring sound, the microphone should be as small as possible. Moreover, a microphone must be designed to compensate for the disturbance caused by its own presence in the sound field.

Acoustic measurements often require the presence of so-called *free-field conditions*, which imply the nonattendance of reflections from obstacles and wall or ground surfaces. For this aim, special rooms have been designed

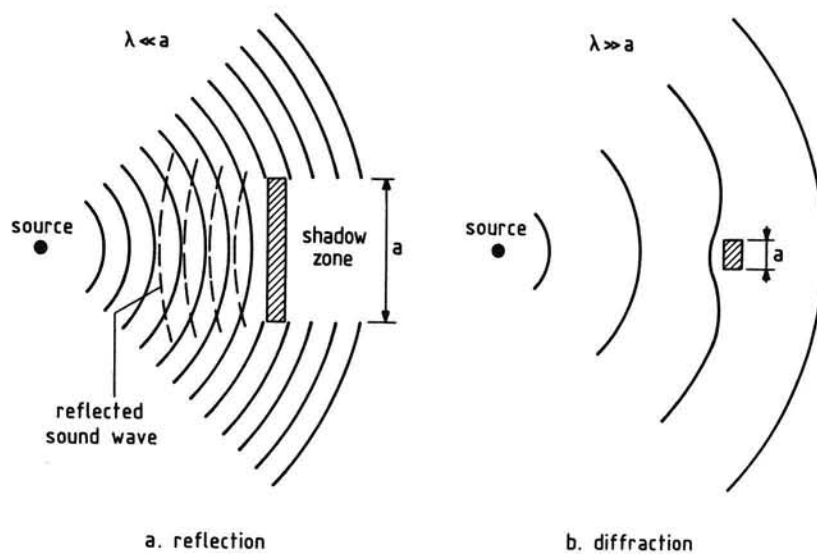


Figure 1.2-3. Sound wave passing an obstacle

in which the sound absorptive construction of the interior surfaces is such that practically no sound is reflected from them. These rooms are called *free-field chambers* or *anechoic chambers*. Rooms having a high wall absorption, but which are not completely echo-free, may be called *dead rooms*.

1.3 DIFFRACTION

As everyone knows, sound can be heard round corners and behind walls. Therefore, it is certainly not true to say that sound waves always travel in straight line.

This bending of sound waves round obstacles is called *diffraction*, and a diffractive wave is thus a sound wave whose wavefront has been changed in direction by an object in the sound field.

As was indicated already in the previous section, bending occurs when the wavelength of the sound is comparable to the dimensions of the obstacle.

Since the wavelength of audible sound varies from about one centimeter to several meters, the wavelength has always the same order of magnitude as the usual objects. For this reason, diffraction effects must be taken into account, even for sound of shorter wavelength.

In order to explain the bending of sound rays, one uses the method of wavefront construction according to the *principle of Huygens*.

As sketched in Figure 1.3-1, Huygens theory states that every vibrating point on a wavefront becomes the origin of a new disturbance. The secondary waves, traveling with the speed of sound, are enveloped by a surface identical in its properties with the wavefront from which the secondary disturbance originated.

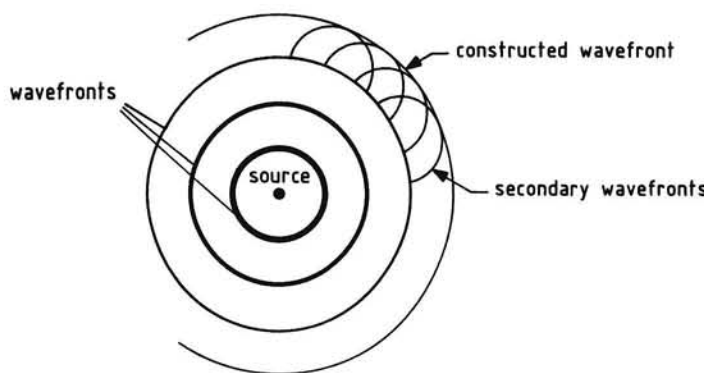


Figure 1.3-1. Huygen's construction of wavefront

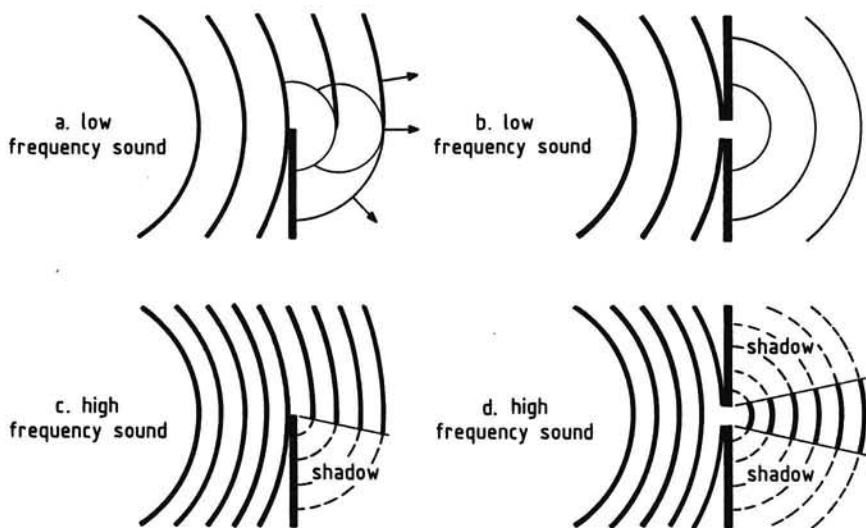


Figure 1.3-2. Effects of diffraction

ces start and this surface forms a new overall wavefront. This implies that each next position of a wavefront can be established from a preceding.

In the case that a solid barrier is placed in the sound field, as in Figure 1.3-2a, we see that secondary waves also provide for a spreading of the sound energy into the space behind the barrier.

Clearly, the sound pressures at a point in the shadow zone are less than they would have been, if the object had been not present.

Figure 1.3-2b indicates what happens when the sound meets a wall with an opening in it. Now the hole acts as were it a new source, radiating spherical sound waves, but with lower sound pressures.

Naturally, the amount of bending, i.e., the distance into the shadow region for which the diffraction produces noticeable effects, depends on the dimensions of the object relative to the wavelength (the frequency) of the sound. Low frequency sound diffuses completely round edges and through holes, whereas high frequency sound forms a more intensive shadow beyond a barrier (Figures 1.3-2c and 1.3-2d).

1.4 REFRACTION

Bending of the sound also occurs when there are *temperature* and *wind gradients* in the atmosphere. According to Equation (1.2-7), the speed of sound depends on the temperature of the air. In an isothermal atmosphere the

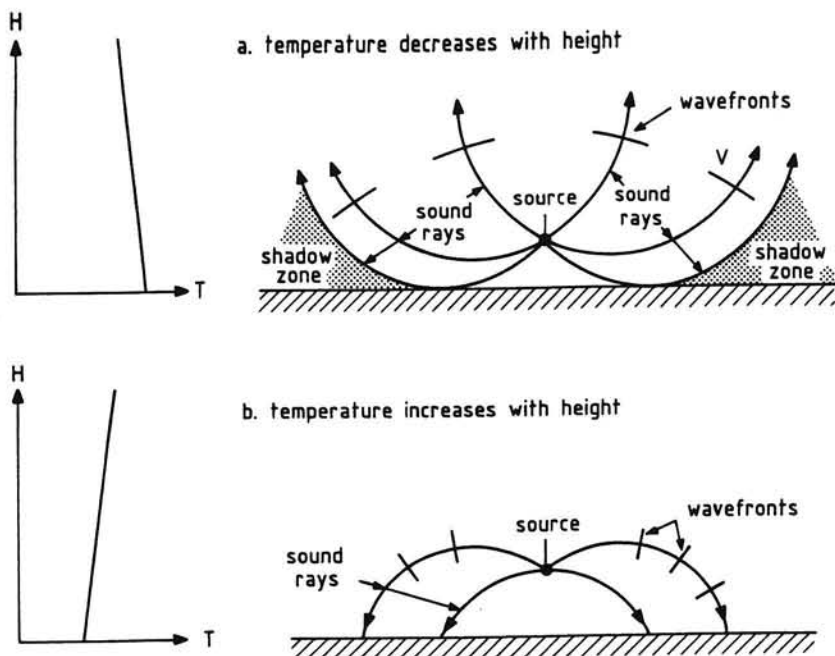


Figure 1.4-1. Refraction of sound due to temperature gradient

speed of sound is constant and sound waves will follow straight paths. However, if the air temperature varies with height, there is a continuous change in direction, which is called *refraction*, resulting in curved sound paths.

Suppose a sound source in an atmosphere at rest in which the temperature decreases with height as in the *International Standard Atmosphere*, I.S.A. (Reference 7).

As portrayed in Figure 1.4-1a, the top of the wavefronts will travel slower than the bottom of the wavefronts. This behavior results in a bending of the waves in the direction away from the higher temperature and toward the lower temperature. This bending of the sound rays in upward direction results in the formation of shadow zones in which the sound pressures are strongly reduced. The condition of a *negative temperature gradient (temperature lapse)* normally exists during daytime on sunny days. The air temperature then decreases with increasing height so that the speed of sound diminishes with height.

On the other hand, in the evening, at night and in the early morning the temperature gradient may be positive. The increase of temperature with

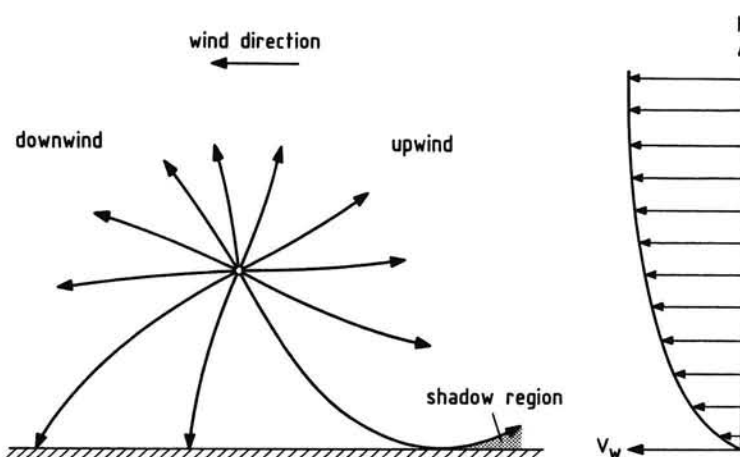


Figure 1.4-2. Refraction of sound due to wind gradient

height is designated as a *temperature inversion*. Now the sound rays are bent toward the ground, reinforcing the sound pressures at ground level around the source (Figure 1.4-1b). Under this condition, it is impossible to have a shadow zone.

Also the presence of a *wind gradient* causes a different propagation speed at upper and lower parts of a wavefront. Consequently, sound will be deflected away from the regions of higher velocity toward regions of lower velocity. Therefore, with the typical *wind profile* of an increasing wind speed with height there will be an upward bending of the sound with a shadow region *upwind* and in *downwind* direction a bending toward the ground, as depicted in Figure 1.4-2.

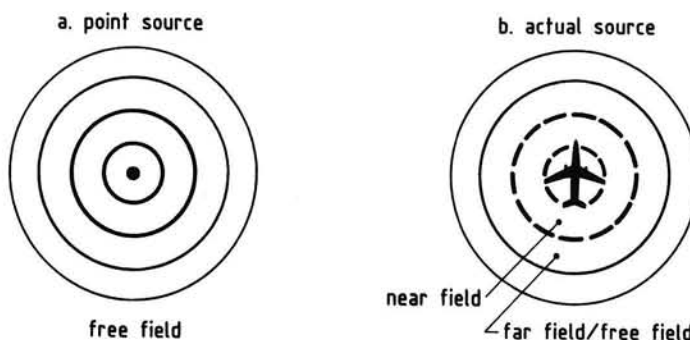


Figure 1.5-1. The occurrence of spherical wavefronts

When both temperature and wind velocity gradients exist, we have the condition that in the direction of the wind the bending of sound is counteracted by a negative temperature gradient, whereas in the upwind direction the shadow formation is intensified.

1.5 SOUND FIELDS

As illustrated in Figure 1.5-1a, the sound energy generated by a point source spreads spherically in all directions, where the wavefronts are imaginary spherical shells surrounding the source. As mentioned already, when this behavior occurs we speak of *free field* conditions. In practice, a free field is a sound field in which the effects of obstacles are imperceptible in the space of interest.

Clearly, as the sound wave travels further from the source its energy is received on an ever larger spherical area. Then, according to Equation (1.2-3), the amplitude of the sound pressure along a given radius varies in inverse proportion to the distance from the source.

A wavefront around an actual sound source with finite dimensions may be considered as spherical if its distance from the source is large in comparison with the dimensions of the source. Therefore, a large part of the sound field surrounding an aircraft can normally be treated as if the sound comes from a single point called the *acoustic center* of the source. Then, as illustrated in Figure 1.5-1b, the sound field consists of two parts, the *far-field*, where the sound pressure is inversely proportional to the distance, and the *near-field*, where the variation of the sound pressure with the distance is a complex function of the radiation characteristics of the source. For this reason, the near-field is usually avoided in making noise measurements.

Generally, the far-field condition will happen at a distance greater than the wavelength of the lowest frequency emitted from the source, or at more than several times the greatest dimension of the source. Obviously, a prerequisite to the occurrence of the far-field condition is the presence of a free sound field.

1.6 ACOUSTIC POWER

The *acoustic power* is the total sound energy emitted by the source per unit of time.

The approximate acoustic powers generated by some typical sound sources are indicated in Figure 1.6-1. A quiet human whisper involves an acoustic power of some 10^{-10} watt and a human shouting produces about 10^{-3} watt. A small propeller-driven airplane radiates 50 watt, while a large jet transport at takeoff may produce 10^3 watt.

From these figures it may be understood that the acoustic powers produced by airplane propulsion devices represent the exhaust of only a very little part of their total power output.

The figures in Figure 1.6-1 also demonstrate the enormous numerical range involved in measuring sound powers. For this reason we usually state not the power, but the corresponding logarithmic quantity, the *power watt level* (PWL). Use of this scale condenses the sound power to numbers which are much more convenient.

The power watt level corresponding to a sound power W is defined as ten times the logarithm to the base ten of the ratio of the acoustic power to the reference power,

$$\text{PWL} = 10 \log \frac{W}{W_0}, \text{ dB} . \quad (1.6-1)$$

In this equation $W_0 = 10^{-12}$ watt is the reference power. The unit of power watt level is *decibel*, abbreviated dB. The lower case 'd' stands for the decimal fraction 'deci' (0.1), and the capital 'B' represents the basic unit named 'bel', in honor of Alexander Graham Bell (1847 - 1922), the inventor of the telephone.

It follows from Equation (1.6-1) that a doubling of the source power is reflected by a small numerical change of only 3 dB. Likewise, a factor of ten

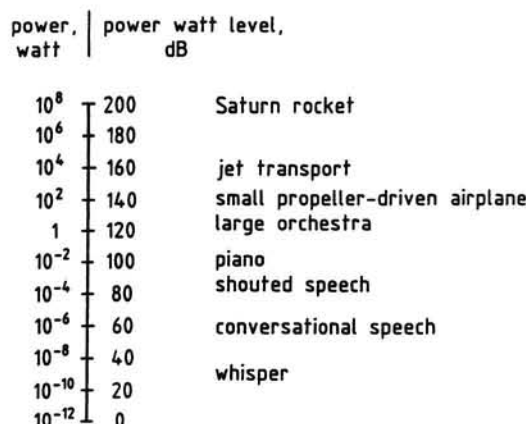


Figure 1.6-1. Relation between sound power and power watt level

change is represented by a ten decibel change. Use of the decibel scale thus reduces the large range of acoustic powers in Figure 1.6-1 to a more manageable range of power watt levels of only 0 to 200 dB.

1.7 SOUND INTENSITY

The sound intensity is the energy per unit time per unit area transmitted by a sound wave, i.e., the sound power per unit area in watt/m².

In the case of a point source in a free field where the sound energy is radiated uniformly in all directions, the intensity is constant at each spherical surface surrounding the source. Under these ideal conditions the relationship between sound intensity and sound power is simply given by

$$I(r) = \frac{W}{4\pi r^2} , \quad (1.7-1)$$

where r is the radius of the sphere.

Apparently, sound intensity is a vector quantity so that its value is only meaningful if also its direction is specified.

The instantaneous sound intensity at a distance r from the source, generally, is given by (Figure 1.7-1):

$$I' = \frac{p' dA dr}{dt dA} , \quad (1.7-2)$$

where p' is the (instantaneous) sound pressure. The numerator of the right-hand term of this equation is the acoustic energy passing through the area dA normal to the direction of travel.

Since $dr/dt = v_r$ is the particle velocity in the direction r , Equation (1.7-2) can be written as

$$I' = p' v_r . \quad (1.7-3)$$

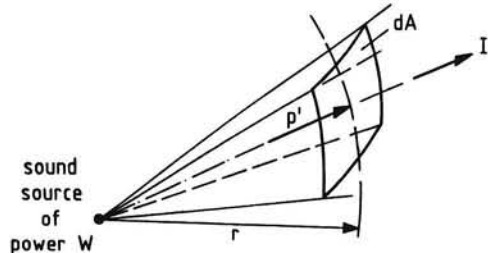


Figure 1.7-1. Sound energy transport

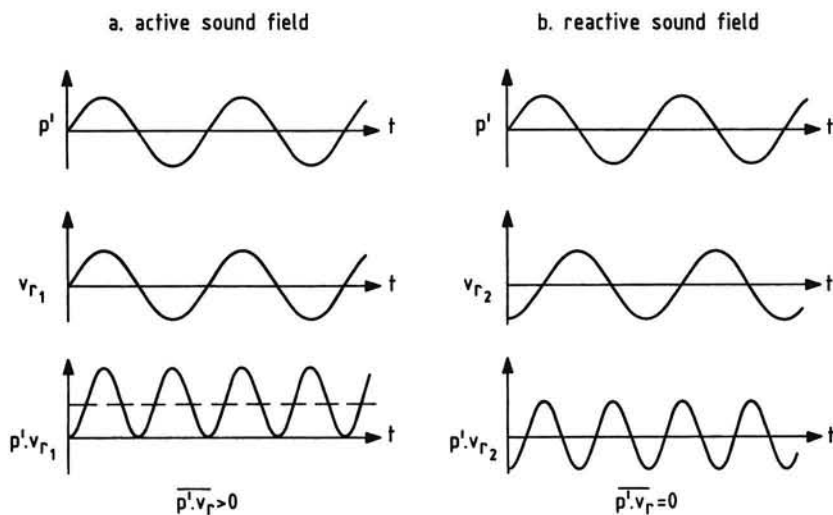


Figure 1.7-2. The active and reactive part of a sound field

The sound intensity is equal to the time-averaged product of the instantaneous sound pressure and the corresponding particle velocity in the same direction,

$$I = \frac{1}{T} \int_0^T p' v_r dt \quad \text{or} \quad I = \overline{p' v_r} . \quad (1.7-4)$$

In the latter expression the bar indicates time averaging.

The particle velocity v_r can essentially be split up into two components,

$$v_r = v_{r1} + i v_{r2} , \quad (1.7-5)$$

where v_{r1} is the active component which is in phase with the sound pressure, the imaginary unit i satisfies the relation $i^2 = -1$, and v_{r2} is the reactive component which is 90° out of phase with the sound pressure.

Only the in-phase particle velocity component will give a time averaged product with p' that is unequal to zero, as illustrated in Figure 1.7-2. Apparently, one of the features of sound intensity is the distinction it makes between the active and reactive part of the sound field. Only in the active part of a sound field an intensity can be present. In a reactive sound field the intensity is zero, which means that there is no net flow of acoustic energy.

The sound intensity that is just audible at 1000 Hz is about 10^{-12} watt/m². On the other end of the scale we have the *threshold of pain* that can be over 100 watt/m². Because of this enormous range of audible sound

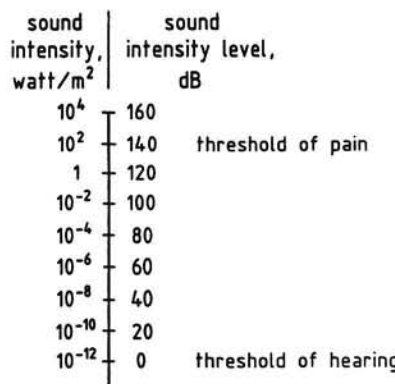


Figure 1.7-3. Relation between sound intensity and sound intensity level

intensities, a ratio of 10^{14} to one, also for the sound intensity a logarithmic scale is used. The *sound intensity level* (SIL) corresponding to a sound intensity I is defined by (Figure 1.7-3),

$$\text{SIL} = 10 \log \frac{I}{I_0} , \text{ dB}, \quad (1.7-6)$$

where I_0 is the reference sound intensity of 10^{-12} watt/m². The value of I_0 thus represents the minimum intensity perceptible by the human ear.

The numerical results of Equation (1.7-6) are given again in decibel, dB.

Another reason for quoting the sound intensity in decibels is that one decibel is about the smallest value that is detectable by the human ear.

Finally, we note that zero decibel does not mean an absence of sound, but only that the value of the sound intensity is equal to the reference value.

1.8 SOUND PRESSURE LEVEL

As will be shown later, in the free field the effective pressure and the sound intensity in the direction of propagation are related by

$$I = \frac{p_e^2}{\rho_\infty c} . \quad (1.8-1)$$

This expression is the acoustical analogy of Ohm's law (current = voltage / resistance). Therefore, the quantity $\rho_\infty c$ is called the *characteristic acoustic resistance* of the medium. For the important case of air at standard sea-level

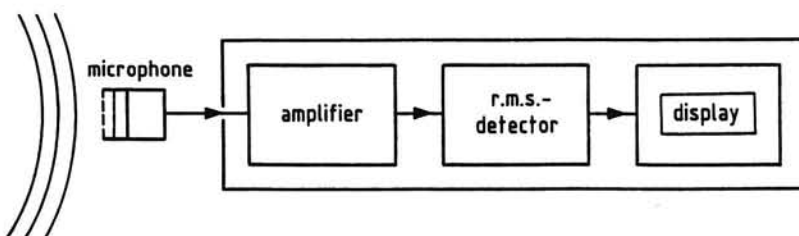


Figure 1.8-1. The basic sound level meter

conditions, where the density is 1.225 kg/m^3 and the speed of sound is 340.29 m/s (Reference 7), we find the product $(\rho_{\infty}c)_0 = 416.86 \text{ kg/m}^2\text{s}$.

The effective pressure is the quantity commonly measured because most microphones used in sound measuring instruments respond to sound pressure.

Essentially, the basic sound level meter consists of a microphone, a processing section and a read-out device (Figure 1.8-1).

The sensing element used for measuring the sound pressures from airplanes is always a *condenser microphone*. It consists of two charged plates which are placed parallel to each other. The outer plate is a very thin diaphragm which vibrates in response of the sound pressure variation. Through the alteration of the separation distance between the plates the capacitance of the sensing element changes, which produces an electrical current in the meter circuit equivalent to the sound pressure. This signal is amplified before the effective pressure is determined in a r.m.s.-detector. Finally, the read-out unit displays the *sound pressure level* (SPL) in decibel according to

$$\text{SPL} = 10 \log \frac{p_e^2}{p_{e0}^2}, \text{ dB}, \quad (1.8-2)$$

where p_{e0} is the reference pressure of $2 \times 10^{-5} \text{ N/m}^2$.

Since the human ear responds to sound intensity, the sound pressure level is determined from the square of the effective pressure.

Commonly, the effective pressure of a sound exhibits a variation with time. In order to measure fluctuating sound pressure levels, the reading is provided with a damping (time-averaging). For sound signals of basically stationary nature, two different responses of the meter display are employed. These are termed *fast* and *slow*, implying an averaging time of 0.125 s and 1.0 s , respectively.

Concerning the perception of sound, it is known that the human ear can observe a variation of the sound pressure level over about one-tenth of a second. This means that the integration time of the sound pressure acting on the eardrum is approximately 0.1 s .

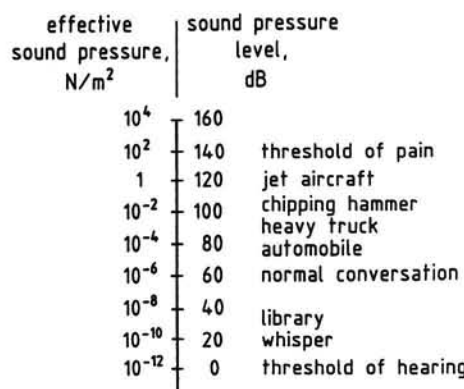


Figure 1.8-2. Relation between effective sound pressure and sound pressure level

The relation between p_e and SPL is indicated in Figure 1.8-2. We see that use of sound pressure level instead of effective pressure reduces the audible range to about 140 dB.

To give some idea of what sound level meter readings represent, in Figure 1.8-2 also are listed the typical sound pressure levels of familiar noise sources. It can be seen from the readings that the decibel scale is by no means in right proportion to one's impression of the loudness of sounds, i.e., the magnitude of the auditory sensation. In this respect, it is of importance to remember that a change of 1 dB is about the smallest value of significance to the human ear. However, only a change of 3 dB may be well perceptible and a 5 dB rise may be judged as clearly perceptible. Approximately, an increase of 10 dB is required before the sound subjectively appears to be twice as loud.

The above observations on the characteristics of the ear leads to the conclusion that it is meaningless to work with an accuracy greater than one dB. In other words, sound level data should always be rounded off to the closest whole decibel value.

From Equations (1.7-6), (1.8-1) and (1.8-2), the relationship between SPL and SIL can be expressed as

$$\text{SPL} = \text{SIL} + 10 \log \frac{I_0}{p_{e0}^2} \rho_\infty c , \text{ dB.} \quad (1.8-3)$$

The reference values $I_0 = 10^{-12} \text{ W/m}^2$ and $p_{e0} = 2 \times 10^{-5} \text{ N/m}^2$ provide that practically SPL equals SIL for air at sea level in the International Standard Atmosphere (I.S.A.), where $(\rho_\infty c)_0 = 416.86 \text{ kg/m}^2 \text{s}$.

Using these values in Equation (1.8-3) furnishes

$$SPL = SIL + 0.2 \text{ , dB.} \quad (1.8-4)$$

When the prevailing air density and the speed of sound deviate strongly from the above mentioned sea-level standard values, a second correction must be applied,

$$SPL = SIL + 0.2 + 10 \log \frac{\rho_{\infty} c}{(\rho_{\infty} c)_0} \text{ , dB.} \quad (1.8-5)$$

Figure 1.8-3 shows this correction as functions of air pressure and temperature. So we see from Equations (1.8-4) and (1.8-5), and Figure 1.8-3 that under virtually all practical atmospheric conditions, the difference between the intensity level and the sound pressure level is less than 1 dB. This observation implies that, practically, the sound pressure level is numerically equal to the sound intensity level.

It should be emphasized that the relationship (1.8-1) and so Equation (1.8-4) and (1.8-5) are only valid in a free field. In an arbitrary reactive sound field there may be a large difference between the intensity level and the sound pressure level. The difference between these two quantities is called the *reactivity index*, which only in a free sound field is practically equal to zero.

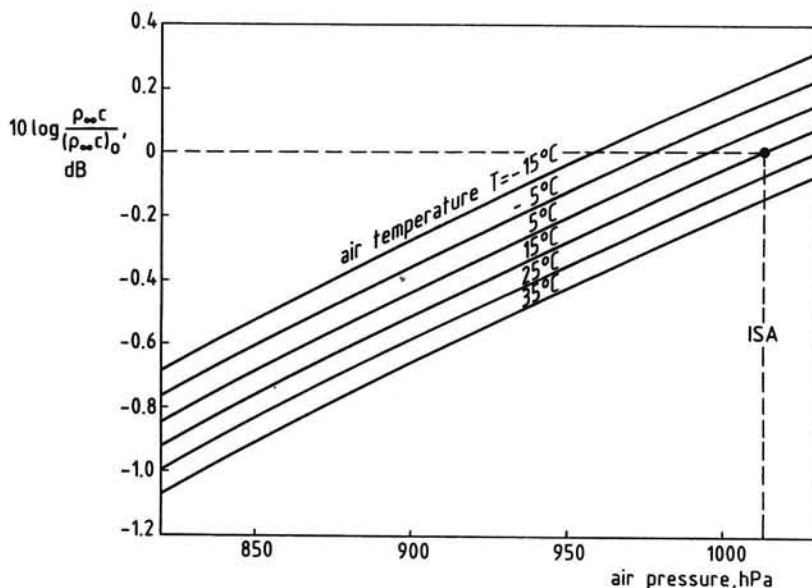


Figure 1.8-3. Dependence of $10 \log \frac{\rho_{\infty} c}{(\rho_{\infty} c)_0}$ on pressure and temperature

1.9 ADDITION OF SOUND PRESSURE LEVELS

If we want to combine the sound pressure levels from two or more independent sound sources, we cannot simply add their decibel values arithmetically because they are logarithmic quantities. To derive an expression for the resultant level we consider two sound sources, each emitting a pure tone with angular frequency ω_1 and ω_2 , respectively (Figure 1.9-1). Then the total sound pressure $p'_m(t)$ at a given point is

$$p'_m(t) = p'_1(t) + p'_2(t) , \quad \text{where} \quad (1.9-1)$$

$$p'_1(t) = \frac{A}{r_1} \cos \omega_1(t - r_1/c) \quad \text{and} \quad (1.9-2)$$

$$p'_2(t) = \frac{B}{r_2} \cos \omega_2(t - r_2/c) . \quad (1.9-3)$$

The square of the resultant effective sound pressure is

$$\begin{aligned} p_e^2_m &= \frac{1}{T} \int_0^T \left[\frac{A}{r_1} \cos \omega_1(t - r_1/c) \right]^2 dt + \frac{1}{T} \int_0^T \left[\frac{B}{r_2} \cos \omega_2(t - r_2/c) \right]^2 dt + \\ &+ \frac{1}{T} \int_0^T \left[\frac{2AB}{r_1 r_2} \cos \omega_1(t - r_1/c) \cos \omega_2(t - r_2/c) \right] dt . \end{aligned} \quad (1.9-4)$$

Employing the trigonometric relationships $\cos^2 x = 0.5(1 + \cos 2x)$ and $\cos x \cos y = 0.5[\cos(x + y) + \cos(x - y)]$, we can integrate Equation (1.9-4) to give

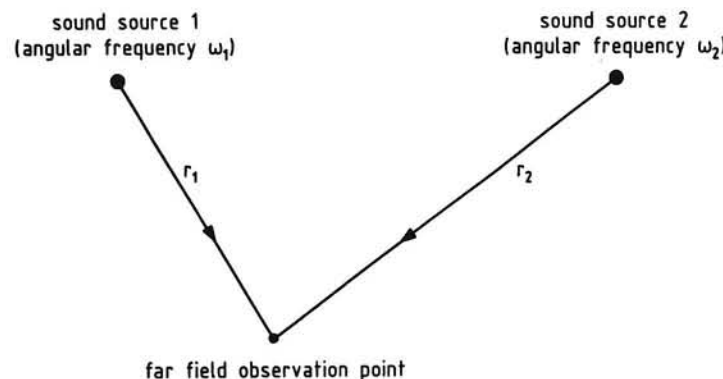


Figure 1.9-1. Combined sound pressure level

$$p_{e_m}^2 = \left[\frac{A}{r_1\sqrt{2}} \right]^2 + \left[\frac{B}{r_2\sqrt{2}} \right]^2 \quad (1.9-5)$$

or with Equation (1.2-6)

$$p_{e_m}^2 = p_{e_1}^2 + p_{e_2}^2 \quad (1.9-6)$$

The resultant sound pressure level becomes

$$SPL_m = 10 \log \left[\frac{p_{e_1}^2 + p_{e_2}^2}{p_{e_0}^2} \right] \quad (1.9-7)$$

Thus, when we combine the sound from two individual sound sources, we must add the squares of the two effective pressures in order to obtain the total sound pressure level.

In terms of the individual sound pressure levels we have

$$SPL_m = 10 \log [10^{SPL_1/10} + 10^{SPL_2/10}] \quad (1.9-8)$$

In the case of N sources we may write

$$SPL_m = 10 \log \sum_{i=1}^N 10^{SPL_i/10} \quad (1.9-9)$$

From Equations (1.9-7) and (1.9-8) it follows that if one of the sources is much less intense than the other, the resultant sound pressure level will not be much greater than the highest level. If we have two similar sources ($p_{e_1} = p_{e_2}$), we see that the level will rise by 3 dB. To produce a 10 dB higher sound pressure level, ten equally intense sources must operate together.

Conversely, obtaining a noticeable decrease of the total level from different sources will require the reduction of the noise radiation from the dominant source.

If the sounds in Figure 1.9-1 are of the same frequency, then integration of Equation (1.9-4) shows that the resultant sound pressure level depends also on the phase difference between the two sound waves,

$$SPL = 10 \log \left[\frac{p_{e_1}^2 + p_{e_2}^2 + 2p_{e_1}p_{e_2} \cos \frac{\omega \Delta r}{c}}{p_{e_0}^2} \right] \quad (1.9-10)$$

where $\Delta r = r_2 - r_1$.

For example, if they are in phase, $\cos \omega \Delta r/c = 1$, giving

$$\text{SPL}_m = 10 \log \left[\frac{p_{e_1} + p_{e_2}}{\frac{p_{e_0}^2}{2}} \right]^2 . \quad (1.9-11)$$

If the two sounds are out of phase, $\cos \omega \Delta r/c = -1$. Then

$$\text{SPL}_m = 10 \log \left[\frac{p_{e_1} - p_{e_2}}{\frac{p_{e_0}^2}{2}} \right]^2 . \quad (1.9-12)$$

It is apparent from Equations (1.9-11) and (1.9-12) that in the case of interference between two sounds of the same frequency and effective pressure, the level will change by any value between plus 6 dB and minus infinity.

1.10 DIRECTIONALITY

In general, each sound source that is large in comparison with the wavelength of the sound it generates tends to be directional. Therefore, the noise fields generated by aircraft always show a very marked directional pattern. As a consequence, a reading obtained in the noise field surrounding an airplane not only depends on the distance from the source but also on the angular location.

The quantity often employed to describe the directionality of a source is the *directivity index* (DI), which is defined as the difference between the sound pressure level in a specified direction θ to the average sound pressure level at the same distance, r ,

$$\text{DI}(\theta) = \text{SPL}(\theta) - \text{SPL}_{av} . \quad (1.10-1)$$

The average sound pressure level, SPL_{av} , is calculated from the acoustic power divided by the surface of the sphere with radius r , i.e., the average intensity in the radial direction,

$$\text{SPL}_{av} = 10 \log \frac{W}{4\pi r^2} , \text{ dB}, \quad (1.10-2)$$

where W is the acoustic power emitted by the source.

Of course, the distance r in Equation (1.10-2) must be sufficiently great that the sound source appears to radiate from a single point called the acoustic center of the source.

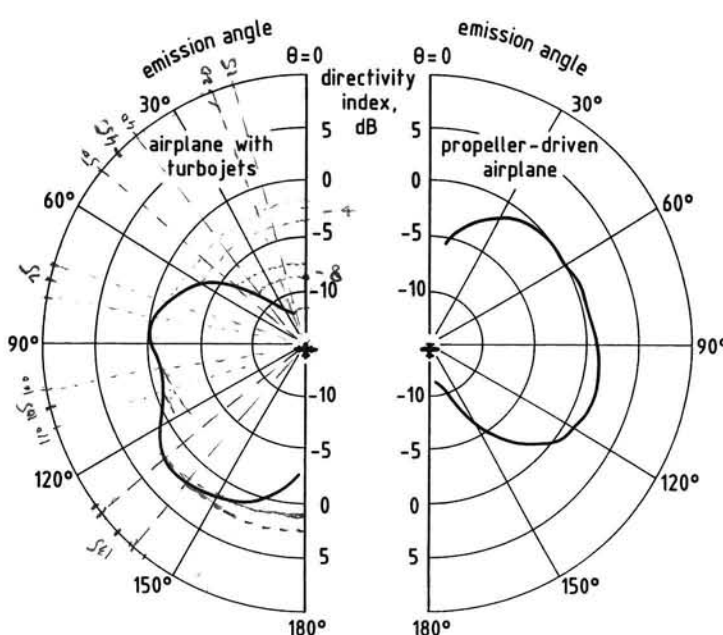


Figure 1.10-1. Directivity index

Typical directivity patterns are shown in Figure 1.10-1. The curves demonstrate that airplanes radiate sound in certain preferential directions.

1.11 IDEALIZED DIRECTIONAL PATTERNS

In order to describe the radiation characteristics of sound sources, it is useful to relate them to certain *elementary sources of sound*.

The most elementary description of sound radiation is obtained by using the *acoustic monopole* which radiates sound energy equally in all directions. The model for this sound source is a pulsating sphere that is periodically changing its volume, forcing the surrounding air to fluctuate. The monopole can be used to model the acoustical effect of a pulsating jet, such as a piston-engine exhaust (Figure 1.11-1a).

Another elementary source of sound is the *dipole* which may be represented by a rigid sphere that oscillates back and forth along a line. The oscillating motion of the forward and rearward hemispheres is of course opposite. This implies a mutual cancellation of the mass flows, but the

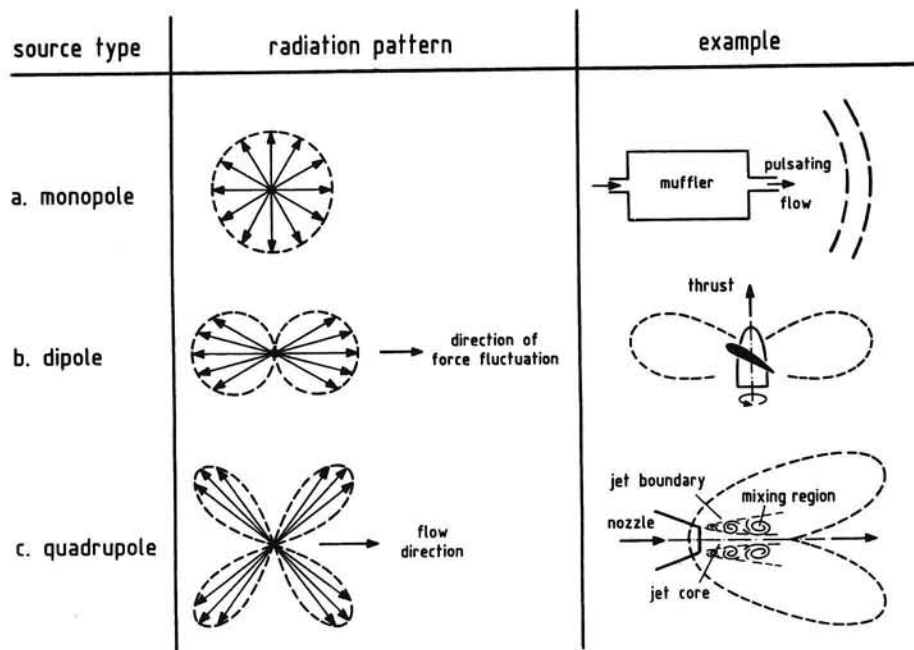


Figure 1.11-1. Elementary sources of sound

motion of the sphere leads to a periodic external force that may be used to describe the effect of an oscillating body (Figure 1.11-1b). Therefore, the dipole is extensively used in analyzing propeller noise. The directional characteristic of the dipole is embodied in $\cos^2\theta$, which means a radiation pattern consisting of two lobes with maximums in the direction of the force.

If two equal and opposite dipoles are placed side by side, the result is a *quadrupole*. This elementary source of sound provides the simplest representation of a noise production involving no mass injection and no externally applied force, but only a shear or moment. These conditions are found in a free wake or jet, thereby excluding both the monopole and the dipole. Hence the quadrupole can be used to describe the way in which noise emission from a wake or jet takes place (Figure 1.11-1c).

When the axes of the force vector and that of the separation vector are perpendicular, we speak about a *lateral quadrupole*. If these axes coincide, the quadrupole is *longitudinal*. The radiation pattern from the lateral quadrupole in Figure 1.11-1c is a four lobe clover leaf pattern.

1.12 TYPES OF SOUND

Sound signals can exhibit two distinct characteristics with respect to its short-term sound pressure variation with time. In consequence, we can classify sounds as *discrete* and *random* or *broadband*.

The simplest form of a discrete sound is the *pure tone*, so called because its sound pressure varies sinusoidally with time. A pure tone, therefore, is a periodic sound, containing only one frequency. The sound pressure amplitude as a function of frequency can thus be represented by a single component as shown in Figure 1.12-1a.

A more complex discrete and periodic sound is a musical tone of which the sound pressure is the sum of a number of sinusoids.

Figure 1.12-1b shows an example of such a non-sinusoidal sound signal which is made up of three pure sine waves with different amplitudes and three frequency components: a fundamental or repetition frequency and two harmonic frequencies or overtones. The fundamental frequency is of course given by the inverse of the period, $f_1 = 1/T$, and the harmonics are integer multiples of the fundamental.

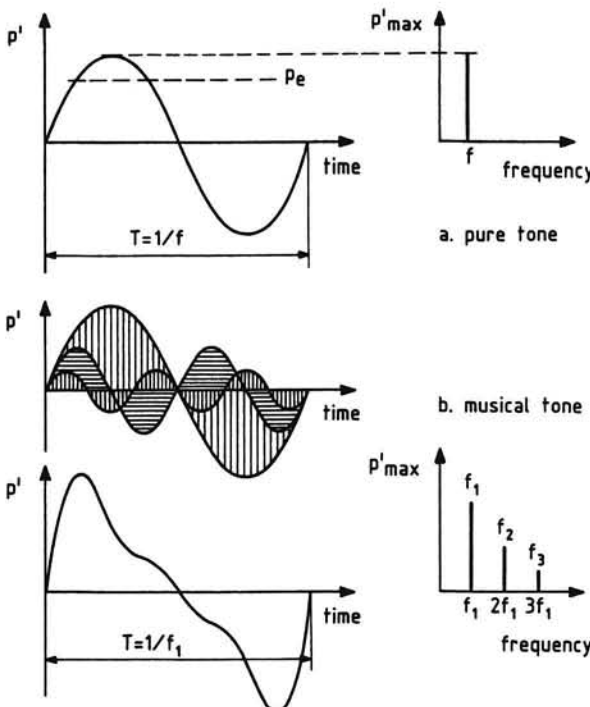


Figure 1.12-1. Types of sound signal

Analysis of a more distorted but still periodic sound signal generally furnishes a very large number of discrete components in the frequency domain at integral multiples of the fundamental frequency to which they are related. This type of sound is exemplified by the sound pressure variation sketched in Figure 1.12-1c, which wave-form may be measured on a propeller-driven airplane (*line spectrum*).

The periodic sound signals indicated so far show always several discrete frequencies which are harmonically related since they can be seen as a combination of a large number of superimposed sinusoids.

Random sounds, contrary to discrete sounds, have no repetition of their sound pressure wave-form over the time period of interest. Moreover, these sounds contain sound pressure amplitudes which fluctuate randomly with respect to time. As portrayed in Figure 1.12-1d, random sound is characterized by a continuous varying frequency distribution over a wide range of frequencies (*continuous spectrum*).

A very special form of random sound is *white noise*, which has a flat frequency spectrum over a specified frequency range.

Practically, noise signals often have characteristics made up of the two above types of sound. For example, the noise from an airplane with turbofan engines, will contain both tone noises arising from the propulsion fan and random (broadband) noise from its jet exhaust. It should also be noticed that in the case of a discrete sound the time period required for the determination of the effective pressure must be one complete period or an integral number of periods. In the case of a random (non-periodic) sound signal, however, the integration time should be long enough

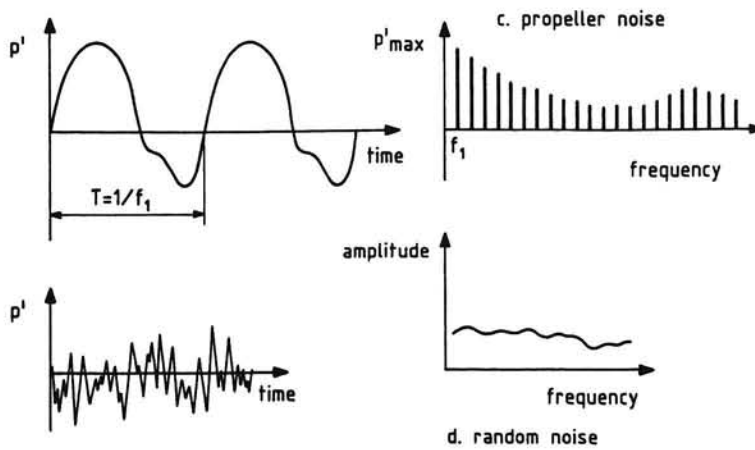


Figure 1.12-1. Continued

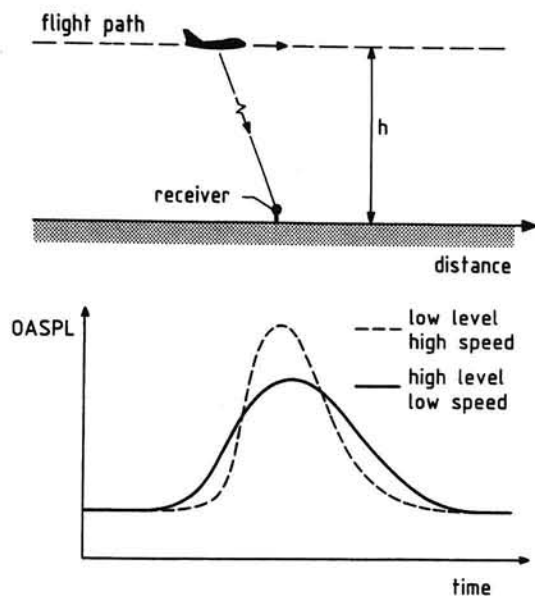


Figure 1.12-2. Sound pressure level time histories

to make the resulting effective sound pressure actually independent of small variations in the length of the integration time.

Sound signals not only exhibit several distinct characteristics according to the time-dependency of the sound pressure, but also to the long-term time-history of the overall sound pressure level, OASPL. For this reason, sound signals are also divided into *continuous* or *stationary sound signals* and *transient* or *non-stationary signals*.

Continuous sounds are those whose sound pressure level remains almost constant over a long time period. In a transient sound the level varies significantly in magnitude with time. The variation may be a steady rise to a peak value followed by a steady fall, as encountered from an aircraft flyover (Figure 1.12-2).

An extreme form is a sharp variation, often with a very high level existing for only a short time, as may be experienced from a gun shot. In this case of very short-duration sound we speak of *impulse* or *impulsive* noise.

A point to note is that when measuring impulse noise, the sound level meter must be used with the time weighting characteristic '*impulse*' in operation. The impulse characteristic has an averaging time of 0.035 s, which is sufficiently short to provide a meter reading which is representative of the

loudness sensation experienced by a listener.

To measure the correct value of the sound pressure level of an impulse noise, a time constant of 50×10^{-6} s or less is used. Together with this *peak* characteristics, a *hold* facility is incorporated in the sound level meter to store the peak value.

1.13 DOPPLER EFFECT

The Doppler effect is the change in observed frequency of a moving source caused by a time rate of change in the distance between source and receiver. If both the source and the receiver are at rest, the sound waves from the source reach the receiver with the speed of sound c in the air. Then the relationship between wavelength and source frequency is given by

$$\lambda = \frac{c}{f} . \quad (1.13-1)$$

If the source moves relative to the receiver, the number of f sound waves which are radiated from the source per second will be contained within a length $(c + dr/dt)$ because this is the velocity of the sound waves approaching the receiver,

$$\lambda' = \frac{c + dr/dt}{f} , \quad (1.13-2)$$

where λ' is the stretched wavelength.

When the airplane moves away from the receiver, as depicted in Figure 1.13-1a, we have $dr/dt > 0$. Then the wavelength is increased in the ratio

$$\frac{\lambda'}{\lambda} = \frac{c + dr/dt}{c} . \quad (1.13-3)$$

Accordingly, the observed frequency is decreased in the ratio

$$\frac{f'}{f} = \frac{c/\lambda'}{c/\lambda} = \frac{1}{1 + \frac{dr/dt}{c}} . \quad (1.13-4)$$

The magnitude of the change in the observed frequency ($f' - f$) is called the *Doppler shift*.

Now suppose, as indicated in Figure 1.13-1a, that the source is an airplane that executes a steady level flight at altitude h . If the flight speed is V and the point of time $t = 0$ coincides with overhead position, we have

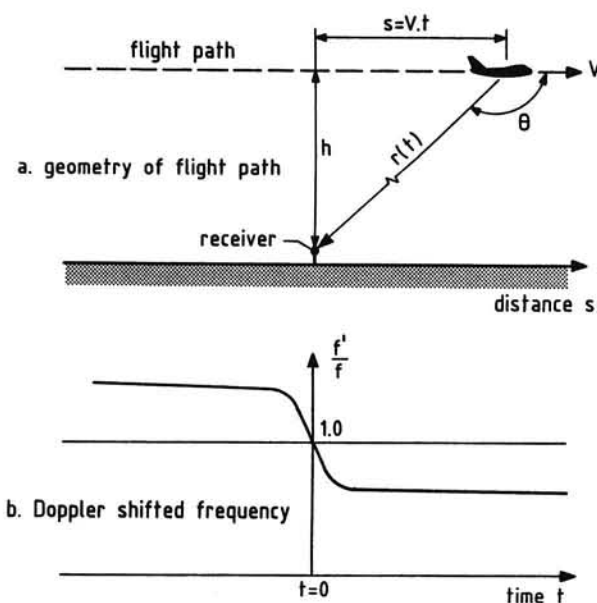


Figure 1.13-1. Doppler effect

$$\frac{dr}{dt} = \frac{d}{dt} \sqrt{h^2 + V^2 t^2} = \frac{V^2 t}{r} . \quad (1.13-5)$$

Insertion of Equation (1.13-5) into Equation (1.13-4) yields

$$\frac{f'}{f} = \frac{1}{1 + \frac{V^2 t}{rc}} . \quad (1.13-6)$$

Using in Equation (1.13-6) the geometrical relationship $r = -V t/\cos\theta$ and the Mach number $M = V/c$, we can write

$$\frac{f'}{f} = \frac{1}{1 - M \cos\theta} . \quad (1.13-7)$$

Apparently, the ratio f'/f is unity at the moment the airplane is overhead ($\theta = 90^\circ$), but is greater than unity when approaching and less than unity when moving away from the receiver (Figure 1.13-1b).

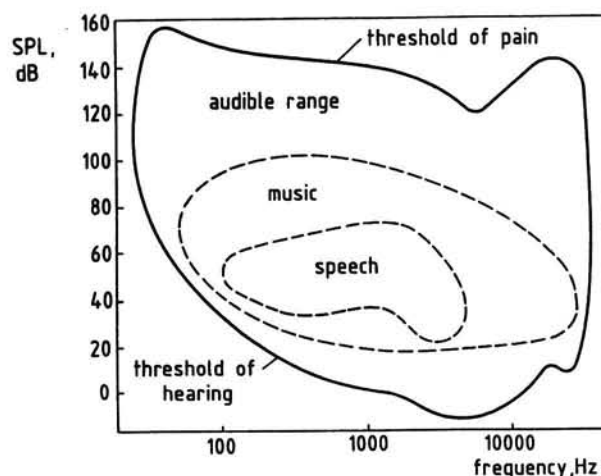


Figure 1.14-1. Hearing range

1.14 LIMITS OF AUDIBILITY

The typical *hearing range* with regard to sound pressure level and frequency is plotted in Figure 1.14-1. All the points inside the closed curve represent audible sound.

As was mentioned earlier, the frequency of audible sound lies between 20 and 20,000 Hz. At 1000 Hz, audible sound ranges from the *threshold of hearing* at about 0 dB to the *threshold of pain* at circa 140 dB. Both these limits vary with frequency and, of course, with the listener's health.

The threshold of hearing can be expected to shift upward with age, particularly in the higher frequency range.

Figure 1.14-1 shows that the human ear is most sensitive to sounds between 2000 and 6000 Hz, and less sensitive at higher and lower frequencies. For example, a 100 Hz tone must be about 20 dB higher than a 1000 Hz tone at the *threshold of audibility*.

The graph of Figure 1.14-1 also indicates speech and music in terms of sound pressure level and frequency. Normal speech comprises frequencies between, say, 200 and 5000 Hz. The performance of music requires a frequency range from about 50 Hz to more than 10,000 Hz.

2 DYNAMICS OF SOUND WAVES

2.1 INTRODUCTION

In this chapter we consider the propagation of sound waves through an atmosphere which, apart from the sound radiation, is uniform and at rest. Also, we make the assumption that the air is inviscid because viscous effects are usually negligible in sound fields. Then, in general, the dynamics of the acoustic disturbances are governed by three physical principles:

- conservation of mass
- conservation of momentum
- conservation of energy.

The first of these principles leads to the equation of continuity. The second principle yields Euler's equations of motion and the third principle furnishes Poisson's relations.

The above mentioned equations form the basis of the mechanics of continuous media. The propagation of sound waves, however, involves a very weak motion of the air from its position at rest. Therefore, in acoustics these initial equations usually can be linearized. In other words, the nonlinear terms in the equations can be neglected, producing a considerable simplification of the dynamics of the sound waves.

The resulting linear theory makes the additional assumptions that the pressure and density variations are very small in comparison with their static (undisturbed) values.

Only the fundamentals of linear acoustics will be discussed in some detail in the following sections of this chapter. For a treatment of the theoretical foundations of nonlinear acoustics, i.e., that part of physics which studies the behavior of strong perturbations, the interested reader is referred to References 13 and 14.

2.2 THE EQUATION OF CONTINUITY

Consider a rectangular axis system $X Y Z$, fixed to the Earth in the field of flow (Figure 2.2-1). The velocity V of the air particles at time t has the components u , v and w along axes X , Y , and Z ,

$$V(x, y, z) = u\mathbf{i} + v\mathbf{j} + w\mathbf{k} , \quad (2.2-1)$$

where \mathbf{i} , \mathbf{j} and \mathbf{k} are the unit vectors in the respective coordinate directions.

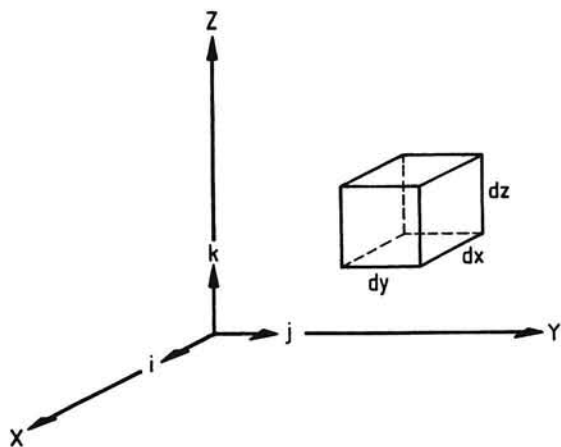


Figure 2.2-1. Elemental volume in the flow field

If ρ is the air density at time t then the mass of air flowing in time dt through the back face of an element of volume $dx dy dz$ is $\rho u dy dz dt$ and through the front face

$$[\rho u + \frac{\partial}{\partial x}(\rho u) dx] dy dz dt .$$

Evidently, the net mass outflow in time dt in the x -direction is

$$\frac{\partial}{\partial x}(\rho u) dx dy dz dt .$$

With the similar contributions from the other faces, the decrease in mass due to the net flux throughout the whole elemental volume in time dt is

$$[\frac{\partial}{\partial x}(\rho u) + \frac{\partial}{\partial y}(\rho v) + \frac{\partial}{\partial z}(\rho w)] dx dy dz dt .$$

The mass originally in the element is $\rho dx dy dz$, and the increase in mass in the volume in time dt is $(\partial \rho / \partial t) dx dy dz dt$.

Hence we can write

$$\frac{\partial \rho}{\partial t} + \frac{\partial}{\partial x}(\rho u) + \frac{\partial}{\partial y}(\rho v) + \frac{\partial}{\partial z}(\rho w) = 0$$

or more concisely

$$\frac{\partial \rho}{\partial t} + \frac{\partial}{\partial x_i}(\rho v_i) = 0 .$$

Equation (2.2-2) is the well-known *equation of continuity*, dealing with elemental volumes of a continuous medium of variable density.

Taking $\rho = \rho_\infty + \rho'$, where ρ_∞ is the static density and ρ' is the

} (2.2-2)

small density increment caused by the wave passing through the air, we have

$$\frac{\partial \rho'}{\partial t} + \frac{\partial}{\partial x} [(\rho_{\infty} + \rho') u] + \frac{\partial}{\partial y} [(\rho_{\infty} + \rho') v] + \frac{\partial}{\partial z} [(\rho_{\infty} + \rho') w] = 0. \quad (2.2-3)$$

In linear acoustics, intrinsically, $\rho' u$, $\rho' v$ and $\rho' w$ involve the products of small quantities and are therefore unimportant in comparison to the other terms in Equation (2.2-3), and hence can be ignored. Accordingly, from Equation (2.2-3), we get

$$\frac{\partial \rho'}{\partial t} + \rho_{\infty} \frac{\partial u}{\partial x} + \rho_{\infty} \frac{\partial v}{\partial y} + \rho_{\infty} \frac{\partial w}{\partial z} = 0. \quad (2.2-4)$$

This equation can be expressed more compactly as

$$\frac{\partial \rho'}{\partial t} + \rho_{\infty} \operatorname{div} V = 0, \quad (2.2-5)$$

where $\operatorname{div} V$ (the divergence of V) is given by:

$$\begin{aligned} \nabla \cdot V &= \left(\frac{\partial}{\partial x} i + \frac{\partial}{\partial y} j + \frac{\partial}{\partial z} k \right) \cdot (ui + vj + wk) \\ &= \frac{\partial u}{\partial x} + \frac{\partial v}{\partial y} + \frac{\partial w}{\partial z}. \end{aligned}$$

Equations (2.2-4) and (2.2-5) are forms of the linearized equation of mass conservation.

It should be noted that when in the element a distributed mass infusion takes place, the continuity equation reads:

$$\frac{\partial \rho'}{\partial t} + \rho_{\infty} \operatorname{div} V = m(x, y, z, t), \quad (2.2-6)$$

where m is the mass injected per unit time and per unit volume ($\text{kg/m}^3\text{s}$).

Finally, it may be noted that the density perturbations may be expressed in terms of the fractional change in density,

$$\rho' = \frac{\rho'}{\rho_{\infty}} \rho_{\infty} = s \rho_{\infty}, \quad (2.2-7)$$

where s is a small parameter which is called the *condensation*.

2.3 EULER'S EQUATIONS

Assuming that external forces are absent and viscous forces are negligible, the motion of the air is due to the pressure forces acting on it.

As shown in Figure 2.3-1, the force on the back face of the element is $p dy dz$, and the force on the front face is $[p + (\partial p / \partial x) dx] dy dz$. Hence the resultant force acting in the x -direction is $-(\partial p / \partial x) dx dy dz$.

Since the mass of the air contained within the element is $\rho dx dy dz$, the equation of motion of the element in x -direction is

$$-\frac{\partial p}{\partial x} dx dy dz = \rho dx dy dz \frac{du}{dt} .$$

For the three components we obtain

$$\left. \begin{aligned} -\frac{1}{\rho} \frac{\partial p}{\partial x} &= \frac{du}{dt} \\ -\frac{1}{\rho} \frac{\partial p}{\partial y} &= \frac{dv}{dt} \\ -\frac{1}{\rho} \frac{\partial p}{\partial z} &= \frac{dw}{dt} \end{aligned} \right\} (2.3-1)$$

The local velocity is a function of time and field coordinates ($V = V(x, y, z, t)$) so that the components of the acceleration are given by

$$\left. \begin{aligned} \frac{du}{dt} &= \frac{\partial u}{\partial t} + \frac{\partial u}{\partial x} \frac{dx}{dt} + \frac{\partial u}{\partial y} \frac{dy}{dt} + \frac{\partial u}{\partial z} \frac{dz}{dt} \\ \frac{dv}{dt} &= \frac{\partial v}{\partial t} + \frac{\partial v}{\partial x} \frac{dx}{dt} + \frac{\partial v}{\partial y} \frac{dy}{dt} + \frac{\partial v}{\partial z} \frac{dz}{dt} \\ \frac{dw}{dt} &= \frac{\partial w}{\partial t} + \frac{\partial w}{\partial x} \frac{dx}{dt} + \frac{\partial w}{\partial y} \frac{dy}{dt} + \frac{\partial w}{\partial z} \frac{dz}{dt} \end{aligned} \right\} (2.3-2)$$

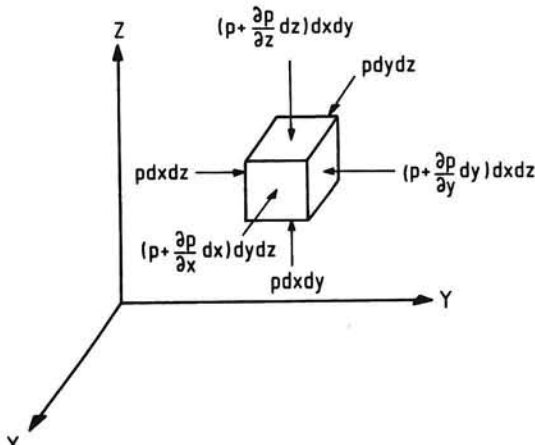


Figure 2.3-1. Pressure forces on a fluid element

Since dx/dt , dy/dt and dz/dt are u , v , and w , respectively, the three accelerations can be written as

$$\begin{aligned}\frac{du}{dt} &= \frac{\partial u}{\partial t} + u \frac{\partial u}{\partial x} + v \frac{\partial u}{\partial y} + w \frac{\partial u}{\partial z} \\ \frac{dv}{dt} &= \frac{\partial v}{\partial t} + u \frac{\partial v}{\partial x} + v \frac{\partial v}{\partial y} + w \frac{\partial v}{\partial z} \\ \frac{dw}{dt} &= \frac{\partial w}{\partial t} + u \frac{\partial w}{\partial x} + v \frac{\partial w}{\partial y} + w \frac{\partial w}{\partial z}\end{aligned}$$

Combining these accelerations with Equation (2.3-1) yields

$$\left. \begin{aligned}\frac{\partial u}{\partial t} + u \frac{\partial u}{\partial x} + v \frac{\partial u}{\partial y} + w \frac{\partial u}{\partial z} &= -\frac{1}{\rho} \frac{\partial p}{\partial x} \\ \frac{\partial v}{\partial t} + u \frac{\partial v}{\partial x} + v \frac{\partial v}{\partial y} + w \frac{\partial v}{\partial z} &= -\frac{1}{\rho} \frac{\partial p}{\partial y} \\ \frac{\partial w}{\partial t} + u \frac{\partial w}{\partial x} + v \frac{\partial w}{\partial y} + w \frac{\partial w}{\partial z} &= -\frac{1}{\rho} \frac{\partial p}{\partial z}\end{aligned}\right\} \quad (2.3-3)$$

This set of equations is known as *Euler's equations of motion of an inviscid fluid*. Using the summation convention, we can write

$$\frac{\partial}{\partial t} (\rho v_i) + \frac{\partial}{\partial x_j} (\rho v_i v_j) + \frac{\partial p}{\partial x_i} = 0 \quad . \quad (2.3-4)$$

We proceed by writing $p = p_\infty + p'$ and $\rho = \rho_\infty + \rho'$, where $p' \ll p_\infty$ and $\rho' \ll \rho_\infty$. Dropping again terms quadratic in the small disturbances, the Equations (2.3-4) reduce to

$$\rho_\infty \frac{\partial u}{\partial t} + \frac{\partial p'}{\partial x} = 0 \quad (2.3-5)$$

$$\rho_\infty \frac{\partial v}{\partial t} + \frac{\partial p'}{\partial y} = 0 \quad (2.3-6)$$

$$\rho_\infty \frac{\partial w}{\partial t} + \frac{\partial p'}{\partial z} = 0 \quad . \quad (2.3-7)$$

If we suppose that in the element there is a distributed externally applied force field $f(x, y, z, t)$ per unit volume, the equations of motion become:

$$\rho_{\infty} \frac{\partial u}{\partial t} + \frac{\partial p'}{\partial x} = f_x(t) \quad (2.3-8)$$

$$\rho_{\infty} \frac{\partial v}{\partial t} + \frac{\partial p'}{\partial y} = f_y(t) \quad (2.3-9)$$

$$\rho_{\infty} \frac{\partial w}{\partial t} + \frac{\partial p'}{\partial z} = f_z(t) . \quad (2.3-10)$$

The Equations (2.3-5) to (2.3-10) are the linearized equations of motion in cartesian coordinates.

2.4 POISSON'S RELATIONS

Poisson's relations are based on the first law of thermodynamics that states that energy is conserved in a thermodynamic system.

Thus, for a system of gas, the energy supplied must equal the sum of the increase in the internal energy of the system and the energy which leaves the system as work.

The differential form of the first law of thermodynamics may be written,

$$dQ = dE + dW , \quad (2.4-1)$$

where dQ is the amount of energy added to the system, dW is the amount of work done by the gas in the system on its surrounding control surfaces, and dE is the corresponding change in internal energy.

It is convenient to employ lower case letters to denote the values of extensive variables per unit mass of gas.

Then, for an incremental change of state of a system of gas,

$$dq = de + dw . \quad (2.4-2)$$

If we assume the absence of gravity and motion, the first term of the right-hand side of Equation (2.4-2) involves solely an increase in internal molecular energy. Assuming, furthermore, that the system experiences a reversible process for which $dw = pd(1/\rho)$, in which $1/\rho$ is the specific volume, we can write

$$dq = de + pd\left(\frac{1}{\rho}\right) . \quad (2.4-3)$$

When we use the concept of enthalpy, h , defined as

$$h = e + \frac{p}{\rho} \quad (2.4-4)$$

then, for an infinitesimal small process,

$$dh = de + p d\left(\frac{1}{\rho}\right) + \frac{1}{\rho} dp . \quad (2.4-5)$$

Combination of Equations (2.4-3) and (2.4-5) yields

$$dq = dh - \frac{1}{\rho} dp . \quad (2.4-6)$$

The specific heat at constant pressure is therefore

$$c_p = \left[\frac{\partial q}{\partial T} \right]_p = \frac{\partial h}{\partial T} . \quad (2.4-7)$$

The specific heat at constant volume is

$$c_v = \left[\frac{\partial q}{\partial T} \right]_v = \frac{\partial e}{\partial T} . \quad (2.4-8)$$

Atmospheric air can be assumed to satisfy the equation of state for a perfect gas, i.e.,

$$\frac{p}{\rho} = R T , \quad (2.4-9)$$

where R is the specific gas constant, and T is the absolute temperature (kelvin). Accordingly, for air the specific heats are related by

$$c_p = \frac{\partial}{\partial T} (e + \frac{p}{\rho}) = \frac{\partial}{\partial T} (e + RT) = c_v + R . \quad (2.4-10)$$

Using Equations (2.4-8) and (2.4-10), we can manipulate Equation (2.4-3) to produce the expression

$$dq = c_p dT - (c_p - c_v) T \frac{dp}{p} . \quad (2.4-11)$$

Normally, it may be assumed that the expansions and compressions of the air particles due to the wave motion are so rapid that there are no appreciable heat losses. In other words, we may assume that the process is adiabatic ($dq = 0$). Then, from Equation (2.4-11),

$$c_p \frac{dT}{T} - (c_p - c_v) \frac{dp}{p} = 0 . \quad (2.4-12)$$

This can be readily integrated and manipulated to the form

$$\frac{p}{T \left[\frac{\gamma}{(\gamma - 1)} \right]} = \text{constant}, \quad (2.4-13)$$

where γ is the ratio of the specific heat at constant pressure to that at constant volume. For atmospheric air we have $\gamma = c_p/c_v = 1.4$.

Using again the perfect gas law, Equation (2.4-9), the latter equation can be transformed to

$$\frac{p}{\rho^\gamma} = \text{constant}. \quad (2.4-14)$$

Equations (2.4-13) and (2.4-14) are called *Poisson's relations*, and provide information on the variations of p , T and ρ in an isentropic process.

To find the relationship between sound pressure and density perturbation, we use Equation (2.4-14), which can be written as

$$\frac{p}{\rho^\gamma} = \frac{p_\infty}{\rho_\infty^\gamma} .$$

With the expressions $p = p_\infty + p'$ and $\rho = \rho_\infty + \rho'$, we can write

$$1 + \frac{p'}{p_\infty} = \left[1 + \frac{\rho'}{\rho_\infty} \right]^\gamma .$$

Using the first two terms of the binomial expansion we get the following linearized form of Equation (2.4-14),

$$p' = \gamma \frac{p_\infty}{\rho_\infty} \rho' . \quad (2.4-15)$$

We now introduce the quantity c given by

$$c^2 = \gamma \frac{p_\infty}{\rho_\infty} . \quad (2.4-16)$$

Using Equation (2.4-16) we can write Equation (2.4-15) in the form

$$p' = c^2 \rho' . \quad (2.4-17)$$

Apparently, an increase of pressure will increase the density.

2.5 THE WAVE EQUATION

If we differentiate Equation (2.3-5) with respect to x , Equation (2.3-6) with respect to y and Equation (2.3-7) with respect to z , we obtain after summation

$$\frac{\partial^2 p'}{\partial x^2} + \frac{\partial^2 p'}{\partial y^2} + \frac{\partial^2 p'}{\partial z^2} = -p_\infty \frac{\partial}{\partial t} \left[\frac{\partial u}{\partial x} + \frac{\partial v}{\partial y} + \frac{\partial w}{\partial z} \right]. \quad (2.5-1)$$

Combination of Equation (2.5-1) with the continuity equation, Equation (2.2-4), yields

$$\frac{\partial^2 p'}{\partial x^2} + \frac{\partial^2 p'}{\partial y^2} + \frac{\partial^2 p'}{\partial z^2} = \frac{\partial^2 \rho'}{\partial t^2}. \quad (2.5-2)$$

Substituting Equation (2.4-17) into Equation (2.5-2) furnishes

$$\frac{\partial^2 p'}{\partial x^2} + \frac{\partial^2 p'}{\partial y^2} + \frac{\partial^2 p'}{\partial z^2} - \frac{1}{c^2} \frac{\partial^2 p'}{\partial t^2} = 0 \quad \text{and} \quad (2.5-3)$$

$$\frac{\partial^2 \rho'}{\partial x^2} + \frac{\partial^2 \rho'}{\partial y^2} + \frac{\partial^2 \rho'}{\partial z^2} - \frac{1}{c^2} \frac{\partial^2 \rho'}{\partial t^2} = 0. \quad (2.5-4)$$

These equations usually are written as

$$\nabla^2 p' - \frac{1}{c^2} \frac{\partial^2 p'}{\partial t^2} = 0 \quad \text{and} \quad (2.5-5)$$

$$\nabla^2 \rho' - \frac{1}{c^2} \frac{\partial^2 \rho'}{\partial t^2} = 0, \quad (2.5-6)$$

where $\nabla^2 = \partial^2/\partial x^2 + \partial^2/\partial y^2 + \partial^2/\partial z^2$ is called the *Laplacian operator*.

Equations (2.5-3) to (2.5-6) are forms of the homogeneous, three-dimensional *wave equation*.

We can modify the above results to the cases of mass injection and the presence of an externally applied force field.

Then the Equations (2.2-6) and (2.3-8) to (2.3-10) hold. The resulting inhomogeneous wave equation, for example, in terms of sound pressure becomes:

$$\nabla^2 p' - \frac{1}{c^2} \frac{\partial^2 p'}{\partial t^2} = -\frac{\partial m}{\partial t} + \nabla \cdot f, \quad (2.5-7)$$

where the two terms on the right-hand side represent the acoustic sources. These terms vanish individually outside the source region. The solutions of

Equation (2.5-7) comprise all the functions describing the propagation of weak, longitudinal, disturbances in a free sound field.

2.6 VELOCITY POTENTIAL

For irrotational velocity fields ($\text{curl } V = 0$) we can use, as a basic dependent variable, the *velocity potential*,

$$\phi = \phi(x, y, z, t) , \quad (2.6-1)$$

such that the particle velocity is given by

$$V = \text{grad } \phi = \nabla \phi , \quad (2.6-2)$$

where the gradient of the scalar function ϕ is defined by

$$\nabla \phi = \left(\frac{\partial}{\partial x} i + \frac{\partial}{\partial y} j + \frac{\partial}{\partial z} k \right) \phi = \frac{\partial \phi}{\partial x} i + \frac{\partial \phi}{\partial y} j + \frac{\partial \phi}{\partial z} k .$$

In cartesian form the particle velocity components are given by

$$u = \frac{\partial \phi}{\partial x} , \quad v = \frac{\partial \phi}{\partial y} \quad \text{and} \quad w = \frac{\partial \phi}{\partial z} . \quad (2.6-3)$$

The possibility to employ the variable ϕ originates from the absence of viscosity through which the rotation of a fluid particle remains always zero.

When the velocity potential is used in the equations of motion to express u , v and w in terms of ϕ , we become from Equations (2.3-5) to (2.3-7):

$$\frac{\partial p'}{\partial x} = -\rho_{\infty} \frac{\partial}{\partial t} \left(\frac{\partial \phi}{\partial x} \right) \quad (2.6-4)$$

$$\frac{\partial p'}{\partial y} = -\rho_{\infty} \frac{\partial}{\partial t} \left(\frac{\partial \phi}{\partial y} \right) \quad (2.6-5)$$

$$\frac{\partial p'}{\partial z} = -\rho_{\infty} \frac{\partial}{\partial t} \left(\frac{\partial \phi}{\partial z} \right) . \quad (2.6-6)$$

These equations can be written much more concisely as

$$\nabla p' = -\rho_{\infty} \frac{\partial}{\partial t} (\nabla \phi) . \quad (2.6-7)$$

The compatibility of the velocity potential with the equations of motion requires that

$$p' = -\rho_{\infty} \frac{\partial \phi}{\partial t} . \quad (2.6-8)$$

When differentiated with respect to time, the Poisson relation, Equation (2.4-17), becomes

$$\frac{\partial p'}{\partial t} = \frac{1}{c^2} \frac{\partial p'}{\partial t} . \quad (2.6-9)$$

Combination of Equation (2.6-9) and the equation of continuity, Equation (2.2-4), yields

$$\frac{1}{c^2} \frac{\partial p'}{\partial t} = -\rho_\infty \left(\frac{\partial u}{\partial x} + \frac{\partial v}{\partial y} + \frac{\partial w}{\partial z} \right) . \quad (2.6-10)$$

According to Equations (2.6-3) and (2.6-8), we have

$$\frac{\partial u}{\partial x} + \frac{\partial v}{\partial y} + \frac{\partial w}{\partial z} = \frac{\partial^2 \phi}{\partial x^2} + \frac{\partial^2 \phi}{\partial y^2} + \frac{\partial^2 \phi}{\partial z^2} \quad (2.6-11)$$

and

$$\frac{\partial p'}{\partial t} = -\rho_\infty \frac{\partial^2 \phi}{\partial t^2} . \quad (2.6-12)$$

By inserting Equations (2.6-11) and (2.6-12) into Equation (2.6-10), we get

$$\frac{\partial^2 \phi}{\partial x^2} + \frac{\partial^2 \phi}{\partial y^2} + \frac{\partial^2 \phi}{\partial z^2} - \frac{1}{c^2} \frac{\partial^2 \phi}{\partial t^2} = 0 \quad \text{or} \quad (2.6-13)$$

$$\nabla^2 \phi = -\frac{1}{c^2} \frac{\partial^2 \phi}{\partial t^2} = 0 . \quad (2.6-14)$$

Equation (2.6-14) is called the *homogeneous three-dimensional scalar wave equation*.

2.7 PLANE WAVES

The plane or one-dimensional wave is the simplest of all radiation waves. It propagates away from the source in one direction only so that the wavefronts always remain parallel to each other. This waveform is of importance because all sound waves become virtually plane at great distances from the source where the radius of curvature of the wavefront is very large.

In this case the sound pressure and the particle velocity are functions of x and t only,

$$p' = p'(x, t) . \quad (2.7-1)$$

For such waves the wave equation, Equation (2.5-3), reduces to

$$\frac{1}{c^2} \frac{\partial^2 p'}{\partial t^2} - \frac{\partial^2 p'}{\partial x^2} = 0 . \quad (2.7-2)$$

The general solution of this equation is

$$p'(x, t) = f_1(x - ct) + f_2(x + ct) . \quad (2.7-3)$$

where f_1 and f_2 are arbitrary functions of the variables $(x - ct)$ and $(x + ct)$, respectively. The function $p'(x, t) = f_1(x - ct) = f_1(\bar{x})$ represents an arbitrary wave traveling without change of its shape at the speed c in the positive x -direction (Figure 2.7-1). Similarly, the function $p'(x, t) = f_2(x + ct)$ describes a wave form in the direction of decreasing x at speed c without change of shape. Obviously, the pressure disturbance travels at speed c , so we identify the quantity c in Equation (2.7-2) as the speed of sound.

From Equations (2.4-9) and (2.4-16), we obtain (see also the previous Equation (1.2-6))

$$c = \sqrt{\gamma \frac{P_\infty}{\rho_\infty}} = \sqrt{\gamma R T_\infty} . \quad (2.7-4)$$

This equation demonstrates that the speed of sound in air depends only on the (absolute) temperature of the air.

A particular waveform is described by Equation (2.7-3) when f_1 and f_2 are harmonic functions. Then we can write

$$p'(x, t) = A \cos \omega(t - x/c) + B \cos \omega(t + x/c) , \quad (2.7-5)$$

where the amplitudes A and B are independent of the distance from the source.

Another important quantity is the *instantaneous particle velocity* u ,

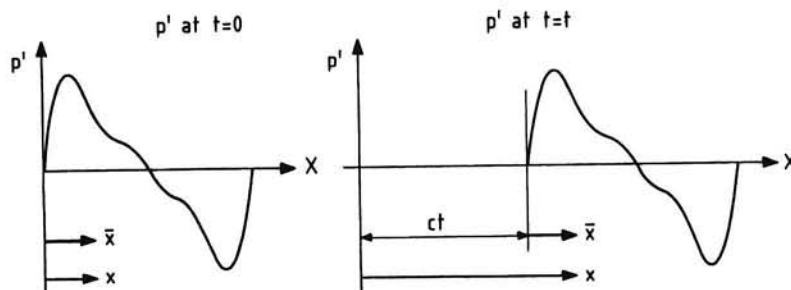


Figure 2.7-1. Plane wave motion

which is the rate at which a given particle oscillates about its equilibrium position when the sound wave passes.

In obtaining the wave equations in Section 2.5, the assumption was made that the acoustic perturbations are small fractions of their static values ($p'/p_{\infty} \ll 1$, $\rho'/\rho_{\infty} \ll 1$). Under these conditions, the particle velocity is also very small relative to the speed of sound.

In order to evaluate the particle velocity, we use the linearized Euler-equation, Equation (2.3-5), repeated here

$$\frac{\partial u}{\partial t} = -\frac{1}{\rho_{\infty}} \frac{\partial p'}{\partial x} . \quad (2.3-5)$$

The particle velocity follows through integrating the pressure gradient with respect to time

$$u = -\frac{1}{\rho_{\infty}} \int \frac{\partial p'}{\partial x} dt . \quad (2.7-6)$$

Now, if we consider the solution $p'(x, t) = A \cos \omega(t - x/c)$, then

$$\frac{\partial p'}{\partial x} = A \frac{\omega}{c} \sin \omega(t - x/c) .$$

Substitution of the latter expression into Equation (2.7-6) and integration with respect to time yields

$$u = \frac{A}{\rho_{\infty} c} \cos \omega(t - x/c) \quad \text{or} \quad (2.7-7)$$

$$u = \frac{p'}{\rho_{\infty} c} . \quad (2.7-8)$$

Similarly, in a wave traveling in the negative x -direction, we find

$$u = -\frac{p'}{\rho_{\infty} c} . \quad (2.7-9)$$

It should be noted that the relationships (2.7-8) and (2.7-9) have a general validity, independent of the occurring waveform.

From Equation (2.7-7) we see that for a sinusoidally varying sound pressure (a pure tone), the particle velocity is also a simple harmonic motion with amplitude

$$u_{\max} = \frac{p_{\max}}{\rho_{\infty} c} = \frac{p_e \sqrt{2}}{\rho_{\infty} c} . \quad (2.7-10)$$

We also see that in a plane progressive wave the sound pressure and the particle velocity are in phase.

As already mentioned in Chapter 1, the constant of proportionality, $\rho_\infty c$, is called the *characteristic acoustic resistance* of the medium.

In order to provide an impression of the magnitude of the particle velocity, we suppose that at a given position the occurring sound pressure level is 100 dB.

By definition the sound pressure level is $10 \log[p_e^2/p_{e_0}^2]$ so that with $p_{e_0} = 2 \times 10^{-5}$ N/m², the effective pressure is found to be

$$p_e = p_{e_0} \sqrt{10^{SPL/10}} = 2 \times 10^{-5} \sqrt{10^{10}} = 2 \text{ N/m}^2.$$

For $\rho_\infty c = 416.86$ kg/m²s (air at 15°C), the particle velocity amplitude is found, from Equation (2.7-10), to be

$$u_{\max} = \frac{2\sqrt{2}}{416.86} = 0.0068 \text{ m/s}.$$

This example demonstrates how small the maximum particle velocity is.

The particle velocity must not be confused with the *molecular velocity* or mean speed of random motion, i.e., the root mean square value of the speed of the molecules in a gas, \bar{v} . According to kinetic theory of gases, the following equation holds (Reference 9):

$$\bar{v} = \sqrt{\frac{8p}{\pi\rho}}. \quad (2.7-11)$$

With the speed of sound $c = \sqrt{\gamma p/\rho}$, Equation (2.7-11) becomes

$$\bar{v} = c \sqrt{\frac{8}{\pi\gamma}} = 1.35c. \quad (2.7-12)$$

This equation shows that the molecular velocity is of the same order of magnitude as the speed of sound and is greater by about 35 percent. For air at standard sea-level temperature the speed of sound is 340.29 m/s. Then, from Equation (2.7-12), the molecular velocity can be obtained as 458.90 m/s.

Comparing the result of Equation (2.7-12) with the above value of u_{\max} in our example shows that the molecular velocity is always very large in comparison with the maximum particle velocity.

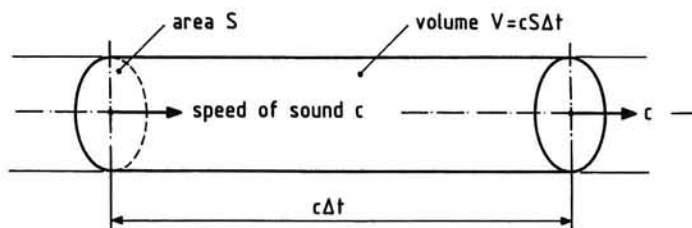


Figure 2.7-2. Derivation of energy density

Using Equation (2.7-8), we readily find the sound intensity, the time average of the product of sound pressure and particle velocity, to be

$$I = \frac{1}{T} \int_0^T p \cdot u dt = \frac{p_e^2}{\rho_\infty c} . \quad (2.7-13)$$

Apparently, in a plane wave the sound intensity is given by the mean square sound pressure divided by the characteristic acoustic resistance.

The energy which passes through an area S in a time Δt is given by

$$E = IS\Delta t . \quad (2.7-14)$$

As portrayed in Figure 2.7-2, the energy passing through S in time Δt is contained in a column of cross-sectional area S and length $c\Delta t$,

$$E = e c S \Delta t = e V , \quad (2.7-15)$$

where $e = E/V$ is termed the *energy density* which has the unit Ws/m^3 .

Equating Equations (2.7-14) and (2.7-15) yields

$$e = \frac{I}{c} . \quad (2.7-16)$$

When Equation (2.7-13) is inserted into Equation (2.7-16), we get

$$e = \frac{p_e^2}{\rho_\infty c^2} . \quad (2.7-17)$$

This equation shows that in a plane wave the energy density is equal to the mean square sound pressure divided by the product of characteristic acoustic resistance and speed of sound.

2.8 SPHERICAL WAVES

A second example of a particular waveform is the spherical wave emanating from a point source. When this wave is centered at the origin of the axis system, both the sound pressure and the particle velocity are functions of radial distance r and time t only,

$$p' = p'(r, t) \quad (2.8-1)$$

$$v_r = v_r(r, t) . \quad (2.8-2)$$

In this case, of course, it is convenient to express the wave equation in spherical polar coordinates. The position of the point P in Figure 2.8-1 is then given by the radial distance r , the angle θ between the line OP and the Z -axis, and the angle ψ between the X -axis and the plane through the Z -axis and the point P . Hence, we must insert into Equation (2.6-13) the relationships, $x = r\sin\theta \cos\psi$, $y = r\sin\theta \sin\psi$, and $z = r\cos\theta$.

Alternatively, here we will directly develop the desired form of the wave equation by applying the three principles of Section 2.1 to an element of volume with sides of lengths $rd\theta$, $r\sin\theta d\psi$, dr (Figure 2.8-2).

Using the acoustic velocity potential,

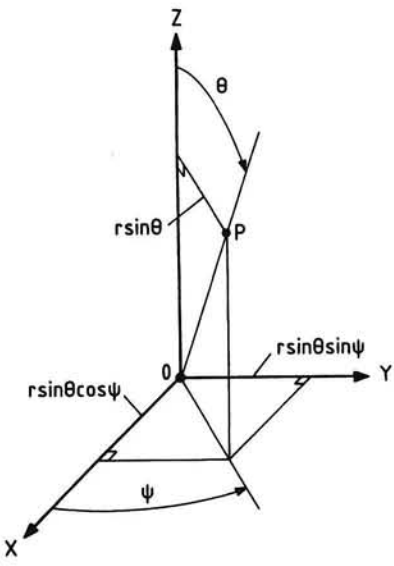


Figure 2.8-1. Spherical coordinates

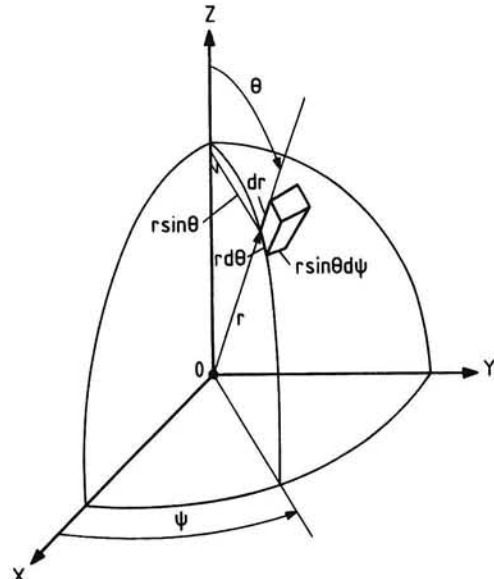


Figure 2.8-2. An element of volume in spherical coordinates

$$\phi = \phi(r, \theta, \psi, t) , \quad \text{we have}$$

$$v_r = \frac{\partial \phi}{\partial r} . \quad (2.8-3)$$

With $p = p_\infty + p'$, the principle of conservation of momentum gives

$$\rho_\infty \frac{\partial v_r}{\partial t} = - \frac{\partial p'}{\partial r} . \quad (2.8-4)$$

This equation of motion demands that (see also Equation (2.6-8))

$$p' = - \rho_\infty \frac{\partial \phi}{\partial t} . \quad (2.8-5)$$

The principle of conservation of mass requires that the sum of the decrease in mass due to the net flux through the faces of the element in time dt and the increase in mass in the element in time dt is equal to zero (cf. Equation (2.2-2)),

$$[\frac{\partial}{\partial r} (\rho v_r) r d\theta r \sin \theta d\psi dr + \frac{\partial \rho}{\partial t} r d\theta r \sin \theta d\psi dr] dt = 0 . \quad (2.8-6)$$

With Equation (2.8-3) and the relationship $\rho = \rho_\infty + \rho'$, we obtain

$$\begin{aligned} & \left[\frac{\partial^2 \phi}{\partial r^2} r d\theta r \sin \theta d\psi + \rho_\infty \frac{\partial \phi}{\partial r} 2 r d\theta \sin \theta d\psi \right] dr + \\ & + r d\theta r \sin \theta d\psi dr \frac{\partial \rho'}{\partial t} = 0 \quad \text{or} \\ & \rho_\infty \frac{\partial^2 \phi}{\partial r^2} + \rho_\infty \frac{2}{r} \frac{\partial \phi}{\partial r} + \frac{\partial \rho'}{\partial t} = 0 . \end{aligned} \quad (2.8-7)$$

Equation (2.4-17), derived from application of the principle of conservation of energy, and Equation (2.8-5) enable us to write the third term of Equation (2.8-7) as

$$\frac{\partial \rho'}{\partial t} = - \frac{\rho_\infty}{c^2} \frac{\partial^2 \phi}{\partial t^2} . \quad (2.8-8)$$

By substituting Equation (2.8-8) into Equation (2.8-7), we derive the wave equation of the form

$$\frac{\partial^2 \phi}{\partial r^2} + \frac{2}{r} \frac{\partial \phi}{\partial r} - \frac{1}{c^2} \frac{\partial^2 \phi}{\partial t^2} = 0 . \quad (2.8-9)$$

In order to discover the solutions for p' we proceed by expressing the wave equation in terms of the sound pressure. Differentiating Equation (2.8-5) with respect to r gives,

$$\frac{\partial p'}{\partial r} = -\rho_\infty \frac{\partial}{\partial t} \left(\frac{\partial \phi}{\partial r} \right) \quad \text{and} \quad \frac{\partial^2 p'}{\partial r^2} = -\rho_\infty \frac{\partial}{\partial t} \left[\frac{\partial^2 \phi}{\partial r^2} \right].$$

Differentiating Equation (2.8-5) twice with respect to t gives

$$\frac{\partial^2 p'}{\partial t^2} = -\rho_\infty \frac{\partial}{\partial t} \left[\frac{\partial^2 \phi}{\partial t^2} \right].$$

Inserting these relations into Equation (2.8-9) furnishes

$$\frac{\partial^2 p'}{\partial r^2} + \frac{2}{r} \frac{\partial p'}{\partial r} - \frac{1}{c^2} \frac{\partial^2 p'}{\partial t^2} = 0. \quad (2.8-10)$$

Continuing the modification process in our quest for finding the solution for the sound pressure, we next consider the product rp' . Differentiating this quantity with respect to r gives

$$\frac{\partial}{\partial r} (rp') = p' + r \frac{\partial p'}{\partial r} \quad \text{and} \quad \frac{\partial^2 (rp')}{\partial r^2} = \frac{\partial p'}{\partial r} + r \frac{\partial^2 p'}{\partial r^2} + \frac{\partial p'}{\partial r}. \quad .$$

Hence,

$$\frac{\partial^2 p'}{\partial r^2} = \frac{1}{r} \frac{\partial^2 (rp')}{\partial r^2} - \frac{2}{r} \frac{\partial p'}{\partial r}. \quad (2.8-11)$$

Combining Equations (2.8-10) and (2.8-11) results in the following expression for the wave equation,

$$\frac{\partial^2 (rp')}{\partial r^2} - \frac{r}{c^2} \frac{\partial^2 p'}{\partial t^2} = 0. \quad (2.8-12)$$

Since r is independent of t , we can write

$$\frac{\partial^2 (rp')}{\partial r^2} - \frac{1}{c^2} \frac{\partial^2 (rp')}{\partial t^2} = 0. \quad (2.8-13)$$

From Equations (2.8-13) and (2.7-2), we see that the wave equation for the quantity rp' is analogous to the plane wave equation. Therefore, the most general solution for rp' is (cf. Equation (2.7-3)),

$$rp'(r,t) = f_1(r - ct) + f_2(r + ct) \quad \text{or} \quad (2.8-14)$$

$$p'(r,t) = \frac{1}{r} [f_1(r - ct) + f_2(r + ct)] . \quad (2.8-15)$$

The two terms on the right-hand side of Equation (2.8-15) represent outward and inward traveling waves, respectively. The latter solution, however, can be excluded since incoming waves are physically impossible in open space. The restriction to the occurrence of only outgoing waves is called *Sommerfeld's radiation condition*. Consequently, Equation (2.8-15) reduces to

$$p'(r,t) = \frac{1}{r} f(r - ct) . \quad (2.8-16)$$

Assuming that f is a harmonic function, we can write in exponential notation

$$p'(r,t) = \frac{A}{r} e^{i\omega(t - r/c)} , \quad (2.8-17)$$

or when using the trigonometric notation

$$p'(r,t) = \frac{A}{r} \cos \omega(t - r/c) , \quad (2.8-18)$$

which expression has already been stated in Chapter 1, Equation (1.2-3), in anticipation of the above analysis.

Note that in Equations (2.8-17) and (2.8-18) the source strength A is a constant. Also note that the sound pressure amplitude varies inversely with the distance r . This behavior is in accordance with a constant value of the power radiated over each spherical surface surrounding the (point) source.

The particle velocity can be determined from the sound pressure by using Equations (2.8-4) and (2.8-17),

$$v_r = -\frac{1}{\rho_\infty} \int \frac{\partial p'}{\partial r} dt = \frac{A}{i\omega\rho_\infty} \left[\frac{i\omega}{cr} + \frac{1}{r^2} \right] e^{i\omega(t - r/c)} \quad \text{or} \quad (2.8-19)$$

$$v_r = \frac{A}{r} \frac{1}{\rho_\infty c} [\cos \omega(t - r/c) + \frac{c}{\omega r} \sin \omega(t - r/c)] . \quad (2.8-20)$$

Comparing Equations (2.8-17) and (2.8-19) shows that normally the sound pressure and the particle velocity are not in phase. In this case the ratio of the sound pressure to the associated particle velocity is called the *characteristic acoustic impedance* and given the symbol Z ,

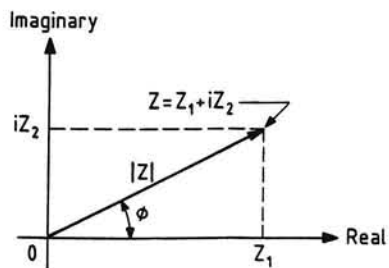


Figure 2.8-3. Complex plane diagram

$$Z = \frac{p'}{v_r} = \rho_\infty c \left[\frac{1 + i \frac{c}{\omega r}}{1 + \left(\frac{c}{\omega r} \right)^2} \right]. \quad (2.8-21)$$

Since Z is a complex number we write (Figure 2.8-3)

$$Z = Z_1 + iZ_2 = |Z|(\cos \phi + i \sin \phi) = |Z|e^{i\phi},$$

where the real component Z_1 is termed the *characteristic acoustic resistance* and the imaginary component Z_2 is termed the *characteristic acoustic reactance*. $|Z|$ is the modulus or absolute value of Z , and ϕ the argument of Z . Furthermore, we have the relations

$$|Z| = \sqrt{Z_1^2 + Z_2^2} \quad \text{and} \quad \phi = \arctan \frac{Z_1}{Z_2}.$$

Applying this to Equation (2.8-21) yields

$$|Z| = \frac{\rho_\infty c}{\sqrt{1 + \left(\frac{c}{\omega r} \right)^2}} \quad \text{and} \quad (2.8-22)$$

$$\phi = \arctan \frac{c}{\omega r}. \quad (2.8-23)$$

Equations (2.8-22) and (2.8-23) indicate that $|Z|$ is less than the characteristic acoustic resistance of the medium, $\rho_\infty c$, and that the phase difference between p' and v_r decreases as r is increased. This means that at greater distances ($r \gg c/\omega$) the simple plane wave equation may be used to describe a spherical wave field. This is in accordance with our observation that at large distances the wavefronts are nearly plane.

As discussed in Chapter 1, the sound intensity is given by the time average of the product of sound pressure and the in-phase particle velocity component of the radial velocity,

$$I = \frac{1}{T} \int_0^T p' v_r dt . \quad (2.8-24)$$

Substitution of Equations (2.8-17) and (2.8-19) into Equation (2.8-24) and performing the integration, we find that

$$I = \frac{1}{\rho_\infty c} \left(\frac{A}{r\sqrt{2}} \right)^2 = \frac{p_e^2}{\rho_\infty c} . \quad (2.8-25)$$

Thus, we see from Equations (2.8-25) and (2.7-13) that both in progressive plane and spherical waves the sound intensity is related to the effective pressure by the same expression. The underlying condition is that the sound-waves are traveling through a free field.

2.9 THE HELMHOLTZ EQUATION

Consider spherical wave motion with harmonic time dependence of angular frequency ω given by Equation (2.8-17), repeated here:

$$p'(r, t) = \frac{A}{r} e^{i\omega(t - r/c)} . \quad (2.8-17)$$

If we differentiate this equation with respect to time, we get

$$\frac{\partial p'}{\partial t} = i\omega \frac{A}{r} e^{i\omega(t - r/c)} \quad \text{and} \quad (2.9-1)$$

$$\frac{\partial^2 p'}{\partial t^2} = -\omega^2 p' . \quad (2.9-2)$$

When we substitute the latter expression into Equation (2.5-5), we find that time harmonic sound waves conform with the form

$$\nabla^2 p' + k^2 p' = 0 , \quad (2.9-3)$$

where $k = \omega/c$ is called the *wavenumber* of the wave, which quantity has the unit of inverse length.

This special form of the wave equation is known as the *Helmholtz equation*, involving harmonic perturbations, and where the time is implicitly present.

3 ELEMENTARY SOURCES

3.1 MONOPOLE SOURCE

The acoustic monopole is visualized here as a pulsating sphere of radius a , centered at the origin of the axis system (Figure 3.1-1). The sound field produced by the motion of the monopole is defined by the radial velocities of its surface.

Assuming a harmonic expansion and retraction, we may write

$$v_{r=a} = v_0 e^{i\omega t}, \quad (3.1-1)$$

where v_0 is the surface velocity amplitude.

Evidently, the sound waves emanating from the source will also have a harmonic time dependence. This simplification of the waveform, however, will cause no loss of generality because the *Fourier's theorem* states that any periodic sound can be regarded as a large number of superimposed sinusoids (see Chapter 7).

According to the previous Equation (2.8-17), the sound pressure generated by our monopole can be written as

$$p'(r, t) = \frac{A}{r} e^{i\omega(t - r/c)}. \quad (3.1-2)$$

The in the preceding chapter derived sound pressure-velocity potential relationship

$$p'(r, t) = -\rho_\infty \frac{\partial \phi_m}{\partial t} \quad Q = 4\pi a^2 v_0 \quad (3.1-3)$$
$$k = \omega/c$$

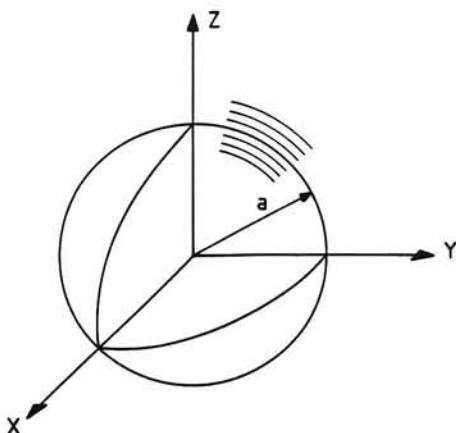


Figure 3.1-1. Pulsating sphere

then enables us to develop the following expression for the monopole velocity potential:

$$\phi_m(r, t) = \frac{i}{\rho_\infty \omega} \frac{A}{r} e^{i\omega(t - r/c)} . \quad (3.1-4)$$

To determine the constant A in this expression, we can use the condition that the particle velocity at the distance $r = a$ is given by

$$(v)_{r=a} = \left[\frac{\partial \phi_m}{\partial r} \right]_{r=a} = v_0 e^{i\omega t} . \quad (3.1-5)$$

From Equation (3.1-4) it follows without difficulty that the derivative of the velocity potential with respect to distance is

$$\frac{\partial \phi_m}{\partial r} = - \frac{i}{\rho_\infty \omega} \frac{A}{r^2} e^{i\omega(t - r/c)} \left(1 + \frac{i\omega r}{c} \right) . \quad (3.1-6)$$

Putting $r = a$ into Equation (3.1-6) and equating the result to Equation (3.1-5), we get

$$- \frac{i}{\rho_\infty \omega} \frac{A}{a^2} e^{i\omega(t - a/c)} \left(1 + \frac{i\omega a}{c} \right) = v_0 e^{i\omega t} . \quad (3.1-7)$$

Solving Equation (3.1-7) for A yields

$$A = - \frac{\rho_\infty \omega v_0 a^2 e^{i\omega a/c}}{i \left(1 + i \frac{\omega a}{c} \right)} . \quad (3.1-8)$$

Substituting Equation (3.1-8) into Equation (3.1-4), finally, gives

$$\phi_m(r, t) = - \frac{v_0 a^2}{\left(1 + i \frac{\omega a}{c} \right)} \frac{1}{r} e^{i\omega(t - \frac{r-a}{c})} . \quad (3.1-9)$$

In dealing with noise emission of airplanes we are especially interested in what happens in the far field. There we have $r \gg a$ so that Equation (3.1-9) may be simplified to

$$\phi_m(r, t) = - \frac{v_0 a^2}{\left(1 + i \frac{\omega a}{c} \right)} \frac{1}{r} e^{i\omega(t - r/c)} . \quad (3.1-10)$$

This equation reveals that the monopole source does not have any directivity and generates spherical waves when placed in a free field.

Differentiating Equation (3.1-10) with respect to time gives the sound pressure as

$$p'(r, t) = -\rho_{\infty} \frac{\partial \phi_m}{\partial t} = \frac{i\omega \rho_{\infty} v_0 a^2}{(1 + i \frac{\omega a}{c})} \frac{1}{r} e^{i\omega(t - r/c)} . \quad (3.1-11)$$

It is an easy matter to perform a few operations with complex numbers to obtain that

$$\frac{i}{(1 + i \frac{\omega a}{c})} = \frac{e^{i \arctan \frac{c}{\omega a}}}{\sqrt{1 + (\frac{\omega a}{c})^2}} . \quad (3.1-12)$$

Using this relationship in Equation (3.1-11) gives

$$p'(r, t) = \frac{\rho_{\infty} v_0 a^2}{r} \frac{\omega}{\sqrt{1 + (\frac{\omega a}{c})^2}} e^{i[\omega(t - r/c) + \arctan \frac{c}{\omega a}]} \text{ or} \quad (3.1-13)$$

$$p'(r, t) = p'_{\max} e^{i[\omega(t - r/c) + \arctan \frac{c}{\omega a}]} , \quad (3.1-14)$$

where

$$p'_{\max} = \frac{\rho_{\infty} v_0 a^2 \omega}{r \sqrt{1 + (\frac{\omega a}{c})^2}} . \quad (3.1-15)$$

With the relationship: $p_e = p'_{\max}/\sqrt{2}$, the effective pressure is found from Equation (3.1-15) to be

$$p_e(r) = \frac{\rho_{\infty} v_0 a^2 \omega}{r \sqrt{2}} \frac{1}{\sqrt{1 + (\frac{\omega a}{c})^2}} . \quad (3.1-16)$$

The radial particle velocity is obtained by differentiating Equation (3.1-10) with respect to r

$$v_r(r, t) = \frac{\partial \phi_m}{\partial r} = v_0 \frac{a}{r} \frac{i \frac{\omega a}{c}}{(1 + i \frac{\omega a}{c})} (1 + \frac{c}{i \omega r}) e^{i \omega(t - r/c)} . \quad (3.1-17)$$

Similar to the development of the relationship (3.1-12), we easily find that

$$1 + \frac{c}{i \omega r} = \sqrt{1 + \left(\frac{c}{\omega r}\right)^2} e^{-i \arctan \frac{c}{\omega r}} . \quad (3.1-18)$$

By using the relationships (3.1-12) and (3.1-18), we can rewrite Equation (3.1-17) as

$$v_r(r, t) = v_0 \frac{a}{r} \frac{\omega a}{c} \frac{\sqrt{1 + \left(\frac{c}{\omega r}\right)^2}}{\sqrt{1 + \left(\frac{\omega a}{c}\right)^2}} e^{i[\omega(t - r/c) + \arctan \frac{c}{\omega a} - \arctan \frac{c}{\omega r}]} . \quad (3.1-19)$$

From Equations (3.1-13) and (3.1-19) we get for the characteristic acoustic impedance (cf. Equations (2.8-22) and (2.8-23)),

$$Z = \frac{p'}{v_r} = \frac{\rho_\infty c}{\sqrt{1 + \left(\frac{c}{\omega r}\right)^2}} e^{i \arctan \frac{c}{\omega r}} . \quad (3.1-20)$$

We again see that the sound pressure and the particle velocity are not in phase but that for large r ($r \gg c/\omega$) the characteristic acoustic impedance becomes nearly real and equal to the characteristic acoustic resistance of the medium $\rho_\infty c$. Comparing Equations (3.1-13) and (3.1-19) then shows that $p' = \rho_\infty c v_r$, as in the case of a plane sound wave.

Employing Equations (3.1-13) and (3.1-19), it is also not hard to derive the following expression for the sound intensity in radial direction in the far field ($c/\omega r \ll 1$):

$$I(r) = \frac{1}{T} \int_0^T p' v_r dt = \frac{\rho_\infty v_0^2 a^4 \omega^2}{2 c r^2} \frac{1}{\sqrt{1 + \left(\frac{\omega a}{c}\right)^2}} . \quad (3.1-21)$$

The sound power is therefore

$$W = I(r)4\pi r^2 = \frac{2\pi\rho_\infty v_0^2 a^4 \omega^2}{c} \frac{1}{\sqrt{1 + (\frac{\omega a}{c})^2}} . \quad (3.1-22)$$

The quantity $\omega a/c$ in the above equations is referred to as the *compactness ratio* since it is the ratio of the circumference of the source to the wavelength of the sound, $\omega a/c = 2\pi a/\lambda$.

The effect of the magnitude of the compactness ratio on the radiation characteristics of the monopole can be seen by comparing the extreme cases where $\omega a/c \gg 1$ and $\omega a/c \ll 1$.

Then from Equations (3.1-16), (3.1-21) and (3.1-22), we obtain:

$$\left. \begin{aligned} p_e(r) &= \frac{\rho_\infty v_0 a c}{r\sqrt{2}} & \omega a/c \gg 1 \\ p_e(r) &= \frac{\rho_\infty v_0 a^2 \omega}{r\sqrt{2}} & \omega a/c \ll 1 \end{aligned} \right\} \quad (3.1-23)$$

$$\left. \begin{aligned} I(r) &= \frac{\rho_\infty v_0^2 a^3 \omega}{2r^2} & \omega a/c \gg 1 \\ I(r) &= \frac{\rho_\infty v_0^2 a^4 \omega^2}{2cr^2} & \omega a/c \ll 1 \end{aligned} \right\} \quad (3.1-24)$$

$$\left. \begin{aligned} W &= 2\pi\rho_\infty v_0^2 a^3 \omega & \omega a/c \gg 1 \\ W &= \frac{2\pi\rho_\infty v_0^2 a^4 \omega^2}{c} & \omega a/c \ll 1 \end{aligned} \right\} \quad (3.1-25)$$

The expressions show that a large pulsating sphere is an effective radiator of acoustic energy. On the contrary, we see that small diameter sources are very weak radiators, except at higher frequencies.

To complete our discussion of monopole sound radiation, we consider the velocity potential for the so-called *point monopole* ($\omega a/c \ll 1$) which, from Equation (3.1-10), can be expressed as

$$\phi_m(r, t) = -\frac{4\pi a^2 v_0}{4\pi r} e^{i\omega(t-r/c)} \quad \text{or} \quad (3.1-26)$$

$$\phi_m(r, t) = -\frac{Q_0}{\rho_\infty 4\pi r} e^{i\omega(t-r/c)}, \quad (3.1-27)$$

where $Q_0 e^{i\omega(t-r/c)} = Q(t)$ is the flow of mass per unit time provided by the pulsating sphere. The sound pressure is then obtained as

$$p'(r, t) = -\rho_\infty \frac{\partial \phi_m}{\partial t} = \frac{1}{4\pi r} \frac{\partial}{\partial t} [Q_0 e^{i\omega(t-r/c)}]. \quad (3.1-28)$$

Inspection of Equations (3.1-27) and (3.1-28) shows that there is a singularity at the origin of the axis system where $r = 0$. In other words, the above results only hold in that part of the sound field which excludes the region occupied by the source.

To describe the entire sound field, we can use the property that the wave equation limits to Laplace's equation as r tends to zero. Hence,

$$\lim_{r \rightarrow 0} \left[\nabla^2 \phi_m - \frac{1}{c^2} \frac{\partial^2 \phi_m}{\partial r^2} \right] = \nabla^2 \phi_m. \quad (3.1-29)$$

This statement may be understood from the fact that differentiation of the velocity potential ϕ_m with respect to r introduces the factor r^3 in the denominator. This implies that the relative importance of $\nabla^2 \phi_m$ in the wave equation increases strongly as r diminishes. Thus, close enough to the point $r = 0$, the wave equation can be approximated by

$$\nabla^2 \phi_m = \nabla \cdot (\nabla \phi_m) = 0. \quad (3.1-30)$$

In mathematical textbooks (e.g., Reference 16), it is shown that according to the *divergence theorem* or *Green's theorem in space*, the integral of the divergence of the vector $\nabla \phi$ taken over the volume of a sphere, with $r = 0$ the center, is equal to the radial gradient of $\nabla \phi_m$, integrated over the surface of the sphere. In formula,

$$\int_V \nabla \cdot (\nabla \phi_m) dV = \int_S \frac{\partial \phi_m}{\partial n} dS. \quad (3.1-31)$$

Using Equation (3.1-27), the right-hand side of Equation (3.1-31) can be written as

$$\begin{aligned}
 & \int_S \frac{\partial}{\partial n} \left[-\frac{Q_0}{\rho_\infty 4\pi r} e^{i\omega(t-r/c)} \right] dS \\
 &= \left[\frac{Q_0}{\rho_\infty 4\pi r^2} e^{i\omega(t-r/c)} + \frac{Q_0}{\rho_\infty 4\pi r} e^{i\omega(t-r/c)} \frac{i\omega}{c} \right] 4\pi r^2 \\
 &= \left[\frac{1}{\rho_\infty} Q_0 + \frac{r}{\rho_\infty} Q_0 \frac{i\omega}{c} \right] e^{i\omega(t-r/c)} . \tag{3.1-32}
 \end{aligned}$$

In the limit, as $r \rightarrow 0$, we obtain

$$\int_S \frac{\partial \phi_m}{\partial n} dS = \frac{1}{\rho_\infty} Q_0 e^{i\omega t} . \tag{3.1-33}$$

If we compare this result with Equations (3.1-29) and (3.1-31), we see that

$$\int_V \left[\nabla^2 \phi_m - \frac{1}{c^2} \frac{\partial^2 \phi_m}{\partial t^2} \right] dV = \frac{1}{\rho_\infty} Q_0 e^{i\omega t} . \tag{3.1-34}$$

This expression reveals that in the source region the wave equation is inhomogeneous. Therefore, the source region is separated from the sound field where the wave equation is homogeneous.

In order to ensure that the right-hand side of Equation (3.1-34) is zero everywhere except at the point $r = 0$, one utilizes the three-dimensional *delta function* $\delta(r)$ (see Reference 6). By definition, this function has the properties that (1) $\delta(r) = \infty$ if $r = 0$, and (2) $\delta(r) = 0$ if $r \neq 0$.

Near $r = 0$ the delta function is sufficiently large that its integral over any volume V enclosing $r = 0$ is unity:

$$\int_V \delta(r) dV = 1 . \tag{3.1-35}$$

Otherwise, because of the properties of the function $\delta(r)$, the integral is equal to zero when V excludes $r = 0$.

Clearly, the right-hand side of Equation (3.1-34) may be expressed as

$$\frac{1}{\rho_\infty} Q_0 e^{i\omega t} = \int_V \frac{1}{\rho_\infty} Q_0 e^{i\omega t} \delta(r) dV . \tag{3.1-36}$$

When this equality is compared with Equation (3.1-34) we find that

$$\nabla^2 \phi_m - \frac{1}{c^2} \frac{\partial^2 \phi_m}{\partial t^2} = \frac{1}{\rho_\infty} Q_0 e^{i\omega t} \delta(r) , \quad (3.1-37)$$

where the term on the right-hand side represents our acoustic monopole source located at the origin of the axis system ($r = 0$).

At this point, let us return to Equation (2.5-7), which furnishes the corresponding inhomogeneous wave equation for the point monopole sound pressure by introducing $m(r,t) = m(t) = Q_0 e^{i\omega t}$ and setting $f(r,t) = 0$ in it. Accordingly, the wave equation is

$$\nabla^2 p - \frac{1}{c^2} \frac{\partial^2 p}{\partial t^2} = -\frac{\partial}{\partial t} (Q_0 e^{i\omega t}) , \quad (3.1-38)$$

where the right-hand side term is equal to zero outside the source region.

3.2 DIPOLE SOURCE

As the model for a dipole source we use a rigid sphere with radius a and density ρ_∞ , whose center oscillates along the Z-axis (Figure 3.2-1).

In the case that the sphere executes a simple harmonic motion about the origin of the axis system, we have

$$w = w_0 e^{i\omega t} . \quad (3.2-1)$$

To find an expression for the velocity potential of the vibrating sphere, ϕ_d , we use the property that if the velocity potential of the monopole, ϕ_m , is a solution of the wave equation, also its derivative with respect to the z-coordinate satisfies the wave equation,

$$\frac{\partial}{\partial z} \left[\nabla^2 \phi_m - \frac{1}{c^2} \frac{\partial^2 \phi_m}{\partial t^2} \right] = \nabla^2 \left[\frac{\partial \phi_m}{\partial z} \right] - \frac{1}{c^2} \frac{\partial^2}{\partial t^2} \left[\frac{\partial \phi_m}{\partial z} \right] = 0 , \quad (3.2-2)$$

where, of course, only the outgoing wave solution need be retained.

In terms of polar coordinates, we may write

$$\frac{\partial}{\partial z} (\phi_m) = \cos \theta \frac{\partial \phi_m}{\partial r} = \phi_d . \quad (3.2-3)$$

Substitution of Equation (3.1-4) into Equation (3.2-3) and performing the differentiation leads to the expression

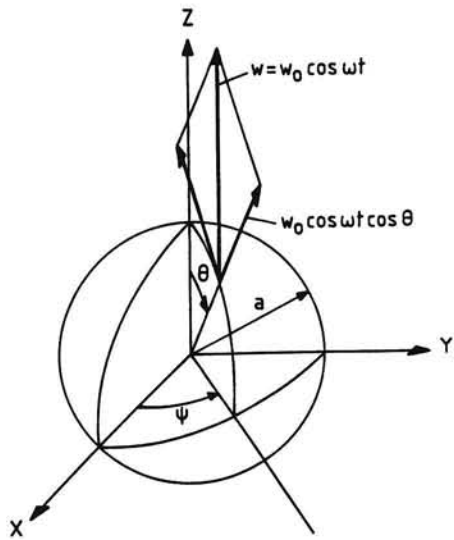


Figure 3.2-1. Oscillating sphere

$$\phi_d(\theta, r, t) = -\cos \theta \frac{i}{\rho_\infty \omega} \frac{A}{r^2} \left[1 + i \frac{\omega r}{c} \right] e^{i\omega(t - r/c)} . \quad (3.2-4)$$

The normal velocity boundary condition at $r = a$ is given by

$$v_{r=a} = \left[\frac{\partial \phi_d}{\partial r} \right]_{r=a} = w_0 e^{i\omega t} \cos \theta . \quad (3.2-5)$$

Then, from Equations (3.2-4) and (3.2-5), we readily find the velocity potential as

$$\phi_d(\theta, r, t) = - \frac{\cos \theta a^3 w_0 (1 + i \frac{\omega r}{c})}{2r^2 \left[1 + i \frac{\omega a}{c} - \frac{1}{2} \left(\frac{\omega a}{c} \right)^2 \right]} e^{i\omega(t - \frac{r-a}{c})} . \quad (3.2-6)$$

We proceed here with considering only the interesting case of a point-dipole source. Then $\omega a / c \ll 1$, and Equation (3.2-6) reduces to

$$\phi_d(\theta, r, t) = -\cos \theta \frac{a^3 w_0}{2r^2} (1 + i \frac{\omega r}{c}) e^{i\omega(t - \frac{r-a}{c})} . \quad (3.2-7)$$

For positions $r \gg a$, we may write

$$\phi_d(\theta, r, t) = -\cos\theta \frac{a^3 w_0}{2r^2} (1 + i \frac{\omega r}{c}) e^{i\omega(t-r/c)} . \quad (3.2-8)$$

The sound pressure and the radial particle velocity, from Equation (3.2-8), are

$$p'(\theta, r, t) = -\rho_\infty \frac{\partial \phi_d}{\partial t} = \rho_\infty \cos\theta \frac{a^3 w_0}{2r^2} (1 + i \frac{\omega r}{c}) e^{i\omega(t-r/c)} i\omega . \quad (3.2-9)$$

$$v_r(\theta, r, t) = \frac{\partial \phi_d}{\partial r} = \cos\theta \frac{a^3 w_0}{2r^2} \left[\frac{2}{r} + i \frac{2\omega}{c} - \frac{\omega^2 r}{c^2} \right] e^{i\omega(t-r/c)} . \quad (3.2-10)$$

The latter equation may be approximated by

$$v_r(\theta, r, t) = -\cos\theta \frac{a^3 w_0}{2r^2} \left[\frac{\omega^2 r}{c^2} - i \frac{2\omega}{c} \right] e^{i\omega(t-r/c)} . \quad (3.2-11)$$

Equations (3.2-9) to (3.2-11) show that the sound pressure and the radial particle velocity have a $\cos\theta$ dependence, and that the perturbations are maximum along the Z-axis ($\cos\theta = 1$) and zero at 90° to the Z-axis.

By expressing Equations (3.2-9) and (3.2-11) in trigonometric form, we obtain

$$p'(\theta, r, t) = -\rho_\infty \cos\theta \frac{a^3 w_0}{2r^2} \omega \left[\frac{\omega r}{c} \cos\omega(t-r/c) + \sin\omega(t-r/c) \right] \quad (3.2-12)$$

and

$$v_r(\theta, r, t) = -\cos\theta \frac{a^3 w_0}{2r^2} \frac{2\omega}{c} \left[\frac{\omega r}{2c} \cos\omega(t-r/c) + \sin\omega(t-r/c) \right] . \quad (3.2-13)$$

The sound intensity in radial direction, from Equations (3.2-12) and (3.2-13), is

$$I(\theta, r) = \frac{1}{T} \int_0^T p'(\theta, r, t) v_r(\theta, r, t) dt = \rho_\infty \cos^2\theta \frac{a^6 w_0^2 \omega}{4r^4 c} \left[\frac{\omega^2 r^2}{2c^2} + 1 \right] . \quad (3.2-14)$$

The far-field form of this expression becomes $\left(\frac{\omega^2 r^2}{2c^2} \gg 1 \right)$:

$$I(\theta, r) = \rho_\infty \cos^2 \theta \frac{1}{8} \frac{a^6 w_0^2 \omega^3}{r^2 c^3} . \quad (3.2-15)$$

This result indicates that the oscillating sphere is strongly directional since the intensity pattern is a figure of eight determined by the $\cos^2 \theta$ factor (Figure 3.2-2).

The sound power follows from integrating the intensity over a spherical surface of radius r , centered at the origin. This integral is

$$W = \int_0^\pi I(\theta, r) 2\pi r \sin \theta r d\theta = \frac{1}{6} \pi \rho_\infty \frac{a^6 w_0^2 \omega^3}{c^3} . \quad (3.2-16)$$

From this expression we see that sound power generated by the dipole rapidly goes down as the frequency is lowered.

In the preceding section we saw that the monopole source corresponds to the introduction of additional mass into the source region, which led to the inhomogeneous wave equation (Equations (3.1-37) and (3.1-38)). In the case of a dipole, however, the air is accelerated back and forth by the oscillations of the forward and rearward hemispheres, leading to a fluctuating force. Then, from Equation (2.5-7), we get at $r = 0$:

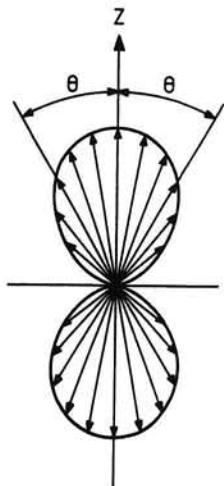


Figure 3.2-2. Sound intensity pattern

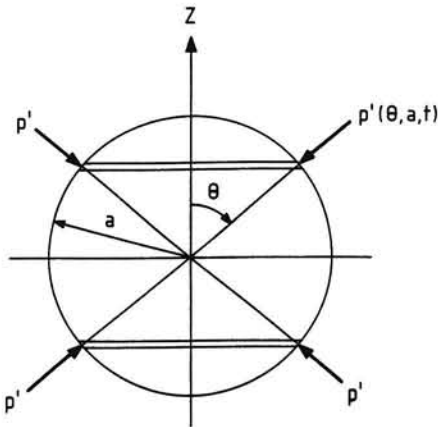


Figure 3.2-3. The pressure on the surface of the sphere

$$\nabla^2 p' - \frac{1}{c^2} \frac{\partial^2 p'}{\partial t^2} = \operatorname{div} f , \quad (3.2-17)$$

where f is the external force applied to unit volume.

The periodic force that the oscillating sphere exerts on the surrounding air is (Figure 3.2-3)

$$F_p(t) = - \int_0^\pi p'(\theta, a, t) \cos \theta 2\pi a \sin \theta a d\theta . \quad (3.2-18)$$

The pressure disturbances on the surface of the sphere, $p'(\theta, a, t)$, follow from the relationship $p' = -\rho_\infty \partial \phi_d / \partial t$, evaluated at $r = a$, where $\phi_d(\theta, r, t)$ is given by Equation (3.2-7).

Thus,

$$F_p(t) = - \int_0^\pi \rho_\infty \pi w_0 a^3 \left(1 + i \frac{\omega a}{c}\right) i \omega e^{i \omega t} \cos^2 \theta \sin \theta d\theta . \quad (3.2-19)$$

Since we are considering a compact source ($\omega a/c \ll 1$), the force $F_p(t)$ is

$$\begin{aligned} F_p(t) &= -\rho_\infty \pi w_0 a^3 i \omega e^{i \omega t} \int_0^\pi \cos^2 \theta \sin \theta d\theta \\ &= \frac{2}{3} \rho_\infty \pi w_0 a^3 i \omega e^{i \omega t} . \end{aligned} \quad (3.2-20)$$

In addition to the above pressure force, a second force is needed to overcome the inertia of the mass of air displaced by the sphere. The latter force can be obtained by applying Newton's second law of motion,

$$F_m(t) = \rho_\infty \frac{4}{3} \pi a^3 \frac{\partial w(t)}{\partial t} = \rho_\infty \frac{4}{3} \pi a^3 w_0 i \omega e^{i \omega t} . \quad (3.2-21)$$

From Equations (3.2-20) and (3.2-21), the total force required to oscillate the dipole is

$$F(t) = \rho_\infty 2 \pi a^3 w_0 i \omega e^{i \omega t} . \quad (3.2-22)$$

It is convenient to relate the sound pressure to the force $F(t)$. To this end, we transform Equation (3.2-9) to the form

$$p'(\theta, r, t) = - \frac{\partial}{\partial r} \left[\rho_\infty \cos \theta \frac{a^3 w_0}{2r} i \omega e^{i \omega(t-r/c)} \right] \quad (3.2-23)$$

with the operator $\frac{\partial}{\partial z}$ inserted for $\cos \theta \frac{\partial}{\partial r}$ (Figure 3.2-1),

$$p'(\theta, r, t) = -\frac{\partial}{\partial z} \left[\rho_\infty \frac{2\pi a^3 w_0 i\omega e^{i\omega(t-r/c)}}{4\pi r} \right]. \quad (3.2-24)$$

From Equations (3.2-22) and (3.2-24) we find the following relationship between the sound pressure produced by a point-dipole source and the total force $F(t)$:

$$p'(\theta, r, t) = -\frac{\partial}{\partial z} \left[\frac{F_0 e^{i\omega(t-r/c)}}{4\pi r} \right], \quad (3.2-25)$$

where F_0 is the amplitude of total force.

Equation (3.2-25) demonstrates that the point-dipole indeed represents a fluctuating force in a given direction. It also describes the sound field in the case that the force is given as a function of time.

3.3 THE QUADRUPOLE AND THE AERODYNAMIC JET NOISE

The exhaust noise behind a jet-engine is generated by the turbulence in the mixing region of the high-velocity jet and the surrounding atmosphere (Figure 3.3-1a).

It has been shown by Lighthill (Reference 11) that for subsonic jets the aerodynamic noise from the turbulence in the exhaust gas stream can be viewed as that due to a distribution of dipoles.

In the following an explanation of the far-field noise radiation characteristics by a jet will be given by considering the turbulence as obtained from a flow

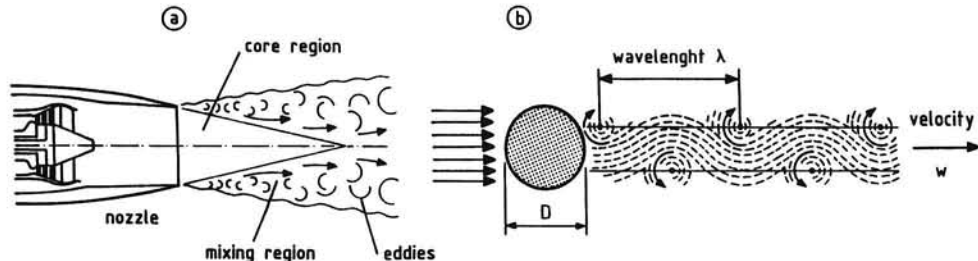


Figure 3.3-1. Jet noise

past a circular cylinder placed at 90° to the direction of the jet. Then a sequence of vortices is developed, which are shed off the cylinder at regular time intervals, alternately from the upper side and from the bottom of the cylinder (Figure 3.3-1b). The procession of alternate vortices imposes periodic cross-forces, which are acoustically equivalent to a regular succession of dipole sources.

We remark that the occurrence of an oscillatory wake is primarily determined by the Reynolds number $R_e = \rho_\infty w D / \mu$, where w is the flow velocity, D is the diameter of the cylinder, and μ is the coefficient of dynamic viscosity. The latter quantity is a state variable, which governs the shear stresses in the wake, and is approximately proportional to $\sqrt{T_\infty}$ over the range of temperatures of the atmosphere (Reference 7).

This periodicity in the flow behind the cylinder is known as the *Kármán vortex street*, named after the Hungarian-born American scientist Theodore von Kármán (1881-1963). The associated momentum transfer to the flow is normal to the direction of the stream, where successive fluctuating motions are out of phase. The scale of the turbulent fluctuations, i.e., the longitudinal spacing λ of the vortex system, is directly related to the diameter D of the cylinder.

On the basis of this model, we may study the sound field as produced by a series of canceling dipoles spaced along the extended engine-centerline. Each pair of dipoles forming a lateral quadrupole, is separated by a spacing $\lambda/2$.

As indicated in Figure 3.3-2, we begin by analyzing a quadrupole of which the dipoles are located at the origin of the axis system ($x = 0, y = 0, z = 0$) and at the point ($x = 0.5\lambda, y = 0, z = 0$).

The sound pressure at a point $P(x, y, z)$ produced by this quadrupole is the sum of the contributions from the two dipoles. Thus

$$p'(x, y, z, t) = p'_1(x, y, z, t) + p'_2(x, y, z, t) . \quad (3.3-1)$$

Using the first two terms of the Taylor expansion, we can express the second term of the right-hand side of Equation (3.3-1) as

$$p'_2(x, y, z, t) = p'_2(x + \frac{\lambda}{2}, y, z, t) - \frac{\lambda}{2} \frac{\partial p'_2}{\partial x} . \quad (3.3-2)$$

The pressure distribution at the point $P'(x + \lambda/2, y, z)$, produced by the dipole at the point $x = \lambda/2, y = 0, z = 0$, is

$$p'_2(x + \frac{\lambda}{2}, y, z, t) = -p'_1(x, y, z, t) . \quad (3.3-3)$$

Combination of Equations (3.3-2) and (3.3-3) and noting that

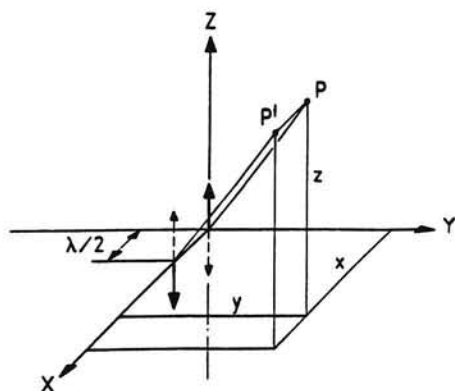


Figure 3.3-2. Location of quadrupole source

$$\frac{\partial p_2'}{\partial x} = -\frac{\partial p_1'}{\partial x}, \text{ furnishes}$$

$$p_2'(x, y, z, t) = -\left[p_1'(x, y, z, t) - \frac{\lambda}{2} \frac{\partial p_1'}{\partial x} \right]. \quad (3.3-4)$$

Substituting this equation into Equation (3.3-1) then yields

$$p'(x, y, z, t) = \frac{\lambda}{2} \frac{\partial p_1'}{\partial x}. \quad (3.3-5)$$

The derivation of Equation (3.3-5) demonstrates that the quadrupole produces a sound because the sound waves emanating from the two dipoles cover different distances to the receiver through which the two signals of opposite strengths do not completely cancel out. In other words, the dipole pairs only generate sound due to the fact that the signals from the individual dipoles do not arrive simultaneously at the observation point. Also of note here is that the occurring sound pressure will depend on frequency.

In Section 3.2, we saw that the velocity potential of the dipole is the partial derivative of the monopole velocity potential with respect to the coordinate in the direction of the dipole axis.

Similarly, it is also apparent from Equations (3.3-5) and (3.2-22) that the sound pressure generated by our quadrupole is the partial derivative with respect to the z-coordinate of the dipole sound pressure expression, so that

$$p'(x, y, z, t) = -\frac{\lambda}{2} \frac{\partial^2}{\partial x \partial z} \left[\frac{\partial}{\partial y} \frac{F_0 e^{i\omega(t-r/c)}}{4\pi r} \right]. \quad (3.3-6)$$

Using the relationship $\partial/\partial z = \cos\theta\partial/\partial r$ and the approximation that $1/r^2 \ll 1/r$, we can transform Equation (3.3-6) into the form

$$\begin{aligned} p'(x, y, z, t) &= -\frac{\lambda}{2} \frac{F_0}{4\pi} \frac{\partial}{\partial x} \left[\cos\theta \frac{\partial}{\partial r} e^{i\omega(t-r/c)} \right] \\ &= \frac{i\omega}{c} \frac{\lambda}{2} \frac{F_0}{4\pi} \frac{\partial}{\partial x} \left[\frac{\cos\theta e^{i\omega(t-r/c)}}{r} \right]. \end{aligned} \quad (3.3-7)$$

This equation can be further developed by recognizing that the fluctuating forces only act in directions normal to the jet velocity. Therefore, as depicted in Figure 3.3-3, the operator $\partial/\partial x$ in Equation (3.3-7) can be replaced by

$$\frac{\partial}{\partial x} = \frac{\partial}{\partial r} \sin\theta .$$

Applying this operator to Equation (3.3-7) and using again $1/r^2 \ll 1/r$ leads to

$$\begin{aligned} p'(x, \theta, t) &= \frac{i\omega}{c} \frac{\lambda}{2} \frac{F_0}{4\pi} \sin\theta \cos\theta \frac{1}{r} \left(-\frac{i\omega}{c} \right) e^{i\omega(t-r/c)} \\ &= \frac{\omega^2}{c^2} \frac{\lambda}{2} \frac{F_0}{4\pi} \frac{1}{2} \sin 2\theta \frac{1}{r} e^{i\omega(t-r/c)} . \end{aligned} \quad (3.3-8)$$

From this equation, the effective pressure produced by a source element of the jet is

$$p_e(r, \theta) = \frac{\omega^2}{c^2} \frac{\lambda}{2} \frac{F_0}{4\pi} \sin 2\theta \frac{1}{2r\sqrt{2}} . \quad (3.3-9)$$

The resulting effective pressure from the entire turbulent flow may be expressed as

$$p_e(r, \theta) \propto \frac{\omega^2}{c^2} \frac{\lambda}{r} F_0 \sin 2\theta . \quad (3.3-10)$$

As would be expected, the effective pressure dies off as $1/r$. Further we see that the sound field has a pronounced directionality, embodied in $\sin 2\theta$. Thus the effective pressure is largest in directions 45 degrees from the direction of the jet (Figure 3.3-4).

Equation (3.3-10) may also be used to indicate how the effective pressure is related to the characteristics of the jet.

According to the formalism of dimensional analysis, the aerodynamic force

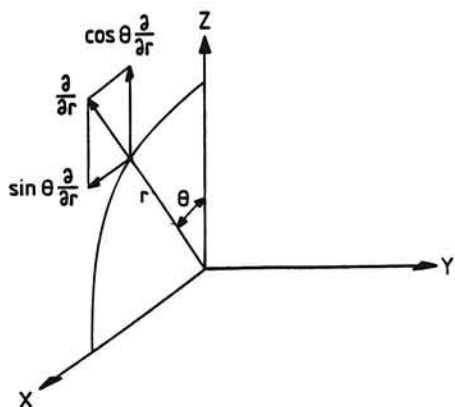
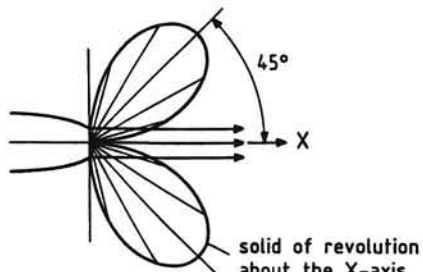
Figure 3.3-3. The operator $\partial/\partial x$ 

Figure 3.3-4. Directional characteristics of the noise from a subsonic jet

F_0 in Equation (3.3-10) will be proportional to $\rho_\infty w^2 \lambda^2$, where the wavelength λ is considered as a characteristic dimension. Thus we obtain

$$p_e(r, \theta) \propto \rho_\infty \frac{\omega^2}{c^2} \frac{\lambda}{r} w^2 \lambda^2 \sin 2\theta . \quad (3.3-11)$$

Writing: $w/\omega\lambda = \alpha$, and inserting this parameter into Equation (3.3-11) gives

$$p_e(r, \theta) \propto \rho_\infty \alpha^{-2} \frac{\lambda}{r} \frac{w^4}{c^2} \sin 2\theta . \quad (3.3-12)$$

The quantity α is directly related to the so-called *Strouhal number*, S , which defines the connection between the flow velocity w , frequency of the phenomenon, and the diameter D of the cylinder,

$$S = \frac{w}{\omega D} .$$

The Strouhal number occurs in several practical problems in aerodynamics. In the case of the Kármán vortex street in Figure 3.3-1b, the Strouhal number has approximately a constant value over a wide range of Reynolds numbers (Reference 10). This means that also α is a constant so that Equation (3.3-12) reduces to

$$p_e(r, \theta) \propto \rho_\infty \frac{\lambda}{r} \frac{w^4}{c^2} \sin 2\theta . \quad (3.3-13)$$

The sound intensity, from Equations (2.8-25) and (3.3-13), is

$$I(r, \theta) = \frac{[p_e(r, \theta)]^2}{\rho_\infty c} \propto \rho_\infty \frac{\lambda^2}{r^2} \frac{w^8}{c^5} (\sin 2\theta)^2 . \quad (3.3-14)$$

The acoustic power follows by integration of the sound intensity over the surface of a hemisphere of radius r . This integral is

$$W = \int_0^\pi I(\theta, r) \pi r \sin \theta r d\theta . \quad (3.3-15)$$

Insertion of Equation (3.3-14) into Equation (3.3-15) and performing the integration readily yields

$$W \propto \rho_\infty \lambda^2 \frac{w^8}{c^5} . \quad (3.3-16)$$

It should be appreciated that in deriving Equation (3.3-16) thermal effects are neglected. Furthermore, no allowance is made for the increase in sound power due to shock waves, which are formed in the flow when the jet velocity approaches the speed of sound. Therefore, Equation (3.3-16) only qualifies the sound power produced by a cold and low-speed jet.

Nevertheless, Equation (3.3-16) demonstrates the importance of the characteristic dimension λ of the turbulence in the flow. Undoubtedly, the most impressive aspect of this equation is the fact that the sound production rises in proportion to w^8 .

This eight power law was first derived by Lighthill in Reference 11, where he considers a fluctuating flow covering a small region within an unbounded uniform medium at rest. His results are based on a survey of the nonlinear and viscous terms in the equations of mass and momentum conservation, and show that the sound is generated under the action of dipole pairs of opposite strengths, i.e. quadrupoles.

Some explanation of Lighthill's approach might be possible by considering the more exact Equations (2.2-2) and (2.3-4). The middle term of the latter, ignored in linearized theory, produces a sound field under the action of stresses of strength $\rho v_i v_j$ per unit volume. After some manipulation we can make inside the source region the equations read (Reference 15):

$$c^2 \frac{\partial^2 p'}{\partial x_i^2} - \frac{\partial^2 p'}{\partial t^2} = - \frac{\partial^2}{\partial x_i \partial x_j} (\rho v_i v_j) . \quad (3.3-17)$$

The double derivative in the term on the right-hand side of this inhomogeneous wave equation reveals that the sound field of turbulence is that of a distribution of quadrupoles.

4 PROPAGATION OF SOUND IN THE ATMOSPHERE

4.1 SPREADING

The sound power emitted by a source spreads out over an increasingly larger surface at increasing distances from the source. Therefore, the sound intensity (the sound power per unit area) falls off when the distance from the source increases.

Considering a nondirectional point source in a free field, we have uniform spherical spreading. Then the sound intensity from a source that is emitting a given sound power diminishes as the square of the distance from the source. In formula (cf. Equation (1.7-1))

$$4\pi r^2 I(r) = \text{constant} . \quad (4.1-1)$$

Note from this equation that the sound intensity decreases to one-quarter for each doubling of the distance r .

Recall from Equations (1.2-4) and (1.2-6) that in the case of simple harmonic motion of a nondirectional point source the effective sound pressure varies inversely as distance,

$$p_e(r) = \left[\frac{1}{T} \int_0^T \left[\frac{A}{r} e^{i\omega(t-r/c)} \right]^2 dt \right]^{1/2} = \frac{A}{r\sqrt{2}} , \quad (4.1-2)$$

where A/r is the local sound pressure amplitude.

The sound pressure level in dB, corresponding to an effective sound pressure $p_e(r)$ is defined by

$$\text{SPL}(r) = 10 \log \frac{p_e^2(r)}{p_{e_0}^2} = 20 \log \frac{p_e(r)}{p_{e_0}} , \quad (4.1-3)$$

where $p_{e_0} = 2 \times 10^{-5}$ N/m² is the reference pressure.

From Equations (4.1-2) and (4.1-3) we see that the difference between the values of the sound pressure level at distances r_1 and r_2 is

$$\text{SPL}(r_1) - \text{SPL}(r_2) = 10 \log \frac{r_2^2}{r_1^2} = 20 \log \frac{r_2}{r_1} . \quad (4.1-4)$$

The relationship (4.1-4) is called the *inverse-distance law* or the *inverse-*

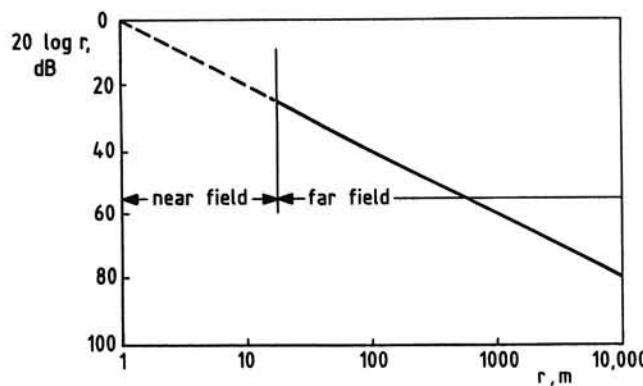


Figure 4.1-1. The inverse square law

square law. It says that the reduction in sound pressure level attributable to spherical divergence is equal to 6 dB for each doubling of distance.

Figure 4.1-1 shows a plot of the sound pressure level versus distance, using a reference distance of $r_1 = 1$ m. Then Equation (4.1-4) can be written as

$$\text{SPL}(r_1) - \text{SPL}(r) = 20 \log r , \quad (4.1-5)$$

where the numerical value of the distance r is in meters.

In practice, the sound source will have finite dimensions. In consequence, as stated already in Section 1.5, the inverse square law will only be true for distances which are large compared with the size of the source, i.e., in the *far field*. There the source can be treated as a *point source*, even though its dimensions are relatively large. Under these conditions the above-mentioned 6 dB variation for a doubling of distance may be used to verify the actuality of the acoustic far-field condition.

The dashed part of the plot in Figure 4.1-1 indicates that for sources of finite size there is a *near field* where the variation of SPL with distance does not obey the inverse square law. In this area the SPL may vary seriously with small changes in distance.

Equation (4.1-1) indicates that for spherical spreading from a point sound source the sound power is numerically equal to the sound intensity when the surface of the sphere surrounding the source is 1 m^2 . The corresponding radius of the sphere follows from

$$4\pi r^2 = 1 \text{ m}^2 \quad \text{or} \quad r = \sqrt{\frac{1}{4\pi}} = 0.282 \text{ m} .$$

Hence, the sound intensity level at a distance of 1 meter from the source is

given by

$$\text{SIL}(r_1) = \text{PWL} - 20 \log \frac{1}{0.282} = \text{PWL} - 11 \text{ , dB.} \quad (4.1-6)$$

When the sound source is located at ground level, the sound power is distributed over the surface of a hemisphere. Then, instead of Equation (4.1-6), we have

$$\text{SIL}(r_1) = \text{PWL} - 8 \text{ , dB.} \quad (4.1-7)$$

Combination of Equation (4.1-6) and the previous Equation (1.8-5) gives

$$\text{SPL}(r_1) = \text{PWL} - 10.8 + 10 \log \frac{\rho_\infty c}{(\rho_\infty c)_0} . \quad (4.1-8)$$

Introducing the latter equality into Equation (4.1-5) yields

$$\text{SPL}(r) = \text{PWL} - 10.8 + 10 \log \frac{\rho_\infty c}{(\rho_\infty c)_0} - 20 \log r . \quad (4.1-9)$$

In order to account for the directionality of the source we may use the *directivity index*, which quantity has been discussed previously in Section 1.10. Then, by combining Equation (4.1-9) and Equation (1.10-1), we obtain

$$\text{SPL}(r, \theta) = \text{PWL} - 10.8 + 10 \log \frac{\rho_\infty c}{(\rho_\infty c)_0} - 20 \log r + \text{DI}(\theta) . \quad (4.1-10)$$

Emphasis is made again that this equation only holds for sound spreading out in a sphere.

4.2 ATMOSPHERIC ATTENUATION OF SOUND

Atmospheric attenuation is the process by which sound energy is absorbed in traveling through the atmosphere. This form of attenuation occurs in addition to spreading and is due primarily to the fact that atmospheric air, like all fluids, exhibits some degree of internal friction. The extra loss caused by atmospheric absorption phenomena learns us that it is not always true to say that viscosity is unimportant in acoustics.

The rate at which sound energy is absorbed during passing through the air is expressed by the *sound attenuation coefficient*, which normally is given in the units of dB per 100 m, and denoted by α . The decrease in sound pressure level due to atmospheric attenuation can thus be written as

$$\Delta \text{SPL} = \alpha \Delta r / 100 \text{ , dB .}$$

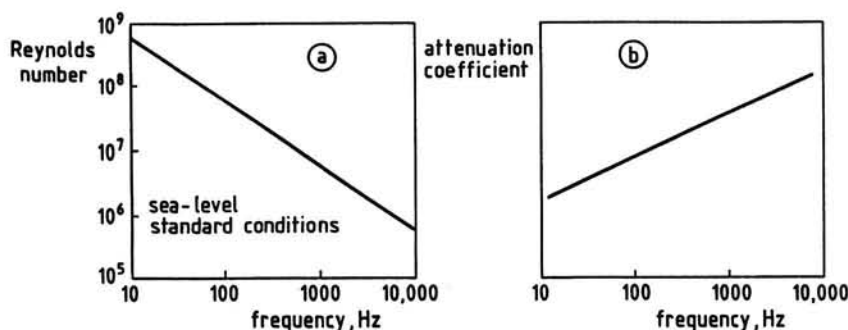


Figure 4.2-1. Effect of frequency on Reynolds number and attenuation rate

When the sound propagates in a homogeneous and quiescent atmosphere the attenuation coefficient is a function primarily of the frequency of the sound. In addition, also the prevailing air temperature and the amount of water vapor in the atmosphere affect the magnitude of the sound absorption.

The atmospheric attenuation coefficient has been found to be relatively small, except at high frequencies (Reference 17).

A qualitative impression of the effect of frequency on the attenuation coefficient may be given by considering the related *Reynolds number*, R_e , of the wave motion, i.e.,

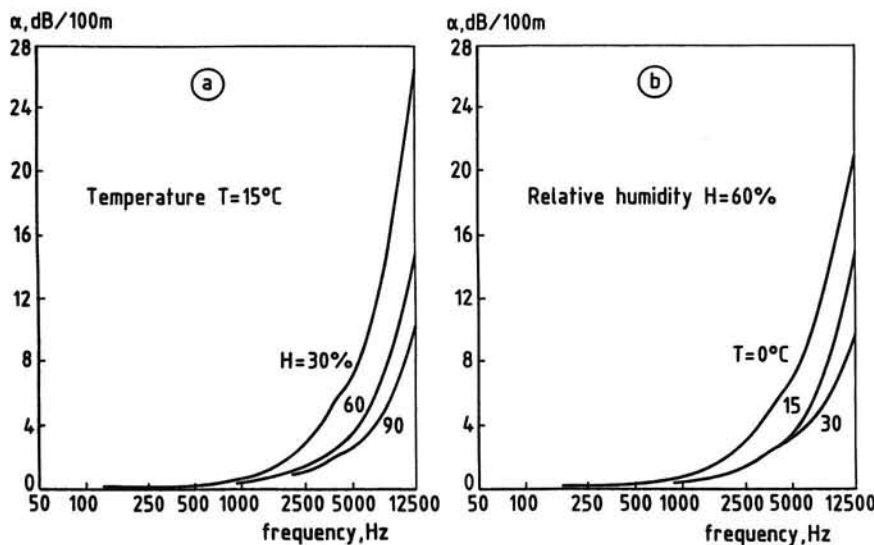


Figure 4.2-2. The attenuation coefficient (from Reference 18)

$$R_e = \frac{\rho_\infty c \lambda}{\mu} = \frac{\rho_\infty c^2}{\mu f}, \quad (4.2-1)$$

where μ is the *coefficient of dynamic viscosity*, which determines the shear stress between air layers moving adjacent to each other at different velocities. The Reynolds number indicates the relative importance of the viscous and pressure forces in the sound field; the lower the value of R_e the more relative important are the viscous effects.

Figure 4.2-1a shows the variation of the Reynolds number with frequency at sea-level standard conditions: $\rho_\infty = 1.225 \text{ kg/m}^3$, $c = 340.249 \text{ m/s}$ and $\mu = 1.7894 \times 10^{-5} \text{ kg/ms}$ (Reference 7). This graph manifests that for sound at the most important frequencies the Reynolds number is of the order 10^7 - 10^8 . Accordingly, we may expect that the effect of viscosity and so the attenuation coefficient is comparatively unimportant.

Since a lower Reynolds number is coupled with a higher sound absorption, the attenuation coefficient will have the tendency to increase with increasing sound frequency (Figure 4.2-1b).

For numerical data the reader is referred to References 18 and 78 (vol. 3), where are listed standard values of the attenuation coefficient as a function of frequency, air temperature and relative humidity.

Relative humidity is the ratio of the prevailing water vapor pressure in the air at a given temperature divided by the saturation vapor pressure at that temperature times 100 percent (Reference 7).

The curves of Figure 4.2-2a are plots of the attenuation coefficient at 15°C for three values of the relative humidity (denoted by the symbol H). Similarly, in Figure 4.2-2b are given the variations of the attenuation coefficient at 60% relative humidity for three values of the air temperature. It appears that at high frequencies the attenuation coefficient diminishes with increasing temperature and humidity.

Figure 4.2-2 also shows that below 1000 Hz the sound absorption coefficient is very small. Consequently, atmospheric attenuation will be of importance for long distance sound propagation.

According to the procedure given in Reference 18, the attenuation coefficient can be expressed as follows:

$$\alpha = 10^{[2.05 \log(f_0/1000) + 1.1394 \times 10^{-3}T - 1.916984]} + \\ + \eta(\delta) \times 10^{[\log(f_0) + 8.42994 \times 10^{-3}T - 2.755624]}, \quad (4.2-2)$$

Table 4.2-1. The factor $\eta(\delta)$

δ	η	δ	η	δ	η	δ	η
0.00	0.000	1.00	1.000	2.30	0.495	4.45	0.245
0.25	0.315	1.10	0.970	2.50	0.450	4.80	0.230
0.50	0.700	1.20	0.900	2.80	0.400	5.25	0.220
0.60	0.840	1.30	0.840	3.00	0.370	5.70	0.210
0.70	0.930	1.50	0.750	3.30	0.330	6.05	0.205
0.80	0.975	1.70	0.670	3.60	0.300	6.50	0.200
0.90	0.996	2.00	0.570	4.15	0.260	7.00	0.200

where

$$\delta = \sqrt{\frac{1010}{f_0}} 10 [\log H - 1.328924 + 3.179768 \times 10^{-2} T] \times \\ \times 10 [-2.173716 \times 10^{-4} T^2 + 1.7496 \times 10^{-6} T^3] ; \quad (4.2-3)$$

- α is the attenuation coefficient in dB/100m for use at the center frequencies of the tertbands (see Chapter 7);
- T is the temperature in °C;
- H is the relative humidity in percent;
- $\eta(\delta)$ is given by Table 4.2-1;
- f_0 is given by Table 4.2-2.

Table 4.2-2. The frequency f_0

tert- band center frequency	f_0 (Hz)	tert- band center frequency	f_0 (Hz)	tert- band center frequency	f_0 (Hz)
50	50	315	315	2000	2000
63	63	400	400	2500	2500
80	80	500	500	3150	3150
100	100	630	630	4000	4000
125	125	800	800	5000	4500
160	160	1000	1000	6300	5600
200	200	1250	1250	8000	7100
250	250	1600	1600	10000	9000

Table 4.2-3. Rate of absorption at 500 Hz

relative humidity %	sound absorption coefficient α in dB/100m									
	temperature °C									
-10	-5	0	5	10	15	20	25	30	35	40
10	0.3	0.5	0.8	1.0	0.9	0.7	0.6	0.5	0.4	0.4
20	0.6	0.8	0.7	0.6	0.5	0.4	0.3	0.3	0.3	0.4
30	0.7	0.6	0.5	0.4	0.3	0.3	0.3	0.3	0.3	0.4
40	0.6	0.5	0.4	0.3	0.2	0.2	0.3	0.3	0.3	0.4
50	0.5	0.4	0.3	0.2	0.2	0.2	0.3	0.3	0.3	0.4
60	0.5	0.3	0.2	0.2	0.2	0.2	0.3	0.3	0.3	0.4
70	0.4	0.3	0.2	0.2	0.2	0.2	0.3	0.3	0.4	0.4
80	0.3	0.2	0.2	0.2	0.2	0.2	0.3	0.3	0.3	0.4
90	0.3	0.2	0.2	0.2	0.2	0.2	0.3	0.3	0.3	0.4
100	0.3	0.2	0.2	0.2	0.2	0.2	0.3	0.3	0.3	0.4

In Reference 18 it is suggested that for airplane noise, the rate of absorption may be represented by its values at a frequency of 500 Hz. Then, from Equations (4.2-2) and (4.2-3), we have

$$\alpha = 10^{(1.1394 \times 10^{-3}T - 2.534095)} + \eta(\delta) 10^{(8.42994 \times 10^{-3}T - 5.6654 \times 10^{-2})}, \quad (4.2-4)$$

where

$$\delta = 1.421267 \times 10^{(\log H - 1.328924 + 3.179768 \times 10^{-2}T)} \times \\ \times 10^{(-2.173716 \times 10^{-4}T^2 + 1.7496 \times 10^{-6}T^3)}. \quad (4.2-5)$$

Numerical values of α determined from the Equations (4.2-4) and (4.2-5) are listed in Table 4.2-3.

4.3 TRANSMISSION OF SOUND FROM ONE AIR LAYER TO ANOTHER

When a sound ray arrives at a plane interface between two air layers with different characteristic resistances, part of the sound is reflected from the boundary and part is transmitted through the boundary with a change in direction of propagation. Incident, reflected and transmitted rays lie all in the same plane normal to the interface plane.

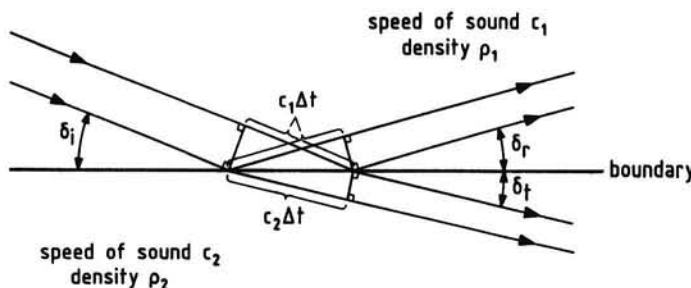


Figure 4.3-1. Refraction at an interface

As shown in Figure 4.3-1, in this section we consider the situation that an infinitesimal segment of a wavefront incident on a horizontal boundary. The path traveled by this wavefront element is the *ray path*. The direction of propagation of the incident sound makes an angle δ_i with the boundary. The reflected and transmitted sound rays are inclined by an angle δ_r and δ_t , respectively. The characteristic resistances of the two media are $\rho_1 c_1$ and $\rho_2 c_2$.

It is convenient to locate the *X*- and *Y*-axes of a rectilinear axis system in the plane of sound propagation, where the *Y*-axis lies along the interface. Then, as depicted in Figure 4.3-2, the distance in the direction of propagation is given by

$$r_i = x \sin \delta + y \cos \delta .$$

Similarly, the distance along the reflected path is given by

$$r_r = -x \sin \delta + y \cos \delta .$$

Using these relations, the three sound pressures in Figure 4.3-1 can be expressed as

$$p'_i = A e^{i\omega[t - (x \sin \delta_i)/c_1 - (y \cos \delta_i)/c_1]} \quad (4.3-1)$$

$$p'_r = B e^{i\omega[t - (x \sin \delta_r)/c_2 - (y \cos \delta_r)/c_2]} \quad (4.3-2)$$

$$p'_t = C e^{i\omega[t + (x \sin \delta_t)/c_1 - (y \cos \delta_t)/c_1]} . \quad (4.3-3)$$

The frequencies of the waves are equal, but the wavelengths in the two air layers are diverse.

The wavelengths of the incident and reflected sounds are the same

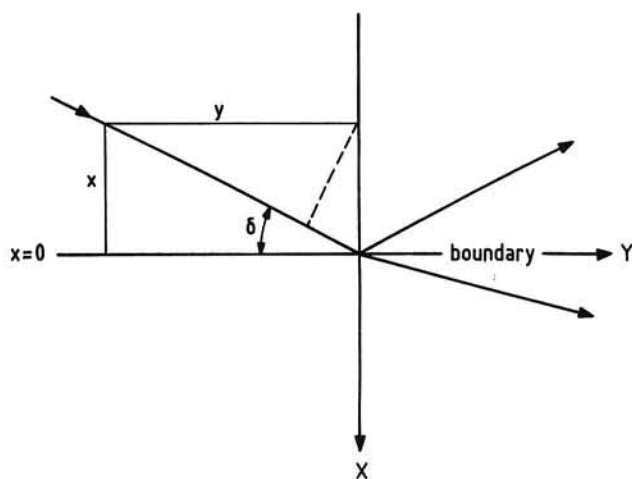


Figure 4.3-2. The axis system

$$\lambda_i = \lambda_r = \frac{c_1}{f} . \quad (4.3-4)$$

The wavelength of the transmitted sound is

$$\lambda_t = \frac{c_2}{f} . \quad (4.3-5)$$

Their relationship is evidently

$$\lambda_t = \lambda_i \frac{c_2}{c_1} . \quad (4.3-6)$$

For continuity across the boundary the intercepts of the wavefronts of the three waves on the dividing plane must be the same. From Figure 4.3-1 we see

$$c_1 \Delta t \sec \delta_i = c_1 \Delta t \sec \delta_r = c_2 \Delta t \sec \delta_t$$

or

$$\lambda_i \sec \delta_i = \lambda_r \sec \delta_r = \lambda_t \sec \delta_t . \quad (4.3-7)$$

Clearly, the angle of incidence δ_i equals the angle of reflection δ_r , and

$$\frac{c_1}{\cos \delta_i} = \frac{c_2}{\cos \delta_t} = \text{constant.} \quad (4.3-8)$$

This equation is known as *Snell's law of refraction*.

The normal components of particle velocity on either side of the boundary must also be identical, for continuity. This requirement may be written as follows:

$$(u_i)_n + (u_r)_n = (u_t)_n .$$

Inserting the relationships $u_i = p_i'/\rho_1 c_1$, $u_r = -p_r'/\rho_1 c_1$ and $u_t = p_t'/\rho_2 c_2$, and using Equations (4.3-1) to (4.3-3), we find

$$\frac{A}{\rho_1 c_1} \sin \delta_i - \frac{C}{\rho_1 c_1} \sin \delta_i = \frac{B}{\rho_2 c_2} \sin \delta_t . \quad (4.3-9)$$

At the interface ($x = 0$) also the sound pressure in the two air layers must be the same, i.e.,

$$p_i' + p_r' = p_t' \quad \text{or}$$

$$A + C = B . \quad (4.3-10)$$

From Equations (4.3-9) and (4.3-10) we obtain

$$\frac{B}{A} = \frac{2\rho_2 c_2 \sin \delta_i}{\rho_2 c_2 \sin \delta_i + \rho_1 c_1 \sin \delta_t} \quad \text{and} \quad (4.3-11)$$

$$\frac{C}{A} = \frac{\rho_2 c_2 \sin \delta_i - \rho_1 c_1 \sin \delta_t}{\rho_2 c_2 \sin \delta_i + \rho_1 c_1 \sin \delta_t} . \quad (4.3-12)$$

The ratio B/A in Equation (4.3-11) is called the *transmission factor*. Similarly, the ratio C/A is termed the *reflection factor*. Notice that both quantities are dependent on the direction of the initial sound wave relative to the interface.

Evidently, when $\rho_2 c_2 \sin \delta_i = \rho_1 c_1 \sin \delta_t$, $B = A$ and $C = 0$. Then all the sound energy travels from the upper region into the lower region and there is no reflection.

From equation (4.3-8), the related value of δ_i for this condition is found to be

$$\delta_i = \sin^{-1} \left[\frac{(c_1/c_2)^2 - 1}{(\rho_2/\rho_1)^2 - 1} \right]^{1/2} . \quad (4.3-13)$$

For this angle to be existent ($0 < \delta_i < 180^\circ$), we have the requirement that

$$\frac{\rho_2}{\rho_1} > \frac{c_1}{c_2} > 1 \quad \text{or} \quad \frac{\rho_2}{\rho_1} < \frac{c_1}{c_2} < 1 .$$

If $c_2 > c_1$, we note from Equation (4.3-8) that $\delta_t < \delta_i$. The critical angle of

incidence $(\delta_i)_c$, corresponding to a refracted ray traveling along the boundary ($\delta_t = 0$), is given by

$$(\delta_i)_c = \cos^{-1} \left[\frac{c_1}{c_2} \right] . \quad (4.3-14)$$

For angles of incidence smaller than $(\delta_i)_c$, no transmission will take place into the lower region so that the sound ray is totally reflected at the boundary.

In the foregoing analysis we tacitly assumed that in crossing the boundary the change of phase was zero. To prove the validity of this presumption we consider a point of time such that $\omega t = \pi/2$ and $x = y = 0$. If the transmitted and reflected sounds differ in phase from the incident sound by α_t and α_r , respectively, Equations (4.3-1) to (4.3-3) furnish

$$p_i' = A e^{i\pi/2} = A \cos \pi/2 = 0 \quad (4.3-15)$$

$$p_t' = B e^{i(\pi/2 + \alpha_t)} = B \cos(\pi/2 + \alpha_t) = -B \sin \alpha_t \quad (4.3-16)$$

$$p_r' = C e^{i(\pi/2 + \alpha_r)} = C \cos(\pi/2 + \alpha_r) = -C \sin \alpha_r . \quad (4.3-17)$$

Equations (4.3-9) and (4.3-10) then become

$$\frac{C}{\rho_1 c_1} \sin \alpha_r \sin \delta_i = - \frac{B}{\rho_2 c_2} \sin \alpha_t \sin \delta_t \quad (4.3-18)$$

$$-C \sin \alpha_r = -B \sin \alpha_t . \quad (4.3-19)$$

Combination of Equations (4.3-18) and (4.3-19) gives

$$\frac{\rho_2 c_2}{\rho_1 c_1} \frac{\sin \delta_i}{\sin \delta_t} C \sin \alpha_r = -B \sin \alpha_t = -C \sin \alpha_r .$$

Obviously, this equality is only possible if $\sin \alpha_r = 0$ or $\alpha_r = 0$ and with that $\alpha_t = 0$, which is in agreement with our results that the transmission factor B/A and the reflection factor C/A are given by real numbers.

The foregoing theory is of special significance to the analysis of airplane noise since sound pressure levels measured close to the Earth's surface are strongly influenced by the presence of the ground surface itself. A detailed discussion on ground plane reflection when measuring flyover noise, however, is deferred until Chapter 8.

4.4 EFFECT OF TEMPERATURE GRADIENTS

In air the speed of sound is proportional to the square root of the absolute temperature:

$$c = \sqrt{\gamma RT} . \quad (4.4-1)$$

Due to the different propagation speeds at upper and lower parts of each wavefront, the sound rays will show a certain curvature (see Section 1.4). Returning to Snell's law, Equation (4.3-8), we see that a sound ray is bent toward the boundary in going into a layer of higher temperature and away from the boundary in going into a layer of lower temperature.

To determine the ray paths through the atmosphere, we assume that the ray is in the XZ -plane and that the air temperature is a function only of height (Figure 4.4-1). The origin of the axis-system coincides with the emission point of the source.

If the positive Z -coordinate is taken vertically downward, the vertical and horizontal components of the propagation speed are given by

$$\frac{dz}{dt} = c \sin \delta \quad (4.4-2)$$

$$\frac{dx}{dt} = c \cos \delta . \quad (4.4-3)$$

When r is the travel distance along the ray path, the radius of curvature of the sound ray, R , is given by

$$R = \frac{dr}{d\delta} , \quad \text{where} \quad (4.4-4)$$

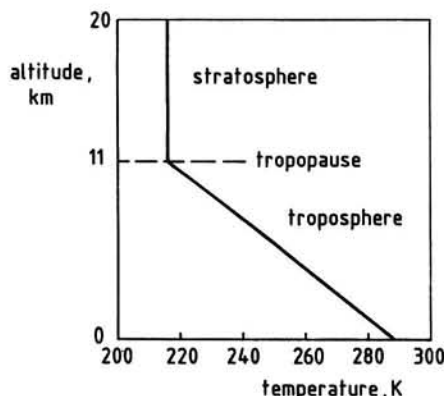
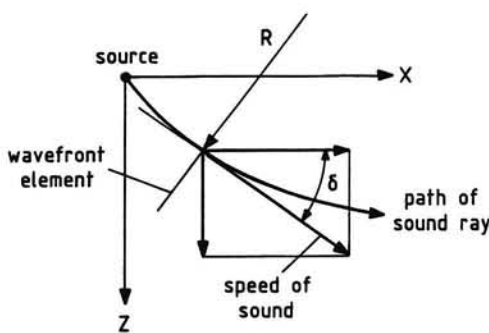


Figure 4.4-1. Curved sound ray. Figure 4.4-2. Temperature variation in I.S.A.

$$dr = \sqrt{(dx)^2 + (dz)^2} . \quad (4.4-5)$$

From Equation (4.3-8) follows

$$\frac{1}{r} = \frac{d\delta}{dR} = -\frac{\cos\delta}{c \sin\delta} \frac{dc}{dR} . \quad (4.4-6)$$

Insertion of $dz/dR = \sin\delta$ yields

$$r = -\frac{c}{\cos\delta \frac{dc}{dz}} \quad \text{or} \quad (4.4-7)$$

$$r = -\frac{c_1}{\cos\delta_1 \frac{dc}{dz}} , \quad (4.4-8)$$

where c_1 is the speed of sound at the source height and δ_1 is the emission angle of the sound ray at the source.

Equation (4.4-8) shows that the curvature of a sound ray is inversely proportional to the gradient of the speed of sound.

As shown in Figure 4.4-2, the air layer adjacent to the surface of the Earth is called the troposphere. This layer is characterized by a decreasing air temperature with height (lapse rate).

In the International Standard Atmosphere (I.S.A.) the troposphere extends to a height of $H = 11$ km. There the temperature gradient is regarded a constant, providing a linear variation of temperature with height (Reference 7).

Thus

$$T = T_0 + \lambda H , \quad (4.4-9)$$

where $\lambda = dT/dH = -0.0065$ K/m and $T_0 = 288.15$ K is the sea-level temperature.

Under these conditions it may be a sufficient approximation to consider also the gradient of the speed of sound as a constant. To calculate the value of the latter gradient we insert Equation (4.4-9) into Equation (4.4-1), giving

$$c = [\gamma R(T_0 + \lambda H)]^{1/2} = \left[c_0 \left(1 + \frac{\lambda H}{T_0} \right) \right]^{1/2} , \quad (4.4-10)$$

where c_0 is the speed of sound at sea level.

Using the first two terms of the binomial expansion we find

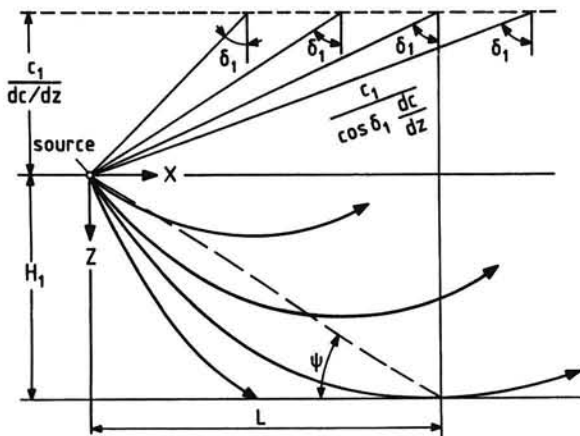


Figure 4.4-3. Refraction of sound rays in an atmosphere with uniform lapse rate

$$c = c_0 + \frac{c_0 \lambda}{2T_0} H = c_0 + \frac{dc}{dH} H , \quad (4.4-11)$$

where $\frac{dc}{dH} = \frac{\lambda c_0}{2T_0}$ is the gradient of the speed of sound.

With $T_0 = 288.15 \text{ K}$, $\lambda = -0.0065 \text{ K/m}$ and $c_0 = 340.249 \text{ m/s}$, we get

$$\frac{dc}{dH} = \frac{c_0 \lambda}{2T_0} = -0.00384 \text{ s}^{-1} . \quad (4.4-12)$$

Noting that $dc/dH = -dc/dz$, we see from Equation (4.4-8) that in the troposphere of the International Standard Atmosphere the radius of curvature of each sound ray is simply a constant and is therefore a circle.

Since $r = dR/d\delta < 0$, the rays are refracted upward symmetrical with respect to the vertical axis through the emission point of the source.

The geometrical construction of Equation (4.4-8) is outlined in Figure 4.4-3, showing that the centers of curvature of the circular paths lie at a level

$$z = -\frac{c_1}{dc/dz} ,$$

at which the speed of sound would be reduced to zero.

An important effect of upward bending of the sound rays is the creation of a shadow zone into which no direct sound can penetrate. This region is determined by the sound ray which just strikes the ground surface.

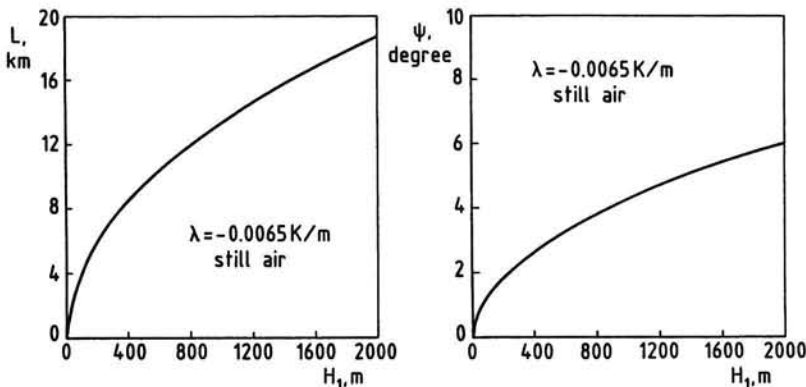


Figure 4.4-4. Location of shadow region

From a consideration of Figure 4.4-3, we find the following relationship:

$$\left[\frac{c_1}{dc/dz} + H_1 \right]^2 = L^2 + \left[\frac{c_1}{dc/dz} \right]^2 , \quad (4.4-13)$$

where L is the horizontal distance between the emission point and the point on which the limiting ray touches the ground surface.

Solving for L furnishes

$$L = \sqrt{H_1 \left[H_1 + \frac{2c_1}{dc/dz} \right]} . \quad (4.4-14)$$

Insertion of Equation (4.4-11) into (4.4-14) yields

$$L = \sqrt{H_1 \left[-\frac{4T_0}{\lambda} - H_1 \right]} . \quad (4.4-15)$$

Since $H_1 \ll -\frac{4T_0}{\lambda}$, Equation (4.4-15) can be approximated by

$$L = \sqrt{-\frac{4T_0}{\lambda} H_1} . \quad (4.4-16)$$

The associated elevation angle is given by

$$\psi = \tan^{-1} \left(\frac{H_1}{L} \right) = \tan^{-1} \sqrt{\frac{-\lambda H_1}{4T_0}} . \quad (4.4-17)$$

In Figure 4.4-4, distance L and angle ψ as a function of source height are presented, using $T_0 = 288.15$ K and $\lambda = -0.0065$ K/m.

Measurement data in Reference 19 indicate that the excess attenuation inside the shadow region increases rapidly away from the shadow boundary and tends to level off to an approximately constant value.

4.5 TEMPERATURE INVERSION EFFECTS

With a temperature inversion, i.e., an increasing air temperature with height (negative lapse rate), sound rays are bent toward the ground.

Assuming a linear variation of speed of sound with height, the sound rays travel from the source along circular arcs. Figure 4.5-1 then shows the construction of ray paths, where the sound is assumed to originate from a point source located on the ground. As derived in the preceding section, the centers of curvature of the ray paths lie on a horizontal line a distance $h_0 = 2 T_0 / \lambda$ below the ground surface.

In addition to the direct path to a receiver near the ground, there are paths involving one or more reflections of the ground at intermediary points between source and receiver. In other words, a large number of sound rays are transmitted to the receiver, the direct ray and reflected rays which take a

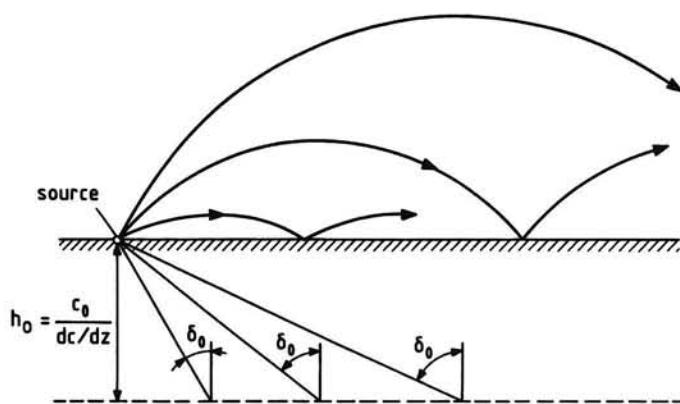


Figure 4.5-1. Propagation in an inversion and reflections at the ground

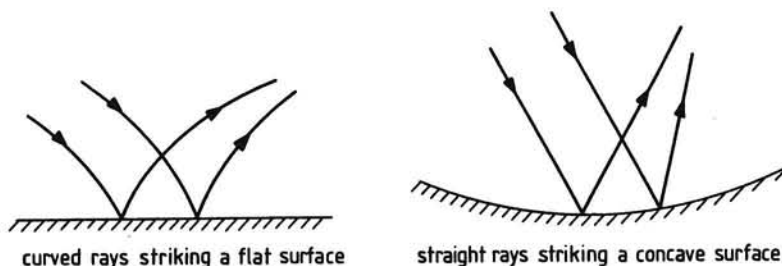


Figure 4.5-2. Convergence of sound rays on reflection from a surface

number of equal skips to the receiver. The result is that reinforcement of sound is possible so that the source may be heard more clearly at a distant position (References 20 to 23).

In addition, focusing of sound on reflection may occur. Convex sound rays are focused by reflection from a flat surface just as straight sound rays are focused by reflection from a concave surface (Figure 4.5-2). These convergence effects will be discussed in Section 4.7.

We may gain some insight into the increased number of ray paths by considering Figure 4.5-3, where, for simplicity, the source and receiver are at the same (small) height h above the ground surface. The horizontal distance x_0 between source and receiver is assumed to be large compared with the height h .

The sound ray indicated in Figure 4.5-3 first touches the ground at a horizontal distance x_s from the source and strikes the surface n times before reaching the receiver.

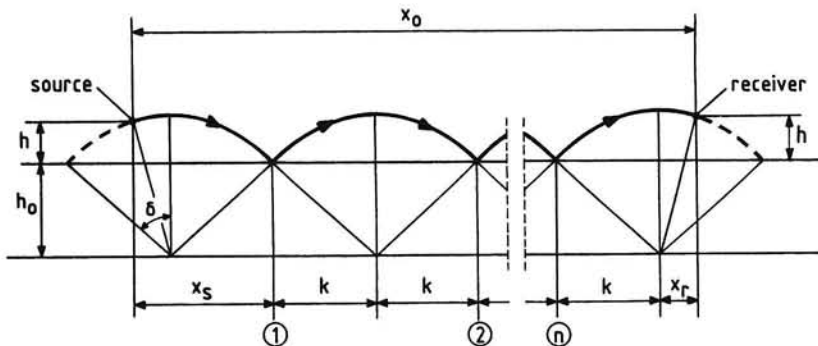


Figure 4.5-3. Ray path between source and receiver involving n ground reflections

The horizontal distance x_r can be written as

$$x_r = \left[(h_0 \tan \delta)^2 + h_0^2 - (h_0 + h)^2 \right]^{1/2} . \quad (4.5-1)$$

Denoting $h_0 \tan \delta = k$, we have

$$x_r = \left[k^2 - (2h_0h + h^2) \right]^{1/2} . \quad (4.5-2)$$

For convenience we set

$$2h_0h + h^2 = b^2 . \quad (4.5-3)$$

Now we get

$$x_r = \left[k^2 - b^2 \right]^{1/2} . \quad (4.5-4)$$

The distance x_0 can be expressed as

$$x_0 = x_s + (2n - 1)k + (k^2 - b^2)^{1/2} , \quad (4.5-5)$$

where n is the number of ground reflections.

Squaring Equation (4.5-5) furnishes

$$\begin{aligned} x_0^2 - 4nx_0k - 2x_0x_s + 2x_0k + 4n^2k^2 + \\ - 4nk^2 - 2kx_s + 4nkx_s + x_s^2 + b^2 = 0 . \end{aligned} \quad (4.5-6)$$

According to Equation (4.5-2) for the distance x_r , we can write down the following expression for the distance x_s :

$$x_s = k + \left[k^2 - (2h_0h + h^2) \right]^{1/2} . \quad (4.5-7)$$

Using Equation (4.5-3), we obtain

$$x_s = k + (k^2 - b^2)^{1/2} . \quad (4.5-8)$$

Solving for k , we have

$$k = \frac{1}{2} \left[x_s + \frac{b^2}{x_s} \right] . \quad (4.5-9)$$

Substitution of Equation (4.5-9) into Equation (4.5-6) yields the following fourth power equation in x_s :

$$\begin{aligned} n(n+1)x_s^4 - (2n+1)x_0x_s^3 + [b^2 + (2n^2 - 1)b^2 + x_0^2]x_s^2 + \\ - (2n-1)b^2x_0x_s + n(n-1)b^4 = 0 . \end{aligned} \quad (4.5-10)$$

Rearranging yields the following quartic equation:

$$[nx_s^2 - x_0x_s + nb^2] [(n+1)x_s^2 + x_0x_s + (n-1)b^2] = 0 \quad . \quad (4.5-11)$$

Equations (4.5-10) and (4.5-11) show that there are in general four possible ray paths for any given value of surface reflections (see also Reference 20). Equation (4.5-11) can be solved for x_s to give

$$x_{s_{1,2}} = \frac{x_0 \pm \sqrt{x_0^2 - 4n^2 b^2}}{2n} \quad (4.5-12)$$

$$x_{s_{3,4}} = \frac{x_0 \pm \sqrt{x_0^2 - 4(n^2 - 1)b^2}}{2(n+1)} \quad . \quad (4.5-13)$$

Remembering that $h_0 = 2T_0/\lambda$, we transform Equation (4.5-3) into

$$b^2 = 4 \frac{T_0}{\lambda} h + h^2 \quad . \quad (4.5-14)$$

Since $h \ll 4T_0/\lambda$, Equation (4.5-14) can be approximated by

$$b^2 = 4 \frac{T_0}{\lambda} h \quad . \quad (4.5-15)$$

Using this relation the solutions (4.5-12) and (4.5-13) become

$$x_{s_{1,2}} = \frac{x_0}{2n} \pm \frac{x_0}{2n} \sqrt{1 - 16 \frac{n^2}{X_0^2} \frac{T_0}{\lambda} h} \quad (4.5-16)$$

and

$$x_{s_{3,4}} = \frac{x_0}{2(n+1)} \pm \frac{x_0}{2(n+1)} \sqrt{1 - 16 \frac{(n^2 - 1)}{x_0^2} \frac{T_0}{\lambda} h} \quad . \quad (4.5-17)$$

From Equations (4.5-16) and (4.5-17) we see that the four ray paths for a given number of surface reflections can exist when the source and receiver are located on the ground or at a small height above the ground surface.

The above results also show that, unless $h = 0$, there is an upper limit to the number of reflections at the surface. This number falls off strongly as the source and receiver heights become greater. Conversely, the number of reflections increases as the strength of the temperature inversion and the horizontal distance between source and receiver are greater.

4.6 COMBINED EFFECT OF WIND AND TEMPERATURE

The refraction of sound has thus far been considered only for a atmosphere in rest. It is known that especially a vertical wind gradient affects the outdoor sound propagation.

Near the Earth's surface the magnitude of the horizontal wind velocity is mainly determined by the prevailing horizontal pressure gradient in the atmosphere and the surface friction. The latter force arises from the relative motion between air and ground surface. The occurring friction force tends to decrease the wind velocity. The retarding effect of the ground is largest near the ground and remains of significance up to a height of about 1000 meters. In this so-called *planetary boundary layer* the wind velocity increases continuously with height, starting from the zero-velocity boundary value at ground level.

The reduction of the wind velocity due to the surface friction depends strongly on the nature of the ground surface.

The typical variation of the wind velocity with height can be represented by power laws, according to the relationship

$$V_w = \bar{V}_{wm} \left[\frac{H}{H_m} \right]^{1/n}, \quad (4.6-1)$$

where \bar{V}_{wm} is the average wind velocity at a certain measurement height H_m . For wind blowing over a relatively smooth surface and under the normal condition of a decreasing air temperature with height, the exponent $1/n$ is approximately equal to $1/7$ (Reference 24).

Figure 4.6-1 shows the wind profiles calculated from Equation (4.6-1), using $n = 7$. Considered are a number of wind velocities measured at a height of 2 m above ground level.

The velocity gradient follows from Equation (4.6-1) as

$$\frac{dV_w}{dH} = \bar{V}_{wm} \frac{1}{n} \left[H \right]^{\frac{1-n}{n}} \left[H_m \right]^{-1/n}, \quad (4.6-2)$$

which decreases gradually as the height becomes greater.

As shown in Figure 4.6.2, if the sound ray is traveling at the speed of sound c relative to the air, and if the horizontal wind velocity is V_w then the apparent propagation speed of an infinitesimal section of a wavefront as seen by an observer fixed in space is the vector sum of V_w and c , the latter being

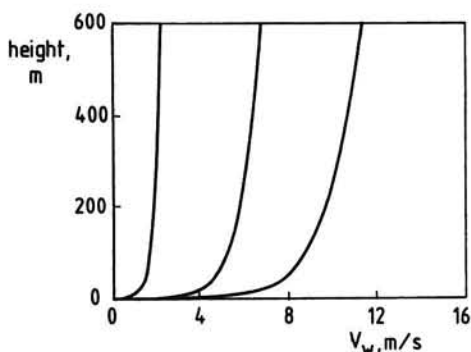


Figure 4.6-1. Typical wind profiles

taken perpendicular to the wavefront element.

The curve drawn in Figure 4.6-2 represents a ray path in a vertical plane relative to an inertial axis-system (cf. Figure 4.4-1).

If the horizontal wind velocity is in the direction of the positive X-axis, the vertical and horizontal components of the propagation speed are given by

$$\frac{dz}{dt} = c \sin \delta \quad (4.6-3)$$

$$\frac{dx}{dt} = c \cos \delta + V_w \quad . \quad (4.6-4)$$

In these equations δ is the angle the wavefront normal makes with the (horizontal) X-axis.

The slope of the ray path follows from Equations (4.6-3) and (4.6-4) as

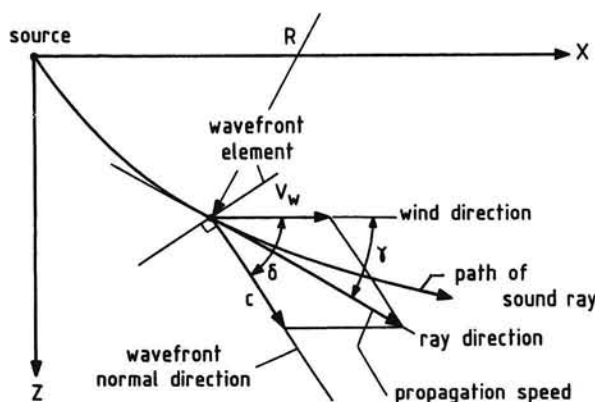


Figure 4.6-2. Ray path in the presence of wind

$$\gamma = \tan^{-1} \left(\frac{dz}{dx} \right) = \tan^{-1} \left(\frac{c \sin \delta}{c \cos \delta + V_w} \right). \quad (4.6-5)$$

The radius of curvature of the sound ray is

$$R = \frac{dr}{d\gamma} = \frac{\sqrt{(dx)^2 + (dz)^2}}{d\gamma}. \quad (4.6-6)$$

From Snell's law of refraction, Equation (4.3-8), we know that when a sound ray arrives at a plane interface between two media with different propagation speeds, the sound can be transmitted into the other region with a change in direction of propagation.

In Figure 4.6-3 is shown the transmission of a wavefront element across such a boundary. Above the interface the speed of sound is c_1 and the wind velocity is V_{w1} . In the region below the interface the speed of sound and wind velocity are c_2 and V_{w2} , respectively.

It may be seen from the construction in Figure 4.6-3 that in the case of relative motion the condition determining the refraction is given by the following equality:

$$\frac{c_1}{\cos \delta_1} + V_{w1} = \frac{c_2}{\cos \delta_2} + V_{w2} \quad \text{or} \quad (4.6-7)$$

$$\frac{c}{\cos \delta} + V_w = \text{constant.} \quad (4.6-8)$$

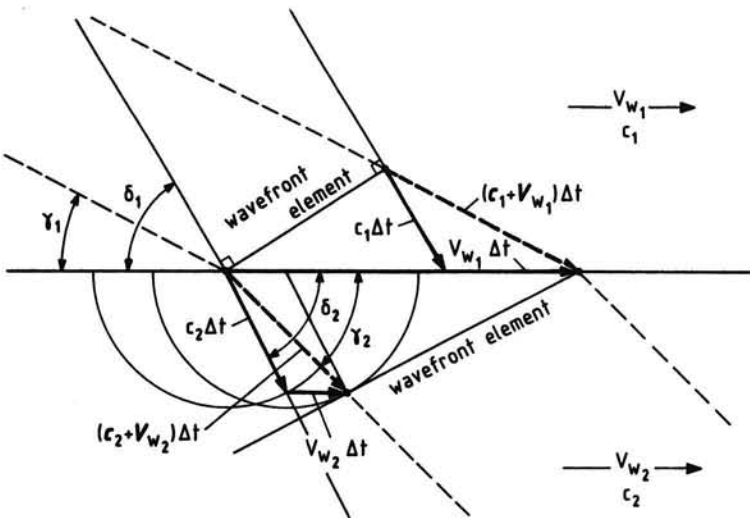


Figure 4.6-3. Refraction of sound by a temperature and wind gradient

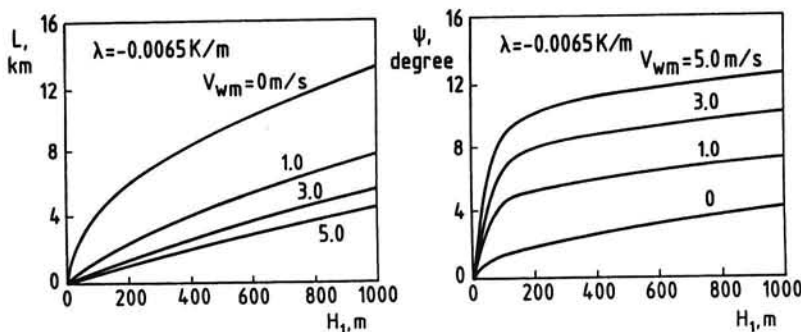


Figure 4.6-4. Location of shadow zone in the presence of wind

This relation is known as *Snell's law of refraction for moving media*, where δ is the angle the wavefront normal makes with the boundary.

Owing to the varying wind gradient the radius of curvature of the sound path in Figure 4.6-2 will vary with height. This implies that an accurate determination of the geometry of the ray paths must involve step by step calculations based on the system of Equations (4.6-2) to (4.6-8). In this manner we can establish the *focusing effects* occurring in downwind direction and the location of the shadow region in upwind direction.

A qualitative picture of the complete radiation pattern around a point sound source has been portrayed already in Figure 1.4-2 of Chapter 1.

In Figure 4.6-4 the location of the *shadow zone* in a combined field of temperature and wind gradients is given. The effects of wind result from numerical integration of the pathlengths.

Considered are wind velocities measured at a height of 2 m above the ground surface. Obviously, the distance to the shadow zone strongly reduces with increasing wind velocity and decreasing source height.

It should be appreciated that the wind has no effect on a sound ray which travels at a right angle to the wind direction. Generally, when the wind vector makes an arbitrary angle with the source-receiver direction, only the components of the wind velocities in the direction of the sound rays affect their curvatures. This situation is considered in Figure 4.6-5, where is sketched the geometry of sound propagation over ground in plan view. The source and receiver are located near the ground and the wind direction is assumed to make an angle β with the source-receiver direction.

Directly downwind, for the temperature lapse condition considered in Figure 4.6-4, the effect of wind typically overrules that of the temperature gradient so that there will be no shadow region. At some distance in upwind

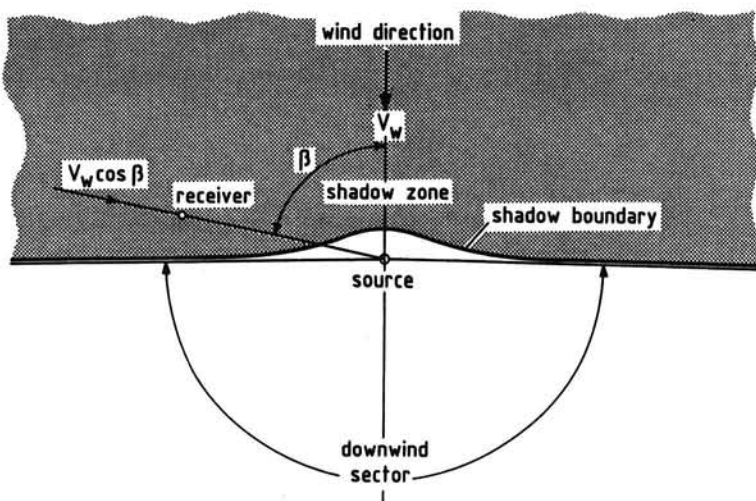


Figure 4.6-5. Typical downwind sector dimensions

direction, there will be a shadow region generated by the wind gradient and augmented by the temperature gradient.

Clearly, the distance to the shadow zone will increase with increasing angle β . Therefore, it might be possible that in a certain downwind direction the negative temperature gradient balances the effect of wind. From the predictions in Figure 4.6-4, however, we must conclude that even for very low wind velocities the effect of wind exceeds the effect of the temperature lapse rate in a large degree. Thus, independent of the magnitude of wind velocity and source height, in all downwind directions the distance to the shadow zone will recede to infinity. In other words, as shown in Figure 4.6-5, for typical daytime conditions it seems realistic to expect that only in the half plane in upwind direction shadow zone formation can take place.

4.7 CONVERGENCE AND DIVERGENCE EFFECTS

In this section we shall examine the *convergence (focusing)* and *divergence* effects of refraction in a velocity gradient.

In order to analyze the effects on measured sound pressure levels, we consider a point source at some height above the ground, radiating a given sound power equally in all directions. As depicted in Figure 4.7-1, a rectangular axis-system is fixed to the source with the origin at the source location. The Z-axis points vertically and is positive in downward direction.

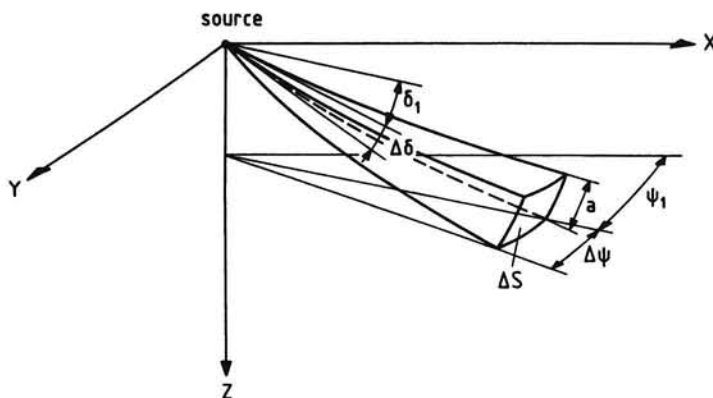


Figure 4.7-1. Curved ray tube

The curved ray tube in Figure 4.7-1 is defined by the four rays with initial angles δ_1 , $\delta_1 + \Delta\delta$, ψ_1 and $\psi_1 + \Delta\psi$. Along the curved path, the angular width $\Delta\psi$ is constant but the angular height $\Delta\delta$ is changed by the slightly different curvatures of the extreme rays in the vertical plane.

The local sound intensity is determined by the sound power confined in the ray tube and the cross-sectional area of the tube. Therefore, the difference between the sound pressure level measured in the presence of a velocity gradient and the sound pressure level with rectilinear propagation can be expressed as

$$\Delta \text{SPL} = 10 \log \frac{r \Delta \delta}{a} , \quad (4.7-1)$$

where r is the straight-line distance between source and measurement point, and a is the local height of the ray tube.

For the sake of simplicity, we limit our analysis to the propagation through an atmosphere where the vertical gradients of sound speed and/or wind velocity are uniform. This assumption implies that in the vertical plane the sound rays consist of circular arcs.

In Figure 4.7-2 are sketched upward refracted sound rays, which shape occurs in an atmosphere where the propagation speed decreases with height.

When the measurement point is chosen on the ground, the tube height at that point is given by

$$a_0 = \Delta x_0 \sin \delta_0 , \quad (4.7-2)$$

where Δx_0 is the horizontal distance along the ground surface between the rays with initial angles δ_1 and $\delta_1 + \Delta\delta$, and δ_0 is the ray angle at ground level.

To calculate the distance Δx_0 , we write

$$\Delta x_0 = x_0 (\delta_1) - x_0 (\delta_1 + \Delta\delta)$$

or

$$\Delta x_0 = -\frac{dx_0}{d\delta_1} \Delta\delta . \quad (4.7-3)$$

From an inspection of the geometric construction of the ray paths in Figure 4.7-2, the following relation is apparent:

$$\left[\frac{c_1}{dc/dz} \tan \delta_1 - x_0 \right]^2 + \left[\frac{c_1}{dc/dz} + z_0 \right]^2 = \left[\frac{c_1}{dc/dz} \frac{1}{\cos \delta_1} \right]^2 \quad (4.7-4)$$

or

$$x_0^2 - 2x_0 \frac{c_1}{dc/dz} \tan \delta_1 + \left[\frac{c_1}{dc/dz} + z_0 \right]^2 - \left[\frac{c_1}{dc/dz} \right]^2 = 0 . \quad (4.7-5)$$

Solving for δ_1 yields

$$\delta_1 = \tan^{-1} \left[\frac{dc/dz}{2x_0 c_1} \left(x_0^2 + \left[\frac{c_1}{dc/dz} + z_0 \right]^2 - \left[\frac{c_1}{dc/dz} \right]^2 \right) \right] . \quad (4.7-6)$$

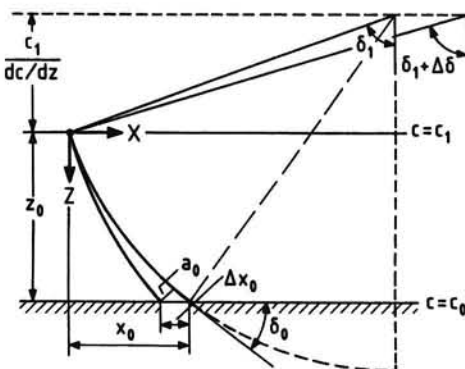


Figure 4.7-2. Geometrical diagram illustrating divergence of sound rays on refraction

The derivative of x_0 with respect to δ_1 follows from differentiating Equation (4.7-5) with respect to δ_1 ,

$$\frac{dx_0}{d\delta_1} = \frac{x_0 \frac{c_1}{dc/dz} \frac{1}{\cos^2 \delta_1}}{x_0 - \frac{c_1}{dc/dz} \tan \delta_1} . \quad (4.7-7)$$

Inserting Equation (4.7-7) into Equation (4.7-3) gives

$$\Delta x_0 = \frac{x_0 \frac{c_1}{dc/dz} \frac{1}{\cos^2 \delta_1}}{\frac{c_1}{dc/dz} \tan \delta_1 - x_0} \Delta \delta . \quad (4.7-8)$$

Combination of Equations (4.7-1), (4.7-2) and (4.7-8) produces

$$\Delta SPL = 10 \log \left[\frac{r_0}{x_0} \frac{\left[\frac{c_1}{dc/dz} \tan \delta_1 - x_0 \right]}{\frac{c_1}{dc/dz} \frac{\sin \delta_0}{\cos^2 \delta_1}} \right] , \quad (4.7-9)$$

where the angle δ_0 follows from Snell's law, Equation (4.3-8),

$$\delta_0 = \cos^{-1} \left[\frac{c_0}{c_1} \cos \delta_1 \right] . \quad (4.7-10)$$

It is an easy matter to show that in the opposite case of sound traveling through an atmosphere where the propagation speed increases with height ($dc/dz < 0$) is given by

$$\Delta SPL = 10 \log \left[\frac{r_0}{x_0} \frac{\left[\frac{c_1}{dc/dz} \tan \delta_1 + x_0 \right]}{\frac{c_1}{dc/dz} \frac{\sin \delta_0}{\cos^2 \delta_1}} \right] . \quad (4.7-11)$$

A numerical consideration of the convergence and divergence effects on the basis of Equations (4.7-9) and (4.7-11) reveals that the ground observed

sound pressure levels only are influenced when there are high velocity gradients, which occur within the typical nonlinear wind velocity profiles near the ground.

The refraction of sound rays traveling downwind within a 1/7 power profile (see Equation (4.6-1)) is reported in Reference 22. The analysis demonstrates that the refraction of sound rays by such a wind profile can cause large deviations from the sound pressure levels in a uniform quiescent atmosphere. The refraction effects seem particularly significant in ground-to-ground sound propagation.

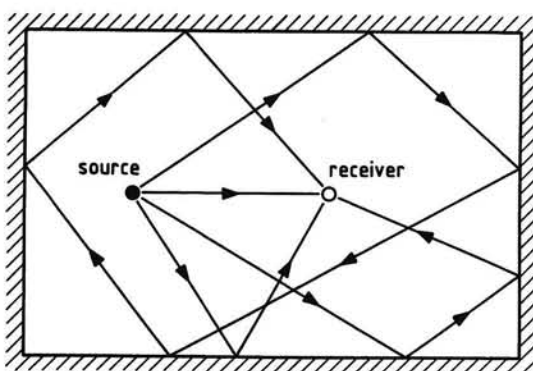


Figure 5.1-1. Direct and reflected sound waves in an enclosure

5 SOUND IN ENCLOSURES

5.1 THE SOUND FIELD

As sketched in Figure 5.1-1, when a sound source is placed in an enclosure every part of the room will be filled with reflected sound waves moving in different directions. Thus the occurring sound pressure at any point in the room will be the sum of the sound pressure of the waves coming directly from the source and the sound pressure created by reflections from the inner walls of the room. Consequently, the observed sound pressure level at a given position in the room will be higher than that of the direct sound.

The typical variation of the total sound pressure level with distance from the source is shown by the curve of Figure 5.1-2.

As remarked already in Chapter 1, close to the source we will find the *near field* in which region, in general, measurements should be avoided.

At some distance from the source the *free field condition* will exist, where the so-called *direct sound pressure level* dominates.

In this part of the sound field the variation of the sound pressure level with distance and angular position, according to Equation (4.1-10), is given by

$$SPL_d(\theta, r) = PWL - 10.8 + 10 \log \frac{\rho_\infty c}{(\rho_\infty c)_0} - 20 \log r + DI(\theta), \quad (5.1-1)$$

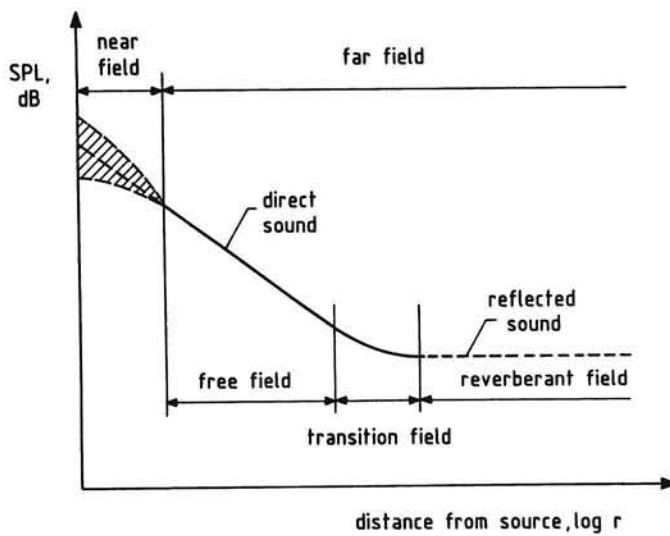


Figure 5.1-2. Variation of sound pressure level with distance in a room

where SPL_d is the direct sound pressure level.

At a certain distance the direct sound pressure level will become equal to the sound pressure level of the reflected waves, SPL_r , (see Section 5.3).

At distances beyond this point the magnitude of the total sound pressure level, being the logarithmic sum of SPL_d and SPL_r , will be determined by that of the reflected sound alone and so remains virtually constant. As indicated in Figure 5.1-2, the region in enclosures in which the reflected sound dominates is termed the *reverberant field*.

5.2 DIFFUSE FIELD

If there are a very large number of reflections coming from all directions, the reverberant field may become a *diffuse field*.

In the latter sound field the sound pressure and particle velocity are uncorrelated in such a manner that the sound energy flow in each point of the field is the same in all directions. For this reason, there is no net flow of acoustic energy so the sound intensity is zero everywhere. The sound pressure level, on the other hand, is unequal to zero and uniform throughout the entire region. Under these conditions, naturally, the Equations (2.7-13) and (2.8-25), relating the effective pressure and sound intensity, cannot hold.

Clearly, we are not only interested in the sound power radiation into the room, but as much in the sound energy time rate that flows into the walls of the room. Therefore, we proceed by developing a relationship between the energy density in a diffuse field and the sound energy passing through a plane of unit area from one side only.

To this end, we consider the sound energy edV contained at a given moment in an element of volume dV (Figure 5.2-1). Because the element dV is part of a diffuse field, the energy density e is the same through the whole of the room. We now consider that portion of the energy initially in the element dV that strikes a plane of unit area dA which is at a distance ε from the element of volume dV and at an angle θ with the radius ε .

Since the energy edV is spread out equally in all directions, the energy falling on the surface element dA can be determined. Treating the waves as plane waves, we get

$$dE_n = \frac{e dV}{4\pi\varepsilon^2} \cos\theta dA , \quad (5.2-1)$$

where $4\pi\varepsilon^2$ is the surface of the spherical shell surrounding the element dV at a distance ε .

The total energy, E_n , that reaches the area dA in a time interval Δt is original-

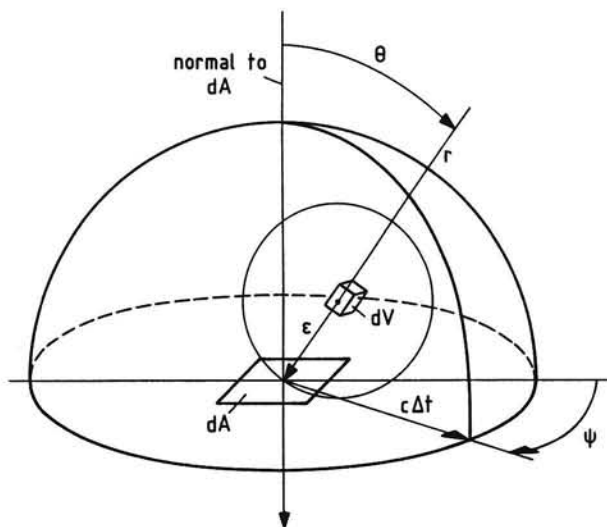


Figure 5.2-1. Diagram illustrating incident intensity
ly within a hemisphere of radius $c\Delta t$, so that

$$E_n = \int_{\text{hemisphere}} \frac{e dV}{4\pi\epsilon^2} \cos\theta dA . \quad (5.2-2)$$

Using spherical polar coordinates (r, θ, ψ), we have $dV = r d\theta r \sin\theta d\psi dr$ so that Equation (5.2-2) can be written as

$$E_n = \frac{e dA}{4\pi} \int_0^{c\Delta t} d\epsilon \int_0^{\pi/2} \cos\theta \sin\theta d\theta \int_0^{2\pi} d\psi . \quad (5.2-3)$$

Integration yields

$$E_n = \frac{e dA}{4} c \Delta t . \quad (5.2-4)$$

So we find for the *incident intensity*, I_n , in a diffuse field, being the time rate of energy passing from one side through a plane of unit area

$$I_n = \frac{e c}{4} . \quad (5.2-5)$$

In Chapter 2 we derived for plane waves traveling in open air the relationship

$$e = \frac{p_e^2}{\rho_\infty c^2} . \quad (2.7-17)$$

We therefore have in a diffuse field

$$I_n = \frac{p_e^2}{4\rho_\infty c} . \quad (5.2-6)$$

This equation shows that the incident intensity of a diffuse sound at a surface is one quarter of the sound intensity from a plane unidirectional wave having the same energy density.

5.3 ABSORPTION

When a sound wave meets a wall surface, usually, most of the incident intensity is reflected into the room, and some is absorbed by the wall. Sound absorbers often are made of porous materials into which air can flow. The amount of absorption then includes transmission of sound energy through passages in the wall to the other side and dissipation in the form of heat due to frictional effects in the pores of the surface material (Figure 5.3-1).

In addition, some sound will be transmitted through the wall, when a forced oscillation of the wall material is generated by the sound pressure (see Section 5.5).

Usually, the *acoustic absorption* properties of each wall surface element S_i are represented by its local *absorption coefficient* α_i , the fraction of the incident intensity that is absorbed by the wall element when sound waves are falling on it equally from all directions.

The value of the absorption coefficient varies with the frequency of the sound and depends strongly on the type of surface material.

The locally absorbed sound power is given by

$$W_{a_i} = I_n \alpha_i S_i . \quad (5.3-1)$$

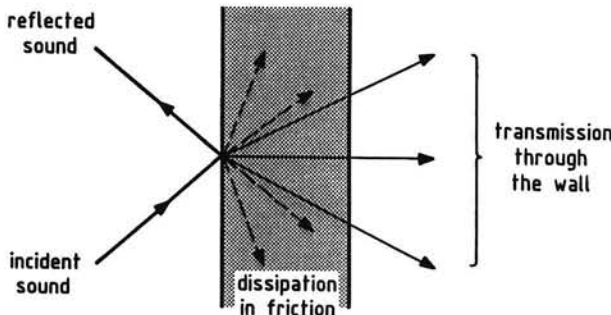


Figure 5.3-1. Reflection, transmission, and dissipation of sound

The total sound power absorbed by the walls is obtained by summation of W_{ai} over the entire wall area S of the room,

$$W_a = I_n \sum \alpha_i S_i . \quad (5.3-2)$$

It is convenient to determine the mean absorption coefficient $\bar{\alpha}$ for the room. This quantity is defined by

$$\bar{\alpha} = \frac{1}{S} \sum \alpha_i S_i , \quad (5.3-3)$$

where $S = \sum S_i$ is the entire wall-surface area.

Thus, the total sound power absorbed in a room can be written as

$$W_a = I_n \bar{\alpha} S . \quad (5.3-4)$$

The quantity $\bar{\alpha}S$ in Equation (5.3-4), having the dimensions of area, is called the *absorption of the room*.

Now we consider two surfaces which absorb the same sound power W_a . If their respective absorption coefficients are α and unity, we have the equality

$$\bar{\alpha}S = S_a , \quad (5.3-5)$$

where S_a is the surface of the perfect absorber, which absorbs as much sound power as the surface with area S and mean absorption coefficient $\bar{\alpha}$.

If the area S_a is measured in square meters, then the absorption is known as *metric sabins*.

Since a perfect absorber can be seen as an open space, the absorption may also be referred to as the *open window area*.

The convenience of employing the idea of open window area is that it can be determined in practical situations without an exact knowledge of the average absorption coefficient of the room.

The rate of change of the total sound energy in the room after starting the source is the difference between the (steady) power radiated into the room by the source and the power absorbed by the walls,

$$V \frac{de}{dt} = W - S_a I_n , \quad (5.3-6)$$

where V is the volume of the enclosure, and e and I_n are the instantaneous values of the energy density and the incident intensity, respectively.

Introducing the relationship $e = 4I_n/c$ into Equation (5.3-6) furnishes

$$\frac{4V}{c} \frac{dI_n}{dt} = W - S_a I_n . \quad (5.3-7)$$

Substitution of $I_n = A + Be^{-\gamma t}$ as a solution yields

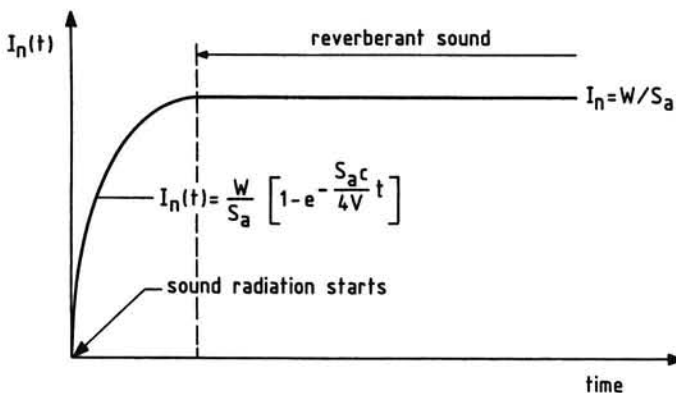


Figure 5.3-2. Rise of incident intensity in a room

$$\gamma = \frac{S_a c}{4V} \quad \text{and} \quad A = \frac{W}{S_a} .$$

Since $I_n = 0$ when $t = 0$, we find $B = -A$ so the increase of the incident intensity from the time the source starts sounding is given by

$$I_n(t) = \frac{W}{S_a} \left[1 - e^{-\frac{S_a c}{4V} t} \right] . \quad (5.3-8)$$

We see that the incident sound intensity in a room approaches to the value (Figure 5.3-2):

$$I_n = \frac{W}{S_a} . \quad (5.3-9)$$

Any numerical consideration on the relationship between $I_n(t)$ and t on the basis of Equation (5.3-8) will manifest that the steady value of I_n is reached almost instantaneously.

In any case, for steady-state conditions the power supplied by the source equals the rate of sound energy loss by absorption.

It is also apparent from Equation (5.3-9) that the magnitude of the steady incident intensity is inversely proportional to the *room absorption*.

Thus, S_a should be small for I_n to be large and vice-versa.

From Equations (5.3-9) and (5.2-6), we readily find the following relationship between the sound pressure level of the reflected sound, SPL_r , the power watt level of the source, and the room absorption in square meters,

$$SPL_r = PWL - 10 \log S_a - 26.0 + 10 \log 4 \rho_\infty c , \text{ dB.} \quad (5.3-10)$$

Using $\rho_\infty c = (\rho_\infty c)_0 = 416.86 \text{ kg/m}^2 \text{s}$, we obtain

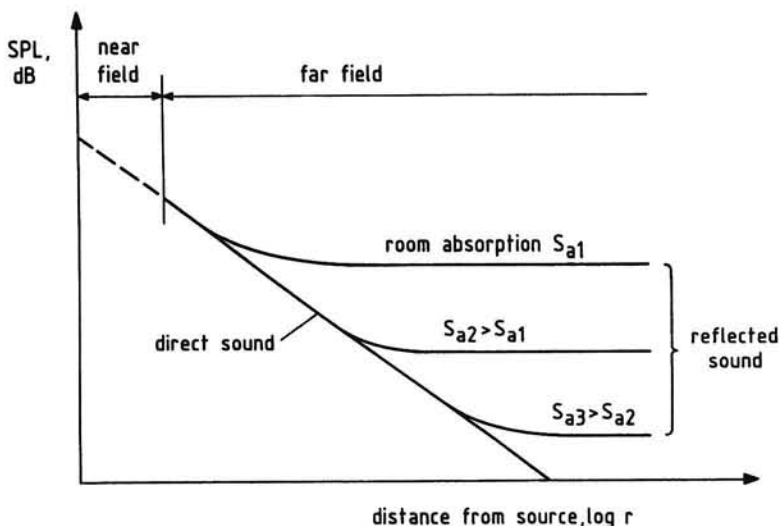


Figure 5.3-3. Sound pressure levels in a room at different absorption S_a

$$\text{SPL}_r = \text{PWL} - 10 \log S_a + 6.2, \text{ dB.} \quad (5.3-11)$$

This equation says that in the case of a diffuse distribution of sound, the sound pressure level SPL_r , decreases with increasing room absorption S_a .

This behavior is illustrated by Figure 5.3-3, in which is sketched the total sound pressure level in a room as a function of distance from the source and room absorption. The curves show that as S_a increases, the total sound pressure level at distances far from the source approaches that of the direct sound alone. On the other hand, in a room with a small amount of absorbent, S_a is low through which the conditions may become so much reverberant that no free field exists. Then the total sound pressure level in the room may be as high as the direct level at points close to the source.

If there is a free-field region, and if in the reverberant field the sound is essentially diffuse, a point can be distinguished at which the sound pressure level of the reflected sound is equal to the direct level (Figure 5.3-4).

Assuming a steady omnidirectional source, the sound power W in Equation (5.3-9) can be written as

$$W = \frac{p_e^2}{\rho_\infty c} 4\pi D^2, \quad (5.3-12)$$

where p_e is the effective pressure produced by the source at the distance D , which may be termed the *reverberation distance*.

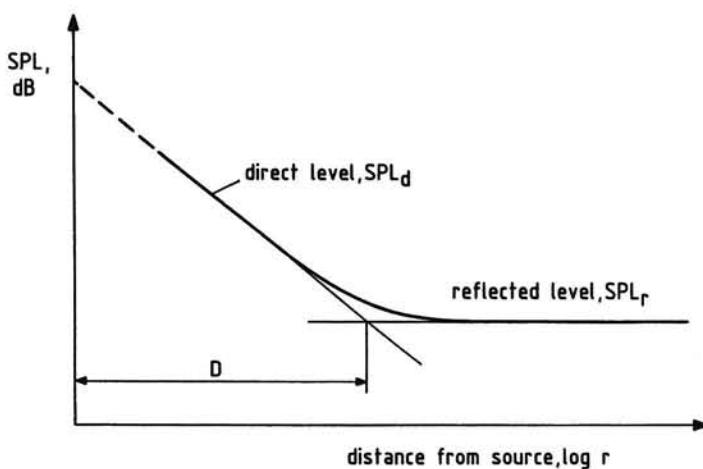


Figure 5.3-4. Reverberation distance

On the other hand, the power absorbed by the wall surface is

$$I_n S_a = \frac{p_e^2}{4 \rho_\infty c} S_a . \quad (5.3-13)$$

Equating the expressions (5.3-12) and (5.3-13) yields

$$D = \frac{1}{4\sqrt{\pi}} \sqrt{S_a} = 0.14 \sqrt{S_a} . \quad (5.3-14)$$

At distances less than D , the direct sound pressure level will supply the main contribution to the total level, while at all distances beyond this point the total level will be essentially equal to the reflected level alone.

Obviously, when one wants to investigate the noise emission from the source, measurements should be made at distances shorter than D . There the direct sound pressure level will be measured, and by integrating this level over a spherical shell surrounding the source, the power watt level of the source may be determined.

In the case that the source is a talker, we also have the requirement that a listener is in the free-field region. It has been found that at the listener's ear the level of speech must be about 10 dB beyond the *reverberant level* to assure reliable speech communications.

The reverberant sound field in a room may be used as a test environment for particular acoustic measurements and for determining the properties of absorbent materials.

Then all the interior wall surfaces must consist of very hard materials in

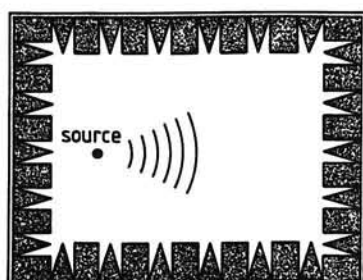


Figure 5.3-5. An anechoic room designed to provide free-field conditions

order to reflect as much sound energy as possible. In addition, sound diffusors, irregularly shaped reflecting surfaces, may be installed to obtain an adequate degree of diffusion. This type of test chamber is called a *reverberation chamber*.

A different facility for noise research testing is the *anechoic chamber* in which essentially free-field conditions are present. In such a room all the wall surfaces are highly absorbent so that reflection of sound fails to appear (Figure 5.3-5).

5.4 REVERBERATION TIME

If the sound source is shut off at a given instant, the reverberant sound field may produce a prolongation of sound during some time. This phenomenon is known as *reverberation* which is an important acoustic property of a room. The length of time for the sound pressure level to drop 60 dB after the source is stopped is defined as the *reverberation time* (Figure 5.4-1).

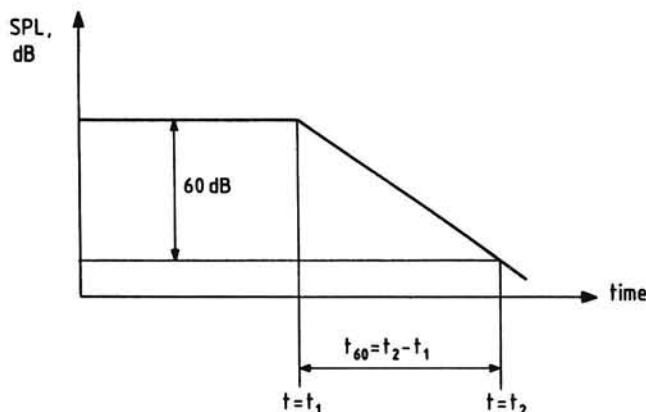


Figure 5.4-1. Definition of reverberation time

When the sound power is zero, from Equation (5.3-7), we have

$$\frac{4V}{c} \frac{dI_n}{dt} = -S_a I_n \quad \text{or} \quad (5.4-1)$$

$$\frac{dI_n}{I_n} = -\frac{cS_a}{4V} dt . \quad (5.4-2)$$

The time needed to obtain a reduction of the sound intensity from I_{n_1} to I_{n_2} is given by

$$\int_0^t dt = -\frac{4V}{cS_a} \int_{I_{n_1}}^{I_{n_2}} \frac{dI_n}{I_n} . \quad (5.4-3)$$

Integration yields

$$t = \frac{4V}{cS_a} \ln \frac{I_{n_2}}{I_{n_1}} . \quad (5.4-4)$$

By inserting $I_{n_2}/I_{n_1} = 10^{-6}$ in Equation (5.4-4) we derive the *Sabine formula* for reverberation time (named after the acoustician W.C. Sabine):

$$t_{60} = 55.3 \frac{V}{cS_a} . \approx \frac{\sqrt{V}}{6S_a} \quad (5.4-5)$$

Equation (5.4-5) indicates that the reverberation time varies directly as the volume of the room, and inversely as the absorption of the room. Thus, as the room volume is larger and the interior surfaces of the room are covered by materials with lower absorption coefficients, the sound pressure level in the room will die out more slowly.

As listed in Table 5.4-1, typical values of reverberation times that may be encountered vary between 0.3 second for small rooms, up to 10 seconds for large churches.

Applying Equation (5.4-5) to a measured reverberation time may provide the absorption for a given room once the volume is known. This means that the

Table 5.4-1 Typical reverberation times

Living rooms	: $0.3 \text{ s} < t_{60} < 1.0 \text{ s}$
Factories	: $2.0 \text{ s} < t_{60} < 3.0 \text{ s}$
Churches	: $3.0 \text{ s} < t_{60} < 10.0 \text{ s}$

magnitude of t_{60} is a direct measure for the absorbing properties of a room. Substituting Equation (5.4-5) into (5.3-14) gives the reverberation distance as

$$D = 1.05 \sqrt{\frac{V}{c t_{60}}} . \quad (5.4-6)$$

This expression shows that by measuring the reverberation time we also are able to determine the reverberation distance.

5.5 NORMAL TRANSMISSION OF SOUND THROUGH A RIGID WALL

The transmission of sound from one medium to another has already been discussed in Section 4.3. Here we shall examine the effects of the presence of a rigid wall on sound propagation.

When a sound wave encounters a partition, the wall may be set into vibration through which sound energy is emitted from the back.

We consider a plane harmonic wave normally incident on a plane rigid wall. Let the wall be free to execute an undamped motion normal to its plane. As indicated in Figure 5.5-1, some sound will be transmitted through the wall and some will be reflected from the wall (cf. Figure 4.3-1).

If we choose our axis system such as to the wall surface lies in the plane $x = 0$, we can write the equation of motion of the surface material as:

$$(A + C - B)e^{i\omega t} = m \frac{dv}{dt} , \quad (5.5-1)$$

where m is the mass of the wall per unit area, and v is the velocity of the wall.

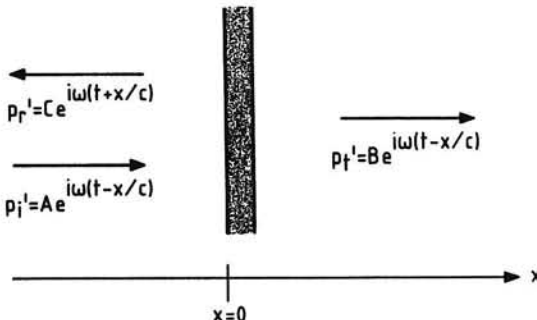


Figure 5.5-1. Sound propagation through a massive wall

According to the previous Equations (2.7-8) and (2.7-9), the relationship between sound pressure and particle velocity in a plane wave is given by

$$u = \pm \frac{p'}{\rho c} . \quad (5.5-2)$$

So the acceleration of the wall element can also be expressed as

$$\frac{dv}{dt} = \frac{d}{dt} \left[\frac{B}{\rho c} e^{i\omega t} \right] = \frac{B}{\rho c} e^{i\omega t} i\omega . \quad (5.5-3)$$

Substitution of Equation (5.5-3) into Equation (5.5-1) furnishes

$$(A + C - B) e^{i\omega t} = \frac{i\omega m}{\rho c} B e^{i\omega t} \quad \text{or} \quad (5.5-4)$$

$$A + C - B = \frac{i\omega m}{\rho c} B . \quad (5.5-5)$$

For velocity continuity, the particle velocities in the air on either side of the wall are equal. Hence

$$\frac{A}{\rho c} e^{i\omega t} - \frac{C}{\rho c} e^{i\omega t} = \frac{B}{\rho c} e^{i\omega t} \quad \text{or} \quad (5.5-6)$$

$$A - C = B . \quad (5.5-7)$$

From Equations (5.5-5) and (5.5-7), we find that the ratio B/A is:

$$\frac{B}{A} = \frac{1}{1 + \frac{i\omega m}{2\rho c}} . \quad (5.5-8)$$

This expression shows there is a phase difference between the incident and transmitted sound pressures at the wall.

By writing $B = B_1 + iB_2 = |B| e^{i\phi}$, where $|B| = \sqrt{(B_1^2 + B_2^2)}$ and $\phi = \tan^{-1}(B_2/B_1)$, from Equation (5.5-8), we readily find,

$$|B| = A \sqrt{\frac{1}{1 + \left[\frac{\omega m}{2\rho c} \right]^2}} \quad \text{and} \quad (5.5-9)$$

$$\phi = \tan^{-1} \left[-\frac{\omega m}{2\rho c} \right] . \quad (5.5-10)$$

The sound intensity in a plane wave is equal to the square of the effective pressure. Hence, the so-called *sound transmission coefficient*, i.e., the ratio of

the sound intensities in transmitted and incident waves, is given by

$$\frac{|B|^2}{A^2} = \frac{1}{1 + \left[\frac{\omega m}{2\rho c} \right]^2}. \quad (5.5-11)$$

Commonly, the sound reduction capability of a wall element is expressed by the *transmission loss*, which quantity is the difference between the sound pressure levels of incident and transmitted sound,

$$TL = SPL_i - SPL_t = 10 \log \frac{A^2}{|B|^2}, \text{ dB.} \quad (5.5-12)$$

With Equation (5.5-9), we then have

$$TL = 10 \log \left[1 + \left[\frac{\omega m}{2\rho c} \right]^2 \right], \text{ dB.} \quad (5.5-13)$$

Equation (5.5-13) indicates that the transmission loss of a wall is dependent on its mass per unit area and that this quantity increases as the frequency of the sound increases.

5.6 THE COINCIDENCE EFFECT

In the preceding section we considered the propagation of sound through a rigid wall, assuming that the wall surface was normal to the direction of wave travel. However, if the incident sound wave is inclined to the normal of the wall surface and if the wall is an infinite, flexible panel, bending in the direction normal to its plane is possible. Under these conditions the sound pressures acting on the plate vary sinusoidally along the *Y*-axis (Figure 5.6-1).

The sound pressures of the incident wave, the transmitted wave, and the reflected wave can be written as (cf. Equations (4.3-1) to (4.3-3)):

$$p'_i = A e^{i\omega[t - (x\sin\delta_i)/c_1 - (y\cos\delta_i)/c_1]} \quad (5.6-1)$$

$$p'_t = B e^{i\omega[t - (x\sin\delta_i)/c_2 - (y\cos\delta_i)/c_2]} \quad (5.6-2)$$

$$p'_r = C e^{i\omega[t + (x\sin\delta_i)/c_1 - (y\cos\delta_i)/c_1]}. \quad (5.6-3)$$

The wavelength of the plate modes in Figure 5.6-1 is called the *trace wavelength* and given here the symbol Λ . The trace wavelength is equal to

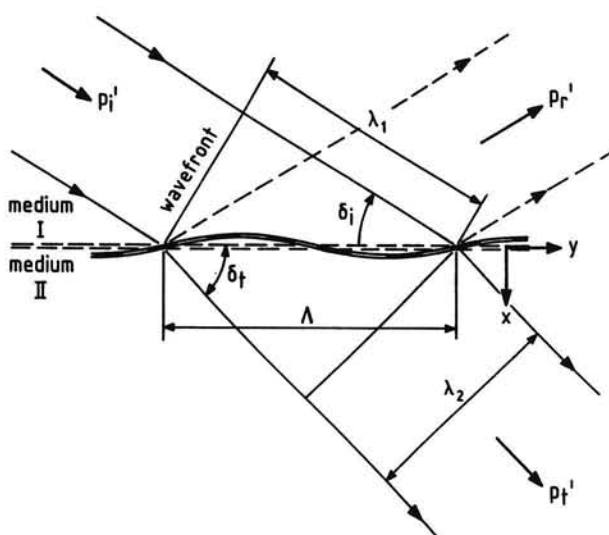


Figure 5.6-1. Flexural waves in a panel

the distance between the intercepts of two successive wavefronts on the plate,

$$\Lambda = \frac{\lambda_1}{\cos \delta_i} . \quad (5.6-4)$$

In the same way, we have

$$\Lambda = \frac{\lambda_2}{\cos \delta_t} . \quad (5.6-5)$$

From Equations (5.6-4) and (5.6-5), we obtain the relationship (cf. Equation (4.3-8)):

$$\cos \delta_t = \frac{c_2}{c_1} \cos \delta_i . \quad (5.6-6)$$

From Equations (5.6-1), (5.6-3) and (5.5-2), we find in medium I the particle velocity normal to the plate to be

$$u_{1x} = \frac{\sin \delta_i}{\rho_1 c_1} A e^{i\omega[t - (x \sin \delta_i)/c_1 - (y \cos \delta_i)/c_1]} + \\ - \frac{\sin \delta_i}{\rho_1 c_1} C e^{i\omega[t + (x \sin \delta_i)/c_1 - (y \cos \delta_i)/c_1]} . \quad (5.6-7)$$

This equation can be integrated with respect to time to give the corresponding particle displacement,

$$\xi_{1x} = \frac{\sin \delta_i}{\rho_1 c_1} \frac{1}{i\omega} A e^{i\omega[t - (x \sin \delta_i)/c_1 - (y \cos \delta_i)/c_1]} + \\ - \frac{\sin \delta_i}{\rho_1 c_1} \frac{1}{i\omega} C e^{i\omega[t + (x \sin \delta_i)/c_1 - (y \cos \delta_i)/c_1]} . \quad (5.6-8)$$

Similarly, in medium II the particle velocity and the particle displacement in x -direction are:

$$u_{2x} = \frac{\sin \delta_t}{\rho_2 c_2} B e^{i\omega[t - (x \sin \delta_t)/c_2 - (y \cos \delta_t)/c_2]} \quad (5.6-9)$$

$$\xi_{2x} = \frac{\sin \delta_t}{\rho_2 c_2} \frac{1}{i\omega} B e^{i\omega[t - (x \sin \delta_t)/c_2 - (y \cos \delta_t)/c_2]} . \quad (5.6-10)$$

The condition for displacement continuity at $x = 0$ may be expressed as

$$\xi_{1x}(x, y, t) \Big|_{x=0} = \xi_{2x}(x, y, t) \Big|_{x=0} = w(x, y, t) , \quad (5.6-11)$$

where w is the flexural displacement of the panel normal to its plane.

Substitution of Equations (5.6-8) and (5.6-10) into Equation (5.6-11) yields the equality

$$w = \frac{\sin \delta_i}{\rho_1 c_1} \frac{1}{i\omega} (A - C) e^{i\omega[t - (y \cos \delta_i)/c_1]} \\ = \frac{\sin \delta_t}{\rho_2 c_2} \frac{1}{i\omega} B e^{i\omega[t - (y \cos \delta_t)/c_2]} . \quad (5.6-12)$$

Using Equation (5.6-12), we can write the displacement of the plate in x -direction in the following form:

$$w = W e^{i\omega[t - (y \cos \delta_t)/c_2]} . \quad (5.6-13)$$

where W is the plate displacement amplitude,

$$W = \frac{\sin \delta_t}{\rho_2 c_2} \frac{1}{i\omega} B . \quad (5.6-14)$$

When the plate has a flexural stiffness of D per unit width, the equation of flexural motion of the plate reads (Reference 8):

$$p_i' + p_r' - p_t' \Big|_{x=0} = m \frac{\partial^2 w}{\partial t^2} + D \frac{\partial^4 w}{\partial y^4} , \quad (5.6-15)$$

where m is the mass of the plate per unit area.

The inertia term in Equation (5.6-15) can be written as

$$m \frac{\partial^2 w}{\partial t^2} = m i \omega \dot{w} . \quad (5.6-16)$$

Similarly, it can be shown that

$$D \frac{\partial^4 w}{\partial y^4} = i m \omega \left[-\frac{D}{m} \frac{\omega^2}{c_2^4} \cos^4 \delta_t \right] \dot{w} . \quad (5.6-17)$$

Inserting Equations (5.6-16) and (5.6-17) into Equation (5.6-15) furnishes

$$p_i' + p_r' - p_t' \Big|_{x=0} = i m \omega \left[1 - \frac{D}{m} \frac{\omega^2}{c_2^4} \cos^4 \delta_t \right] \dot{w} . \quad (5.6-18)$$

When we put Equation (5.6-5) into Equation (5.6-18), we get

$$p_i' + p_r' - p_t' \Big|_{x=0} = i m \omega \left[1 - \frac{D}{m} \frac{1}{\omega^2} \left(\frac{2\pi}{\Lambda} \right)^4 \right] \dot{w} . \quad (5.6-19)$$

Apparently, the transmitted sound pressure is maximum when

$$\frac{D}{m} \frac{1}{\omega^2} \left(\frac{2\pi}{\Lambda} \right)^4 = 1 . \quad (5.6-20)$$

Under these conditions the transmitted sound pressure is found to be the same as the incident pressure. In other words, the plate transmits all the sound energy incidenting on it ($TL = 0$). This phenomenon is known as the *coincidence effect* because the incident sound wave coincides with the natural mode of bending of the surface of the panel.

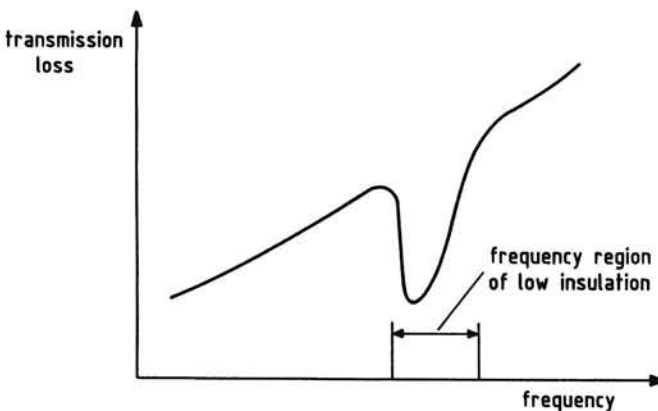


Figure 5.6-2. The coincidence dip

The particular frequency of the incident sound at which this occurs is

$$f_c = \frac{2\pi}{\Lambda^2} \sqrt{\frac{D}{m}} , \quad (5.6-21)$$

where f_c is called the *resonance frequency*.

In practice, for a plate of given stiffness and mass, there is a frequency region of low insulation (Figure 5.6-2).

As a final point, we remark that the sound pressure required to produce unit wall velocity is called the *impedance of the plate*.

From Equations (5.6-18) and (5.6-6) we obtain

$$Z_p = im\omega \left[1 - \frac{D}{m} \frac{\omega^2}{c_1^4} \cos^4 \delta_i \right] . \quad (5.6-22)$$

This equation shows that Z_p is evidently an imaginary number.

5.7 STANDING SOUND WAVES

In this section we return to the problem of a plane wave that is reflected from a plane, rigid boundary which is placed normal to the direction of propagation of the wave (see Figure 5.5-1). The reflected wave, of course, travels in opposite direction along the same line as the incident wave.

Using trigonometric notation, the sum of the two sound pressures is

$$p'(x, t) = A \cos \omega(t - x/c) + C \cos \omega(t + x/c) . \quad (5.7-1)$$

Suppose, firstly, that perfect reflection occurs so that the waves have the same amplitude. Then, from Equation (5.7-1), the resultant sound pressure is found to be

$$p'(x, t) = 2A \cos \omega t \cos \omega x/c . \quad (5.7-2)$$

Using in Equation (5.7-2) the relationships $\omega = 2\pi f$, $T = 1/f$ and $\lambda = c/f$, we get

$$p'(x, t) = 2A \cos 2\pi \frac{t}{T} \cos 2\pi \frac{x}{\lambda} . \quad (5.7-3)$$

Equation (5.7-3) demonstrates that at any position on the X-axis the sound pressure varies with time according to $\cos 2\pi t/T$, while the amplitude varies along the X-axis according to $2A \cos 2\pi x/\lambda$. Thus, the wave does not move,

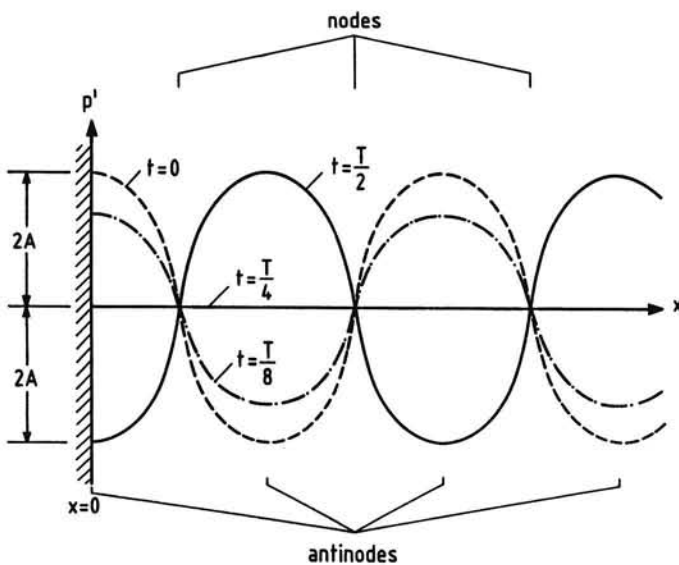


Figure 5.7-1. Standing sound wave

but simply oscillates in amplitude.

For this reason, the combination of two simple-harmonic waves of equal amplitude is called a *standing wave*.

At equally spaced points along the X-axis where $x = (n + 1/2)\lambda/2$, $n = 0, 1, 2$, etc., the sound pressure is zero, independent of time. These points are called the *nodes* of a standing wave. On the other hand, at points where $x = n\lambda/2$, the amplitude of the sound pressure has its maximum value. These points are known as *antinodes*.

A plot of the variation of the sound pressure along the X-axis at different points of time is given in Figure 5.7-1. The graph illustrates that the interaction of two traveling waves of equal amplitude results simply in a series of maxima and minima in sound pressure as the observer moves along the X-axis. At the wall the sound pressure has its maximum value.

As we saw previously in Section 2.7, the particle velocity can be obtained by integrating the gradient of the sound pressure with respect to time,

$$u = -\frac{1}{\rho} \int \frac{\partial p'}{\partial x} dt . \quad (5.7-4)$$

When we put Equation (5.7-3) into Equation (5.7-4), we obtain for the particle velocity

$$u(x,t) = -\frac{2A}{\rho c} \sin \omega t \sin \omega x/c = \frac{2A}{\rho c} \sin 2\pi t/T \sin 2\pi x/\lambda . \quad (5.7-5)$$

Comparing Equation (5.7-5) with Equation (5.7-3) reveals that in a standing wave the particle velocity is 90° out of phase with the sound pressure. Thus, at the points where the sound pressure has its maximum value the particle velocity is zero and vice-versa.

This observation indicates that a standing wave is an example of a reactive sound field where the acoustic energy does not propagate and the sound intensity is zero everywhere.

When the amplitudes A and C of the incident and the reflected waves are unequal, then from Equation (5.7-1), the sum of the two sound pressures can be written as

$$\begin{aligned} p'(x, t) &= A \cos \omega(t - x/c) + A \cos \omega(t + x/c) - (A - C) \cos \omega(t + x/c) \\ &= 2A \cos \omega t \cos \omega x/c - (A - C) \cos \omega(t + x/c) . \end{aligned} \quad (5.7-6)$$

This expression shows that if the reflecting surface does not reflect all energy of the original wave, the resultant wave consists of a standing wave and an additional traveling wave.

The combination of standing and progressive waves is specified by the *standing wave ratio* R , defined by

$$R = \frac{p_{e_{\max}}}{p_{e_{\min}}} . \quad (5.7-7)$$

From Equation (5.7-1) the effective pressure is found as follows (cf. Equation (1.9-10)):

$$p_e = \left[\frac{1}{2} (A^2 + C^2 + 2AC \cos 2\omega x/c) \right]^{\frac{1}{2}} . \quad (5.7-8)$$

This means that the standing wave ratio is

$$R = \frac{A + C}{A - C} . \quad (5.7-9)$$

We thus see that the effect of imperfect reflection from the boundary ($C < A$) is to blur the nodes and the antinodes.

5.8 MEASUREMENT OF SOUND INTENSITY

As described in Section 1.7, the sound intensity vector component in the direction r is given by the time averaged product of the local sound pressure and the associated in-phase particle velocity component,

$$I_r = \overline{p'v_r} . \quad (5.8-1)$$

In Sections (2.7) and (2.8) of Chapter 2 we saw that when a plane or spherical wave propagates in a free sound field, the sound intensity in the direction of propagation is

$$I = \frac{p_e^2}{\rho_\infty c} , \quad (5.8-2)$$

where p_e is the effective pressure (r.m.s. sound pressure) and $\rho_\infty c$ the specific resistance of the medium.

Experience has shown, however, that actually the sound intensity for any waveform is also given by Equation (5.8-2), provided that the sound wave is traveling in a free field.

An example of a sound field in which Equation (5.8-2) does not hold is an ideal diffuse field where $I = 0$, which means that there is no net flow of acoustic energy. At each point in the sound field the energy flow is the same in all directions so that all the energy remains in the sound field.

Also in a purely reactive sound field the intensity is zero since, by definition, the particle velocity is precisely 90° out of phase with the sound pressure. An example of this type of sound field is an ideal standing wave.

Returning to Figure 5.1-2, we see that in an enclosure free-field conditions only are present in the neighborhood of the sound source. In the transition and reverberant parts of the sound field the sound intensity can only be determined by using Equation (5.8-1), that is, by measuring p' and v_r versus time.

The sound pressure can easily be obtained by employing a *pressure microphone*, but a direct measurement of particle velocity is certainly not a simple matter.

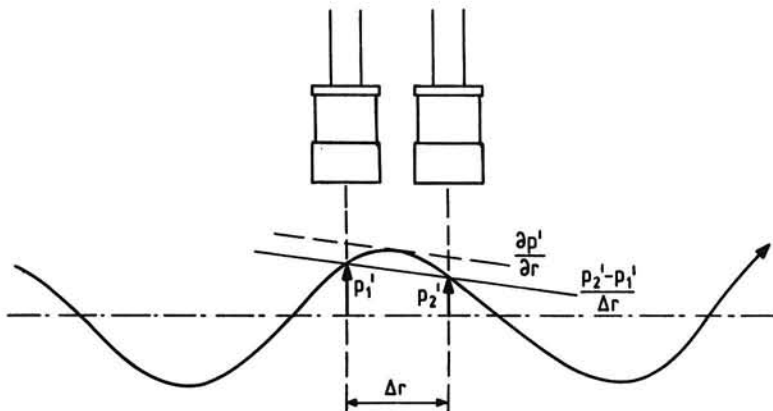


Figure 5.8-1. Measurement of pressure gradient

A convenient way of measuring the sound intensity is the use of two equal microphones located at two closely spaced points aligned along the direction of sound propagation (Figure 5.8-1). The method is based on the linearized Euler Equation:

$$\frac{\partial v_r}{\partial t} = - \frac{1}{\rho_\infty} \frac{\partial p'}{\partial r} \quad (5.8-3)$$

which gives

$$v_r = - \frac{1}{\rho_\infty} \int \frac{\partial p'}{\partial r} dt . \quad (5.8-4)$$

Practically, it may be acceptable to write

$$v_r = - \frac{1}{\rho_\infty} \int \frac{(p_2' - p_1')}{\Delta r} dt , \quad (5.8-5)$$

where $(p_2' - p_1')$ is the measured sound pressure difference and Δr is the known separation distance between the two microphones.

The sound intensity vector component in the direction r can now be expressed as

$$I_r = - \frac{1}{2\rho_\infty \Delta r} \overline{(p_2' + p_1') \int (p_2' - p_1') dt} , \quad (5.8-6)$$

where the sound pressure is assumed to be equal to the average of p_1' and p_2' . For a deeper study of the 2-microphone method and the different principles of processing the two microphone signals, the reader is directed to Reference 25.

6 ATTENUATION OF SOUND IN DUCTS

6.1 CHANGE IN CROSS-SECTIONAL AREA

When in a duct there is an abrupt change of area of cross-section, part of the sound incident on the juncture is transmitted down the duct and part of the sound is reflected back toward the source (Figure 6.1-1). Thus, the transmission of sound energy can be influenced by employing appropriate discontinuities in a duct. This feature is often used in duct systems designed to provide noise reduction in engine exhausts. Sound attenuation obtained in this manner is named *reactive attenuation*.

In analyzing the transmission and reflection at a junction, we shall assume that the duct walls are rigid and that the acoustic wavelength is considerably larger than the diameter of the duct. In other words, we shall assume one-dimensional wave motion of low frequency sound.

Furthermore, we shall assume that there is no reflected wave in the duct beyond the juncture, i.e., we shall simplify the situation to a reflection-free termination in a tube of infinite length.

Considering harmonic waves of angular frequency ω , the sound pressures in Figure 6.1-1 can be expressed as

$$p_a'(x,t) = A e^{i\omega(t-x/c)} \quad (6.1-1)$$

$$p_b'(x,t) = B e^{i\omega(t-x/c)} \quad (6.1-2)$$

$$p_c'(x,t) = C e^{i\omega(t+x/c)} \quad . \quad (6.1-3)$$

The subscripts a , b and c are used to denote the incident, transmitted and reflected waves, respectively. The positive x -direction is taken as the direction of propagation of the incident sound wave.

For continuity of mass flow at the area change ($x = 0$), we have the requirement

$$\rho S_1(u_a + u_c) = \rho S_2 u_b \quad . \quad (6.1-4)$$

Using the previous Equation (5.5-2), the particle velocities u in Equation (6.1-4) can be expressed in terms of sound pressure, giving

$$\rho S_1 \left[\frac{A e^{i\omega t}}{\rho c} - \frac{C e^{i\omega t}}{\rho c} \right] = \rho S_2 \frac{B}{\rho c} e^{i\omega t} \quad . \quad (6.1-5)$$

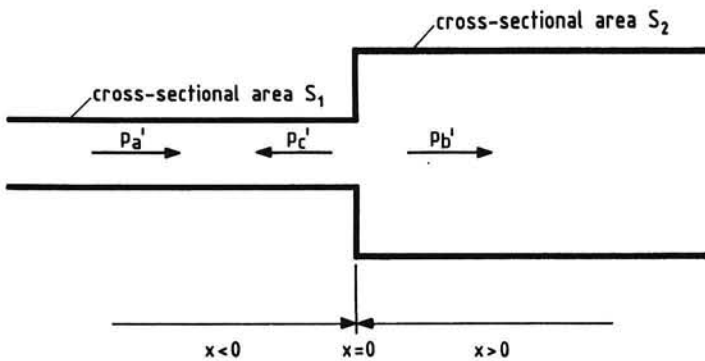


Figure 6.1-1. Duct with change in the cross-sectional area

Since ρ and c remain the same, they will cancel out, leaving

$$S_1(A - C) = S_2B \quad . \quad (6.1-6)$$

The second condition that must hold is that the sound pressure is continuous at the junction. This gives

$$p'_a + p'_c = p'_b \quad \text{or} \quad (6.1-7)$$

$$A + C = B \quad . \quad (6.1-8)$$

Elimination of C from Equations (6.1-6) and (6.1-8) furnishes the transmission factor

$$\frac{B}{A} = \frac{2}{1 + S_2/S_1} \quad . \quad (6.1-9)$$

Solving Equations (6.1-6) and (6.1-8) for C/A produces the reflection factor

$$\frac{C}{A} = \frac{1 - S_2/S_1}{1 + S_2/S_1} \quad . \quad (6.1-10)$$

Equation (6.1-9) shows that at any juncture where the duct cross-sectional area increases, only a fraction of the sound energy is transmitted down the duct.

From Equations (6.1-6) and (6.1-8) it is also apparent that

$$S_1(A^2 - C^2) = S_2B^2 \quad . \quad (6.1-11)$$

This equality says that energy is conserved. This observation is in accordance with our conservation relations at $x = 0$, which imply that the transmission of sound across the junction is not reduced by absorption of sound energy, but only by reflection of energy at the junction.

Because the area of the wavefront changes at the juncture, we only can express the sound attenuation (the transmission loss) in terms of power watt level,

$$\Delta \text{PWL} = 10 \log \frac{W_a}{W_b}, \quad (6.1-12)$$

where W_a is the incident sound power and W_b is the transmitted sound power. With the relationships $W = IS = p_e^2 S / pc$ and $p_e = p'_{max} / \sqrt{2}$ we get

$$\Delta \text{PWL} = 10 \log \frac{A^2 S_1}{B^2 S_2}. \quad (6.1-13)$$

Insertion of Equation (6.1-9) yields

$$\Delta \text{PWL} = 10 \log \frac{(1 + S_2/S_1)^2}{4 S_2/S_1}. \quad (6.1-14)$$

Note from Equation (6.1-14) that ΔPWL is independent of the direction of the wave motion. Thus, a constriction in the duct will cause the same attenuation as a widening of the duct.

6.2 SINGLE-EXPANSION CHAMBER

A simple and effective sound attenuation device consists of a duct which is equipped with an enlargement or expansion chamber. This so-called *reactive*

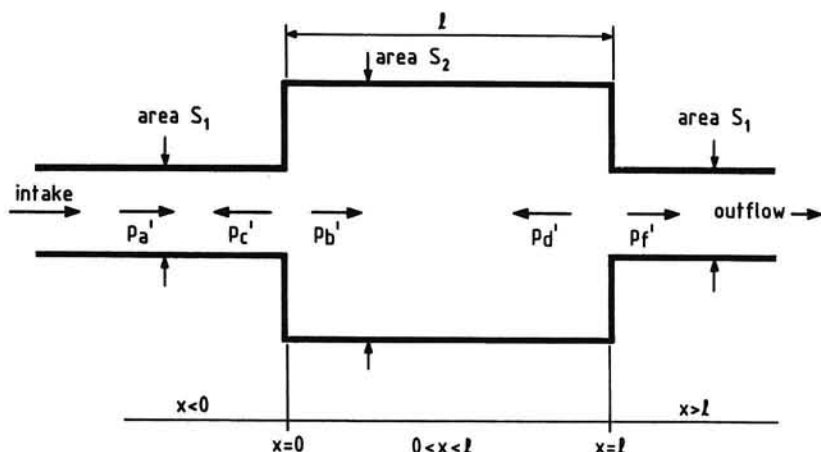


Figure 6.2-1. A single-expansion chamber

attenuator provides attenuation by utilizing the sound reflections from the junctures at which the cross-sectional area changes. A *single-expansion chamber* may have a cylindrical duct with inlet and outlet tubes of equal cross-sectional area located at the two ends of the chamber (Figure 6.2-1). If all waves are assumed to be plane and harmonic, then we can write

$$p'_a = Ae^{i\omega(t-x/c)} \quad \text{in} \quad x < 0 \quad (6.2-1)$$

$$p'_b = Be^{i\omega(t-x/c)} \quad \text{in} \quad 0 < x < l \quad (6.2-2)$$

$$p'_c = Ce^{i\omega(t+x/c)} \quad \text{in} \quad x < 0 \quad (6.2-3)$$

$$p'_d = De^{i\omega(t+x/c)} \quad \text{in} \quad 0 < x < l \quad (6.2-4)$$

$$p'_f = Fe^{i\omega(t-[x-l]/c)} \quad \text{in} \quad x > l \quad . \quad (6.2-5)$$

The subscripts *a* and *c* refer to the incident and reflected waves ahead of the chamber, *b* and *d* to the waves inside the chamber, and *f* refers to the transmitted wave beyond the expansion chamber.

The equations for continuity of mass flow and pressure at $x = 0$ are

$$\rho S_1(u_a + u_c) = \rho S_2(u_b + u_d) \quad (6.2-6)$$

or with Equation (5.5-2)

$$S_1(A - C) = S_2(B - D) \quad \text{and} \quad (6.2-7)$$

$$p'_a + p'_c = p'_b + p'_d \quad \text{or} \quad (6.2-8)$$

$$A + C = B + D \quad . \quad (6.2-9)$$

Similarly, at $x = l$, the relations are

$$\rho S_2(u_b + u_d) = \rho S_1 u_f \quad \text{or} \quad (6.2-10)$$

$$S_2(Be^{-i\omega l/c} - De^{i\omega l/c}) = S_1 F \quad \text{and} \quad (6.2-11)$$

$$p'_b + p'_d = p'_f \quad \text{or} \quad (6.2-12)$$

$$Be^{-i\omega l/c} + De^{i\omega l/c} = F \quad . \quad (6.2-13)$$

Solving Equations (6.2-7), (6.2-9), (6.2-11) and (6.2-13) for the ratio A/F results in

$$\frac{A}{F} = \frac{(S_2/S_1 + 1)^2}{4S_2/S_1} e^{i\omega l/c} - \frac{(S_2/S_1 - 1)^2}{4S_2/S_1} e^{-i\omega l/c} \quad \text{or} \quad (6.2-14)$$

$$\frac{A}{F} = \cos \omega l/c + i \frac{1}{2} \left[\frac{S_1}{S_2} + \frac{S_2}{S_1} \right] \sin \omega l/c . \quad (6.2-15)$$

The drop in sound pressure level, i.e., the transmission loss in dB becomes

$$TL = 10 \log \left| \frac{A}{F} \right|^2 = 10 \log \left[1 + \frac{1}{4} \left[\frac{S_1}{S_2} - \frac{S_2}{S_1} \right]^2 \sin^2 \omega l/c \right] . \quad (6.2-16)$$

Notice that in deriving Equation (6.2-16), as we also did in the preceding section, we assumed the occurrence of one-dimensional wave motion and the absence of sound reflection from the exit of the attenuator.

Equation (6.2-16) indicates that the transmission loss is zero when $\sin \omega l/c = 0$, i.e., when

$$\frac{\omega l}{c} = n\pi , \quad (6.2-17)$$

where n is any integer ($n = 0, 1, 2, 3, \dots$ etc.).

On the other hand, the attenuation is maximum when $\sin \omega l/c = \pm 1$, i.e., when

$$\frac{\omega l}{c} = (2n+1)\frac{\pi}{2} . \quad (6.2-18)$$

Thus, at a given frequency and speed of sound, the optimum length of the expansion chamber is given by

$$l = (2n+1)\frac{\pi c}{2\omega} = (2n+1)\frac{c}{4f} . \quad (6.2-19)$$

Evidently, the length of the chamber determines the frequencies attenuated so that the chamber must have a particular length to provide the possible peak attenuation at the frequency of the sound. The length at which this peak attenuation occurs is inversely proportional to the frequency of the sound.

Returning to Equation (6.2-16) we see that the magnitude of the peak attenuation is a function of the *expansion ratio* S_2/S_1 only.

In Figure 6.2-2 is plotted TL as functions of $\omega l/c$ and S_2/S_1 . The curves illustrate the cyclic nature of the attenuation and the fact that the transmission loss increases as the ratio S_2/S_1 is greater.

If it is necessary to increase the transmission loss of a reactive attenuator, an effective means is to place a number of expansion chambers in series and to join them with either external or internal tubes (Reference 26). As an example, a sketch of a *double-expansion chamber* with internal connecting tube is given in Figure 6.2-3.

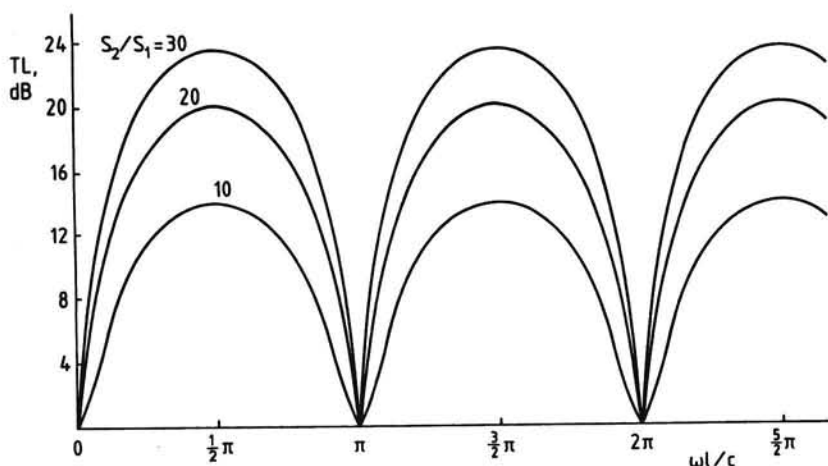


Figure 6.2-2. Attenuation characteristics for single-expansion chamber

The derivation of the expression for the transmission loss provided by this muffler configuration is left to the reader as an exercise. Using the symbols as indicated in Figure 6.2-3, the result is

$$TL = 10 \log \left[\cos(\omega l_2/c) - \left(\frac{S_2}{S_1} - 1 \right) \sin(2\omega l_2/c) \tan(\omega l_1/c) \right]^2 + \\ + \left[\frac{1}{2} \left\{ \left(\frac{S_2}{S_1} + \frac{S_1}{S_2} \right) \sin(2\omega l_2/c) + \left(\frac{S_2}{S_1} - 1 \right) \tan(\omega l_1/c) \times \right. \right. \\ \left. \left. \times \left(\frac{S_2}{S_1} + \frac{S_1}{S_2} \right) \cos(2\omega l_2/c) - \left(\frac{S_2}{S_1} - \frac{S_1}{S_2} \right) \right\} \right]^2 . \quad (6.2-20)$$

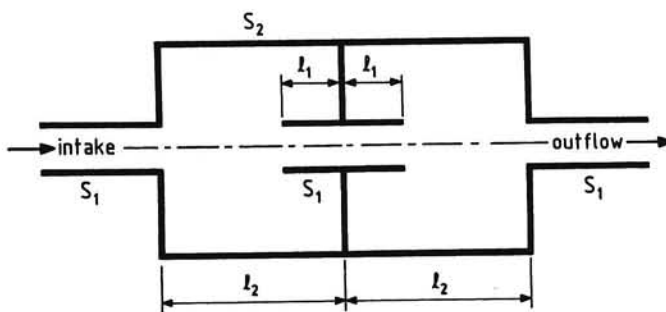


Figure 6.2-3. Schematic diagram of double-expansion chamber muffler

At this point, emphasis is made again that a reactive attenuator reduces only the amount of energy that flows into the outlet tube. This reduction of the transmitted sound is attended by a corresponding increase in the reflected sound. A proportion of the total sound energy will be lost from the attenuator by the occurrence of vibration of the duct walls and another proportion is transformed into heat.

Also a comment is in order concerning the assumption underlying the preceding analyses, that there is no net flow of air or gas in the ducts. In an actual exhaust system, for example, the gas that transports the sound energy is in motion.

The question of the effect of forward velocity on the characteristics of sound radiation is treated in Chapter 11 of this book. The results obtained there indicate that the effect of uniform mean flow without shear on sound transmission will be a function of $(1 - M)^2$, where M is the Mach number corresponding to the flow velocity.

As stated in Reference 26, the permissible engine back pressure limits the Mach number in the exhaust tube to a value appreciably less than one. In the practical range of expansion ratios, the gas velocity inside the expansion chamber is therefore much lower than the outlet tube so that $(1 - M)^2 \approx 1$. Consequently, the gas velocity will have no noticeable effect on the transmission loss of a single expansion chamber muffler. However, in the case of a multiple expansion chamber muffler, the gas velocity in the connecting tube(s) may be so high that the attenuation is changed seriously.

6.3 CLOSED SIDE BRANCH TUBE

In this section we consider the muffler configuration of a duct with a closed tube as a side branch (Figure 6.3-1). Now, in the duct reflection of sound occurs where the side branch leaves, whereby we assume that there is no reflection from the juncture of the branch tube with the duct.

Using the simplification that the tube cross-sectional area is equal to the cross-sectional area of the duct, the boundary conditions of continuity of pressure and mass flow at the discontinuity ($x = y = 0$) become

$$p'_a + p'_c = p'_b \quad (6.3-1)$$

$$p'_t + p'_r = p'_b \quad (6.3-2)$$

$$\rho S(u_a + u_c) = \rho S u_b + \rho S u_t + \rho S u_r . \quad (6.3-3)$$

In these equations the subscripts t and r refer to the incident and reflected

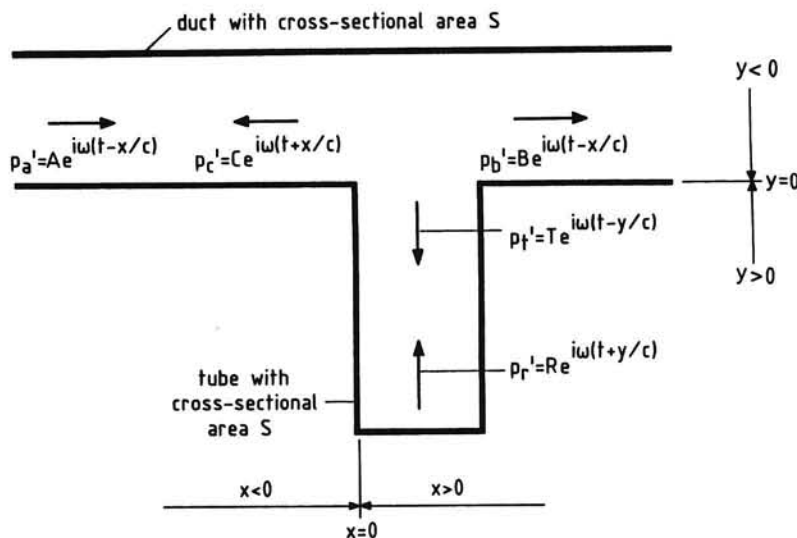


Figure 6.3-1. Duct with a closed side branch tube

waves inside the side branch tube, respectively.

Assuming harmonic, plane waves, we have at $x = y = 0$:

$$A + C = B \quad (6.3-4)$$

$$T + R = B \quad (6.3-5)$$

$$A - C = B + T - R \quad . \quad (6.3-6)$$

The boundary condition at the outer end of the tube gives

$$\rho S(u_t + u_r) = 0 \quad \text{or} \quad T e^{-i\omega l/c} - R e^{i\omega l/c} = 0 \quad . \quad (6.3-7)$$

Thus the reflection factor inside the tube at the juncture is

$$\frac{R}{T} = e^{-i2\omega l/c} \quad . \quad (6.3-8)$$

By elimination of C , T , and R from Equations (6.3-4) to (6.3-7) we find the transmission loss as

$$TL = 10 \log \frac{A^2}{|B|^2} = 10 \log \left(1 + \frac{1}{4} \tan^2 \omega l/c \right) \quad , \text{ dB} \quad . \quad (6.3-9)$$

From Equation (6.3-9) we see that the transmission loss is zero at zero frequency, and that this quantity increases with increasing frequency. We also see that a tube of length l will provide a complete cancellation of the incident sound wave by the reflected wave if the length l is a multiple of $\lambda/4$.

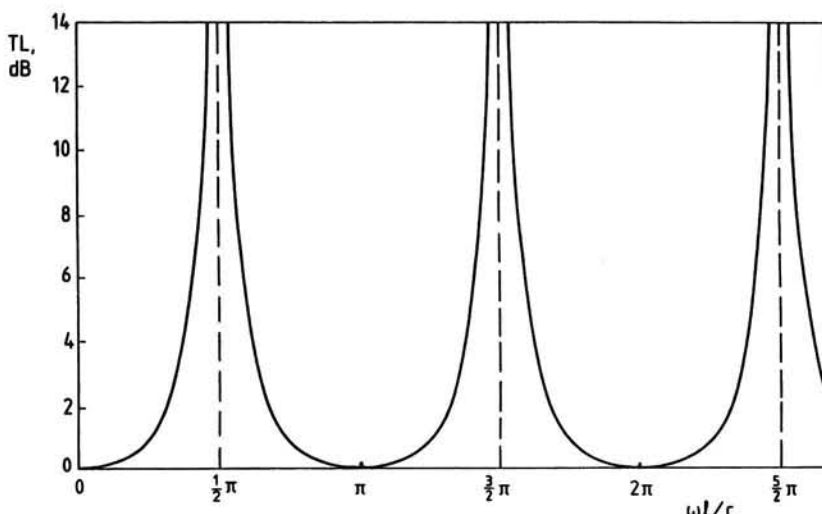


Figure 6.3-2. Attenuation characteristics for closed side branch tube

The attenuation characteristics of the closed side branch tube is presented in Figure 6.3-2. The calculations show that high transmission loss values only are obtained within very narrow frequency regions.

6.4 HELMHOLTZ RESONATOR

As we have already noted in Section 5.3, sound energy is absorbed whenever a sound strikes a porous material into which air can flow. Such materials, e.g., *acoustic foam*, are often used as *resistive attenuators* and are especially effective at higher frequencies where the *absorbent lining* can be relatively thin.

At low frequencies adequate absorption can be obtained by using *resonant cavities* in the surface material. To explain the principles that underlie the workings of this type of absorbent we consider a volume V , having a small circular opening of area S_k and length l (Figure 6.4.1). Such an enclosure with a small opening is called a *Helmholtz resonator*.

Consider the situation that the sound field outside the resonator has a harmonic time dependence,

$$p'_k = K e^{i\omega t} \quad . \quad (6.4-1)$$

The sound pressure p'_k forces the air in the neck to move back and forth so that the air inside the cavity undergoes also alternate compressions and expansions. Clearly, we have the following relationship between the density

variation in the resonator and the shift of the air particles in the neck:

$$\rho'_r = \frac{\rho_\infty x S_k}{V} . \quad (6.4-2)$$

Assuming adiabatic conditions, the sound pressure within the resonator is related to the density disturbance by the linearized Poisson equation, Equation (2.4-17),

$$p'_r = c^2 \rho'_r . \quad (6.4-3)$$

Combining Equations (6.4-2) and (6.4-3) gives

$$p'_r = \frac{c^2 \rho_\infty x S_k}{V} . \quad (6.4-4)$$

From Equations (6.4-1) and (6.4-4), the force acting on the mass of air in the neck can be written as

$$(p'_k - p'_r) S_k = K e^{i\omega t} S_k - \frac{c^2 \rho_\infty x S_k^2}{V} . \quad (6.4-5)$$

Neglecting the effects of friction, we find the equation of motion for the air in the neck of the resonator as

$$\rho_\infty l \frac{d^2 x}{dt^2} + \frac{c^2 x \rho_\infty S_k}{V} = K e^{i\omega t} . \quad (6.4-6)$$

Note that this equation contains the assumption that the air in the neck of the resonator oscillates as a unit of constant mass, i.e., as a solid piston.

The solution of the differential equation (6.4-6) will be of the form

$$x = x_0 e^{i\omega(t+\phi)} . \quad (6.4-7)$$

Differentiating Equation (6.4-7) with respect to time, we obtain

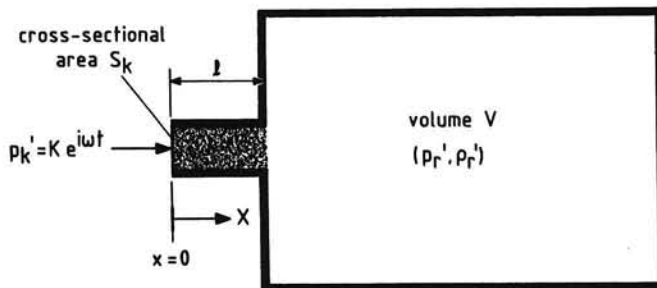


Figure 6.4-1. Helmholtz resonator

$$\frac{dx}{dt} = x_0 i \omega e^{i\omega(t+\phi)} \quad \text{and} \quad (6.4-8)$$

$$\frac{d^2x}{dt^2} = -x_0 \omega^2 e^{i\omega(t+\phi)} \quad . \quad (6.4-9)$$

Substitution of Equations (6.4-7) and (6.4-9) into Equation (6.4-6) furnishes

$$-\rho_\infty l x_0 \omega^2 e^{i\omega(t+\phi)} + \frac{x_0 c^2 \rho_\infty S_k}{V} e^{i\omega(t+\phi)} = K e^{i\omega t} \quad . \quad (6.4-10)$$

The integration constants x_0 and ϕ are found by insertion of known boundary values into Equation (6.4-10).

From substitution of $t = \pi/(2\omega)$ we deduce $\phi = 0$. At $t = 0$,

$$\left[\frac{\rho_\infty c^2 S_k}{V} - \rho_\infty l \omega^2 \right] x_0 = K \quad \text{so that} \quad x_0 = \frac{K}{\rho_\infty \left[\frac{c^2 S_k}{V} - l \omega^2 \right]} \quad .$$

Using the above results in Equation (6.4-7) produces

$$x = \frac{K e^{i\omega t}}{\rho_\infty \left[\frac{c^2 S_k}{V} - l \omega^2 \right]} \quad . \quad (6.4-11)$$

Combining Equation (6.4-4) and (6.4-11) results in a single expression for the sound pressure in the cavity, namely,

$$p_r' = \frac{\frac{c^2 S_k}{V}}{\left[\frac{c^2 S_k}{V} - l \omega^2 \right]} K e^{i\omega t} \quad . \quad (6.4-12)$$

The particle velocity and the mass flow in the neck are obtained from Equation (6.4-11) as

$$u_k = \frac{dx}{dt} = \frac{i \omega K e^{i\omega t}}{\rho_\infty \left[\frac{c^2 S_k}{V} - l \omega^2 \right]} \quad . \quad (6.4-13)$$

$$m_k = \rho_\infty u_k S_k = \frac{i\omega S_k K e^{i\omega t}}{\left[\frac{c^2 S_k}{V} - l \omega^2 \right]} . \quad (6.4-14)$$

Equations (6.4-12) to (6.4-14) show that when $c^2 S_k / V = \omega^2 l$ the sound pressure in the resonator cavity, the particle velocity in the neck, and the mass flow m_k become infinite.

Obviously, this is unrealistic and what actually happens is that the particle velocity is reduced to finite but yet very high values by the frictional effects owing to the rapid alternating motion in the neck of the resonator.

The presence of viscosity has very little effect on the frequency for maximum amplitude (Reference 12). Hence, the so-called *resonant frequency* is given by

$$f_r = \frac{c}{2\pi} \sqrt{\frac{S_k}{Vl}} . \quad (6.4-15)$$

At this particular frequency the small pressure variations at the neck produce large velocities into the resonator, resulting in considerable viscous dissipation of acoustic energy.

A weakness of using a Helmholtz resonator to provide sound attenuation is that this device is especially effective at and near the frequency of resonance which is determined by the dimensions of the resonator. Tuning of the resonator to a particular frequency may be accomplished by varying either the volume of the cavity or the dimensions of the neck, or both.

The next section will be devoted to deriving the equation for the transmission loss due to a single resonator in a side branch.

6.5 SINGLE RESONATOR IN A SIDE BRANCH

To attenuate sound moving through a duct a Helmholtz resonator can be linked to the side of the duct. A schematic diagram of a single resonator is shown in Figure 6.5-1 with the symbols that are used indicated.

At the boundary ($x = 0$) both the pressure and mass flow must be identical, for continuity.

The pressure equality for the assumed plane-wave transmission furnishes:

$$A + C = B . \quad (6.5-1)$$

Continuity of mass flow yields:

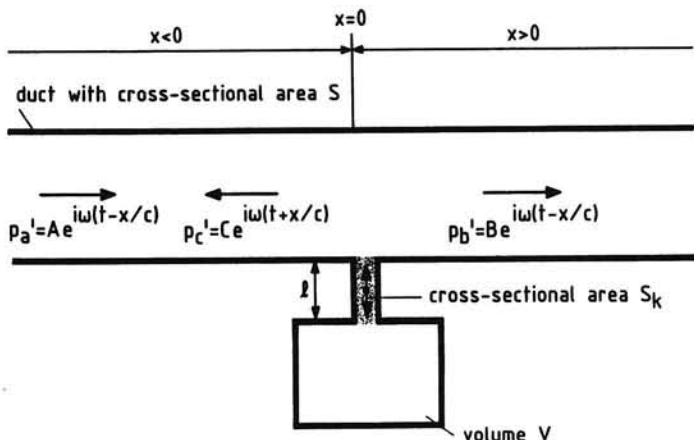


Figure 6.5-1. Duct with resonator

$$\rho S(u_a + u_c) = m_k + \rho S u_b , \quad (6.5-2)$$

where m_k is the rate of mass flowing into the resonator. Using again the plane-wave relationship $p' = \pm \rho c u$ for each of these waves, we obtain from Equation (6.5-2):

$$\frac{S}{c}(A - C)e^{i\omega t} = m_k + \frac{S}{c}B e^{i\omega t} . \quad (6.5-3)$$

An expression for the mass flow m_k is given in the previous section (Equation (6.4-14)), repeated and renumbered below for convenience:

$$m_k = \frac{i\omega S_k K e^{i\omega t}}{\left[\frac{c^2 S_k}{V} - l\omega^2 \right]} . \quad (6.5-4)$$

Solving Equations (6.5-1), (6.5-3) and (6.5-4) for B in terms of A , we get the transmission factor

$$\frac{B}{A} = \frac{1}{1 + \frac{1}{2S} \left[\frac{c}{i\omega V} + \frac{i\omega l}{c S_k} \right]^{-1}} . \quad (6.5-5)$$

The corresponding transmission loss in dB is easily found as

$$TL = 10 \log \frac{A^2}{|B|^2} = 10 \log \left[1 + \frac{1}{4S^2} \left(\frac{c}{\omega V} - \frac{\omega l}{c S_k} \right)^{-2} \right] . \quad (6.5-6)$$

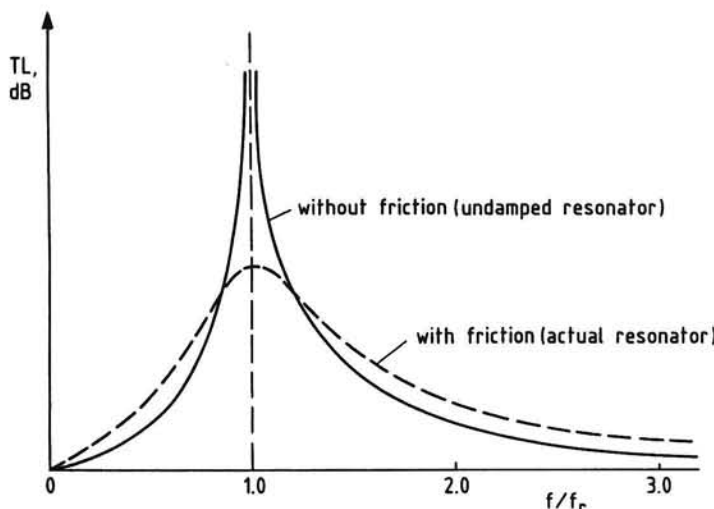


Figure 6.5-2. The effect of adding resistance on the attenuation of a resonator muffler

Using the resonant frequency derived in Section 6.4:

$$f_r = \frac{c}{2\pi} \sqrt{\frac{S_k}{Vl}} , \quad (6.4-15)$$

we can transform Equation (6.5-6) into the form

$$TL = 10 \log \left[1 + \frac{\frac{VS_k}{4S^2l}}{\left[\frac{f}{f_r} - \frac{f_r}{f} \right]^2} \right] , \text{ dB.} \quad (6.5-7)$$

Equations (6.5-6) and (6.5-7) show that the transmission loss rises to infinity at the frequency of resonance. Apparently, the action of a frictionless resonator provides a complete cancellation of the incident sound energy in the duct. As remarked already in Section 6.4, due to the presence of viscosity, in the resonator neck a finite velocity and so a finite attenuation occurs at the resonant frequency. At the same time, generally, adding resistance increases the transmission loss at higher and lower frequencies than the resonant frequency (Figure 6.5-2).

Helmholtz resonators have a great practical meaning because of their

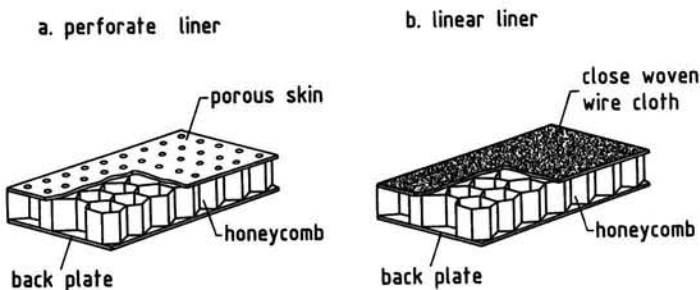


Figure 6.5-3. Acoustic lining materials

application to *mufflers* used for quieting piston-engine exhaust noise. Resonators are also of importance in the construction of sound absorbent duct linings. Then the attenuation material consists of a perforated or porous sheet covering a series of small cavities (Figure 6.5-3). Each cavity functions as a Helmholtz resonator so that the *acoustic lining* exploits both the principles of reactive and resonance attenuation as discussed in Sections 6.3 and 6.4. Of course, its sound attenuation properties can be influenced by varying the porosity of the skin and the cavity dimensions.

Present noise reduction measures applied to turbofan engines involve the use of large areas of lining in the intake and discharge ducts (Figure 6.5-4).

As depicted in Figure 6.5-3, two typical lining structures may be distinguished. The first form, the so-called *perforate liner* or *narrow-band resonator*, is composed of a perforated-plate facesheet bonded to a metal honeycomb, which in turn is attached to a solid backplate, to form a honeycomb sandwich structure. The second design is the so-called *linear liner* or *resistive attenuator*. Now the honeycomb structure is covered by a porous layer through which some additional resistive attenuation is obtained. The

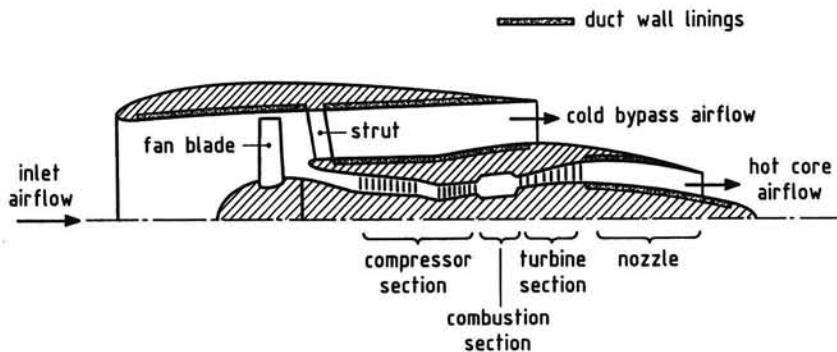


Figure 6.5-4. Acoustic treatment of turbofan engine

latter configuration may provide a better absorption over an enlarged bandwidth of frequencies, and may hold its qualities over a broad range of flight conditions.

6.6 HIGHER ORDER MODES IN DUCTS

The analyses so far have been concerned with the case of plane-wave propagation through rigid ducts. However, in the case of higher-frequency sound we are faced with additional waves, the so-called *higher order modes* of the duct. These waves arise from interference between multiple reflections from the inner walls of the rigid duct, and are characterized by the fact that their pressure distribution over the cross-section of the duct is not uniform. For the higher order modes, the sound pressure depends on the form of the duct cross section since a rigid duct requires that the normal particle velocity is zero at the walls.

Undoubtedly, the most common geometry for ducts employed in propulsion systems is a circular cross section. This gives a solution in terms of Bessel functions with which the reader may be less familiar than trigonometric functions.

To illustrate this phenomenon, we therefore consider a rectangular duct with breadth in y -direction b and depth in z -direction d . The X -axis is oriented parallel to the longitudinal axis of the duct at one corner of the duct walls.

Assuming harmonic time dependence, we can write the homogeneous wave equation as (see Equation (2.9-3))

$$\frac{\partial^2 \phi}{\partial x^2} + \frac{\partial^2 \phi}{\partial y^2} + \frac{\partial^2 \phi}{\partial z^2} + k^2 \phi = 0 , \quad (6.6-1)$$

where the wave number $k = \omega/c$ satisfies the condition:

$$k^2 = k_x^2 + k_y^2 + k_z^2 . \quad (6.6-2)$$

We solve this boundary-value problem by the standard method of separation of variables, yielding solutions of the form

$$\phi(x, y, z, t) = f_1(x)f_2(y)f_3(z)f_4(t) , \quad (6.6-3)$$

where

$$f_1(x) = A_x e^{-ik_x x} + B_x e^{ik_x x} \quad (6.6-4)$$

$$f_2(y) = A_y e^{ik_y y} + B_y e^{-ik_y y} \\ = A_y \cos k_y y + B_y \sin k_y y \quad (6.6-5)$$

$$\begin{aligned}f_3(z) &= A_z e^{ik_z z} + iB_z e^{-ik_z z} \\&= A_z \cos k_z z + B_z \sin k_z z\end{aligned}\quad (6.6-6)$$

$$f_4(t) = e^{i\omega t} . \quad (6.6-7)$$

The wall boundary conditions are

$$\frac{\partial \phi}{\partial y} = 0 \text{ at } y = 0, \quad y = b \quad \left. \right\} \quad (6.6-8)$$

and

$$\frac{\partial \phi}{\partial z} = 0 \text{ at } z = 0, \quad z = d . \quad \left. \right\}$$

Then the characteristic function $f_2(y)$ can be written as

$$f_2(y) = A_{xm} \cos\left(\frac{m\pi y}{b}\right) , \quad (6.6-9)$$

where $m = 0, 1, 2, \dots$ represents an infinite number of possibilities.

Similarly, we obtain for $f_3(z)$

$$f_3(z) = A_{zn} \cos\left(\frac{n\pi z}{d}\right) , \quad n = 0, 1, 2, \dots \quad (6.6-10)$$

From Equation (6.6-2), we see that for a given mode (m, n) , the component of the wave number vector in the x -direction is

$$k_x = \pm k_{mn} = \pm \sqrt{k^2 - \left(\frac{m\pi}{b}\right)^2 - \left(\frac{n\pi}{d}\right)^2} . \quad (6.6-11)$$

By the principle of superposition, the complete solution is

$$\begin{aligned}\phi(x, y, z, t) &= \sum_{m=0}^{\infty} \sum_{n=0}^{\infty} \cos\left(\frac{m\pi y}{b}\right) \cos\left(\frac{n\pi z}{d}\right) \times \\&\quad \times \left[A_{mn} e^{i(\omega t - k_{mn} x)} + B_{mn} e^{i(\omega t + k_{mn} x)} \right] ,\end{aligned}\quad (6.6-12)$$

where A_{mn} and B_{mn} are constants.

In Equation (6.6-12), the terms

$$\cos\left(\frac{m\pi y}{b}\right) \cos\left(\frac{n\pi z}{d}\right) A_{mn} e^{i(\omega t - k_{mn}x)}$$

and

$$\cos\left(\frac{m\pi y}{b}\right) \cos\left(\frac{n\pi z}{d}\right) B_{mn} e^{i(\omega t + k_{mn}x)}$$

represent waves going in the positive and negative x -direction, respectively. Returning to Equation (6.6-11), it can be seen that the higher modes are traveling at an axial speed:

$$c_{mn} = \frac{\omega}{k_{mn}} = \frac{\omega}{\sqrt{k^2 - \left(\frac{m\pi}{b}\right)^2 - \left(\frac{n\pi}{d}\right)^2}} . \quad (6.6-13)$$

This propagation speed is greater than the speed of sound in free space $c = \omega/k$ which occurs at the fundamental or plane-wave mode, the $m = n = 0$ case.

At very high frequencies the speed c_{mn} is very large. As the frequency of the sound decreases, also the speed c_{mn} falls off. There exists a frequency at which for a given mode (m, n) the speed c_{mn} becomes imaginary. This particular frequency is called the *cutoff frequency*, because below this frequency there is no transfer of sound energy.

From Equation (6.6-13), the condition for the cutoff frequency is

$$f_{mn} = \frac{\omega_{mn}}{2\pi} = \frac{c}{2} \sqrt{\left[\left(\frac{m}{b}\right)^2 + \left(\frac{n}{d}\right)^2\right]} . \quad (6.6-14)$$

At frequencies lower than f_{mn} , the dependence of the amplitude of the mode on distance in the positive x -direction is through $\exp(-|k_{mn}|x)$, and for waves going in the negative x -direction through $\exp(|k_{mn}|x)$.

This means that there is an exponential decay with distance along the duct. The lower the excitation frequency is, compared to the cutoff frequency, the faster is the attenuation resulting in no propagation.

In conclusion, remember that the complete solution for the velocity potential inside a rigid duct shows that there may be an infinite number of modes for the transmission of sound energy. However, only the plane-wave mode exists at any frequency. A finite number of higher order modes are possible at frequencies which are greater than the cutoff frequency.

7 FREQUENCY SPECTRA

7.1 GENERAL

In the preceding chapters we have been considering the generation and transmission of pure tones only. However, as already pointed out in Section 1.12, the sound power output of a noise source is usually distributed over a large range of frequencies.

The availability of the source frequency spectra at a given distance and at various emission angles is essential in finding the dominant source component and so in reducing noise at source. Also, accounting for noise attenuation by the propagation through the atmosphere and making efficient use of absorbent materials, demand a knowledge of the distribution of the sound intensity with respect to frequency.

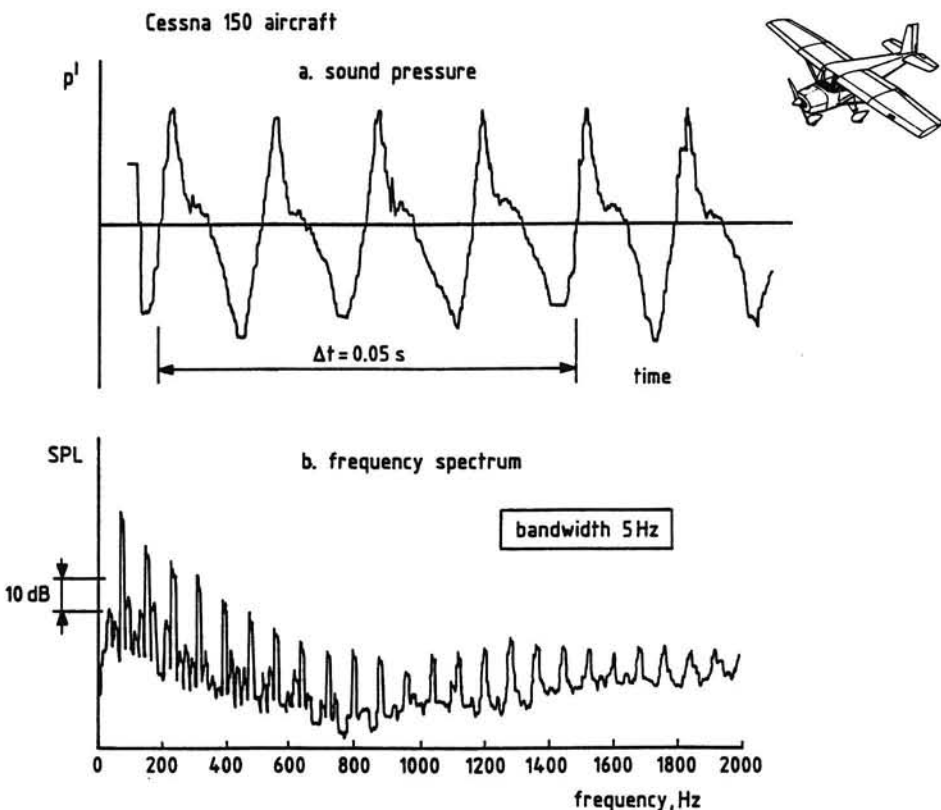


Figure 7.1-1. Sound pressure time history and frequency content for propeller airplane under static conditions

Moreover, as will be discussed in Chapter 9, the frequency content determines the perceived loudness since the sensitivity of the human ear depends on the sound frequency.

Figure 7.1-1a shows the highly periodic time history of the sound pressure variation obtained from static noise measurements of a small propeller-driven airplane; see also the introductory Figure 1.12-1c. The corresponding frequency spectrum is given in Figure 7.1-1b. The latter chart clearly demonstrates the discrete frequency characteristics of propeller-driven airplane noise.

In Figure 7.1-2a is presented the stationary noise signal from a small jet-airplane powered by two turbofan-engines. The related spectrogram (Figure 7.1-2b) indicates that the noise consists of a mixture of broadband noise and individual tones.

The airplane of Figure 7.1-1 is single-engined and has a two-bladed, ungeared propeller, driven by a four-cylinder piston-engine. The peak level in

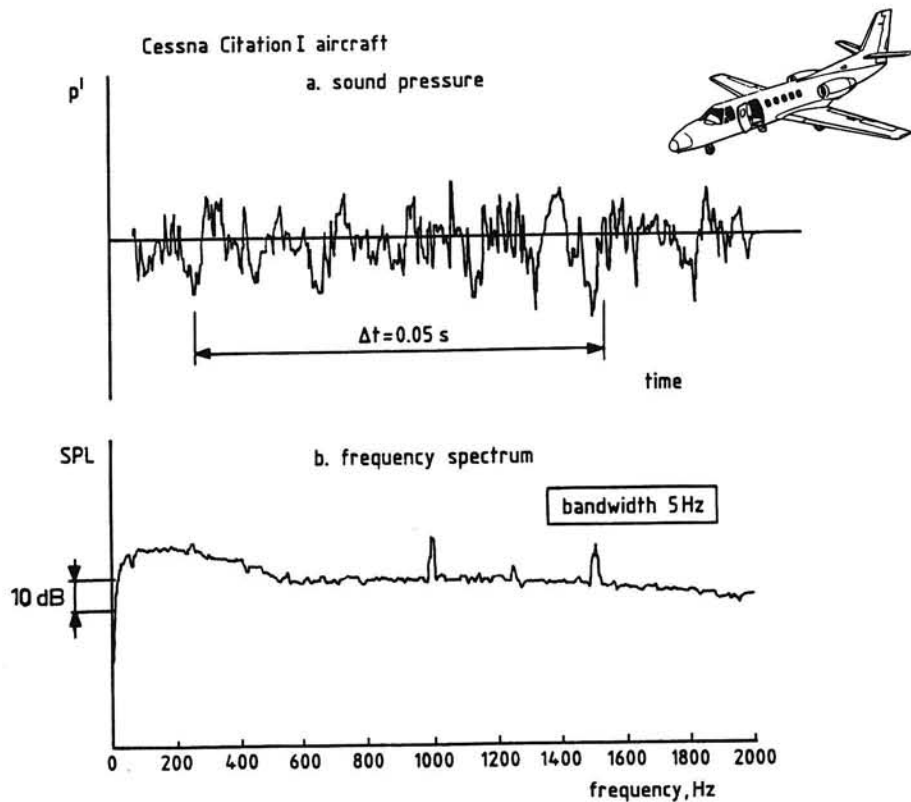


Figure 7.1-2. Sound pressure time history and frequency content for turbofan airplane operating statically

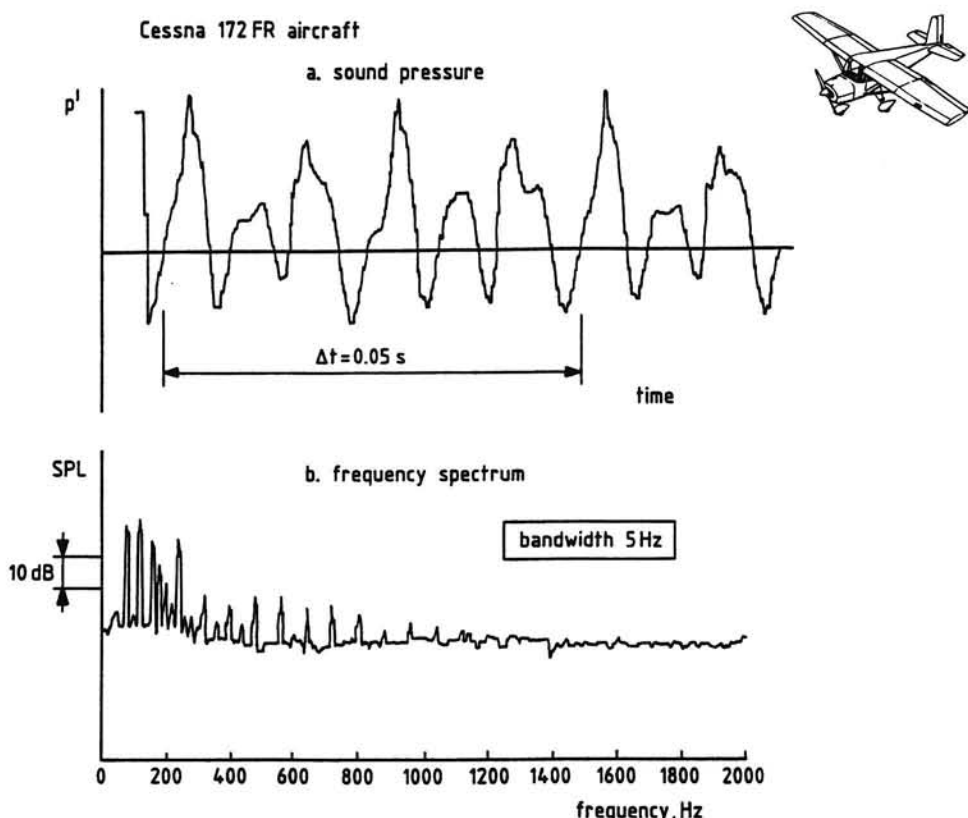


Figure 7.1-3. Sound pressure time history and frequency content for propeller airplane operating statically

Figure 7.1-1b is associated with the *propeller blade passage frequency* and the *engine exhaust firing frequency*. The rest of the peaks are higher harmonics, i.e., integral multiples of the blade passage frequency. Typical are the relative high sound pressure levels at low order harmonics.

The propeller blade passage frequency, f_1 , is given by the relationship:

$$f_1 = B \frac{n_p}{60} , \text{ Hz} \quad (7.1-1)$$

where B is the number of propeller blades and n_p is the propeller rotational speed in rpm (rotations per minute). With $B = 2$ and $n_p = 2400 \text{ rpm}$, we have

$$f_1 = 2 \times \frac{2400}{60} = 80 \text{ Hz} .$$

Since the engine is operating on the four-stroke cycle principle, see Chapter 12, the corresponding relationship for the exhaust firing frequency, f_e , is

$$f_e = N \frac{n/2}{60} , \text{ Hz} \quad (7.1-2)$$

where N is the number of cylinders and n is the engine rotational speed in rpm. With $N = 4$ and $n = n_p = 2400$ rpm we thus find $f_e = f_1$.

Because of this condition the contributions from propeller and engine cannot be separated in the spectrum.

When individual cylinders have different characteristics it may be possible that noise components are found at multiples of the *cylinder firing frequency*, f_c , where

$$f_c = \frac{n/2}{60} , \text{ Hz} . \quad (7.1-3)$$

Figure 7.1-3 shows the sound pressure time history and the associated frequency spectrum measured of a single-engine small airplane with a two-bladed, ungeared propeller driven by a six-cylinder piston-engine. Since now $f_e \neq f_1$, propeller and engine noise components may be discerned in the frequency spectrum.

The spectra in Figures 7.1-1b to 7.1-3b are derived from *frequency analysis*, that is the procedure of determining the contributions to the total sound pressure level made by the individual frequencies. The mathematical basis for all frequency analysis procedures is the *Fourier transform* which we deal with in brief in the following section.

7.2 FOURIER TRANSFORM

The mathematical operation for resolving a sound signal into its frequency components is based on the *Fourier theorem*, which states that any periodic time function can be represented as a series of pure tones of increasing frequency.

The *Fourier series* corresponding to the periodic function $f(t)$ is given by (Reference 16):

$$f(t) = \sum_{k=0}^{\infty} (A_k \cos 2\pi k f_1 t + B_k \sin 2\pi k f_1 t) , \quad (7.2-1)$$

where the *Fourier coefficients* are

$$A_0 = \frac{1}{T} \int_0^T f(t) dt \quad (7.2-2)$$

$$A_k = \frac{2}{T} \int_0^T f(t) \cos 2\pi k f_1 t dt \quad (k = 1, 2, 3, \dots) \quad (7.2-3)$$

$$B_k = \frac{2}{T} \int_0^T f(t) \sin 2\pi k f_1 t dt \quad (k = 1, 2, 3, \dots) . \quad (7.2-4)$$

In these equations T is the period and $f_1 = 1/T$ is the fundamental frequency of the sound signal.

The separate terms of Equation (7.2-1) are called *harmonics* and their frequencies are integer multiples of the fundamental mode.

Note that in the Fourier series corresponding to an odd function, $f(-x) = -f(x)$, only sine terms are present. On the contrary, the Fourier series corresponding to an even function, $f(-x) = f(x)$, consists of cosine terms only.

A complex notation for the Fourier series can be obtained by employing the Euler identities:

$$\cos x = \frac{1}{2} (e^{ix} + e^{-ix}) \quad \text{and} \quad \sin x = \frac{1}{2i} (e^{ix} - e^{-ix}) .$$

Then, it is an easy matter to transform Equation (7.2-1) into the form

$$f(t) = \sum_{k=-\infty}^{\infty} C_k e^{i 2\pi k f_1 t} , \quad (7.2-5)$$

where the complex Fourier spectrum coefficients C_k are obtained from the integral

$$C_k = \frac{1}{T} \int_0^T f(t) e^{-i 2\pi k f_1 t} dt . \quad (7.2-6)$$

As an example we consider the square wave of Figure 7.2-1a. Fourier analysis of this periodic function yields the series:

$$f(\omega t) = \frac{A}{2} + \sum \frac{2A}{k\pi} \sin k \omega t \quad (k = 1, 3, 5, \dots) . \quad (7.2-7)$$

The result shows that a square wave is represented in the frequency domain by an infinite number of discrete lines at the odd harmonics of the fundamental frequency (Figure 7.2-1b).

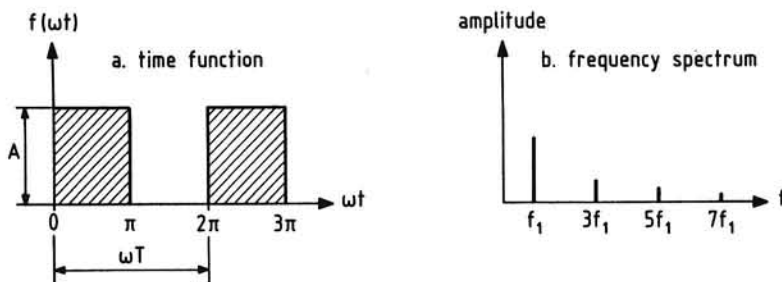


Figure 7.2-1. Square wave and its spectrum

It is quite obvious that usually the function $f(t)$ is not directly integrable. Then, the spectrum coefficients must be determined by approximate integration procedures. To perform this operation, a number of algorithms and instruments have been developed.

We may also be faced with the difficulty of a broadband (random) time signal which, naturally, is a nonperiodic noise whose instantaneous amplitude is not specified at any instant.

Fortunately, it is feasible to extend Equation (7.2-6) to the case of stationary random noises if we allow the periodic time to tend to infinity. To explain this we consider the sound pressure variation for a random signal as shown in the upper part of Figure 7.2-2.

For this time function we express the Fourier spectrum coefficients in the form of Equation (7.2-6) for a time length T .

Clearly, by letting $T \rightarrow \infty$ the fundamental frequency dies out to a small quantity Δf and the harmonics become $k\Delta f$ which may be denoted by f .

Apparently, the discrete frequencies of the spectrum are compressed such that the coefficients C_k become a continuous function of frequency.

Equation (7.2-6) can now be expressed as

$$\begin{aligned} \lim_{T \rightarrow \infty} C_k &= \lim_{T \rightarrow \infty} \frac{1}{T} \int_0^T p'(t) e^{-i2\pi ft} dt \\ &= \Delta f \int_{-\infty}^{\infty} p'(t) e^{-i2\pi ft} dt . \end{aligned} \quad (7.2-8)$$

We may write Equation (7.2-8) in the form

$$C(f) = \int_{-\infty}^{\infty} p'(t) e^{-i2\pi ft} dt . \quad (7.2-9)$$

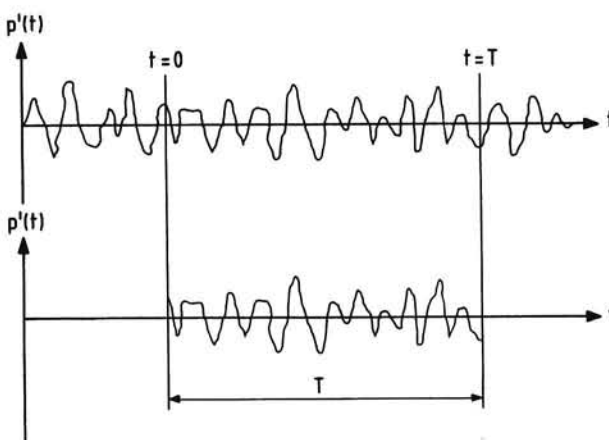


Figure 7.2-2. Frequency analysis of broadband noise

This equation transforms for each frequency the time function $p'(t)$ into its complex frequency elements $C(f)$. The function $C(f)$ is called the *Fourier transform* of $p'(t)$.

A relationship similar to that between Equations (7.2-6) and (7.2-9) exists for the time function (7.2-5), which can be represented as an integral of its spectrum elements:

$$p'(t) = \int_{-\infty}^{\infty} C(f) e^{i2\pi ft} df . \quad (7.2-10)$$

Equation (7.2-10) shows that the time function $p'(t)$ can be obtained from its frequency elements. The function $p'(t)$ is known as the *inverse Fourier transform* of $C(f)$. The two Equations (7.2-9) and (7.2-10) are called the *Fourier transform pair*.

For the various techniques of calculating the Fourier coefficients specialized text-books must be consulted; see e.g. Reference 27.

In order to demonstrate the use of the Fourier transform pair, in the following we will solve the problem of finding the Fourier transform of a rectangular time function. The function $f(t)$ may be defined as (Figure 7.2-3):

$$f(t) = \begin{cases} A, & |t| < T/2 \\ 0, & |t| > T/2 \end{cases} . \quad (7.2-11)$$

From Equation (7.2-9) the transform of $f(t)$ is

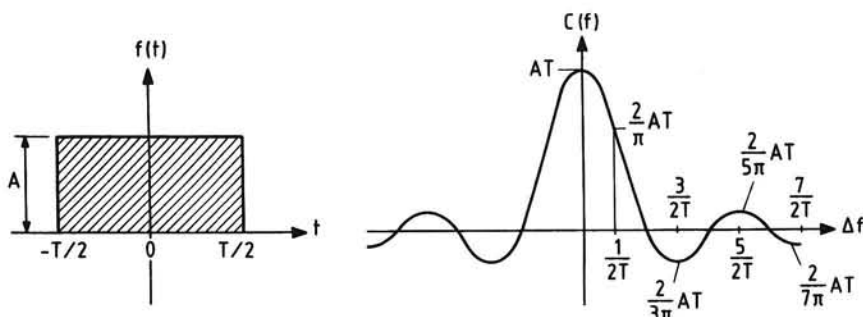


Figure 7.2-3. Fourier transform of rectangular time function

$$\begin{aligned}
 C(f) &= \int_{-T/2}^{T/2} A e^{-i2\pi f t} dt = -\frac{A}{i2\pi f} \int_{-T/2}^{T/2} de^{-i2\pi f t} \\
 &= -\frac{A}{i2\pi f} [e^{-i\pi f T} - e^{i\pi f T}] = A T \frac{\sin \pi f T}{\pi f T} . \quad (7.2-12)
 \end{aligned}$$

For $f = 0$, we obtain $C(f) = A T$ since $\lim_{x \rightarrow 0} \frac{\sin x}{x} = 1$.

The function (7.2-12) is also plotted in Figure 7.2-3, showing that we have successive amplitudes at $\Delta f = 1/2T, 3/2T, 5/2T$, etc.

Conversely, it is illustrative to determine $f(t)$ from Equations (7.2-10) and (7.2-12). Together these give

$$\begin{aligned}
 f(t) &= \int_{-\infty}^{\infty} A \frac{\sin \pi f T}{\pi f} e^{i2\pi f t} df = \frac{A}{2\pi} \int_{-\infty}^{\infty} \frac{1}{i2\pi f} [e^{i\pi f T} - e^{-i\pi f T}] e^{i2\pi f t} d2\pi f \\
 &= \frac{A}{2\pi} \int_{-\infty}^{\infty} \frac{1}{i2\pi f} e^{i\pi f T} [1 - e^{-i2\pi f T}] e^{i2\pi f t} d2\pi f \\
 &= \frac{A}{2\pi} \left[\int_0^{\infty} \frac{[1 - e^{-i2\pi f T}]}{i2\pi f} e^{i2\pi f(t+T/2)} d2\pi f + \int_0^{\infty} \frac{[1 - e^{i2\pi f T}]}{-i2\pi f} e^{-i2\pi f(t+T/2)} d2\pi f \right] \\
 &= \frac{A}{i2\pi} \int_0^{\infty} [e^{i2\pi f(t+T/2)} - e^{i2\pi f(t-T/2)} - e^{-i2\pi f(t+T/2)} + e^{-i2\pi f(t-T/2)}] \frac{d2\pi f}{2\pi f} \\
 &= \frac{A}{\pi} \int_0^{\infty} \left[\frac{\sin 2\pi f(t+T/2)}{2\pi f} - \frac{\sin 2\pi f(t-T/2)}{2\pi f} \right] d2\pi f . \quad (7.2-13)
 \end{aligned}$$

Generally, the integral $F(u) = \int_0^\infty \frac{\sin ux}{x} dx$ from calculus is:

$$F(u) = \pi/2 \text{ for } u > 0; F(u) = 0 \text{ for } u = 0; F(u) = -\pi/2 \text{ for } u < 0.$$

Accordingly, the integral (7.2-13) is A for $-1/2 T < t < 1/2 T$ and zero for $1/2 T < t < -1/2 T$. This result is precisely $f(t)$ as defined by Equation (7.2-11).

For stationary random noise signals Equation (7.2-9) tends to zero since $p'(t)$ has a zero mean value. This problem is remedied by basing the analyses on a finite time interval.

As illustrated in the lower part of Figure 7.2-2, considering a length of time T and replacing the sound pressures outside this range by zero, we can write

$$C(f) = \int_0^T p'(t) e^{-i2\pi ft} dt , \quad (7.2-14)$$

where $p'(t)$ is given by Equation (7.2-10).

Now the values of $C(f)$ become unequal to zero because the time interval has a finite length.

The corresponding variation of sound intensity with frequency follows from the mean square pressures in infinitesimal frequency intervals. For nonperiodic stationary functions the mean square value is given by

$$\overline{[f(t)]^2} = \lim_{T \rightarrow \infty} \frac{1}{T} \int_0^T [f(t)]^2 dt . \quad (7.2-15)$$

In order to ensure that the average remains finite, the limit is taken as T approaches infinity (Reference 8).

From Equations (7.2-10) and (7.2-15) we obtain the mean square pressure as

$$\begin{aligned} \overline{[p'(t)]^2} &= \lim_{T \rightarrow \infty} \frac{1}{T} \int_0^T [p'(t)]^2 dt = \lim_{T \rightarrow \infty} \frac{1}{T} \left[\int_0^T p'(t) dt \int_{-\infty}^{\infty} C(f) e^{i2\pi ft} df \right] \\ &= \lim_{T \rightarrow \infty} \frac{1}{T} \left[\int_{-\infty}^{\infty} C(f) df \int_0^T p'(t) e^{i2\pi ft} dt \right] \\ &= \int_{-\infty}^{\infty} \lim_{T \rightarrow \infty} \frac{|C(f)|^2}{T} df . \end{aligned} \quad (7.2-16)$$

Equation (7.2-16) may be rewritten as

$$\overline{[p'(t)]^2} = \int_{-\infty}^{\infty} P(f) df , \quad (7.2-17)$$

where the quantity $P(f) = \lim_{T \rightarrow \infty} |C(f)|^2/T$ is called the *power spectral density*.

It should be appreciated that the power spectral density represents the sound intensity per unit frequency interval and thus must be integrated over a finite frequency interval to yield a finite intensity.

7.3 BANDWIDTH

In order to determine the spectral composition of a sound signal several frequency analysis systems are available today. For a detailed discussion on the principles of the workings of existing appliances by which the audible frequency range can be divided into smaller ranges, the reader is also referred to the specialized literature on this subject. Here, it is suffice to say that two types of *analyzers* can be distinguished: (1) constant bandwidth analyzers, and (2) constant percentage bandwidth analyzers. It may be noted that the term *bandwidth* originates from the use of *bandpass filters*, which have the property of transmitting only the sound power of the components lying within a particular *passband* of width Δf , and attenuating totally all the energy at frequencies outside the selected passband.

Constant percentage bandwidths are characterized by the fact that the frequency interval increases as the frequency increases. The *center frequency* of a passband, f_i , is defined by the geometric mean of its limiting frequencies, i.e., the midpoint on a logarithmic scale:

$$\log f_i = \frac{1}{2} [\log f_u + \log f_l] \quad \text{or} \quad f_i = \sqrt{f_u f_l} , \quad (7.3-1)$$

where f_u is the upper limiting frequency of a band and f_l the lower limiting frequency.

The largest constant percentage bandwidths are *octave bands*, over which the frequency doubles. Then, from Equation (7.3-1) we see that the upper limiting frequency is $2^{1/2}$ times the center frequency, and that the center frequency is $2^{1/2}$ times the lower limiting frequency. Thus

$$\left. \begin{aligned} f_u &= 2 f_l \\ f_u &= 2^{1/2} f_i \\ f_i &= 2^{1/2} f_l \end{aligned} \right\} \quad (7.3-2)$$

Dividing the bandwidth by the center frequency produces

$$\frac{\Delta f}{f_i} = \frac{f_u - f_l}{f_i} = \sqrt{2} - \frac{1}{\sqrt{2}} = \frac{1}{\sqrt{2}} = 0.71 \quad . \quad (7.3-3)$$

This result shows that the passband encompasses a frequency range equal to 71% of the mid-frequency.

From the relations (7.3-2) it also follows that the center frequency of each successive octave band is twice the center frequency of the previous one.

It may be remarked that the width of an octave band represents one-eighth of the frequency range covered by the familiar musical instruments. In order to demonstrate this connection, a top view of the piano keyboard is shown in Figure 7.3-1.

Preferred frequencies for acoustical measurements are established by the *International Organization for Standardization* (Reference 28). Table 7.3-1 lists the recommended series of octave band center frequencies and the corresponding limits of the passbands. The center frequencies given in this table are computed from the formula

$$f_i = 10^{3n/10}, \quad (7.3-4)$$

where n is an integer which is called the *band number* ($n = 0-14$).

Usually, however, not the band numbers, but the center frequencies are used to identify the passbands.

The sound pressure level within a specified frequency band is called the *pressure band level* (PBL). The sound pressure level for the sound

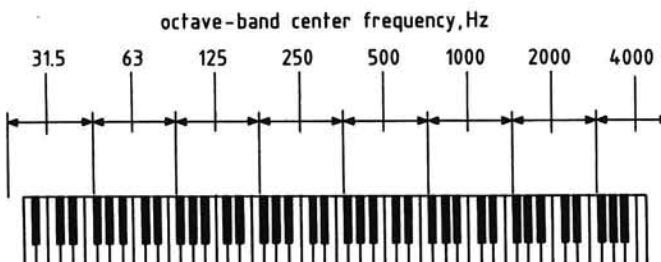


Figure 7.3-1. Piano keyboard frequency range

Table 7.3-1 Octave bands

band number, n	center frequency, Hz	passband, Hz	band number, n	center frequency, Hz	passband, Hz
1	2	1.41 - 2.82	8	250	178 - 355
2	4	2.82 - 5.62	9	500	355 - 708
3	8	5.62 - 11.2	10	1000	708 - 1410
4	16	11.2 - 22.4	11	2000	1410 - 2820
5	31.5	22.4 - 44.7	12	4000	2820 - 5620
6	63	44.7 - 89.1	13	8000	5620 - 11200
7	125	89.1 - 178	14	16000	11200 - 22400

intensity contained within a band 1 Hz wide centered at a specified frequency is termed the *pressure spectrum level* (PSL) of a sound at the specified frequency.

If, as is depicted in Figure 7.3-2, we assume equal intensity per unit frequency bandwidth, i.e., white noise, the pressure spectrum level is constant. The plotted points show that the associated pressure band level increases with frequency. In this case the relationship between the two levels is

$$PBL = 10 \log \frac{p_e^2 \Delta f}{p_{e_0}^2} = PSL + 10 \log \Delta f , \quad (7.3-5)$$

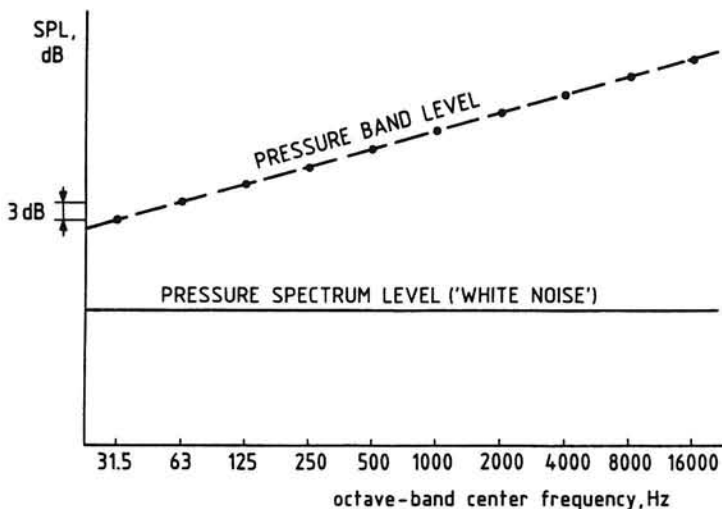


Figure 7.3-2. Pressure band level versus octave-band center frequency for white noise emission

or with Equation (7.3-3)

$$\text{PBL} = \text{PSL} + 10 \log 0.71 f_i . \quad (7.3-6)$$

From Equation (7.3-6) we conclude that the pressure band level increases with frequency at a rate of 3 dB per octave band.

It may be noted that another special form of broadband noise is *pink noise*, whose pressure spectrum level decreases with frequency such that the pressure band level remains constant for each band.

When more information about a complex sound is desired, it is convenient to space the frequencies by fractions of an octave interval. For example, the audible range can be divided into *half-octave bands*, of which the bandwidths are defined by:

$$\left. \begin{aligned} f_u &= 2^{1/2} f_l \\ f_u &= 2^{1/4} f_i \\ f_i &= 2^{1/4} f_l \end{aligned} \right\} \quad (7.3-7)$$

This gives

$$\frac{\Delta f}{f_i} = \frac{f_u - f_l}{f_i} = 2^{1/4} - \frac{1}{2^{1/4}} = 0.35 . \quad (7.3-8)$$

The center frequencies may be computed from the relationship:

$$f_i = 10^{2n/10} \quad (n = 0 - 28) \quad (7.3-9)$$

Now the center frequency of each consecutive half-octave band is $2^{1/2}$ times the center frequency of the preceding one.

All existing procedures for describing aircraft noise require measurement data of the noise produced in *1/3-octave bands (tertsbands)*. Their bandwidths are defined as follows:

$$\left. \begin{aligned} f_u &= 2^{1/3} f_l \\ f_u &= 2^{1/6} f_i \\ f_i &= 2^{1/6} f_l \end{aligned} \right\} \quad (7.3-10)$$

Equation (7.3-10) gives us

Table 7.3-2 One-third-octave bands

band number, n	center frequency, Hz	passband, Hz	band number, n	center frequency, Hz	passband, Hz
1	1.25	1.12 - 1.41	23	200	178 - 224
2	1.6	1.41 - 1.78	24	250	224 - 282
3	2	1.78 - 2.24	25	315	282 - 355
4	2.5	2.24 - 2.82	26	400	355 - 447
5	3.15	2.82 - 3.55	27	500	447 - 562
6	4	3.55 - 4.47	28	630	562 - 708
7	5	4.47 - 5.62	29	800	708 - 891
8	6.3	5.62 - 7.08	30	1000	891 - 1120
9	8	7.08 - 8.91	31	1250	1120 - 1410
10	10	8.91 - 11.2	32	1600	1410 - 1780
11	12.5	11.2 - 14.1	33	2000	1780 - 2240
12	16	14.1 - 17.8	34	2500	2240 - 2820
13	20	17.8 - 22.4	35	3150	2820 - 3550
14	25	22.4 - 28.2	36	4000	3550 - 4470
15	31.5	28.2 - 35.5	37	5000	4470 - 5620
16	40	35.5 - 44.7	38	6300	5620 - 7080
17	50	44.7 - 56.2	39	8000	7080 - 8910
18	63	56.2 - 70.8	40	10000	8910 - 11200
19	80	70.8 - 89.1	41	12500	11200 - 14100
20	100	89.1 - 112	42	16000	14100 - 17800
21	125	112 - 141	43	20000	17800 - 22400
22	160	141 - 178			

$$\frac{\Delta f}{f_i} = \frac{f_u - f_l}{f_i} = 2^{1/6} - \frac{1}{2^{1/6}} = 0.23 , \quad (7.3-11)$$

or a bandwidth of 23% of the center frequency.

For white noise emission, the reading on consecutive tertbands is increased by one dB. The ratio of two adjacent tertband center frequencies is $2^{1/3}$ and the relationship between center frequency and band number is

$$f_i = 10^{n/10} \quad (n = 0 - 43) . \quad (7.3-12)$$

The set of standardized 1/3-octave center frequencies is given in Table 7.3-2.

Finally, we may mention the subdivision into 1/12-octave bands (see the piano keyboard in Figure 7.3-1), where the frequency intervals are defined by:

$$\left. \begin{aligned} f_u &= 2^{1/12} f_l \\ f_u &= 2^{1/24} f_i \\ f_i &= 2^{1/24} f_l \end{aligned} \right\} \quad (7.3-13)$$

and $\Delta f/f_i = 0.058$.

The relationship between center frequency and band number is given by

$$f_i = 10^{n/40} \quad (n = 0 - 169) \quad (7.3-14)$$

and the ratio of two successive center frequencies is $2^{1/12}$.

7.4 EFFECT OF BANDWIDTH ON MEASURED SPECTRA

The noise data portrayed in the previous Figures 7.1-1 and 7.1-3 were obtained from measurements made of two different propeller airplanes operating statically. The noise source of Figure 7.1-1a was a Cessna 150 aircraft, having a two-bladed, fixed-pitch propeller directly driven by a four-cylinder piston-engine. The noise source of Figure 7.1-3 was a Cessna 172FR aircraft which also is equipped with a two-bladed, ungeared, constant speed propeller. The source of power, however, is now a six-cylinder piston-engine. Both airplanes were tested at an engine speed of 2400 rpm.

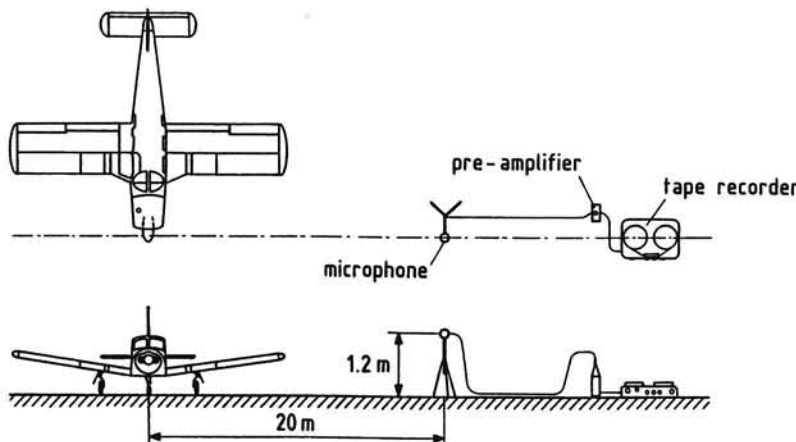


Figure 7.4-1. Schematic layout of noise test facility (not to scale)

As depicted in Figure 7.4-1, the microphone was mounted on a pole at a height of 1.2 m above ground level and located in the extension of the propeller plane, at a distance of 20 m from the propeller axis. It should be noted that placement of the microphone at a height of 1.2 m is the most frequently employed method to acquire airplane noise data since the human ear is usually somewhere between a height of 0.8 m (sitting) and 1.6 m (standing). Accordingly, 1.2 m seems an acceptable mean to measure noise levels as perceived by people on the ground.

The noise was measured by use of a Brüel & Kjaer (B&K) 4144 pressure-type condenser microphone with a foam windshield, a pre-amplifier (B&K 2204 sound level meter), and a Nagra IV D tape recorder. By means of a B&K 2031 Narrow Band Spectrum Analyzer, frequency analyses in 400 channels were made. A full-scale frequency range of 0-2000 Hz was selected, providing a constant bandwidth of 5 Hz.

Extremely detailed pictures of the frequency contents are shown in Figure 7.4-2, where a full-scale frequency range of 500 Hz is used, giving a

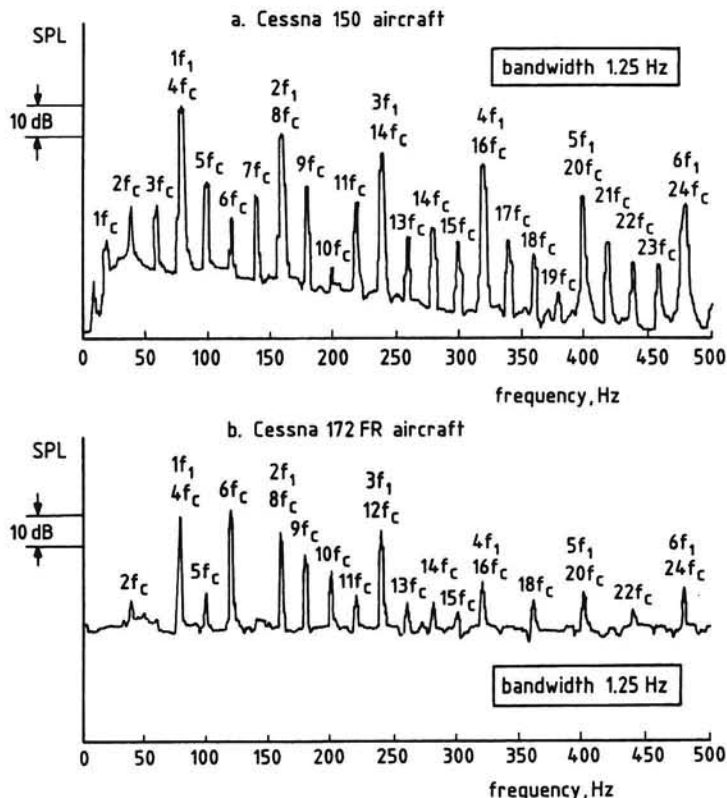


Figure 7.4-2. Narrow-band spectra

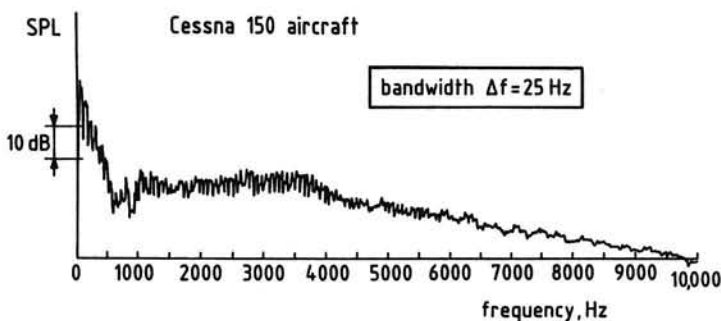


Figure 7.4-3. Propeller airplane noise spectrum

bandwidth of only 1.25 Hz. In both spectra, the repetitive pattern of the cylinder firing frequency is now undoubtedly discernible.

Since for the Cessna 172FR airplane the engine exhaust firing frequency and the blade passage frequency are not harmonically related, it is not difficult to separate the noise from propeller and engine ($f_1 = 80 \text{ Hz}$ and $f_e = 6 f_c = 120 \text{ Hz}$).

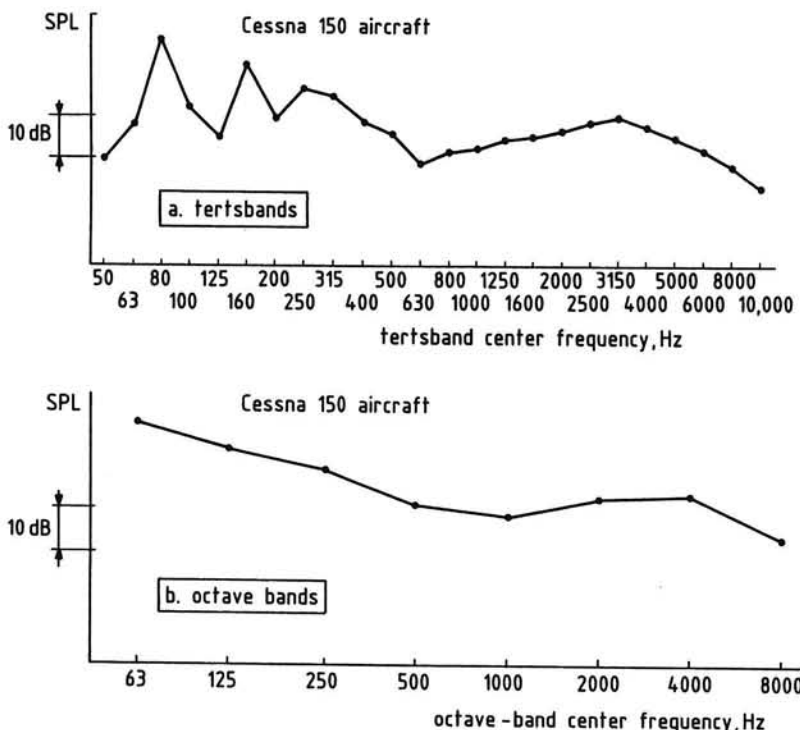


Figure 7.4-4. Propeller airplane noise spectra

To demonstrate the effect of increasing the bandwidth on the shape of the spectrum, the spectrum plotted in Figure 7.1-1b is shown in Figure 7.4-3 for constant frequency bands with a width of 25 Hz. Apparently, with the larger bandwidth it is less easier to recognize the individual harmonics.

Figure 7.4-4a shows how the noise spectrum in Figure 7.1-1b appears when measured in successive one-third octave bands.

The pressure band levels are represented by the plotted points. The straight lines joining the points are drawn to bring out the general shape of the spectrum. However, reading sound pressure levels in between the points is meaningless.

Figure 7.4-4b shows the spectrogram of the same noise as in Figure 7.4-4a plotted in octave bands. These frequency spectra demonstrate that the wider the frequency band, the less clearly visible do the individual harmonics become in the analysis. Especially at higher frequencies the discrete components are seen in a more diluted form since a number of harmonics may be confined within a single passband.

7.5 MEASURED SPECTRA FROM FLYOVERS

Basically, the primary single qualification of a noise source is the total acoustic energy radiated into the air per unit time (the acoustic power). A complete description must include also the distribution of the total acoustic power with regard to space and frequency.

Practically, the external noise field generated by an airplane may be defined by the tertsbandsound pressure level spectra at a given distance from the source for a number of emission angles. For a complete specification, of course, these spectra have to be known for a range of operating conditions of the airplane. In this respect it is important to note that also the configuration of the airplane, i.e., landing gear position, flap angle, air brake and spoiler deflections, and number of operative engines, may have a noticeable influence on the directional characteristics of the sound field.

The above acoustic data can be derived from continuous tape recordings made of the sound signal produced by a test airplane during a level or climbing flight at constant airspeed and powersetting over a ground-based noise measuring station. These flyover test procedures are widely used in the study of airplane noise, as well as in noise certification (References 29 to 32). Although the objective of this chapter is to present the characteristics of frequency spectra, some brief, but necessary, description is given below of the particular test procedure which forms the basis of the results to be presented in this section (References 31 and 32).

Therefore, an example of a graphic result of the overall sound pressure level versus immission time as recorded during a straight-line flyover by a small

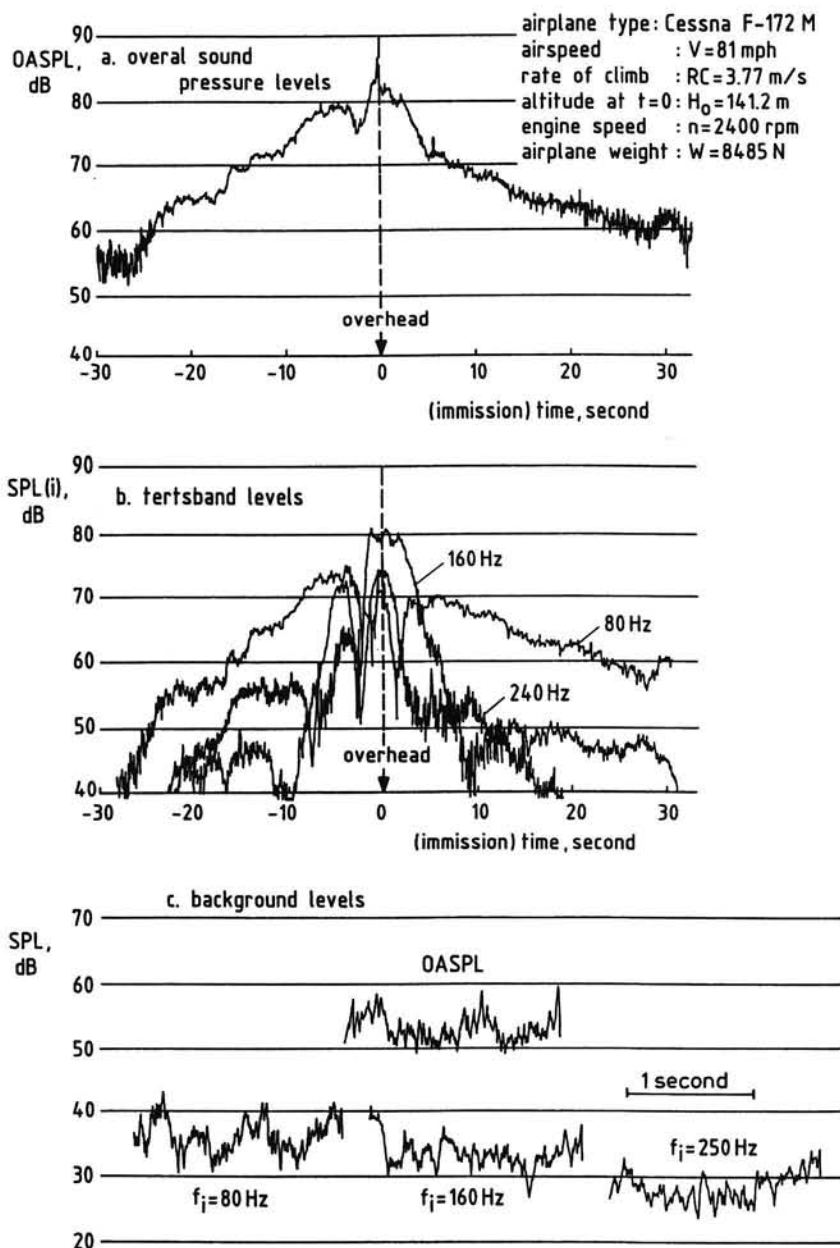


Figure 7.5-1. Sound pressure level time histories

Table 7.5-1 Data of the airplane type CESSNA F-172M

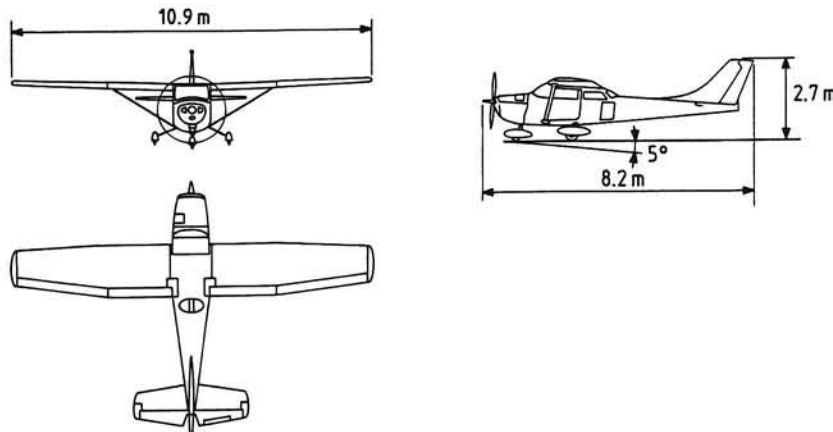
Gross weight	: 10240 N
Empty weight	: 5540 N
Wing span	: 10.9 m
Wing area	: 16.2 m ²
Propeller type	: direct drive; fixed pitch
Propeller diameter	: 1.91 m
Top speed at sea level	: 224 km/h
Maximum rate of climb at sea level	: 3.3 m/s
Speed for maximum rate of climb	: 143 km/h

propeller-driven airplane is shown in Figure 7.5-1a. The test airplane, a Cessna F-172M, is a single-engine small airplane, having a two-bladed, fixed-pitch propeller, directly driven by a four-cylinder piston-engine. Figure 7.5-2 is a dimensioned three-view of the airplane.

Characteristic data are tabulated in Table 7.5-1. The noise time-history was measured with the microphone positioned at a height of 1.2 m above a grass-covered surface. A schematic of the testing layout is shown in Figure 7.5-3.

It should be appreciated that for measurements on aircraft in flight the presence of a stable atmosphere with low surface winds (10 knots or less) is a prerequisite for obtaining proper results.

Additionally, the ground surface in the vicinity of the measuring location should be essentially flat terrain exhibiting no excessive sound absorption

*Figure 7.5-2. General arrangements of the airplane type Cessna F-172M*

characteristics such as might be produced by trees or shrubbery. The measurement site should be well isolated from urban noise sources and airways, and well away from obstructions which may significantly influence the sound field from the test airplane.

As discussed earlier in Section 1.12, the sound pressure level measured below the flight path increases with time from the background noise level to a peak value at approximately overhead position and then falls off into the ambient. Therefore, measuring noise from aircraft in flight introduces not only the effect of Doppler shift on observed frequencies, but also the complication of a nonstationary (transient) sound signal. Therefore, the sample time is restricted so the resulting overall noise levels and frequency spectra may be of less quality than those obtained from static measurements.

The overall sound pressure level (OASPL) in Figure 7.5-1a can be analyzed by sequential filtering to obtain one-third octave band sound pressure level time histories (Figure 7.5-1b). Also recordings must be made of ambient (background) noise levels to correct the measured sound pressure levels in each tertband if necessary. Figure 7.5-1c shows time-histories of typical low background noise.

To convert the tertband sound pressure levels, $SPL(i)$, to basic sound source quantities, the distance r_e between airplane and microphone and emission angle θ must be known as a function of time (Figure 7.5-3).

Setting the *emission time* $t_e = 0$ at overhead time and observing that both the airspeed V and rate of climb RC are constant, the following equations for r_e and θ can be derived:

$$r_e = \left[(H_0 + (RC)t_e)^2 + (Vt_e)^2 + d^2 \right]^{\frac{1}{2}} \quad (7.5-1)$$

$$\theta = \pi - \cos^{-1} \left[\frac{Vt_e + H_0(RC)/V}{r_e} \right], \quad (7.5-2)$$

where H_0 is overhead altitude and d is the lateral error as indicated in Figure 7.5-3.

In relating the measured sound pressure levels to the emission angle we have the complication that owing to the finite speed of sound, the signal emitted by the source at the emission time t_e arrives at the microphone at a later time, the *immission time* t ,

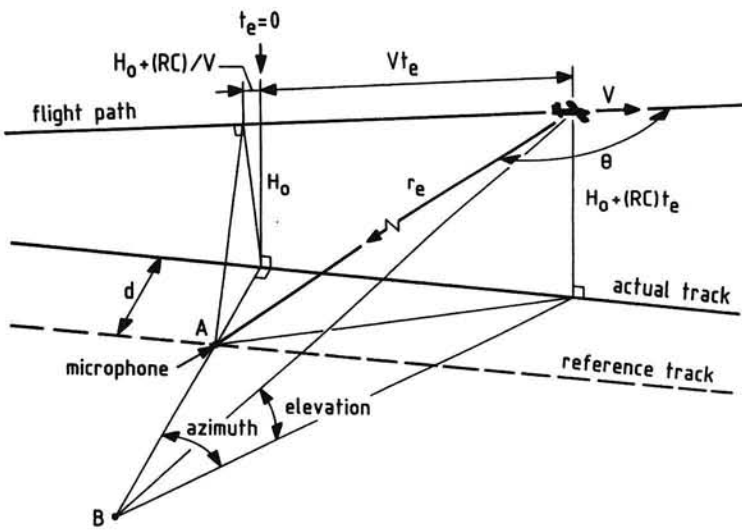


Figure 7.5-3. Test site geometry

$$t = t_e + r_e/c \quad . \quad (7.5-3)$$

By combining Equations (7.5-1) and (7.5-3), and noting that $(RC)^2 \ll V^2$, we find

$$t_e = \frac{(c^2 t - H_0(RC)) - [2c^2 H_0(RC)t + (c^2 - V^2)(H_0^2 + d^2) + V^2 c^2 t^2]^{1/2}}{c^2 - V^2}, \quad (7.5-4)$$

where c is the (mean) speed of sound in the actual atmosphere.

To compare the noise characteristics of different airplane types the tertband sound pressure levels may be converted to a certain reference distance. Usually, a reference distance of one meter from the hypothetical acoustic center of the source is employed, which sound pressure level is denoted as $SPL_1(i, \theta)$. The conversion can be performed by applying the *inverse distance law* taking into account atmospheric attenuation:

$$SPL_1(i, \theta) = SPL_r(i, \theta) + 20 \log r_e + \alpha r_e \quad , \quad (7.5-5)$$

where the attenuation coefficient α may be determined from the previous Equation (4.2-2). The required information of flight condition and airplane position can be obtained by tracking methods such as radar tracking, theodolite triangulation, or photographic scaling techniques.

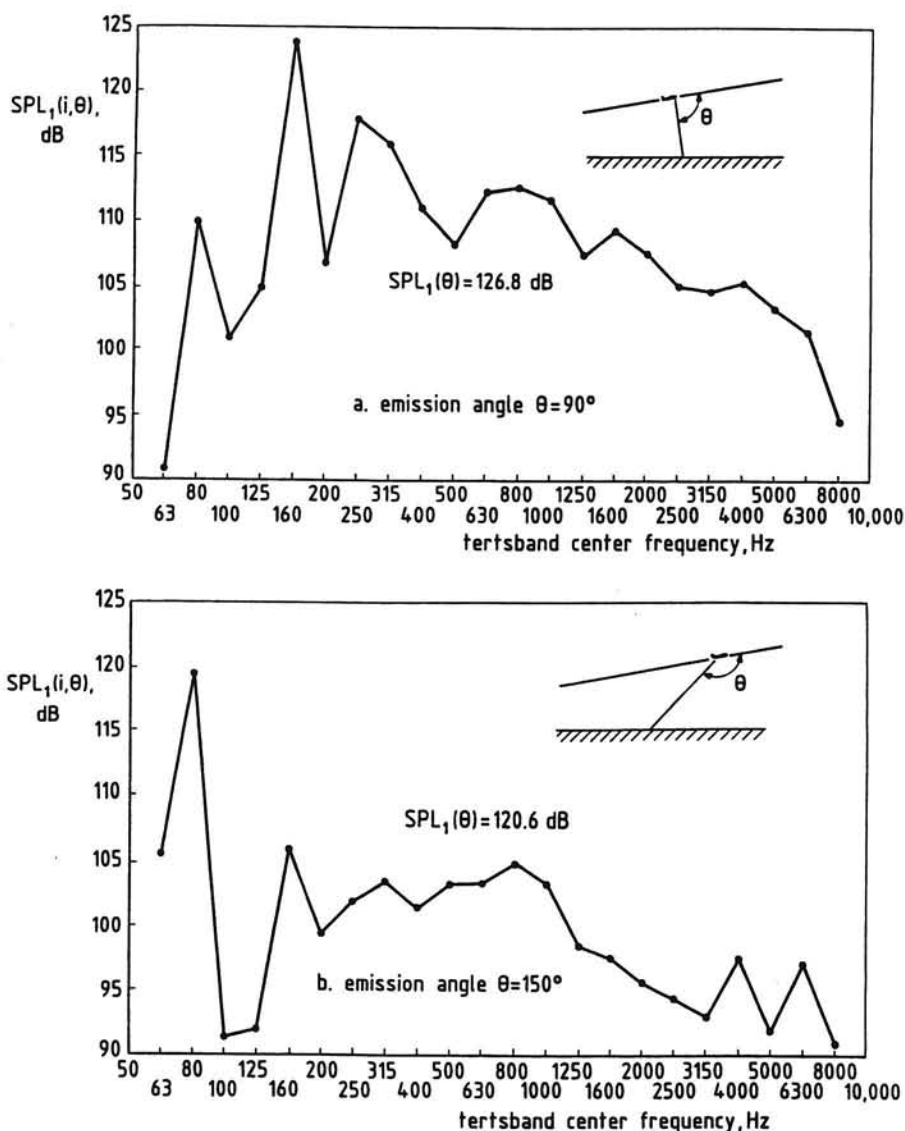


Figure 7.5-4. Flyover tertsband spectra

In the present measurement procedure, photographs taken at known positions *A* and *B* in Figure 7.5-3, were employed to determine airspeed, rate of climb and the position of the airplane at regular intervals. The camera in point *B*, located normally to the vertical flight plane, was synchronized in time to the sound recording, resulting in known sound pressure levels, $SPL_r(i, \theta)$, for each known airplane position.

By taking into account the effects of background noise level, speed of sound, distance and atmospheric attenuation, the tertsbands spectra at unity distance for a series of emission angles are obtained.

Figure 7.5-4 shows two examples of tertsbands spectra resulting from the flyover in Figure 7.5-1a.

Figure 7.5-4a gives the spectrum at the instant the airplane is approximately overhead. It appears that the contribution to the overall sound pressure level of the tertsbands containing the second harmonic frequency is of greater importance than the tertsbands containing the blade passage frequency. On the other hand, from Figure 7.5-4b we note that when the airplane is heard at a large emission angle the fundamental frequency is the most intense. This spectrum is similar to the result shown in Figure 7.4-4a, which was obtained from static measurements. It is worth noting that the major importance of the second harmonic frequency as occurring at overhead position is typical for a range of emission angles near the propeller plane.

The dependence of the spectral content on test geometry can be explained by considering the effects of ground plane reflections on measured noise levels, as will be seen in the next chapter.

8 GROUND REFLECTION

8.1 OBSERVED SOUND PRESSURE LEVEL

A major problem in the interpretation of results from noise measurements are the effects of ground reflected sound, which must be removed from the measured noise levels before the free-field noise characteristics of the source become visible.

The geometry of the problem occurring under typical in-flight noise test conditions is outlined in Figure 8.1-1, where the airplane is in straight flight at a subsonic speed over a ground noise measuring station. The microphone is at a height h_m above the ground.

The airplane is assumed to generate sound as a point source, and the atmosphere is considered as quiet, isothermal and homogeneous. We also make the simplifying assumption that the ground surface is specularly reflecting, requiring that the ground surface is flat and that the irregularities in the ground surface are small when compared to the wavelengths of the sound.

At a given emission time t_e the airplane is at an instantaneous position given by altitude H and emission angle θ . A direct sound ray travels from the airplane the distance r_{e_1} to the microphone and arrives at the microphone at

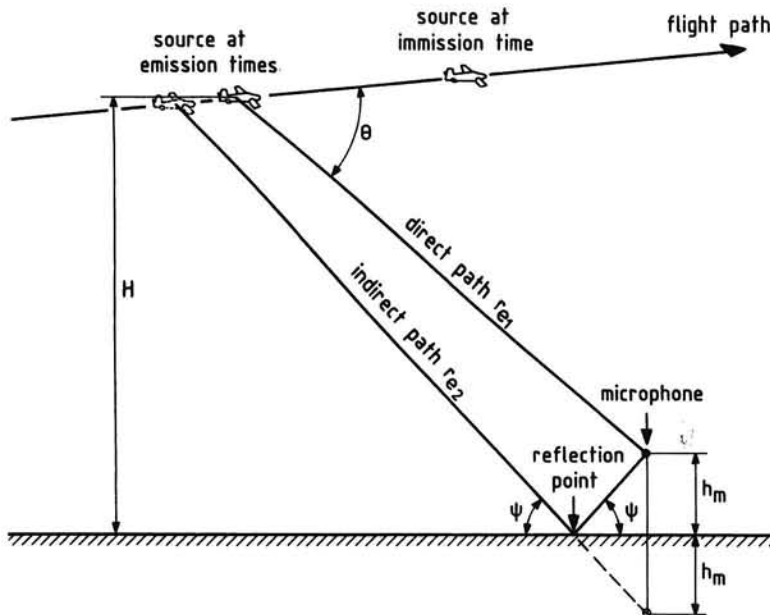


Figure 8.1-1. Sound propagation geometry from flyover

an immission time $t = t_e + r_{e_1}/c$. At the same arrival time t also a reflected ray strikes the microphone. The travel distance of this reflected ray is equal to the distance r_{e_2} to the microphone image. Since r_{e_2} is always greater than r_{e_1} , the reflected sound is emitted slightly earlier than the direct sound. This time interval is given by

$$\Delta t = \frac{r_{e_2} - r_{e_1}}{c}. \quad (8.1-1)$$

However, for the sake of simplicity, we will ignore the small displacement of the noise source in the interval Δt , and the effects of the ground on observed sound pressure levels will be analyzed on the basis of the radiation geometry of Figure 8.1-2. Note that in this figure the subscripts "e" denoting the ray pathlengths have been emitted to abridge the equations in this chapter.

At a given frequency the sound pressure at the receiver is the sum of the sound pressures caused by the direct ray and the reflected ray,

$$p'_m(r, t) = \frac{A}{r_1} e^{i\omega(t - r_1/c)} + Q \frac{A}{r_2} e^{i\omega(t - r_2/c)}, \quad (8.1-2)$$

where A is the amplitude of the sound pressure at unity distance from the source and Q is the *reflection factor*.

To include a change of amplitude as well as phase on reflection in Equation (8.1-2) a complex notation for the reflection factor must be used,

$$Q = |Q| e^{i\phi}, \quad (8.1-3)$$

where $|Q|$ is the ratio of magnitudes of reflected and direct waves and ϕ is the phase change.

The effective sound pressure at the receiver is given by

$$p_{e_m}(r) = \left[\frac{1}{T} \int_0^T [p'_m(r, t)]^2 dt \right]^{1/2}. \quad (8.1-4)$$

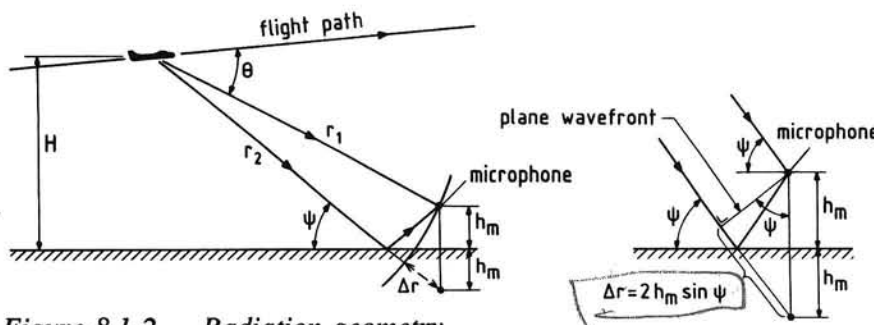


Figure 8.1-2. Radiation geometry

Substitution of Equation (8.1-2) into Equation (8.1-4) yields after integration (cf. Equation (1.9-10)):

$$p_{e_m}(r) = \left[\left(\frac{A}{r_1\sqrt{2}} \right)^2 + |\mathcal{Q}|^2 \left(\frac{A}{r_2\sqrt{2}} \right)^2 + |\mathcal{Q}| \frac{A^2}{r_1 r_2} \cos(\omega \frac{\Delta r}{c} + \phi) \right]^{1/2}, \quad (8.1-5)$$

where $\Delta r = r_2 - r_1$.

The effective sound pressure from the direct sound is

$$p_{e_d}(r) = \left[\frac{1}{T} \int_0^T \left[\frac{A}{r_1} \cos \omega(t - r_1/c) \right]^2 dt \right]^{1/2} = \frac{A}{r_1\sqrt{2}}. \quad (8.1-6)$$

Combining Equations (8.1-5) and (8.1-6) produces the expression

$$p_{e_m}(r) = p_{e_d}(r) \left[1 + \left(\frac{r_1}{r_2} \right)^2 |\mathcal{Q}|^2 + 2 \frac{r_1}{r_2} |\mathcal{Q}| \cos(\omega \frac{\Delta r}{c} + \phi) \right]^{1/2}. \quad (8.1-7)$$

A sound level meter at the receiver position will display the sound pressure level according to

$$\text{SPL}_m = 10 \log \frac{p_{e_m}^2}{p_{e_0}^2}, \quad (8.1-8)$$

where p_{e_m} is the root-mean-square sound pressure given by Equation (8.1-7) and p_{e_0} is the reference pressure of $2 \times 10^{-5} \text{ N/m}^2$.

We may define the *ground effect* as the difference between the measured sound pressure level at a given emission angle, $\text{SPL}_m(r, \theta)$ and the sound pressure level at the same emission angle, $\text{SPL}_d(r, \theta)$, which would occur in the free field:

$$\Delta \text{SPL}(r, \theta) = \text{SPL}_m(r, \theta) - \text{SPL}_d(r, \theta). \quad (8.1-9)$$

From the above definition, reinforcement due to ground reflection yields a positive value of the ground effect. Cancellation effects appear as negative values of ΔSPL .

From Equations (8.1-7) to (8.1-9), we get

$$\Delta \text{SPL}(r, \theta) = 10 \log \left[1 + \left(\frac{r_1}{r_2} \right)^2 |\mathcal{Q}|^2 + 2 \frac{r_1}{r_2} |\mathcal{Q}| \cos(\omega \frac{\Delta r}{c} + \phi) \right]. \quad (8.1-10)$$

In deriving this equation, atmospheric attenuation is neglected since the difference between the reflected and direct pathlengths will be small when compared to the total lengths.

Equation (8.1-10) predicts that the reflected sound can change the measured sound pressure level at a given frequency by any value between a 6 dB rise and negative infinity.

The pathlength difference between the two rays is obtained from the geometry of Figure 8.1-2, as follows:

$$\Delta r = \left[(H + h_m)^2 + \left(\frac{H + h_m}{\tan \psi} \right)^2 \right]^{1/2} - \left[(H - h_m)^2 + \left(\frac{H + h_m}{\tan \psi} \right)^2 \right]^{1/2}, \quad (8.1-11)$$

where h_m is the receiver height and ψ is the angle of incidence of the reflected sound with the ground surface.

Since H is much greater than h_m and also $H \gg \Delta r$, it can easily be found that Equation (8.1-11) is very well approximated by

$$\Delta r = 2 h_m \sin \psi. \quad (8.1-12)$$

This simplification suggests the use of a plane wave model at the reflection point, as also is illustrated in Figure 8.1-2.

Inserting Equation (8.1-12) into Equation (8.1-10) furnishes with $\omega = 2\pi f$:

$$\Delta SPL(r, \theta) = 10 \log \left[1 + \left(\frac{r_1}{r_2} \right)^2 |Q|^2 + 2 \frac{r_1}{r_2} |Q| \cos \left(\frac{4\pi f}{c} h_m \sin \psi + \phi \right) \right]. \quad (8.1-13)$$

Equations (8.1-10) and (8.1-13) clearly show that ground interference effects arise from the pathlength difference between direct and reflected waves, and from a phase change on reflection of the indirect wave at the ground surface. Let, for the purpose of this discussion, the quantity $r_1/r_2|Q| \approx 1$ and the phase change $\phi \approx 0$. Then, for the airplane at overhead ($\psi = 90^\circ$), the variation of ΔSPL with frequency is as plotted in Figure 8.1-3, where the customary receiver height of 1.2 m is used.

The graph shows that at the time of passing overhead during a flyover, cancellation of the first harmonic frequency measured from propeller noise can actually occur, as can reinforcement of the corresponding second harmonic frequency.

From Equation (8.1-13), we establish that the frequencies at which reinforcement occurs are given by

$$f = \frac{ck}{2h_m \sin \psi}, \quad (8.1-14)$$

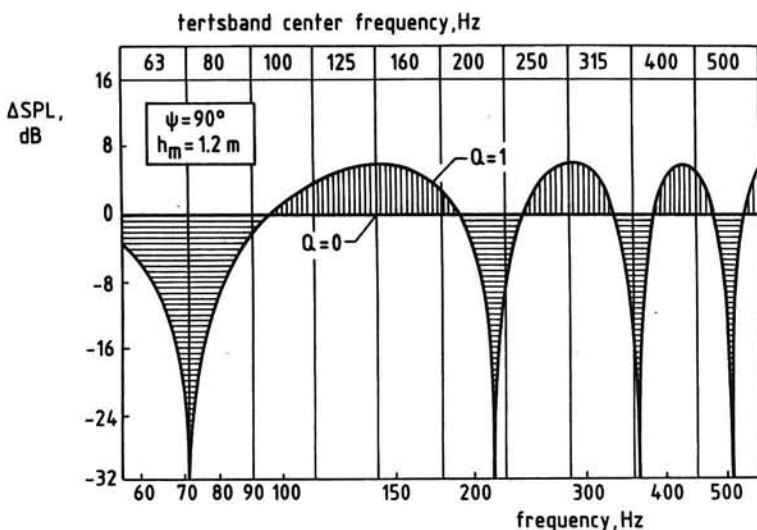


Figure 8.1-3. Ground effect from a hard boundary

where k is an integer ($k = 0, 1, 2, \dots$).

On the other hand, cancellation occurs when the frequencies are equal to

$$f = \frac{c(k + \frac{1}{2})}{2h_m \sin \psi} \quad (8.1-15)$$

Figure 8.1-4 shows for $h_m = 1.2$ m the constructive and destructive interference frequencies according to Equations (8.1-14) and (8.1-15) as a function of angle of incidence ψ .

Undoubtedly, the plots of the difference between measured and free-field sound pressure levels in Figure 8.1-3 and 8.1-4 reflect the discrepancies between the frequency spectra given in the previous Figures 7.5-4a and 7.5-4b. The latter data resulted from noise tests of a small propeller-driven airplane operating above a typical short-grass-covered landingstrip with the microphone placed at a height of 1.2 m. These spectra demonstrated that when the noise reaches the ground at a large angle of incidence, the tertsband containing the second harmonic frequency is the most intense. On the other hand, when the noise strikes the ground at a small incidence angle, the tertsband enclosing the first harmonic frequency is the most important. This phenomenon is further confirmed by Figure 8.1-5, which presents a tertsband frequency spectrum resulting from in-flight noise measurements made at such a side-line location that the angle of incidence reached a maximum value of only 19.2° . In spite of the fact that the associated emis-

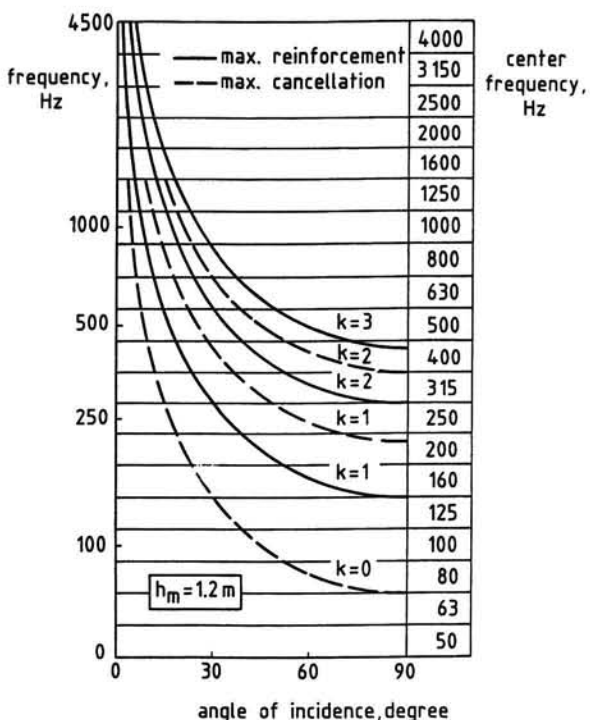


Figure 8.1-4. Constructive and destructive ground reflection frequencies as a function of incidence angle

sion angle was 90° , a dominating first harmonic frequency was obtained. It is clear from the spectral irregularities, as illustrated above, that varying the incidence angle significantly changes the frequencies at which cancellations and reinforcements occur.

With regard to propeller-driven airplane noise measurements, it is also apparent that the effects of ground reflection infer that small deviations in propeller rotational speed can cause significant changes to the noise level at a 1.2 m pole microphone.

Equation (8.1-13) also predicts that, starting from the position at ground level and depending on angle of incidence and observed frequency, elevating the microphone will result in a decreasing ground effect. If the sound level meter reading reaches a minimum value, the ground effect and the corresponding total phase change are given by

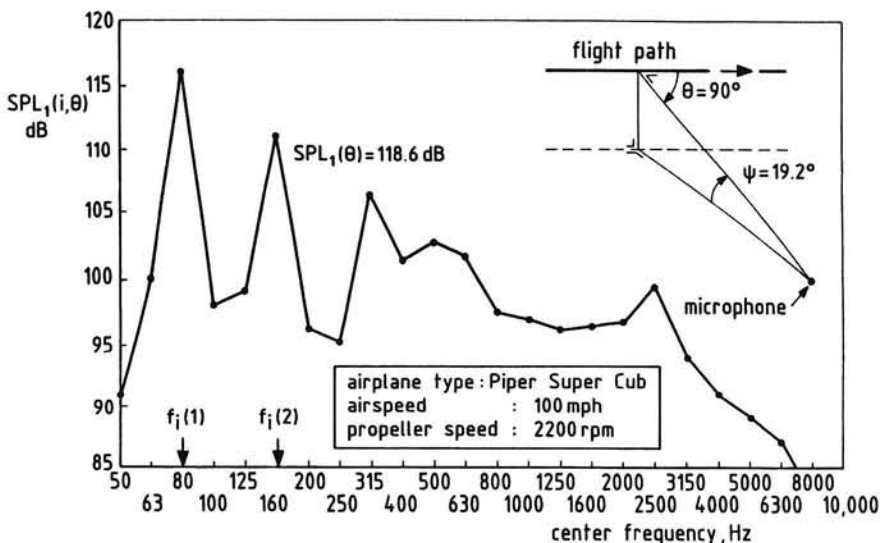


Figure 8.1-5. Tertsband spectrum of propeller-airplane flyover noise

$$\Delta \text{SPL}_{\min}(f, \psi) = \text{SPL}_{\min} - \text{SPL}_d = 10 \log \left[1 - \frac{r_1}{r_2} |Q| \right]^2 \quad (8.1-16)$$

and

$$\frac{4\pi f}{c} h_m \sin\psi + \phi = \pi \quad (8.1-17)$$

Further increase of the microphone height will deliver an increasing sound pressure level value, until a maximum reading occurs, which means that the total phase change has become equal to 2π .

Then

$$\Delta \text{SPL}_{\max}(f, \psi) = \text{SPL}_{\max} - \text{SPL}_d = 10 \log \left[1 + \frac{r_1}{r_2} |Q| \right]^2. \quad (8.1-18)$$

For a given frequency and angle of incidence, the latter three equations in three unknowns can provide the free-field sound pressure level, SPL_d , as well as the amplitude and phase of the complex reflection factor Q .

8.2 EFFECT OF FINITE-WIDTH FILTERS

Equation (8.1-10) for the prediction of ground effect has been developed for discrete frequency sound. Since airplane noise analyses usually are made within finite frequency intervals, the interference effects may be seen in a more diluted form. This may especially be true in the case of jet-propelled aircraft, of which the noise is broadband in nature.

To make appropriate ground effect predictions, the pure-tone equation must be integrated over each frequency band. Thus $\Delta SPL =$

$$\Delta SPL = 10 \log \frac{\int_{f_l}^{f_u} [p_e(f)]^2 \left[1 + \left(\frac{r_1}{r_2} \right)^2 |\mathcal{Q}(f)|^2 + 2 \frac{r_1}{r_2} |\mathcal{Q}(f)| \cos \left(\frac{\omega}{c} \Delta r + \phi(f) \right) \right] df}{\int_{f_l}^{f_u} [p_e(f)]^2 df} \quad (8.2-1)$$

where f_u and f_l are the upper and lower limiting (cutoff) frequencies of the frequency band.

In the following, the analysis is restricted to the case of a band-limited white spectrum, i.e., a noise having a constant spectral density across each frequency interval (see Sections 7.2 and 7.3).

Then, the broadband equivalent of Equation (8.1-10) becomes

$$\Delta SPL = 10 \log \frac{\int_{f_l}^{f_u} \left[1 + \left(\frac{r_1}{r_2} \right)^2 |\mathcal{Q}(f)|^2 + 2 \frac{r_1}{r_2} |\mathcal{Q}(f)| \cos \left(\frac{\omega}{c} \Delta r + \phi(f) \right) \right] df}{f_u - f_l} \quad (8.2-2)$$

Assuming that the amplitude and phase of the complex reflection factor are constants within each frequency interval and equal to their values at the center frequencies, Equation (8.2-2) reduces to

$$\Delta SPL = 10 \log \left[1 + \left(\frac{r_1}{r_2} \right)^2 |\mathcal{Q}_i|^2 + 2 \frac{r_1}{r_2} |\mathcal{Q}_i| \frac{\int_{f_l}^{f_u} \cos \left(\frac{\omega}{c} \Delta r + \phi_i \right) df}{f_u - f_l} \right]. \quad (8.2-3)$$

In the case of an analysis at constant bandwidth, Equation (8.2-3) can be written as

$$\Delta \text{SPL} = 10 \log \left[1 + \left(\frac{r_1}{r_2} \right)^2 |Q_i|^2 + 2 \frac{r_1}{r_2} |Q_i| \frac{\sin \pi \frac{\Delta r}{c} \Delta f}{\pi \frac{\Delta r}{c} \Delta f} \cos (2\pi \frac{\Delta r}{\lambda_i} + \phi_i) \right]. \quad (8.2-4)$$

where $\Delta f = f_u - f_l$ and $\lambda_i = 2c/(f_u + f_l)$. The reflection coefficient Q_i is evaluated at the (arithmetic) mean frequency $f_i = (f_u + f_l)/2$ of the filterband. For constant percentage bandwidth analysis Equation (8.2-3) becomes

$$\begin{aligned} \Delta \text{SPL} = 10 \log & \left[1 + \left(\frac{r_1}{r_2} \right)^2 |Q_i|^2 + 2 \frac{r_1}{r_2} |Q_i| \frac{\sin \pi \frac{\Delta r}{\lambda_i} \frac{\Delta f}{f_i}}{\pi \frac{\Delta r}{\lambda_i} \frac{\Delta f}{f_i}} \times \right. \\ & \times \left. \cos \left(2\pi \frac{\Delta r}{\lambda_i} \sqrt{1 + \frac{1}{4} \left(\frac{\Delta f}{f_i} \right)^2} + \phi_i \right) \right], \end{aligned} \quad (8.2-5)$$

where $f_i = \sqrt{(f_u f_l)}$ and $\lambda_i = c/f_i$. The subscript i in Equation (8.2-5) indicates that the values are evaluated at the (geometric) center frequencies of the respective passbands. For one-third octave band filters $\Delta f/f_i$ is 0.23 (see Equation (7.3-11)).

Based on Equation (8.2-1), in References 33 and 34 formulae are derived which predict ground effect for various assumed spectrum shapes.

8.3 PLANE WAVE REFLECTION COEFFICIENT

Application of Equation (8.1-13) requires knowledge of the reflection factor Q over the frequency range of interest and over the zone of angles of incidence involved.

An expression for Q follows from the requirement that the complex ratio between the sound pressure at a point on the surface and the velocity of air particles at the surface, the latter due to a motion of the surface itself or else to a motion of air into pores in the ground, equals the acoustic impedance of the surface, (*surface impedance*),

$$Z_g = \frac{p_m'(r,t)}{v_g(r,t)}. \quad (8.3-1)$$

The unit of Z_g is kg/s m^2 .

Using the radiation geometry in Figure 8.3-1a, the sound pressure at the reflection point for a harmonic time dependence, from Equation (8.1-2), is given by ($r_2 = r_1 = r$)

$$p_m'(r, t) = (1 + Q) \frac{A}{r} e^{i\omega(t - r/c)} . \quad (8.3-2)$$

The corresponding particle velocity into the ground, from the previous Equation (5.5-2), is found to be

$$v_g(r, t) = \frac{\sin\psi}{\sin\psi_g} \frac{1}{\rho_\infty c} (1 - Q) \frac{A}{r} e^{i\omega(t - r/c)} , \quad (8.3-3)$$

where ψ_g is the angle to the horizontal subtended by the reflected wave in the ground medium, as depicted in Figure 8.3-1a.

Note that in deriving Equation (8.3-3) we have assumed the occurrence of a plane wave of sound incident obliquely on the ground surface.

In this connection, it is worthwhile to realize that in-flight operations practically mean long distance sound propagation and angles of incidence in the 30-90 degrees region. This means that the sound field can be very well approximated by plane wave propagation.

For a homogeneous isotropic ground medium, the incident and refracted angles are related by (cf. Equation (4.3-8)):

$$k_g \cos\psi_g = k \cos\psi , \quad (8.3-4)$$

where k_g is the wavenumber or propagation constant in the ground medium and k is the wavenumber in the air.

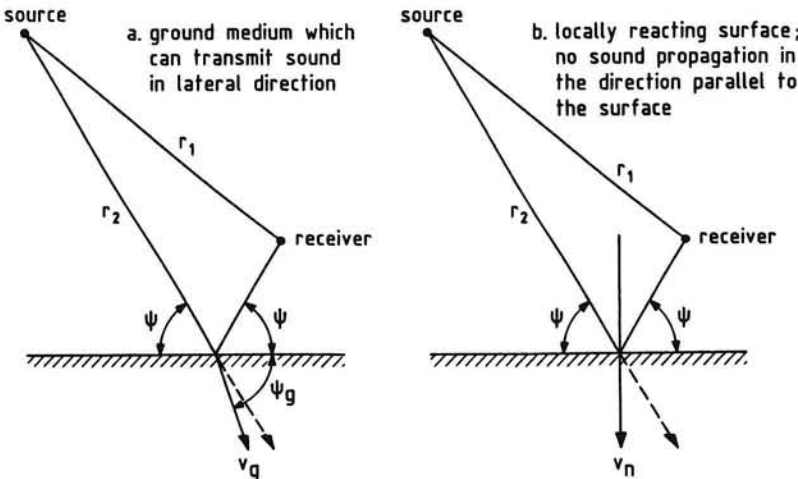


Figure 8.3-1. Reflection and refraction of sound at the ground surface

Solving Equation (8.3-1) to (8.3-3) for Q yields

$$Q_p = \frac{\frac{Z_g}{\rho_\infty c} \sin \psi - \sin \psi_g}{\frac{Z_g}{\rho_\infty c} \sin \psi + \sin \psi_g} . \quad (8.3-5)$$

The subscript p is used to denote that Equation (8.3-5) is based on the plane wave concept. The ratio of the surface impedance Z_g to the characteristic resistance of the ambient air $\rho_\infty c$, usually, is called the *specific impedance of the surface*.

Anticipating later conclusions, it may be assumed that the ground surfaces commonly employed in airplane noise testing behave if they are *locally reacting*. This term is used to denote the conditions under which lateral propagation through the ground is absent or can be ignored (Figure 8.3-1b).

In this case the characteristics of a particular ground surface may be represented by the *normal surface impedance*, Z_n , which quantity relates the sound pressure applied to a surface to its normal particle velocity v_n ,

$$Z_n = \frac{p'_n(r,t)}{v_n(r,t)} . \quad (8.3-6)$$

Equation (8.3-5) then reduces to

$$Q_p = |Q_p| e^{i\beta} = \frac{\frac{Z_n}{\rho_\infty c} \sin \psi - 1}{\frac{Z_n}{\rho_\infty c} \sin \psi + 1} . \quad (8.3-7)$$

If the normal surface impedance $Z_n = Z_{n_1} + iZ_{n_2}$ has a real part, acoustic energy will be absorbed at the surface, whereas a purely imaginary impedance causes only a change of phase on reflection. For a perfectly reflecting surface ($Q_p = 1$) the phase change is zero, and Z_n must be infinite.

Practically, Z_n may be very large, but its value will always remain finite. Then, Q_p is only equal to one for normal incidence ($\sin \psi = 1$). The actual value of Z_n is dependent on frequency but not on the angle of incidence.

The amplitude and phase of the plane wave reflection factor are related to the real and imaginary components of the impedance Z_n by the following equations:

$$|Q_p| = \frac{\left[\left[\left(\frac{Z_{n_1}}{\rho_\infty c} \right)^2 + \left(\frac{Z_{n_2}}{\rho_\infty c} \right)^2 \right] \sin^2 \psi - 1 \right]^2 + \left(2 \frac{Z_{n_2}}{\rho_\infty c} \sin \psi \right)^2}{\left[\left(\frac{Z_{n_1}}{\rho_\infty c} \right)^2 + \left(\frac{Z_{n_2}}{\rho_\infty c} \right)^2 \right] \sin^2 \psi + 2 \frac{Z_{n_1}}{\rho_\infty c} \sin \psi + 1}^{1/2} \quad (8.3-8)$$

$$\beta = \tan^{-1} \left[\frac{2 \frac{Z_{n_1}}{\rho_\infty c} \sin \psi}{\left[\left(\frac{Z_{n_1}}{\rho_\infty c} \right)^2 + \left(\frac{Z_{n_2}}{\rho_\infty c} \right)^2 \right] \sin^2 \psi - 1} \right]. \quad (8.3-9)$$

Equations (8.3-8) and (8.3-9) show that at a given angle ψ the plane wave reflection factor is completely defined by the components of the complex specific normal surface impedance.

The next section will be devoted to presenting information about the surface impedance of some typical ground surfaces used for airplane noise measurements.

8.4 SURFACE IMPEDANCE DATA

The discussion in the preceding section showed that in order to determine the sound pressure level above a reflecting plane, the surface impedance of the ground must be known.

Experimental results for the surface impedance of grassland in dry conditions are reported in Reference 35. Similar data on the acoustic impedance of grass-covered ground surfaces in dry and wet conditions are presented in Reference 36.

Figure 8.4-1 shows both sets of data, where the real and imaginary components of the surface impedance in the nondimensional form $Z/\rho_\infty c$ are plotted against frequency.

The data in Figure 8.4-1a were obtained from in situ measurements using two different interference methods.

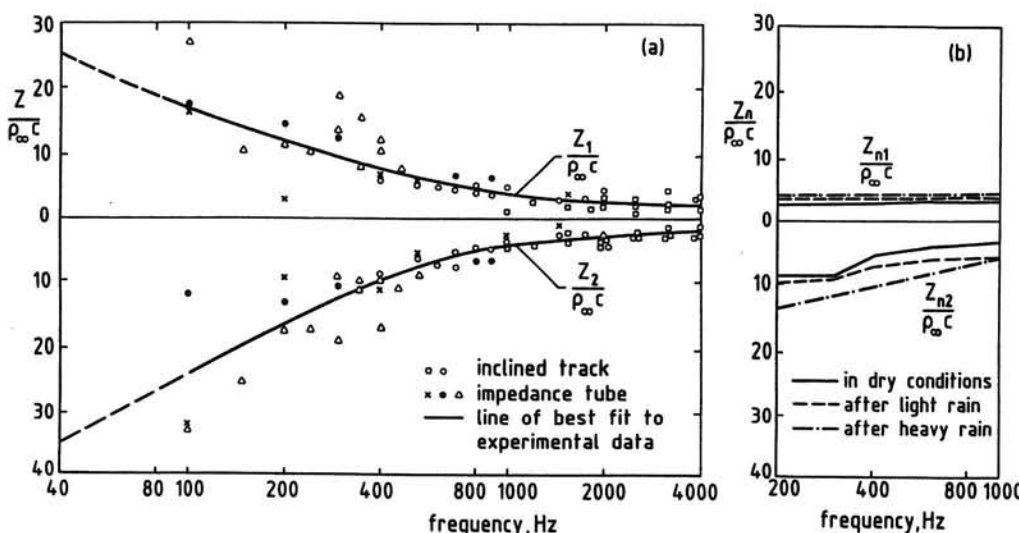


*Figure 8.4-1. Specific surface impedance of grass-covered flat ground.
(a) Taken from Reference 35, and (b) from Reference 36*

One used an *impedance tube* or *standing wave apparatus* placed vertically on the ground. As shown in Figure 8.4-2a, the impedance tube is simply a tube containing a sample of the ground material. At the other end of the tube there is a sound generator, emitting pure tones of given amplitude. A probe microphone is movable in the tube.

The sound waves travel through the tube and are then partly reflected at the test sample. As the microphone is moved between the source and the ground sample, alternate cancellation and reinforcement will occur due to the pathlength difference between the direct and indirect waves and to a phase change on reflection at the surface of the sample. From the resulting series of maxima and minima in sound pressure level and their respective distances from the ground sample, the reflection factor and thence the real and imaginary parts of the surface impedance can be calculated according to the procedures described in Sections 8.1 and 8.3.

In the other interference method one used a stationary sound source suspended above the ground sample and a microphone receiver which was moved along an inclined path (Figure 8.4-2b). By this technique surface impedances could be determined at incidence angles from 15 to 21 degrees.

Similar outdoor noise tests were made at normal incidence to measure the impedance values of Figure 8.4-1b.

Comparing in Figure 8.4-1a the data at oblique incidence with those obtained

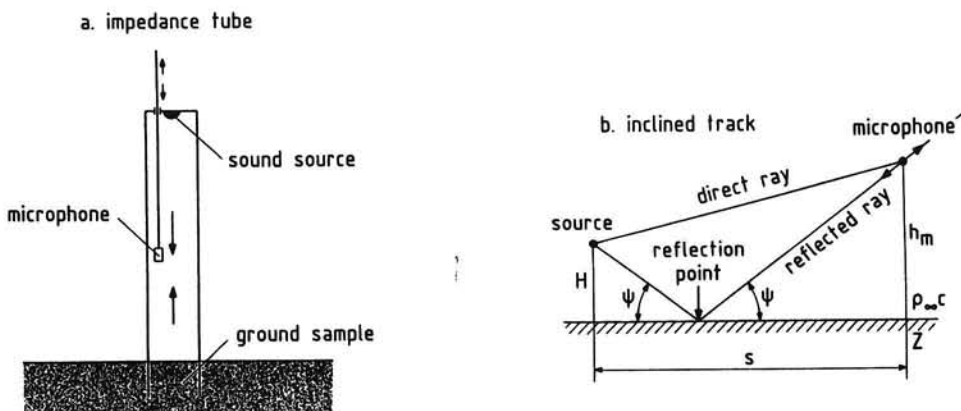


Figure 8.4-2. Measurement of surface impedance

at normal incidence demonstrates that both parts of the surface impedance tend to be functions of frequency only. This implies that grassland may have the acoustic properties of a locally reacting porous medium. Consequently, grassy surfaces may be described by a normal surface impedance.

The measurement data in Figure 8.4-1b indicate that the presence of moisture hardly affects the magnitude of the normal surface impedance of grass-covered ground. In other words, the impedance is not very sensitive to weather.

According to Reference 37, the specific normal impedance of real soil surfaces can be represented by using a model of the acoustic properties of fibrous absorbent materials.

This model, originally developed in Reference 38, gives the real and imaginary components of the specific normal acoustic impedance as

$$\frac{Z_n}{\rho_\infty c} = \left[1 + 9.08 \left(\frac{f}{\sigma} \right)^{-0.75} \right] + i \left[11.9 \left(\frac{f}{\sigma} \right)^{-0.73} \right], \quad (8.4-1)$$

where f is frequency and σ is a single specifying model parameter. The latter quantity depends on the type of terrain and the condition of the ground surface. For several values of σ , the components of the specific normal surface impedance are shown in Figure 8.4-3. A comparison of the curves with the experimental data in Figure 8.4-1 indicates that relevant values of σ pertaining to grass-covered surfaces are in the range of 100-400.

As matter of interest, it may be noted that measurement data of the acoustic impedance of grassland and other natural surfaces, such as stubble, sand, gravel, and snow, are collected together in Reference 39.

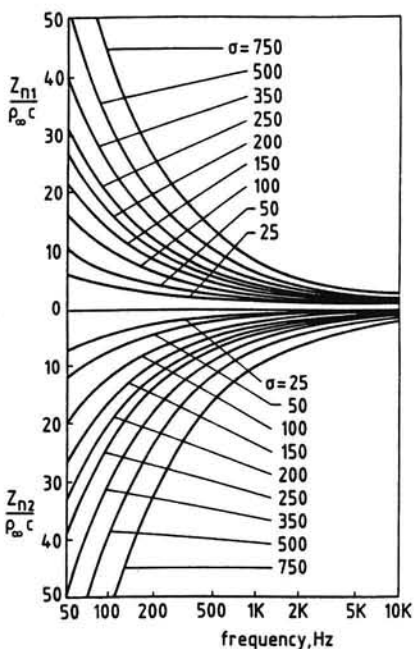


Figure 8.4-3. Model impedance

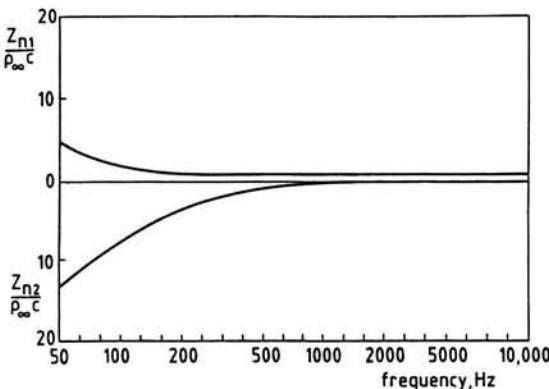


Figure 8.4-4. Crushed stone impedance

A ground surface commonly used in static full scale engine noise tests is the crushed stone surface. Figure 8.4-4 presents measured specific normal impedances for this type of ground surface (Reference 40).

Contrary to the more natural surfaces, data on the acoustic impedance of hard solid surfaces such as concrete or asphalt are extremely limited. A rough figure for the input parameter in Equation (8.4-1) pertaining to concrete may be $\sigma = 750$ (Reference 41). A much greater value for the specific

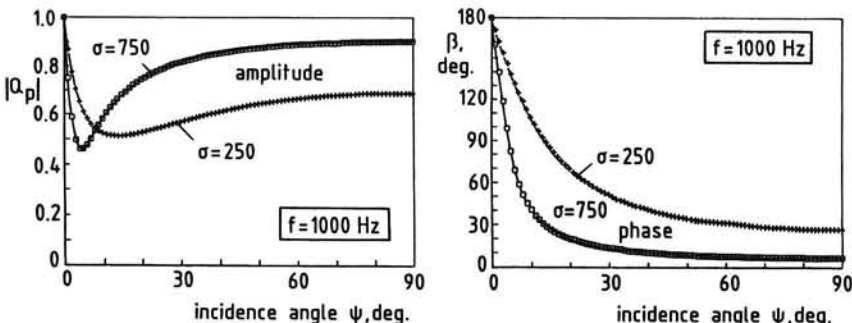


Figure 8.4-5. Plane wave reflection factor

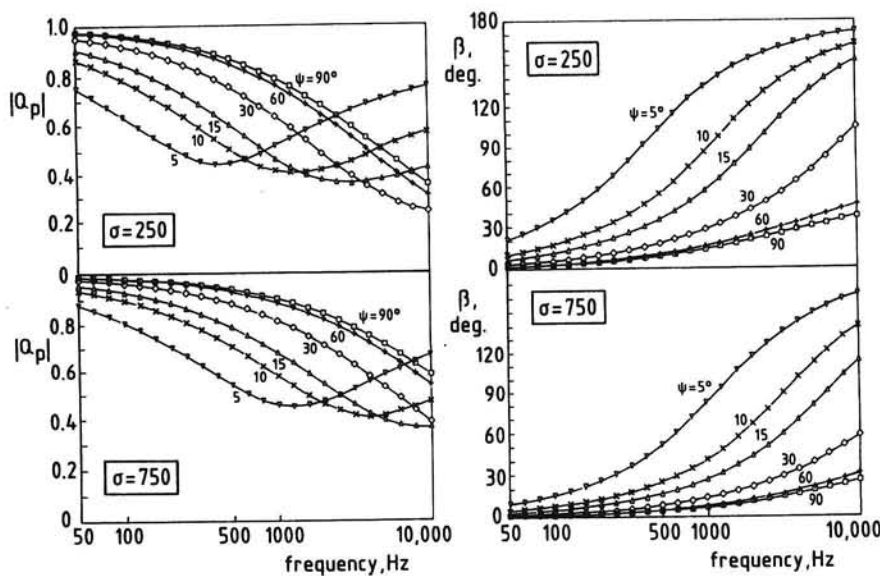


Figure 8.4-6. Plane wave reflection factor

impedance of a hard surface is mentioned in Reference 40, which source suggests the use of the following empirical formula:

$$\frac{Z_n}{\rho_\infty c} = 100(1+i) . \quad (8.4-2)$$

This expression indicates that the impedance of concrete and asphalted surfaces not only may satisfy the local reaction boundary condition assumption, but also that the impedance might possibly be independent of frequency.

Figure 8.4-5 shows for a frequency of 1000 Hz the variations of the amplitude and phase of the plane wave reflection factor with angle of incidence. The data given there relate to grass-covered and hard surface impedance values according to Equation (8.4-1), using a model parameter σ of 250 and 750, respectively.

The way in which amplitude and phase vary with frequency, is shown in Figure 8.4-6.

From Figures 8.4-5 and 8.4-6 it can be seen that, except within the zone of very small incidence angles, hard surfaces exhibit acoustic properties very similar to those of a perfect reflector of acoustic energy.

8.5 VALIDITY OF PLANE WAVE APPROXIMATION

Regardless of the magnitude of the ground impedance, from Equations (8.3-5) and (8.3-7) it follows that at grazing incidence ($\psi = 0$) the plane wave reflection factor Q_p is equal to minus one. Thus, when the sound waves propagate parallel to the ground surface, complete cancellation of the sound pressure is predicted.

It has been observed experimentally, however, that this cancellation does not occur. This problem has led to the development of improved theory, where the sound field above an absorbing flat surface due to a point source is composed of a direct contribution from the source and a second contribution from a modified image source, rather than a simple point image as considered before. The difference between the modified image and the simple point image, allowing a finite sound pressure to exist at near grazing angles of incidence, is referred to often as the *ground wave*.

Specific formulae obtained from relevant theory describing the sound field near a locally reacting flat ground surface from a spherically-radiating point monopole source under flyover circumstances are summarized in Reference 42. There, for the appropriate cases of a rigid boundary and $kr_2 > 1$, the reflection factor for spherical waves is expressed in terms of an expansion of elementary plane waves,

$$Q = |Q| e^{i\phi} = Q_p + (1 - Q_p) F(p) . \quad (8.5-1)$$

The second term on the right-hand side of Equation (8.5-1) represents the ground wave mentioned above.

The function $F(p)$ describes the interaction of the curved wavefront with a flat ground surface of finite impedance, and is defined by the following equation:

$$F(p) = 1 - \sqrt{\pi} p e^{p^2} \operatorname{erfc}(p) , \quad (8.5-2)$$

where p is given by

$$p = -i \sqrt{\frac{ikr_2}{2}} \left(\sin \psi + \frac{\rho_\infty c}{Z_n} \right) . \quad (8.5-3)$$

If the wavefront is plane ($r_2 \rightarrow \infty$), then $|p| \rightarrow \infty$ and $F(p) \rightarrow 0$.

For reasonably large values of p the asymptotic expansion of the error function complement is used in Equation (8.5-2), which yields

$$F(p) = -2\sqrt{\pi} p e^{p^2} H(-Re p) + \left[\frac{1}{2p^2} - \frac{1 \times 3}{(2p^2)^2} + \frac{1 \times 3 \times 5}{(2p^2)^3} - \dots \right], \quad (8.5-4)$$

where $H(-Re p)$ is the unit stepfunction, which is unity when its argument is positive and zero when its argument is negative.

The first term on the right of Equation (8.5-4) is known as the *surface wave*, which may be a significant component of the total sound field in the case of a hard boundary.

In order to extend Equation (8.5-2) to smaller values of $|p|$ the power series expansion of $\text{erfc}(p)$ is used, which yields

$$F(p) = 1 - \sqrt{\pi} p e^{p^2} + 2p \left[1 + \frac{2p^2}{1 \times 3} + \frac{(2p^2)^2}{1 \times 3 \times 5} + \dots \right]. \quad (8.5-5)$$

From a numerical justification it appeared that for a transition value of $|p| = 3$ the two expansions are well matched.

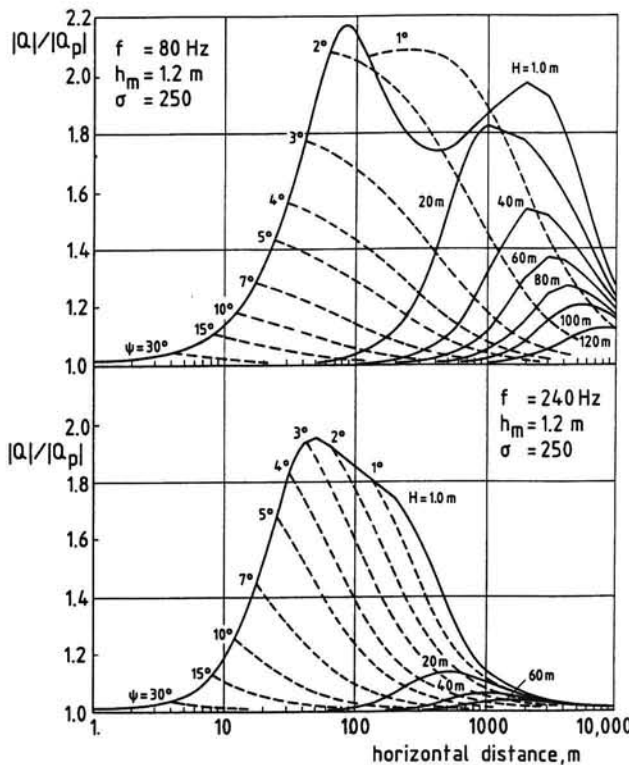


Figure 8.5-1. Validity of plane wave theory

The significance of sound propagation by spherical waves can be illustrated by examining the ratio

$$\frac{Q}{Q_p} = \frac{|Q|}{|Q_p|} e^{i(\phi-\beta)} . \quad (8.5-6)$$

For several heights of the source, both reflection factors were computed as a function of the horizontal separation between source and receiver. For frequencies of 80 and 240 Hz, the ratio $|Q|/|Q_p|$ is shown in Figure 8.5-1, where also are plotted curves of constant angle of incidence.

Considered is the case of a receiver height of 1.2 m and a grass-covered surface. The impedance was calculated by Equation (8.4-1), using a model-parameter $\sigma = 250$.

From Figure 8.5-1 and subsequent computations it follows that with increasing frequency the difference between the two reflection factors approaches to zero. The curves in Figure 8.5-1 also indicate that under flyover circumstances, which practically mean a region of incidence angles between 30 and 90 degrees, the plane wave reflection factor will provide essentially identical results.

Only when the source is at a very low altitude and for ground-based geometries, the spherical wave appears to be a required mode of propagation.

8.6 ACQUISITION OF FREE-FIELD NOISE LEVELS

There are two main reasons why the acquisition of free-field noise data is of practical significance in the field of aeronautical acoustics. First, noise data must be fully representative of the source and not be influenced by local variable conditions, and second, the free-field sound pressure level spectra are required when measured spectra must be extrapolated to any ground position and receiver height.

It may also be noted that there is an increasing tendency to execute noise measurements under both static and flight conditions since it has been recognized that differences exist in the noise characteristics of airplanes operating statically and in forward flight. In order to be able to interpret and compare data from both types of noise testing, the interference effects from ground plane reflections must be removed from the recordings.

On the one side, flyover measurements introduce the complication of a radiation geometry which changes continually with time. Moreover, we are faced with the problem of a restricted sample time due to the nonstationary (transient) sound signal and the effect of Doppler-shift on observed frequen-

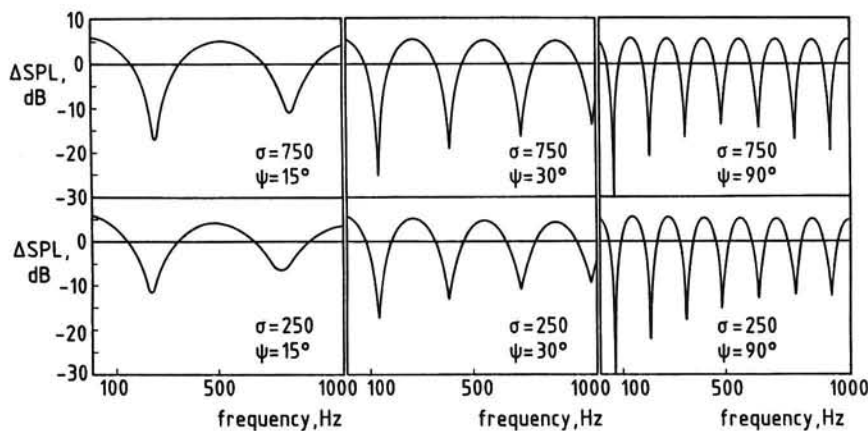


Figure 8.6-1. Ground effect predictions ($h_m = 1.2\text{m}$)

cies. On the other hand, the analytical description of the interference effects is strongly simplified by the fact that under forward flight conditions the noise source can be considered as a point source and that close the ground plane wave propagation can be assumed.

The general characteristics of the ground effect predicted by using Equation (8.1-13), the plane wave reflection factor according to Equations (8.3-8) and (8.3-9), and model values of the surface impedance given by Equation (8.4-1) can be demonstrated by particular examples.

Figure 8.6-1 shows the computed variation of ΔSPL as functions of incidence angle and frequency for a receiver height of 1.2 m. Considered are the cases of propagation over a hard solid surface ($\sigma = 750$) and over grassland ($\sigma = 250$). As mentioned already in Section 8.5, the ground effect predictions at incidence angles in the range of 30-90 degrees represent flyover conditions, whereas grazing incidence angles below 15° are of particular interest when the noise source is near the ground, as in the case of static noise testing.

At the 1.2 m receiver position, ground interference effects appear to be very sensitive to incidence angle and so to the position of the airplane relative to the receiver. In fact, no band level will remain the same by a variation in airplane position. Clearly, there is an orderly progression of reflection-induced sound pressure level variations as the airplane approaches and recedes, which causes that defining the free-field noise characteristics is especially a serious problem when the airplane is near overhead position.

Another important observation is that natural surfaces such as grassland produce ground reflection effects very similar to those produced by hard solid surfaces.

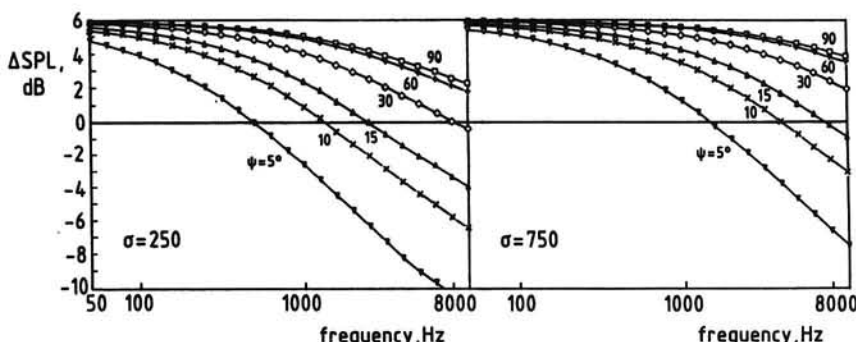


Figure 8.6-2. Ground effect predictions ($h_m = 0$)

In Figure 8.6-2 predictions of ΔSPL are given for a receiver placed on the ground ($h_m = 0$ m). Under this condition, both direct and reflected waves arrive in phase, resulting approximately in a pressure doubling with no attended cancellations.

Indeed we see from Figure 8.6-2 that the ground effect at all frequencies and incidence angles of practical interest is essentially constant ($\Delta\text{SPL} = 4\text{-}6$ dB). Only at near-grazing incidence there will be a systematic deviation from pressure doubling which occurs as a function of frequency and incidence angle. The deviations are due to the finite impedance of the ground surface (see also Reference 43).

At this point, it should be noted that, in fact, virtually all of the research programs on airplane noise have been conducted using the standard microphone height of 1.2 m until a few years ago. This microphone placement, however, introduces significant and confusing interference effects between direct and reflected waves which cause a distortion of the free-field noise spectra, particularly at low frequencies and large incidence angles.

In this respect, it is of importance to remember that a significant proportion of the sound generated by airplanes is contained in the low-frequency range ($f < 1000$ Hz). This is especially the case for propeller-driven airplanes.

Obviously, only when there is a precise knowledge of the radiation geometry as a function of emission time and the acoustic properties of the local terrain, it is possible to abstract ground effects from forward flight data with sufficient accuracy to obtain free-field spectra. The theoretical predictions in Figure 8.6-2 clearly indicate that placing the microphone very close to an acoustically hard surface, may be an effective measure to overcome the problems introduced by unwanted reflections.

Under flyover conditions, the conversion to free-field levels requires then simply the subtraction of 6 dB from all one-third octave band sound pressure levels.

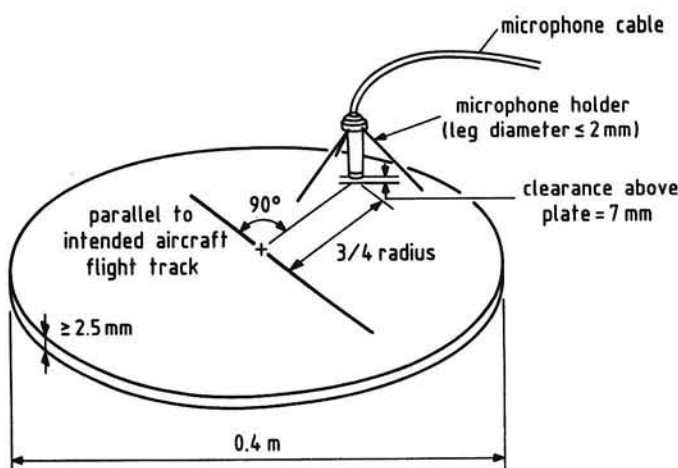


Figure 8.6-3. Inverted ground-level microphone assembly

Investigations involving many different ground microphone configurations have shown that a microphone with its protective grid mounted in an inverted position to a metal plate represents an optimum configuration for airplane noise testing. The surface of the plate should be carefully made flush with the ground surface in order to minimize diffraction effects due to impedance discontinuities between acoustically hard and soft surfaces at the edge of the ground plate. Also, the plate should be painted white to avoid local surface effects from solar heating.

Inverted microphone arrangements currently are used for full scale static engine operations, model scale noise measurements, and for in-flight testing. An example of an inverted ground-level microphone assembly developed for in-flight noise testing of propeller-driven airplanes is shown in Figure 8.6-3. Used is a circular 0.4 m diameter, at least 2.5 mm thick metal, white-painted plate, which must be placed horizontally and made flush with the surrounding ground plane with no cavities below the plate. The microphone is fixed by a holder such that the microphone diaphragm is 7 mm above and parallel to the ground plate. It has been found that the best microphone position is at 3/4 radius from the plate center in a direction normal to the flight track of the test airplane (Reference 44).

8.7 EXCESS GROUND ATTENUATION

In the preceding sections we have seen that airplane noise levels usually are measured at a position directly below the flightpath.

When these measurement data are used to predict the sound pressure levels observed at points lateral to the flight track, we must take into account the effects of spherical spreading and atmospheric absorption.

When the airplane is at a shallow angle with respect to the ground observation point, an extra attenuation may occur due to the fact that at the two receiver positions there is a different ground effect. The latter contribution to the losses is called *excess ground attenuation* (EGA) which, by definition, is the difference in the overall sound pressure level between that measured underneath the flightpath and that observed to the side of the flight track, when received at the same emission angle and source-receiver distance,

$$\text{EGA} = \text{OASPL}_c - \text{OASPL}_s , \quad (8.7-1)$$

where the subscripts *c* and *s* denote centerline and sideline position, respectively.

A positive value of EGA thus represents an attenuation in excess of that due to spherical divergence and atmospheric attenuation.

Figure 8.7-1 illustrates the geometrical relations between the two receiver positions and the flightpath. The airplane is at a point *A* on its flightpath, which, for simplicity, is assumed to be horizontal. The centerline receiver in

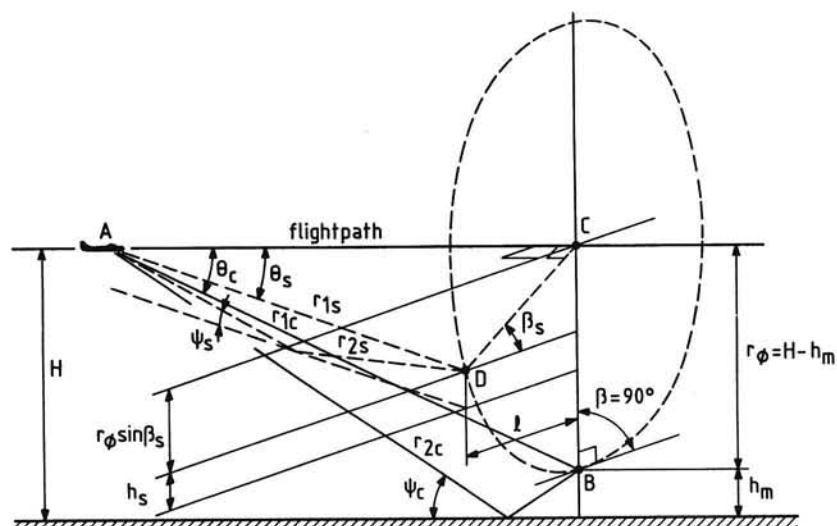


Figure 8.7-1. Geometrical model for excess ground attenuation

point B is at a height h_m directly above the flight track. Point C on the flightpath represents overhead position, i.e., the nearest distance of approach to the centerline receiver. The distance between points B and C is denoted by $r_\phi = H - h_m$, where H is the flight altitude.

The direct sound travels to the centerline receiver along a straight path $r_{1c} = r_\phi / \sin \theta_c$, where θ_c is the emission angle.

The sideline receiver in point D is at a distance l normal to the flight track and at a height h_s above an auxiliary surface parallel to and above the initial ground surface such that the slant ranges r_{1c} and r_{1s} , and the emission angles θ_c and θ_s , are the same. The lateral distance l is defined by the elevation angle β_s .

The procedure for obtaining EGA is illustrated by the two particular examples given in Figure 8.7-2. Considered is the case of $\theta = 90^\circ$, $r_1 = 1000$ m, $h_m = h_s = 1.2$ m, flight over a real soil surface ($\sigma = 100$), and an elevation angle $\beta_s = 1^\circ$.

The predictions in Figure 8.7-2 are based on typical 1-meter free-field tertsband spectra of a turbojet-powered airplane and an airplane with turbofan engines (from Reference 45).

Adjustments were made to the one meter levels to account for spherical spreading and atmospheric attenuation, according to the correction procedures described in Chapter 4. In this way the free-field tertsband levels were

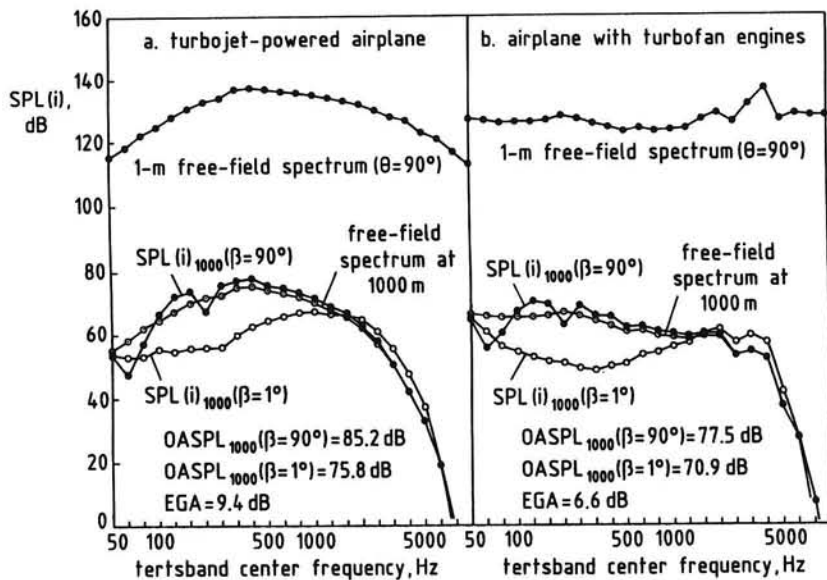


Figure 8.7-2. Noise frequency spectra of jet-driven aircraft

corrected to a slant range of 1000 m, assuming standard day weather conditions of 15°C, 70% relative humidity, and no wind.

Next, the ground effects were added to the 1000 m free-field sound pressure levels for an elevation angle $\beta = 90^\circ$ (measurement point) and $\beta_s = 1^\circ$ (ground observation point), using the spherical wave reflection factor according to Equation (8.5-1).

The ground effect over a 1/3-octave band was obtained from an integration of the mean sound square pressures, assuming that the noise source has a constant spectral density across each tertband, and that within a given tertband the reflection factor is essentially constant. Then, from Equation (8.2-5), we have

$$\Delta \text{SPL} = 10 \log \left[1 + \left(\frac{r_1}{r_2} \right)^2 |Q_i|^2 + 2 \frac{r_1}{r_2} |Q_i| \frac{\sin \alpha}{\alpha} \cos(\beta + \phi_i) \right] , \quad (8.7-2)$$

where

$$\begin{aligned} \alpha &= \pi f_i \frac{\Delta r}{c} \frac{\Delta f}{f_i} = 0.23 \pi f_i \frac{\Delta r}{c} \\ \beta &= 2\pi f_i \frac{\Delta r}{c} \sqrt{1 + \frac{1}{4} \left(\frac{\Delta f}{f_i} \right)^2} = 2.01 \pi f_i \frac{\Delta r}{c} . \end{aligned}$$

Finally, to obtain the EGA values, the corrected tertband levels were summed as follows (cf. Equation (1.9-9)):

$$\text{OASPL} = 10 \log \sum_{n=0}^{43} 10^{\text{SPL}(i)/10} , \quad (8.7-3)$$

where n is the band number.

The above examples clearly show that the value of EGA not only is a complicated function of surface impedance, radiation geometry, and atmospheric conditions, but also depends on spectral content, i.e., on aircraft type and thrust setting.

9 NOISE MEASURES

9.1 LOUDNESS LEVEL

If two pure tones of equal frequency are compared, the ear will judge the sound with the highest sound pressure level as the sound with the highest *loudness*.

Based on the reactions of a large number of listeners (*sound juries*), the loudness levels of pure tones have been established.

The results are shown in Figure 9.1-1 in the form of so-called *equal loudness level contours*. These curves, which have been internationally standardized, give the sound pressure levels of single-frequency sounds that are equally loud (Reference 46).

The unit of loudness level is the *phon*. The numerical value of the phon is defined as the free-field sound pressure level of a pure tone of 1000 Hz, heard in frontal incidence, that sounds equally loud. The value 0 phon corresponds to the threshold of hearing and the value of 120 phon to the threshold of pain.

It can be seen from Figure 9.1-1 that the human ear is less responsive to frequencies below 1000 Hz and above 6000 Hz. The curves also show that the sensitivity to frequency is more pronounced at lower phon values than at high phon values.

For example, a 100 Hz tone must be 24 dB higher than a 1000 Hz tone at a

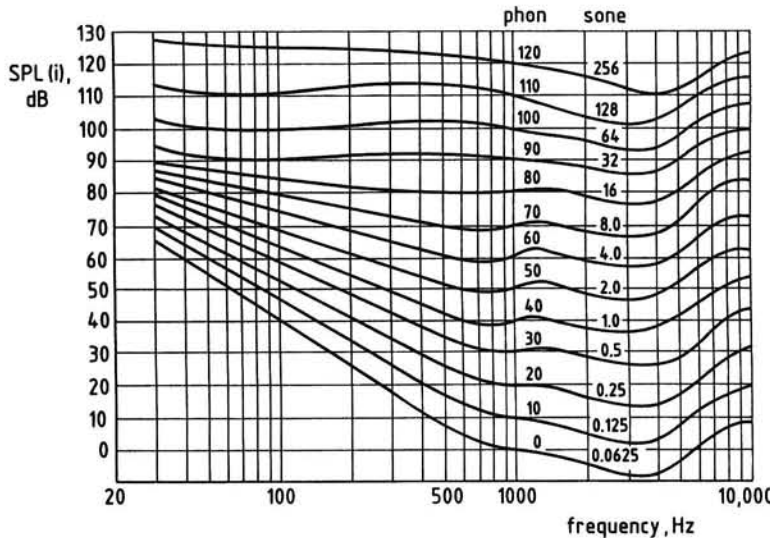


Figure 9.1-1. Equal loudness contours for pure tones

level of 40 phon and 9 dB higher at a level of 70 phon in order to give the same subjective impression of loudness.

Loudness-judgment tests also have shown that an increase of the loudness level of 10 phon corresponds to approximately a doubling of the perceived loudness.

By analogy with the relationship between sound pressure level and sound intensity, the loudness level is used as a basis for calculating the loudness.

The relationship between loudness s and loudness level p is defined by

$$s = 2^{(p-40)/10} \quad (9.1-1)$$

For any value of the loudness, the loudness level can be found from Equation (9.1-1), rewritten as

$$p = 40 + 33.3 \log s \quad (9.1-2)$$

The unit of loudness is the *sone*. By definition, a loudness level of 40 phon is taken equal to a loudness of 1 sone.

Figure 9.1-2 gives the relationship between loudness in sone and loudness level in phon, as computed from Equation (9.1-1). Using this equation, the equal loudness contours in Figure 9.1-1 have also been labeled in terms of sone.

The significance of employing the loudness scale according to Equation (9.1-1) is that the numerical value of the loudness doubles when the loudness level increases by 10 phon, i.e., when the sound approximately is judged as twice as loud.

The overall perceived loudness of a complex sound depends on several complicating factors, particularly in the case of random sound or noise. For example, of significance in determining the overall loudness is the

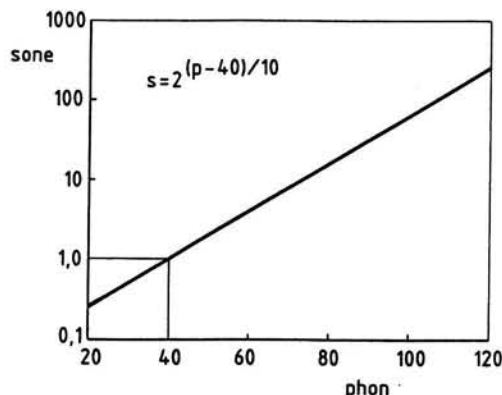


Figure 9.1-2. Graph showing the relationship between the units sone (loudness) and phon (loudness level)

effect of *masking*. This term indicates the phenomenon that a low frequency component may prevent a listener from hearing a lower amplitude component at a higher frequency.

It may be noted that masking also concerns the reduction of the audibility of a sound by the presence of another sound (Reference 12). The latter form of masking is highly relevant in communication when background noise masks speech.

To calculate a value for the true subjective response of the ear, the following empirical formulae have been developed for adding the sone values of the individual frequency bands:

$$S = s_{max} + 0.30 [\Sigma s - s_{max}] \quad \text{for 1/1-octave bands} \quad (9.1-3)$$

$$S = s_{max} + 0.20 [\Sigma s - s_{max}] \quad \text{for 1/2-octave bands} \quad (9.1-4)$$

$$S = s_{max} + 0.15 [\Sigma s - s_{max}] \quad \text{for 1/3-octave bands} \quad (9.1-5)$$

In these equations S is the overall sone value, Σs the sum of the sone values in all frequency bands, and s_{max} the greatest value of s .

Finally the total loudness is converted back into an overall phon value using Equation (9.1-2),

$$L_L = 40 + 33.3 \log S , \quad (9.1-6)$$

where L_L is the total loudness level in phon.

9.2 PERCEIVED NOISE LEVEL

When dealing with noise from airplane flyovers, frequently the measure *perceived noise level* (PNL) is used instead of loudness level. The unit of this computed quantity is *perceived noise deciBel*, designated PNdB.

Perceived noise level has been developed in the same way as the phon scale, namely by investigating the reactions of a large number of people (Reference 47).

These experiments made clear that people are more sensitive to complex sounds containing high frequency components than they are to high frequency pure tones.

As presented in Figure 9.2-1, the results are available in the form of *equal noisiness curves*. These curves are the equivalents of the equal loudness contours in sone in the previous Figure 9.1-1. Noisiness is expressed in *nøy*, the unit value being the noisiness of a *tertsband* of random sound centered on 1000 Hz heard in diffuse sound field condition at a sound pressure level of

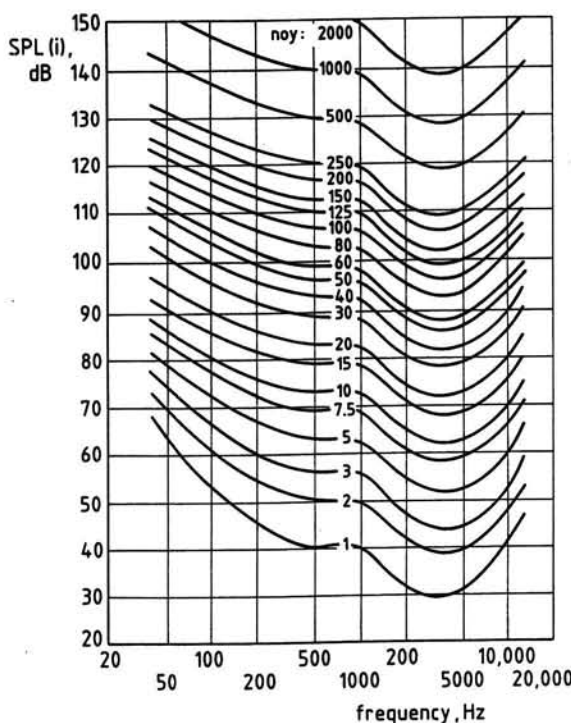


Figure 9.2-1. Equal noisiness curves

40 dB. Accordingly, the equal noisiness curves in Figure 9.2-1 relate the tertsbands sound pressure levels to a *noy-value*, n , in each 1/3-octave band. The noy values thus found are summed in the manner prescribed by Equation (9.1-5):

$$N = n_{\max} + 0.15 \left[\sum n - n_{\max} \right], \quad (9.2-1)$$

where n_{\max} is the number of noys in the tertsbands having the greatest noy value, and $\sum n$ is the sum of the noy values in all bands. Practically, the summation is restricted to the 24 one-third octave bands covering the range of center frequencies from 50 to 10,000 Hz; band numbers 17 to 40 (see Table 7.3-2).

The overall noy value N is converted into perceived noise level, in the same way as sone values are converted into phons, i.e.,

$$L_{PN} = 40 + 33.3 \log N, \quad PNdB, \quad (9.2-2)$$

where L_{PN} is the symbol for perceived noise level (PNL).

Obviously, when the value of N doubles, the perceived noise level is increased by 10 PNdB.

The perceived noise level of a sound signal having a pronounced spectral irregularity may be adjusted by a so-called *tone correction*, which has been introduced to account for the increased noisiness of audible discrete frequency components such as found in airplane flyover noise.

For the calculation procedure to determine this correction, the reader is referred to Section 9.5. Adding this penalty to the perceived noise level yields the *tone corrected perceived noise level* (TPNL), expressed in TPNdB.

9.3 MEASURING LOUDNESS LEVELS

In addition to linear response, which allows the measurement of sound pressure levels, frequency weighting filters are incorporated in sound level meters to measure sound levels that reflect the loudness caused by a complex sound.

The filters make a correction for each sound pressure level according to frequency. As presented in Figure 9.3-1, four weighting filters have been standardized, designated A, B, C and D.

The A-weighting filter weights a sound approximately according to the inverted equal loudness contour of 40 phon in Figure 9.1-1. The B and C filters correspond to the equal loudness contours of 70 and 100 phon, respectively. The D-weighting filter has been especially developed for airplane

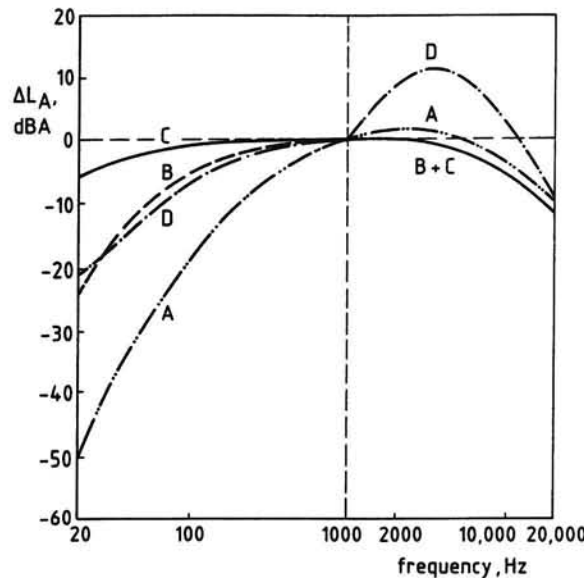


Figure 9.3-1. Frequency weighting characteristics

Table 9.3-1. A-weighting corrections for tertsbands

center frequency, Hz	correction $\Delta L_A(i)$, dBA	center frequency, Hz	correction $\Delta L_A(i)$, dBA
20	-50.5	800	-0.8
25	-44.7	1000	0.0
31.5	-39.4	1250	0.6
40	-34.6	1600	1.0
50	-30.2	2000	1.2
63	-26.2	2500	1.3
80	-22.5	3150	1.2
100	-19.1	4000	1.0
125	-16.1	5000	0.5
160	-13.4	6300	-0.1
200	-10.9	8000	-1.1
250	-8.6	10000	-2.5
315	-6.6	12500	-4.3
400	-4.8	16000	-6.6
500	-3.2	20000	-9.3
630	-1.9		

noise measurements and weights the signal in a way which approximates to the equal noisiness curve of 40 noy in Figure 9.2-1.

To indicate that meter readings thus obtained represent weighted sound levels and not sound pressure levels, they are designated AL, BL, CL or DL, and expressed in dBA, dBB, dBC or dBd.

It should be noted that the A-weighting is found to work well for loudness comparisons at all levels. Therefore, at the present time, the A-weighted sound level, AL (symbol L_A), is by far the most widely employed basic noise measure for assessing sounds of all levels, and is frequently specified for rating sounds, regardless of level. Moreover, it has been found that the numerical value of L_A is virtually equal to that of perceived noise level, except for a constant of 14 dB:

$$L_A = L_{PN} - 14 \quad , \quad (9.3-1)$$

Depending on the shape of the frequency spectrum, the above relation is uncertain within approximately ± 3 dB.

From Figure 9.3-1, we see that the A-weighting characteristic adjust the frequency response mainly by attenuating the lower frequencies. The relative

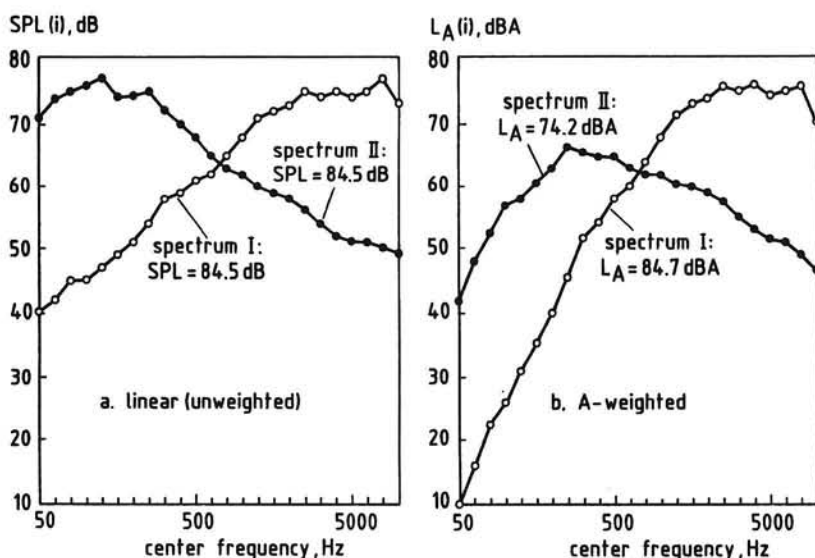


Figure 9.3-2. Effect of frequency weighting on noise level

response may be approximated by:

$$\Delta L_A = -145.528 + 98.262 \log f - 19.509 (\log f)^2 + 0.975 (\log f)^3 . \quad (9.3-2)$$

Table 9.3-1 lists the weighting corrections for tertsbands center frequencies. For a given tertsbands sound pressure level spectrum, the computation formula for the overall A-weighted sound level is:

$$L_A = 10 \log \sum 10^{\frac{10}{10}} , \text{ dBA} , \quad (9.3-3)$$

where $L_A(i) = SPL(i) + \Delta L_A(i)$ is the corrected band level.

The overall value of AL, of course, depends on spectrum type. To illustrate the effect of A-weighting on sound level we consider Figure 9.3-2, where are shown two sound spectra occurring at the same distance and angular location relative to the source. Spectrum I might be the characteristic *whine* of an airplane propelled by turbojet engines, and spectrum II might represent the *droning* of an airplane driven by gasturbine engines equipped with afterburners (Figure 9.3-3).

Afterburning is a method to achieve a temporary increase in engine thrust by burning extra fuel in the afterburner duct. When the afterburner is off, the afterburner duct serves as a basic engine exhaust nozzle.

Although the spectrum shapes in Figure 9.3-2a differ markedly from one another, in this hypothetical case their overall sound pressure levels (SPL) have the same

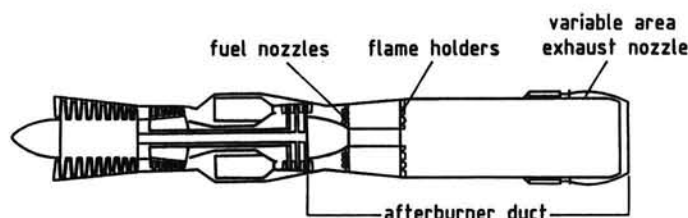


Figure 9.3-3. Turbojet with afterburner

value. However, the higher degree of annoyance caused by the high frequency components in spectrum I finds expression in a greater dBA value of the overall noise level L_A when compared with that of the low frequency noise of spectrum II (Figure 9.3-2b).

As discussed earlier in Chapters 7 and 8, tertband spectra of propeller-driven airplane noise show relative high sound pressure levels at the blade passage frequency and at the second harmonic of the fundamental. When the A-weighting is applied, however, the contributions from these low order harmonics are considerably reduced.

Figure 9.3-4, where the linear spectrum (sound pressure level spectrum) of the previous Figure 7.5-4a is repeated, indicates that higher order harmonics control the corresponding A-weighted noise level.

Finally, we note that AL is the noise evaluation measure used for the certification of propeller-driven-small airplanes (see Chapter 10).

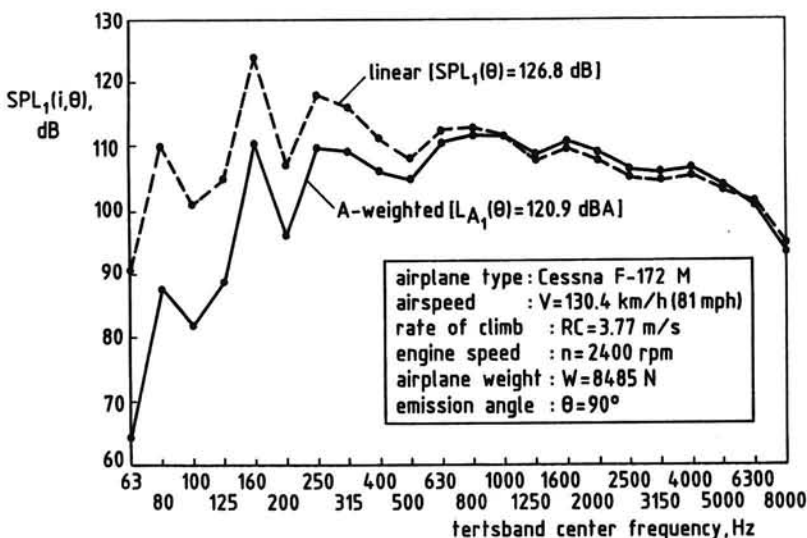


Figure 9.3-4. Effect of weighting on flyover tertband spectrum

9.4 EFFECT OF DURATION

During the flyover of an airplane, the noise level observed at a point on the ground gradually intensifies until it reaches its maximum value and then gradually again falls off.

One way to quantify the noise of a transient signal from a single airplane flyover is to use the maximum A-weighted sound level, MAL (symbol $L_{A\max}$), or the maximum tone corrected perceived noise level, MTPNL (symbol $L_{TPN\max}$).

Since the human ear responds not only to the maximum observed noise level, but also to the time-history of the noise, the effect of duration on loudness and noisiness may be included in the measurement and assessment of transient noise.

To account for the time variation in sound pressure level we may consider the total amount of sound energy delivered to the recipient during the event divided by the measurement time period (Figure 9.4-1a). This energy integration provides a single number descriptor of time-varying sound which is called *equivalent sound pressure level* (ESPL). Mathematically:

$$L_{eq,T} = 10 \log \left[\frac{1}{T} \int_0^T \frac{[p_e(t)]^2 dt}{p_{e_0}^2} \right] = 10 \log \left[\frac{1}{T} \int_0^T 10^{\frac{SPL(t)}{10}} dt \right], \text{ dB.} \quad (9.4-1)$$

In Equation (9.4-1), $L_{eq,T}$ is the symbol for equivalent sound pressure level, T

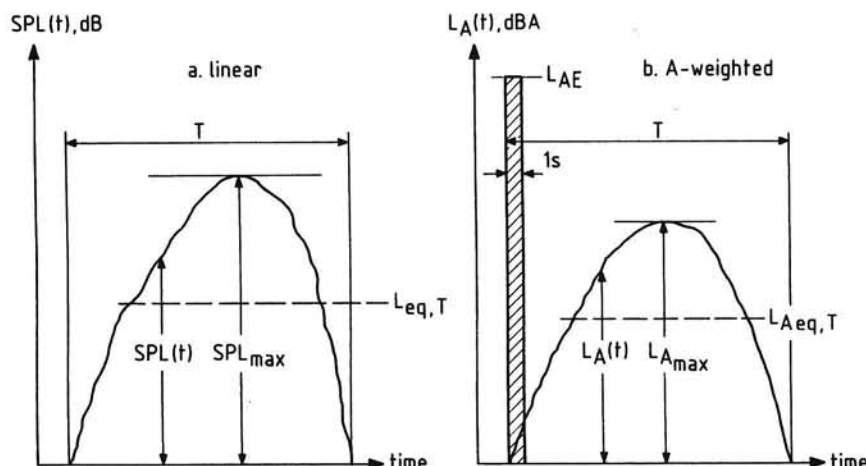


Figure 9.4-1. Time-integrated noise measures

is the time interval over which is measured, and $SPL(t)$ is the sound pressure level at any instant during the flyover.

Apparently, the equivalent sound pressure level represents the constant sound pressure level which would give the same total acoustic energy to the recipient as the actual transient sound received over the same time period T .

A well-known and important descriptor for the subjective loudness of an airplane flyover noise is the *equivalent A-weighted sound level* (EAL), expressed in dBA.

By performing continuous integration for a specified time period T , the formula is:

$$L_{A\text{ eq}, T} = 10 \log \left[\frac{1}{T} \int_0^T 10^{\frac{L_A(t)}{10}} dt \right], \text{ dBA.} \quad (9.4-2)$$

In this equation $L_{A\text{ eq}, T}$ is the symbol for EAL and $L_A(t)$ is the instantaneous A-weighted sound level (Figure 9.4-1b).

Both $L_{eq,T}$ and $L_{A\text{ eq}, T}$ can be measured directly with an integrating sound level meter set to the appropriate weighting. The readings also have the advantage of being comparable with noises other than that of aircraft.

In order to eliminate the influence of the magnitude of the measurement duration T on the resultant sound level, the *sound exposure level* (SEL) should be employed. The numerical value of this quantity is equal to that of a given equivalent A-weighted sound level when normalized to a time period of one second (see Figure 9.4-1b). Sound exposure level is also expressed in units dBA. In formula:

$$L_{AE} = 10 \log \left[\frac{1}{T_1} \int_0^T 10^{\frac{L_A(t)}{10}} dt \right], \text{ dBA} \quad (9.4-3)$$

where L_{AE} is the symbol for sound exposure level and T_1 is the reference time of one second.

A special case of SEL is the *single event noise exposure level*, SENEL. This noise descriptor differs from SEL in that the computation is made for those transient sounds which exceed a certain level.

EAL is related to SEL by the following relationship:

$$L_{A\text{ eq}, T} = L_{AE} - 10 \log \frac{T}{T_1}, \text{ dBA.} \quad (9.4-4)$$

The use of SEL allows a direct comparison of the loudness of transient

sounds. It also enables us to determine the overall level of multiple event noise exposure by summing the individual SEL values energetically,

$$L_{Aeq,T} = 10 \log \sum_{j=1}^N 10^{\frac{L_{AE}(j)}{10}} - 10 \log \frac{T}{T_1}, \quad (9.4-5)$$

where N is the number of events, $L_{AE}(j)$ is the sound exposure level for the j^{th} event, and T is a specified time period.

The first term of the right-hand side of Equation (9.4-5) may be called the cumulative sound exposure level (CSEL).

Equation (9.4-2) requires continuous integration of A-weighted sound level for a specified time period. For discrete sampling the computation formula is

$$\left[L_{Aeq,T} = 10 \log \left[\frac{1}{n} \sum_{k=1}^n 10^{\frac{L_A(k)}{10}} \right], \text{ dBA}, \right] \quad (9.4-6)$$

where $L_A(k)$ is the instantaneous A-weighted sound level for sample k , and n is the number of samples in the measurement time T .

Another time-integrated single number descriptor of airplane flyover noise is the *effective perceived noise level* (EPNL), expressed in EPNdB units. It is derived from PNL, and includes both pure-tone and duration corrections. The effective perceived noise level is defined, mathematically, as

$$L_{EPN} = 10 \log \left[\frac{1}{T_{10}} \int_0^T 10^{\frac{L_{TPN}(t)}{10}} dt \right], \quad (9.4-7)$$

where L_{EPN} is the symbol for effective perceived noise level, T_{10} is the normalizing constant of 10 seconds, $L_{TPN}(t)$ is the instantaneous tone corrected perceived noise level, and T is the integration time.

Usually, the time period T is defined as the time interval during which the sound level is within 10 dB of its maximum value since only the highest levels will contribute significantly to the resultant noise level. The corresponding time interval when using the above approximation is known as the *10 dB-down time*.

For practical purposes EPNL is computed from TPNL values determined at discrete 0.5 second time intervals throughout the period of the flyover noise (see Section 9.5). Then, the computation formula for the effective perceived noise level can be written as:

$$L_{EPN} = 10 \log \left[\frac{\Delta t}{T_{10}} \sum_{k=t_1}^{t_2} 10^{\frac{L_{TPN}(k)}{10}} \right], \quad (9.4-8)$$

where $\Delta t = 0.5$ s, and t_2 and t_1 are the points of time closest to those instants when TPNL is 10 TPNdB less than its maximum value, and k denotes the k^{th} time segment within the duration interval.

Returning to the noise time-histories in Figure 1.12-2, we may understand that the number of time samples increases as the flight speed and altitude are lower.

By substitution of $T_{10} = 10$ s and $\Delta t = 0.5$ s, we can rewrite Equation (9.4-8) as

$$L_{EPN} = 10 \log \left[\sum_{k=t_1}^{t_2} 10^{\frac{L_{TPN}(k)}{10}} \right] - 13. \quad (9.4-9)$$

The effective perceived noise level is often expressed as the algebraic sum of maximum perceived noise level (MTPNL) and a duration allowance, designated by the symbol Δ . Thus

$$L_{EPN} = L_{TPN_{\max}} + \Delta. \quad (9.4-10)$$

From Equations (9.4-9) and (9.4-10), we have

$$\Delta = 10 \log \left[\sum_{k=t_1}^{t_2} 10^{\frac{L_{TPN}(k)}{10}} \right] - 13 - L_{TPN_{\max}}. \quad (9.4-11)$$

It may be noted that Δ is usually negative.

As will be discussed in Chapter 10, the measure EPNL is used in noise certification of all civil subsonic jet air-planes and heavy propeller-driven airplanes.

To describe the noisiness caused by a succession of airplane flyovers, the measure *cumulative perceived noise level* (CPNL) may be used:

$$L_{CPN} = 10 \log \left[\sum_{j=1}^N 10^{\frac{L_{EPN(j)}}{10}} \right] + 10 \log \frac{T_{10}}{T_1}, \quad (9.4-12)$$

where L_{CPN} is the symbol for cumulative noise exposure level, $L_{EPN(j)}$ is the effective perceived noise level for the j^{th} event, and N is the number of events.

In parallel to Equation (9.4-5) we may use the measure *equivalent cumulative perceived noise level* (ECPNL):

$$L_{ECPN} = 10 \log \left[\sum_{j=1}^N 10^{\frac{L_{EPN}(j)}{10}} \right] + 10 - 10 \log \frac{T}{T_1} , \quad (9.4-13)$$

where L_{ECPN} is the symbol for ECPNL, and T is a specified exposure time in seconds.

In view of the importance of effective perceived noise level, the next section will be devoted to the procedure of calculating this noise measure.

9.5 CALCULATION OF EFFECTIVE PERCEIVED NOISE LEVEL

As we have learned in the preceding section, the effective perceived noise level in units EPNdB is a single event noise descriptor based on one-third octave band data used to certify most types and classes of commercial aircraft for flyover noise.

In this section we will describe the calculation procedure of EPNL according to the international standards for noise emission by aircraft (Reference 29). These requirements are set by the *International Civil Aviation Organization* (ICAO), a special agency in the United Nations, which is responsible for making rules and regulations in consultation with all member states.

The equations given in the preceding sections of this chapter that we shall use here are repeated and renumbered for the sake of convenience.

In deriving effective perceived noise level, the sound pressure level spectrum must be measured at half-second time intervals throughout the time period of the flyover. Each spectrum must consist of 24 tertbands with a center frequencies from 50 Hz to 10,000 Hz (band numbers 17 to 40; see Table 7.3-2).

The instantaneous sound pressure level in each tertband, $SPL(i,k)$, must be converted to a noy value, $n(i,k)$, by reference to the tables in Appendix A, or to the mathematical formulation of these tables given in reference 29 (see also Figure 9.2-1). The noy values thus obtained are combined in the manner prescribed by the following expression:

$$N(k) = n_{\max}(k) + 0.15 \left[\left(\sum_{i=17}^{40} n(i,k) \right) - n_{\max}(k) \right] , \quad (9.5-1)$$

where $n_{\max}(k)$ is the largest of the noy values $n(i,k)$. To avoid confusion with the noy values, the band number is denoted here by the letter i , instead of n as used originally in Chapter 7.

The overall noy value $N(k)$ is converted back into perceived noise level, $L_{PN}(k)$, by use of the relation:

$$L_{PN}(k) = 40 + \frac{10}{\log 2} \log N(k) . \quad (9.5-2)$$

In the case that the flyover sound pressure level spectra show pronounced spectral irregularities, a tone correction, $C(k)$, must be added to the perceived noise level. Thus,

$$L_{TPN}(k) = L_{PN}(k) + C(k) , \quad (9.5-3)$$

where $L_{TPN}(k)$ is the symbol for tone corrected perceived noise level (TPNL) for the k^{th} one-half second increment of time.

An example of tone correction calculation is presented in Table 9.5-1 (see page 201), illustrating the step by step procedure given below. The numbers heading each column correspond to step numbers in the calculation procedure.

1. For each spectrum, list the tertband sound pressure levels, $SPL(i,k)$, beginning with band number $i = 19$ ($f_i = 80$ Hz) and ending with band number $i = 40$ ($f_i = 10,000$ Hz).
2. Calculate the so-called *slopes*, i.e., the differences in sound pressure level, $s(i,k)$, where $s(i,k) = SPL(i,k) - SPL[(i - 1), k]$.
3. Determine the changes in slope, $\Delta s(i,k)$, where $\Delta s(i,k) = s(i,k) - s[(i - 1), k]$.
4. Shade the cells with those values of $s(i,k)$ where the absolute value of change in slope, $\Delta s(i,k)$, is greater than five.
5. Shade the cell with $SPL(i,k)$ if the shaded value of the slope $s(i,k)$ is positive and algebraically greater than the slope $s[(i - 1), k]$.
6. Shade the cell with $SPL[(i - 1), k]$ if the shaded value of the slope $s(i,k)$ is zero or negative and the slope $s[(i - 1), k]$ is positive.
7. Omit all shaded values of $SPL(i,k)$ and calculate new values $SPL'(i,k)$ as follows:
 - a. For the shaded sound pressure levels in bands 19 to 39, set the

adjusted sound pressure level equal to the arithmetic mean of the preceding and following sound pressure levels,

$$\text{SPL}'(i, k) = \frac{1}{2} [\text{SPL}[(i-1), k] + \text{SPL}[(i+1), k]] .$$

- b. If the SPL value of the highest frequency band $i = 40$ ($f_i = 10,000$ Hz) is shaded, set

$$\text{SPL}'(40, k) = \text{SPL}(39, k) + s(39, k) .$$

8. For all non-shaded $\text{SPL}(i, k)$, set $\text{SPL}'(i, k) = \text{SPL}(i, k)$.
9. Compute new slopes $s'(i, k)$, including one for the fictitious band $i = 41$, as follows:

$$s'(19, k) = s'(20, k)$$

$$s'(i, k) = \text{SPL}'(i, k) - \text{SPL}'[(i-1), k]$$

$$s'(41, k) = s'(40, k) .$$

10. For band numbers 19 to 39 compute the arithmetic mean of three adjacent slopes,

$$\bar{s}(i, k) = \frac{1}{3} [s'(i, k) + s'[(i+1), k] + s'[(i+2), k]] .$$

11. Compute ultimate adjusted sound pressure levels, $\text{SPL}''(i, k)$, by starting with band number $i = 19$ and proceeding to band number $i = 40$ as follows:

$$\text{SPL}''(19, k) = \text{SPL}(19, k)$$

$$\text{SPL}''(i, k) = \text{SPL}''[(i-1), k] + \bar{s}[(i-1), k] .$$

12. Determine the difference, $F(i, k)$, between the original sound pressure level and the ultimate adjusted sound pressure level where

$$F(i, k) = \text{SPL}(i, k) - \text{SPL}''(i, k) .$$

Note only values of $F(i, k)$ equal to or greater than three.

13. Determine the discrete frequency corrections, $C(i, k)$, using the following equations (see also Figure 9.5-1):

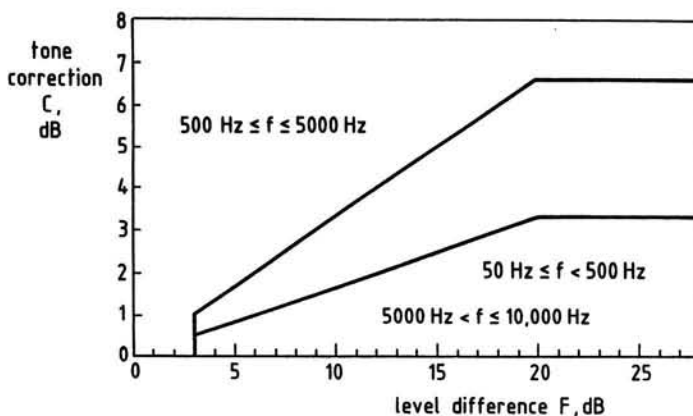


Figure 9.5-1. Tone correction C

$$\left. \begin{array}{ll} C(i,k) = 0 & F(i,k) < 3 \\ C(i,k) = F(i,k)/3 & 3 \leq F(i,k) < 20 \\ C(i,k) = 6\frac{2}{3} & 20 \leq F(i,k) \end{array} \right\} \text{for bands in the frequency range: } 500 \text{ Hz} \leq f \leq 5000 \text{ Hz}$$

$$\left. \begin{array}{ll} C(i,k) = 0 & F(i,k) < 3 \\ C(i,k) = F(i,k)/6 & 3 \leq F(i,k) < 20 \\ C(i,k) = 3\frac{1}{3} & 20 \leq F(i,k) \end{array} \right\} \text{for bands in the frequency ranges: } 50 \text{ Hz} \leq f < 500 \text{ Hz} \text{ and } 5000 \text{ Hz} < f \leq 10,000 \text{ Hz.}$$

14. The maximum value of $C(i,k)$ determined in step 13 defines the tone correction $C(k)$ which, according to Equation (9.5-3), should be added to $L_{PN}(k)$ to derive $L_{TPN}(k)$.

Repeating the above procedure for each k^{th} increment of time yields the TPN-time history. Of course, at some point of time the maximum TPN value, $L_{TPN_{max}}$, occurs.

Figure 9.5-2 gives a sketch of a flyover noise time history, where the points of time t_1 and t_2 are to be determined as follows:

Table 9.5-1. Determination of tone correction

step		1, 5, 6	2, 4	3	7, 8	9	10	11	12	13, 14
i	f_i , Hz	SPL (i,k)	s (i,k)	Δs (i,k)	SPL' (i,k)	s' (i,k)	\bar{s} (i,k)	SPL'' (i,k)	F (i,k)	C (i,k)
19	80	71			71	-5	-1	71		
20	100	66	-5		66	-5	+3	70		
21	125	76	+10	+15	73	+7	+31/6	73		
22	160	80	+4	-6	80	+7	+10/3	78 1/6		
23	200	85	+5	+1	81.5	+1.5	-5/3	81.5	3.5	0.6
24	250	83	-2	-7	83	+1.5	-9/6	79 5/6	3 1/6	0.5
25	315	75	-8	-6	75	-8	-4/3	78 1/3		
26	400	78	+3	+11	77	+2	+5/3	77		
27	500	79	+1	-2	79	+2	+1	78 2/3		
28	630	80	+1	0	80	+1	+1	79 2/3		
29	800	80	0	-1	80	0	+1	80 2/3		
30	1k	82	+2	+2	82	+2	+2/3	81 2/3		
31	1.25k	83	+1	-1	83	+1	+2/3	82 1/3		
32	1.6k	82	-1	-2	82	-1	+2/3	83		
33	2k	84	+2	+3	84	+2	+8/3	83 2/3		
34	2.5k	85	+1	-1	85	+1	+11/6	86 1/3		
35	3.15k	90	+5	+4	90	+5	+4/3	88 1/6		
36	4k	100	+10	+5	89.5	-0.5	-4/3	89.5	10.5	3.5
37	5k	89	-11	-21	89	-0.5	-17/6	88 1/6		
38	6.3k	86	-3	+8	86	-3	-13/3	85 1/3		
39	8k	91	+5	+8	81	-5	-5	81	10	1.7
40	10k	76	-15	-20	76	-5		76		
41	12.5k					-5				

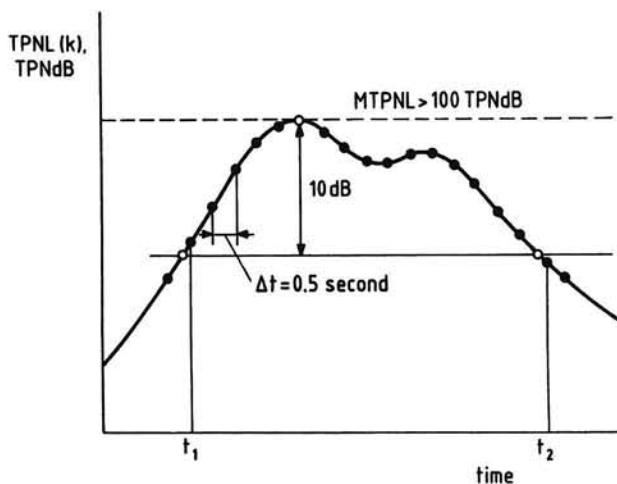


Figure 9.5-2. Typical variation of airplane flyover noise

- If the value of $L_{TPN_{max}}$ is greater than 100 TPNdB, t_1 is the first point of time after which L_{TPN} becomes greater than $L_{TPN_{max}} - 10$ and t_2 is the point of time after which L_{TPN} remains constantly less than $L_{TPN_{max}} - 10$.
- If $L_{TPN_{max}}$ is less than 100 TPNdB, t_1 is the first point of time after which L_{TPN} becomes greater than 90 TPNdB and t_2 is the point of time after which L_{TPN} remains constantly less than 90 TPNdB.
- If $L_{TPN_{max}}$ is less than 90 TPNdB, L_{EPN} is taken as equal to $L_{TPN_{max}}$.

The computation formula for the effective perceived noise level can be written as

$$L_{EPN} = 10 \log \left[\frac{\Delta t}{T_{10}} \sum_{k=t_1}^{t_2} 10^{\frac{L_{TPN}(k)}{10}} \right], \quad (9.5-4)$$

where $\Delta t = 0.5$ s, $T_{10} = 10$ s, and $t_2 - t_1$ is the time interval in seconds defined by the points of time corresponding to the value $L_{TPN_{max}} - 10$ or 90 TPNdB, as specified above.

9.6 NOISE CONTOURS

The noise heard on the ground near an airport from which an airplane is taking off, or toward it is approaching to land can be presented by plotting lines of constant noise level.

These so-called *single-event noise contours* or *footprints* give the noise level at any particular point on the ground expressed in one of the single number noise descriptors treated in the preceding sections.

Each contour encloses the area where the noise levels are in excess of the cited level. An example of a single-event noise contour produced by a takeoff maneuver of a transport airplane is portrayed in Figure 9.6-1.

As depicted in Figure 9.6-2, the takeoff path of the airplane with all engines operating may be divided into the following phases:

- ground run
- first segment climb (takeoff thrust, flaps and landing gear down)
- second segment climb (takeoff thrust and flaps down, landing gear up)
- third segment climb (maximum climb thrust, flaps and landing gear up)
- continued climb (reduced thrust).

To improve rate of climb the landing gear is retracted soon after liftoff. Shortly after the thrust setting is reduced to maximum climb thrust.

Once a safe altitude has been reached thrust may be reduced again to less than maximum climb thrust since satisfactory climb performance may also be attained at a considerable lower engine thrust setting. This so-called *thrust cutback procedure* may yield lower noise levels than are observed during a full thrust climb, where the airplane reaches a greater distance from the ground.

Noise footprints as sketched in Figure 9.6-1 may also be used to investigate the effects of noise abatement techniques and to demonstrate how much less noise is generated by new or modified airplanes compared to older or unmodified versions.

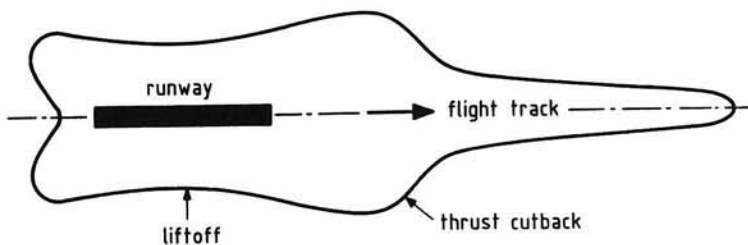


Figure 9.6-1. Typical takeoff footprint

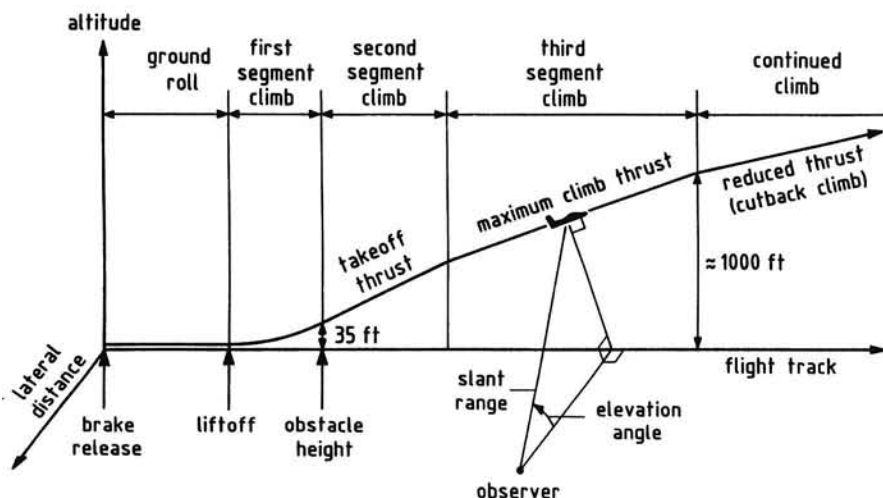


Figure 9.6-2. Transport airplane takeoff path

The construction of noise footprints requires calculation of the noise level at a large number of ground observations points around the airport and connecting lines through individual points with equal level.

Calculation of noise level at a given observation point caused by an individual airplane is based on knowledge of the noise characteristics of the airplane, the location of its flight path relative to the observation point, and engine power and airspeed at each point along the flight path.

The noise emission characteristics, usually, are specified by the relationship between observed (peak) noise level under the flight path, shortest distance between source and receiver (slant range distance), and power setting. These *noise-thrust/power-distance* data are given for reference atmospheric conditions. They can be obtained by executing flyover noise measurements with the microphone located on the flight track, as illustrated by the example in the previous Figure 7.5-1. The resulting noise-power-distance curves for the small propeller-driven airplane considered there, are presented in Figure 9.6-3.

When the airplane is close to the ground, noise propagates at low angles of incidence to the sideline. Under these conditions it may be necessary to apply adjustments to the noise levels of Figure 9.6-3 to account for excess ground attenuation (EGA). Then, according to our discussion in Chapter 8, noise levels observed at sideline locations are lower than the levels at locations directly below the airplane at the same distance. At small elevation angles an additional attenuation caused by airframe shielding may also be of importance (Reference 48).

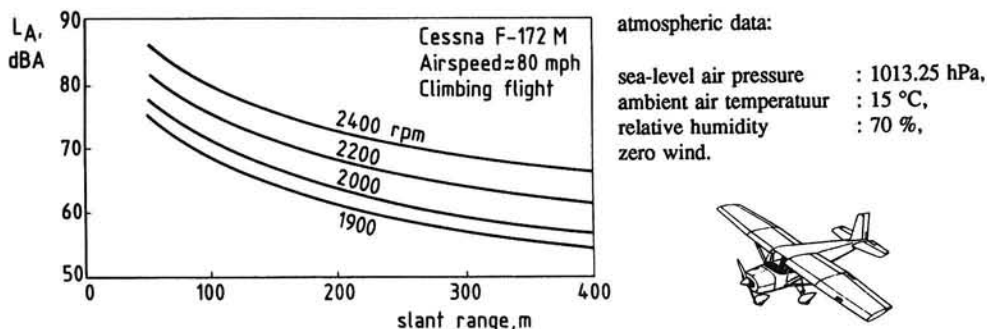


Figure 9.6-3. Noise-power-distance graph for a small propeller-driven airplane

The total noise level reduction from ground effects and shielding is termed *lateral noise attenuation* (References 49 and 50).

A detailed description of a method for computing noise contours around airports is presented in Reference 51. To simplify the calculations, airplane performance and noise data are developed for certain computational reference conditions. The influences of vertical gradients of wind and temperature, moisture content, and other real-life conditions such as local topographical features are left out of account.

9.7 INDICES OF TOTAL NOISE EXPOSURE

Measures used to quantify the impact of noise in airport communities due to the air traffic activities are called *noise indices*.

A large number of indices have been established in the different countries and have been raised to regulations on the assessment of total airplane noise exposure around airports on an individual national basis. All these airport annoyance measures are based on acoustical descriptors such as sound exposure level (SEL), effective perceived noise level (EPNL), maximum perceived noise level (MPNL), or maximum A-weighted sound level (MAL). They may also incorporate weightings of these single event levels depending on the time of day or night and of the year at which they occur. Also weightings on the number of airplane movements within a specified time period may be made.

The principles of the various noise indices will be illustrated in the following by reference to a few typical examples (Reference 52).

1. Day-night average level (DNL).

The day-night average level is the equivalent A-weighted sound level integrated on the basis of the squared pressures over a 24 hour period.

The noise levels occurring at nighttime are increased by 10 dB in order to account for the increased annoyance cause by noise heard during the nighttime hours 2200 to 0700. The difference of 10 dB between the noise levels acceptable during day and night is adopted from experience gained with regard to industrial noise. The question of noise disturbed sleep will be discussed in more detail in Section 9.8.

The index DNL, which has been developed in the U.S.A. as a measure for environmental noise, is a modification to the basic $L_{Aeq,T}$ defined by Equations (9.4-2) and (9.4-6).

DNL can be determined by continuous integration of A-weighted sound level for a 86400 second (24 hour) period:

$$L_{DN} = 10 \log \left[\frac{1}{86400} \int_0^{86400} w(t) 10^{\frac{L_A(t)}{10}} dt \right], \quad (9.7-1)$$

where L_{DN} is the symbol for DNL, w is time of day weighting factor (from 0700 to 2200, $w = 1$; from 2200 to 0700, $w = 10$), t is time in seconds.

For discrete sampling of A-weighted sound level, the computation formula reads:

$$L_{DN} = 10 \log \left[\frac{1}{n} \sum_{k=1}^n w(k) 10^{\frac{L_A(k)}{10}} \right], \quad (9.7-2)$$

where $w(k)$ is the time of day weighting factor for sample k , $L_A(k)$ is A-weighted sound level for sample k , and n is the number of samples in a 24-hour period. For sounds with time varying fluctuations as observed from aircraft flyovers, one uses L_{AE} instead of L_A (cf. Equation (9.4-13)).

2. Weighted equivalent continuous perceived noise level (WECPNL).

This noise index also quantifies the total noise exposure over a 24-hour period. It is based on EPNL and applies a 10 dB correction to nighttime levels from 2200 to 0700 hours. In addition, an appropriate weighting for monthly temperature values is included.

For continuous time integration of perceived noise level the equation for WECPNL is as follows:

$$L_{WECPN} = 10 \log \left[\frac{1}{86400} \int_0^{86400} w(t) 10^{\frac{L_{TPN}(t)}{10}} dt \right] + s , \quad (9.7-3)$$

where L_{WECPN} is the symbol for WECPNL, w is the time of day weighting factor (from 0700 to 2200, $w = 1$; from 2200 to 0700, $w = 10$), t is time in seconds, and s is the seasonal weighting factor, as tabulated below.

condition	s , EPNdB
- less than 100 hours per month at or above 20°C	-5
- more than 100 hours per month at or above 20°C and less than 100 hours at or above 25.6°C	0
- more than 100 hours per month at or above 25.6°C	5

In practice, WECPNL is determined from ECPNL according to Equation (9.4-13):

$$L_{WECPN} = 10 \log \left[\frac{5}{8} 10^{\frac{L_{ECPN_d}}{10}} + \frac{3}{8} 10^{\frac{L_{ECPN_n}}{10}} \right] + s , \quad (9.7-4)$$

where L_{ECPN_d} is the ECPNL during the daytime hours, and L_{ECPN_n} is the ECPNL during the nighttime hours.

3. Noise and number index (NNI).

The noise and number index uses the average (i.e., on an energy basis) maximum perceived noise level and the number of flyovers heard during one day or one night.

The index has been developed in Great Britain for community noise assessment, and is determined by the following formula (Reference 1):

$$\begin{aligned} NNI &= \bar{L}_{TPN\max} + 15 \log N - 80 \\ &= 10 \log \left[\frac{1}{N} \sum_{j=1}^N 10^{\frac{L_{TPN\max}(j)}{10}} \right] + 15 \log N - 80 , \end{aligned} \quad (9.7-5)$$

where N is the number of events during the exposure time, and $L_{TPN\max}(j)$ is

the maximum perceived noise level occurring during the j^{th} event. The constant 80 in Equation (9.7-5) is introduced to set the lower limit of annoyance at about 80 PNdB. In other words, the noise and number index only includes observed noise levels greater than 80 PNdB.

4. Noise load (B).

The noise load in Kosten units (K_e) combines average (i.e., on an energy basis) maximum A-weighted sound level with the number of passages heard within the period of one year. Appropriate weightings are made for the time of day and night.

Noise load is used for the quantification of noise pollution in the vicinity of commercial airports and military airfields in the Netherlands, and is computed from the following equation:

$$B = 20 \log \left[\sum_{j=1}^N w(j) 10^{\frac{L_{A\max}(j)}{15}} \right] - 157 , K_e , \quad (9.7-6)$$

where N is the number of events per year, $L_{A\max}(j)$ is the maximum A-weighted sound level occurring during the j^{th} event, and $w(j)$ is the time of day weighting factor for event j , as specified below.

time of movement	weighting factor w	time of movement	weighting factor w
0600 - 0700	8	2000 - 2100	4
0700 - 0800	4	2100 - 2200	6
0800 - 1800	1	2200 - 2300	8
1800 - 1900	2	2300 - 0600	10
1900 - 2000	3		

We remark at this point that around the general aviation airfields in the Netherlands a modification of the basic $L_{A\text{eq}, T}$ according to Equation (9.4-5) is employed to quantify the noise load in dBA-units:

$$B_{GA} = 10 \log \left[\sum_{j=1}^N w(j) 10^{\frac{L_{AE}(j)}{10}} \right] - 10 \log \frac{T}{T_1} , \quad (9.7-7)$$

where the subscript "GA" denotes general aviation, N is the number of events during a relevant period of twelve hours ($T = 43200$ s), and $w(j)$ is a time of day weighting factor for event j .

For the surroundings of the general aviation airstrips, where a high per-

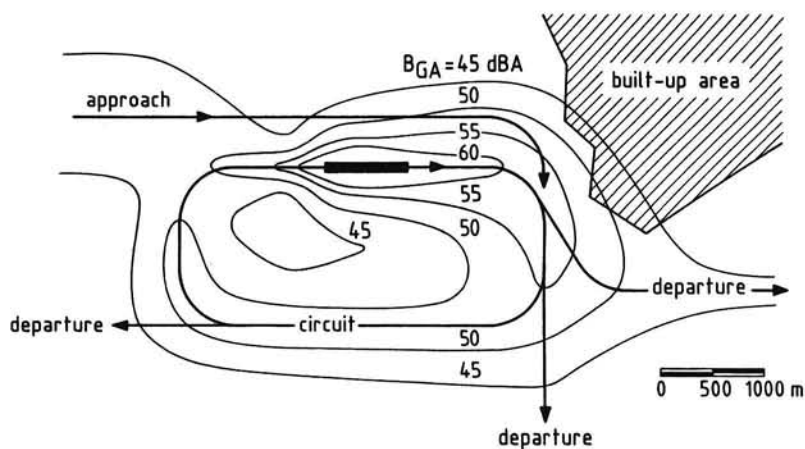


Figure 9.7-1. Computed noise load contours around a general aviation airstrip; circuit altitude is 152 m (500 ft)

percentage of the airplane operations consists of touch-and-go training, the long duration of the noise from airplanes in the traffic pattern is a major contributing factor to the annoyance. This explains the use of a $L_{Aeq,T}$ -type unit in Equation (9.7-7) instead of maximum A-weighted sound level.

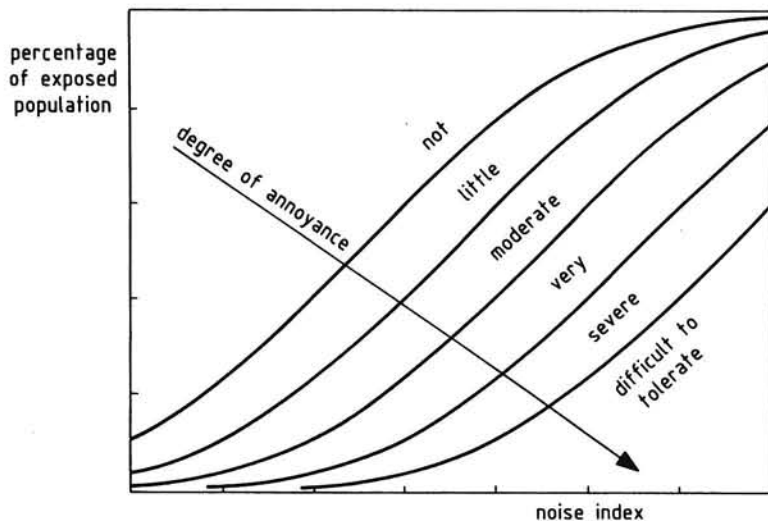


Figure 9.7-2. Typical relations between noise exposure level and percentage of people annoyed

Using a particular noise index, community noise impact around a commercial airport or a military airfield can be visualized by drawing contours of constant total noise exposure on a local map.

As an example, B_{GA} -contours are presented in Figure 9.7-1, where a total number of 520 airplane operations is considered (Reference 53).

Computed contours may be published at regular times to indicate the changing noise situation at an airport and its surroundings. The noise exposure zones enclosed by the contours provide a basis for land use planning and noise abatement procedures.

On the basis of social surveys, the noise and number index (NNI) and the noise load (B) have been correlated with the percentage of people disturbed by the noise of aircraft operations as well as with the experienced degree of annoyance. The typical plot for the annoyance levels has the form shown in Figure 9.7-2.

Accordingly, noise exposure zones not only may indicate where around an airport noise nuisance happens, but they are also useful to quantify the number of people annoyed by aviation noise and to estimate the noise problem in terms of subjective human response.

9.8 NOISE INDUCED SLEEP DISTURBANCE

It has been recognized that the human tolerance to noise nuisance is much greater during the day than during the night. In other words, a sound which people would ignore in the daytime, would be an annoying noise at night.

In addition to interviewing people, physiological monitoring of sleepers under laboratory conditions has been carried out to study the effects of noise on sleep. Results reported in Reference 54 indicate that noise induced sleep disturbances do not appear below levels of 50 to 60 dBA. Another result of this investigation is presented in Figure 9.8-1, where the solid line gives the allowable

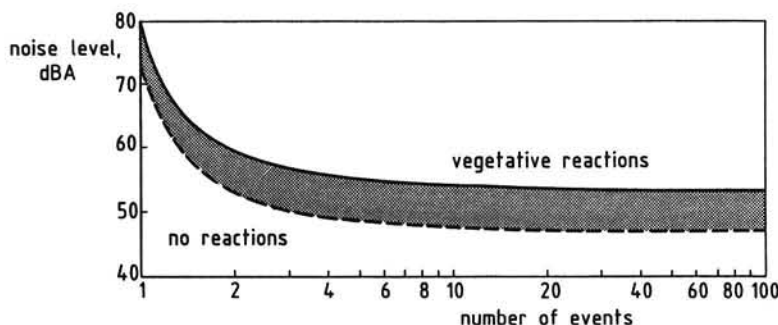


Figure 9.8-1. Sleep disturbance (Griefahn-curves)

peak A-weighted noise level as a function of the number of nighttime exposures, accepting that the number of awakenings by the noise is equal to 10 percent of the number of people living in a given residence.

The above relationship can be expressed by

$$L_{A\max} = (-0.09 + 0.129N - 0.0018N^2)^{-1} + 53.16, \text{ dBA}, \quad (9.8-1)$$

where N is the number of events.

The dash curve in Figure 9.8-1 represents the boundary below which no reactions to noise exposure during sleep are aroused. The term 'no reactions' means that only short duration reactions and/or eye movements occur; in the present case also with a probability of 10 percent.

9.9 LOSS OF HEARING FROM NOISE EXPOSURE

As shown schematically in Figure 9.9-1, the main components of the human ear are the *outer ear*, the *middle ear*, and the *inner ear*.

The outer ear consists of the *pinna*, the *external auditory canal*, and the *eardrum* which is a thin membrane closing off the external canal. The sound pressures in the air causes the eardrum to vibrate.

The air-filled cavity of the middle ear contains three interconnected small bones or ossicles called the *hammer*, *anvil* and *stirrup*. These bones, by the attachment of the first to the eardrum and the connection of the third with the

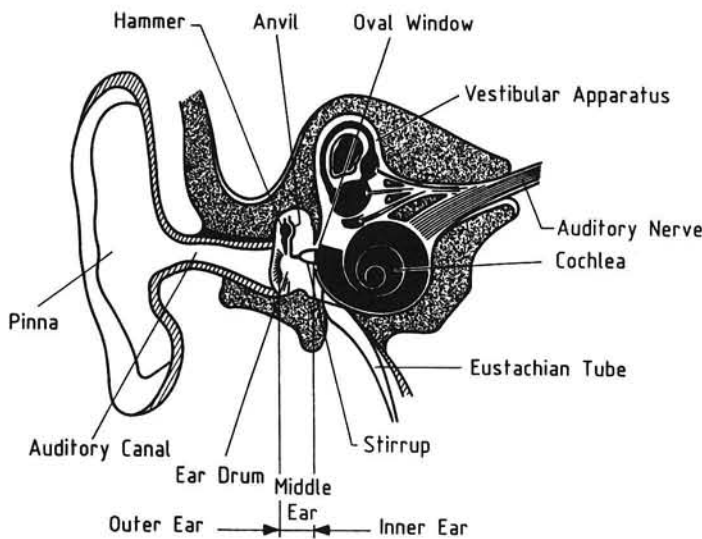


Figure 9.9-1. A schematic drawing of the auditory system

oval-window membrane, convert the sound pressures in the air into movements of the fluid in the *cochlea*, which is the organ of hearing in the cavity of the inner ear.

Equalization of pressure inside the middle ear is obtained by means of the *Eustachian tube*, which connects the middle ear to the throat and nose.

The various components in the outer and inner ear not only act as transmitters but also as amplifiers of acoustic energy.

The fluid-filled cochlea is a snail-shaped tube which is divided longitudinally into two parts by the *basilar membrane* (not indicated). Within the cochlea, on the surface of the basilar membrane is the *organ of Corti* which contains *sensory cells* or *hair cells* and the endings of the *auditory nerve*.

The basilar membrane is forced into vibration by the movements of the fluid in the cochlea. These vibrations are transmitted to the hair cells which in turn transform the vibrations into neural impulses which, finally, are conveyed to the brain by the auditory nerve.

For completeness, it may be mentioned that the inner ear also contains the vestibular apparatus. The function of this organ is related to the maintenance of balance.

As has been stated previously in Chapter 1, our auditory system deteriorates with age. The normal loss of hearing due to the aging process is named *presbyacusias*. This form of hearing loss is apparently caused by degeneration of the hair cells in the inner ear, and appears to affect the higher tones, as depicted in Figure 9.9-2a.

In addition, long-term exposure to high noise levels or exposure to an excessive single impulse noise can cause permanent damage to the hair cells. The corresponding hearing loss is called *nerve deafness*. Of course, injury to

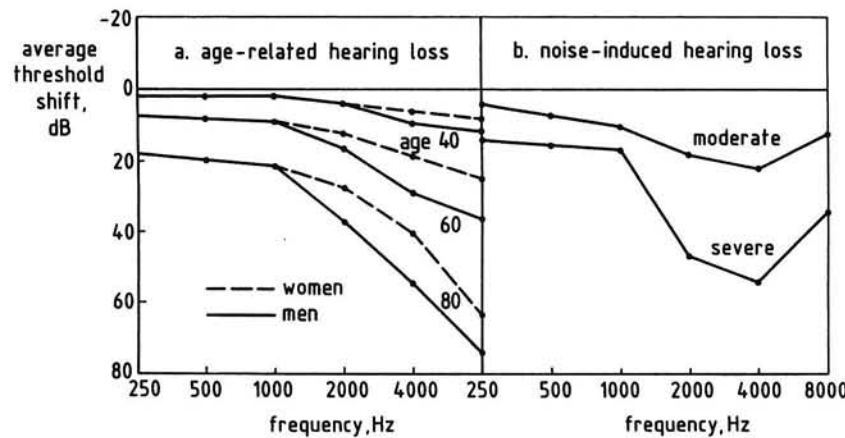


Figure 9.9-2. Typical shifts in the threshold of hearing for pure tones

the hair cells is beyond repair.

Nerve deafness is related to both level of noise and exposure duration. The greater the noise level and/or duration, the greater the hearing impairment.

Figure 9.9-2b illustrates the hearing loss due to detriment of the hair cells from prolonged exposure to high noise levels. Typically, the drop in sensitivity is greatest in the higher frequency range with a pronounced dip around 4000 Hz.

To protect employees in noisy work situations against permanent hearing loss, damage risk criteria have been set forth by a number of countries (Reference 3).

All standards define the *permissible noise dose* which, on an energy basis, is a maximum steady noise level in dBA, $L_{A\max}$, experienced for a working day of 8 hours or a working week of 40 hours.

As shown in Figure 9.9-3, most standards prescribe a value of 90 dBA as an upper limit to avoid permanent damage to the auditory system, and allow a 3 or 5 dBA increase in $L_{A\max}$ per halving of exposure duration.

The ratio of the total noise dose and permissible noise dose is called the *composite noise exposure index* (CNEI), and is expressed in percent. This quantity can be written as

$$\text{CNEI} = \frac{\int_0^{T_{ref}} 10^{L_A(t)/10} dt}{T_{ref} 10^{L_{A\max}/10}} \times 100\% , \quad (9.9-1)$$

where T_{ref} is the *reference duration* (8 or 40 hours).

Normally, the *actual total noise dose* is made up of a number of

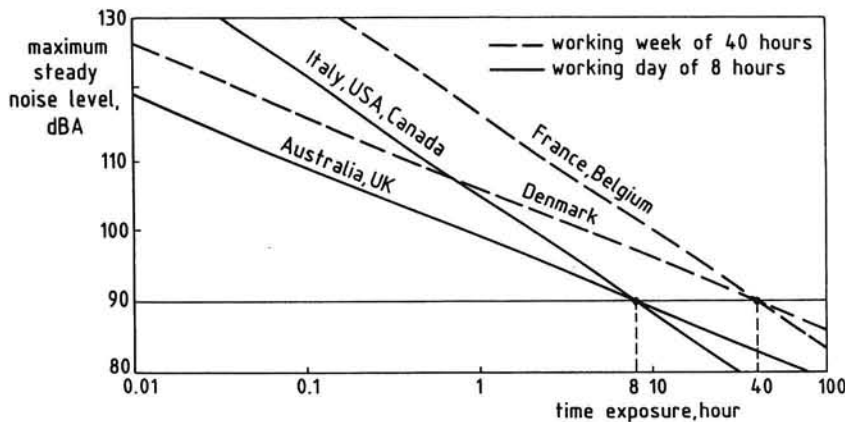


Figure 9.9-3. Standards on noise dose

partial doses to which an employee is subjected during the whole working day or week. Then, using Equation (9.4-3), we may write

$$\text{CNEI} = \frac{\sum_{j=1}^N 10^{L_{AE}(j)/10}}{T_{ref} 10^{L_{A\max}/10}} \cdot 100\% , \quad (9.9-2)$$

where N is the number of partial doses during the reference time.

Clearly, a composite noise exposure index of more than 100% means that someone is being exposed to unacceptable noise dose levels.

The standards define an overriding noise level limit (usually 115 dBA) in order that a worker may be subjected to a noise level in excess of the maximum value if the associated partial noise dose is counteracted by staying some time at a less noisy place such that the total noise dose remains below that allowable.

It should be noted that the above procedure is inadequate to estimate permanent effects due to an *impulse noise* with a duration less than one second. In this case the risk of hearing loss depends especially on its *peak sound pressure level*. In general, one supposes that exposure to an impulse noise level greater than 140 dB will cause hearing impairment.

We conclude our discussion of noise induced hearing loss by stating that very noisy environments should be avoided, and if this is impossible, ear protection by means of *ear plugs* or *ear muffs* is a necessity for conservation of hearing.

10 NOISE CERTIFICATION

10.1 INTRODUCTION

The object of this chapter is to outline the current international standards on noise emission for civil aircraft. In this respect, it is of interest to remark that in 1944 the *International Civil Aviation Organization* (ICAO) was established by the *Chicago Convention on International Civil Aviation*.

As mentioned earlier, ICAO is a special UN-agency charged with the execution of standardization activities on technical and operational aspects of civil aviation. Through the requirements developed by ICAO, and to which all member states have to comply, safe and efficient international air traffic is maintained and enhanced worldwide.

These standards and recommended practices (SARPs) are laid down in documents termed *Annexes to the Chicago Convention*.

In the ICAO definition *Standards* are a set of specifications, the uniform application of which is recognized as *necessary* for the safety or regularity of international air navigation. *Recommended Practices* are similar specifications, of which the uniform application is considered as *desirable* for the safety, regularity or efficiency of international air navigation.

The Standards and Recommended Practices for aircraft noise, laid down in *Annex 16, Environmental Protection*, were adopted by the ICAO Council for the first time in 1971 for subsonic jet-powered civil airplanes.

This first edition of Annex 16 was developed as a direct result of the *Special Meeting on Aircraft Noise in the Vicinity of Aerodromes*, which was convened in Montreal in 1969 under the auspices of ICAO.

Several editions of Annex 16 have since been published; the latest in 1988 where all provisions relating to environmental aspects of aviation are included (Reference 29).

It may be noted that Annex 16 consists of two Volumes, each divided in several Parts. Volume I (1988) deals with the requirements on noise emissions, and Volume II (1981) gives the provisions related to aircraft engine emissions.

The *noise certification standards* contained in Annex 16 have been developed by the *Committee on Aircraft Noise* (CAN), instituted by ICAO in 1970. In 1983, CAN has been renamed *Committee on Aviation Environmental Protection* (CAEP).

Up until now, ICAO-CAN/CAEP has had eight meetings at regular time intervals, the first in 1970 and the latest in 1986.

Due to the development and application of noise reduction technology there

has been a steady decrease in noise emissions from new type aircraft, through which the ICAO was able to establish more stringent noise requirements for completely new designs of aircraft. In addition, similar standards have been formulated and became effective for other types of aircraft.

The current noise level standards and methodologies are described in the Chapters 2-10 of Part II of the 1988 edition of Annex 16 / Volume I. Each chapter is devoted to particular types or type of aircraft, defined by the type of propulsion system, weight-category, and date of application for the prototype certificate of airworthiness, as follows:

CHAPTER 2. Subsonic jet airplanes for which the application for certificate of airworthiness for the prototype was accepted before 6 October 1977.

CHAPTER 3. a. Subsonic jet airplanes for which the application for certificate of airworthiness for the prototype was accepted on or after 6 October 1977.

b. Propeller-driven airplanes of a maximum takeoff mass greater than 5700 kg for which the application for certificate of airworthiness for the prototype was accepted on or after 1 January 1985 and before 17 November 1988.

c. Propeller-driven airplanes of a maximum takeoff mass greater than 9000 kg for which the application for certificate of airworthiness for the prototype was accepted on or after 17 November 1988.

CHAPTER 4. Supersonic airplanes.

CHAPTER 5. Propeller-driven airplanes of a maximum takeoff mass greater than 5700 kg for which the application for certificate of airworthiness for the prototype was accepted before 1 January 1985.

CHAPTER 6. Propeller-driven airplanes of a maximum takeoff mass not exceeding 9000 kg for which the application for certificate of airworthiness for the prototype was accepted before 17 November 1988.

- CHAPTER 7. Propeller-driven airplanes with short takeoff and landing field lengths (STOL airplanes).
- CHAPTER 8. Helicopters.
- CHAPTER 9. Installed auxiliary power units (APU) and associated aircraft systems during ground operations.
- CHAPTER 10. Propeller-driven airplanes of a maximum takeoff mass not exceeding 9000 kg for which the application for certificate of airworthiness for the prototype was accepted on or after 17 November 1988.

Standards and Recommended Practices for supersonic airplanes and propeller-driven STOL airplanes are not yet developed.

For supersonic airplanes the provisions of Annex 16 / Chapter 2 applicable to the older types of subsonic jet airplanes may be used as guidelines for noise certification.

Guidelines provided in Attachment B of Annex 16 / Volume I may be used for noise certification of propeller-driven STOL airplanes (see Section 10.4).

For the sake of brevity, in subsequent sections of this chapter we will only review the Chapters 3, 6, 7 and 10 of Annex 16 / Volume I, thus excluding not only helicopters but also earlier types of jet airplanes and their derived versions. Although this chapter exclusively deals with ICAO Requirements and Recommendations, it is worth mentioning that in the U.S.A. by action of the *Federal Aviation Administration* (FAA), the first domestic noise level standards became effective already on 1 December 1969 in the form of Part 36 in the *Federal Aviation Regulations* (FAR). These so-called FAR Part 36 Stage 1 standards are applicable to subsonic transport category airplanes and to all subsonic turbojet-powered aircraft regardless of category. Of course, the FAR Part 36 Stage 1 requirements and their refinements and extensions (Stages 2 and 3), are almost identical to the noise rules established by ICAO.

Flight tests to demonstrate compliance with *noise limits* require the availability of test sites that are surrounded by relatively flat terrain having no excessive sound absorption characteristics. Obstructions which may influence the sound field from the test airplane must be absent.

Airplane position data relative to the microphone must be determined by a method independent of normal flight instrumentation such as radar tracking, theodolite triangulation, photographic scaling techniques or other methods to be approved by the certificating authority of the State issuing the certification.

The test and noise measurement procedures must be acceptable to the local certificating authority. Also all measuring equipment must be approved.

Needless to say, for further details and any application of these noise level standards the reader always should consult the original ICAO-documents.

10.2 ANNEX 16 / VOLUME I / CHAPTER 3

The noise requirements of Annex 16 / Chapter 3 relate to:

- All subsonic jet airplanes other than airplanes which require a runway length of 610 m or less at maximum certificated mass for airworthiness, in respect of which the application for certificate of airworthiness for the prototype was accepted by the certificating authority, on or after 6 October 1977.
- All propeller-driven airplanes of over 5700 kg maximum certificated takeoff mass for which the application for certificate of airworthiness for the prototype was accepted by the certificating authority, on or after 1 January 1985 and before 17 November 1988, except where the standards of Annex 16 / Chapter 10 apply.
- All propeller-driven airplanes of over 9000 kg maximum certificated takeoff mass for which the application for certificate of airworthiness for the prototype was accepted by the certificating authority, on or after 17 November 1988.

When performing noise certification under Annex 16 / Chapter 3, the airplane must execute a series of landing and takeoff maneuvers over the following three measurement stations (Figure 10.2-1):

1. On the approach to landing, at a point on the extended centerline of the runway and at a distance of 2000 m from the threshold (*approach reference noise measurement point*). This corresponds to a position 120 m vertically beneath the approach reference flight path originating from the aiming point on the runway 300 m beyond the threshold.
2. On takeoff, at a point on the extended centerline of the runway and at a distance of 6500 m from the start of takeoff roll (*flyover reference noise measurement point*).
3. On takeoff, at a point on a line parallel to and 450 m from the runway centerline

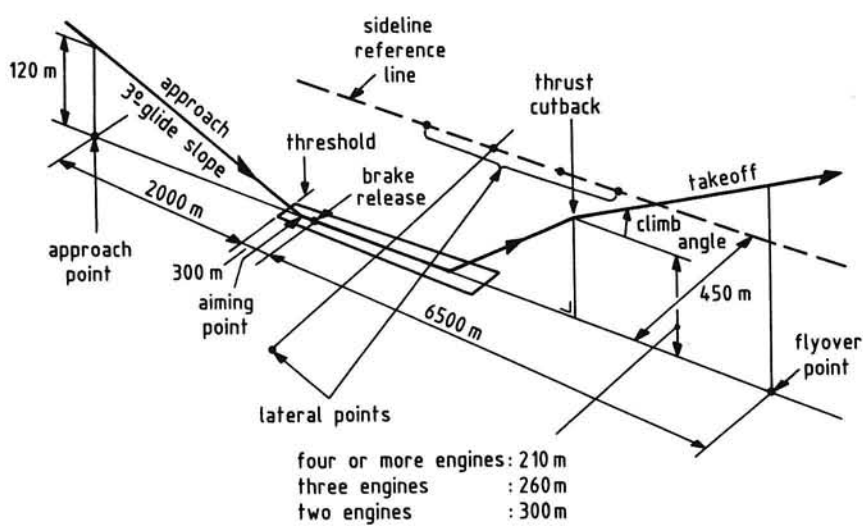


Figure 10.2-1. ICAO / Annex 16 / Chapter 3 measuring locations and reference trajectories

where the noise level is maximum during takeoff (*lateral reference noise measurement point*).

With regard to lateral noise, sufficient measurement points must be used to demonstrate that the maximum noise level has been determined. Also simultaneous measurements must be made at one test noise measurement point at a symmetrical position on the other side of the runway.

The approach reference flight path indicated in Figure 10.2-1 must be calculated as follows:

1. The speed of the airplane must be stabilized and the airplane must follow a 3°-glide path.
2. The approach must be executed at an airspeed of not less than $1.3 V_{MS} + 10$ knot with thrust stabilized during approach and over the measuring point, and continued to a normal touchdown. The speed V_{MS} is the calibrated minimum stalling speed for the airplane in the landing configuration (see Reference 7).
3. The constant approach configuration as used in the airworthiness certification tests, but with the landing gear down, must be maintained throughout the approach reference procedure.

4. The mass of the airplane at the touchdown must be the maximum landing mass permitted in the approach configuration at which noise certification is requested.
5. The most critical (that which produces the highest noise level) configuration with normal deployment of aerodynamic control surfaces including lift and drag producing devices, at the mass at which certification is requested must be used.

The takeoff reference trajectory must be determined as follows:

1. Takeoff thrust must be used from start of takeoff roll to the point where at least the following height above the runway level is reached:
 - airplanes with one or two engines : 300 m (985 ft);
 - airplanes with three engines : 260 m (855 ft);
 - airplanes with four engines or more : 210 m (690 ft).
2. After reaching the height specified in 1 above, the thrust must not be reduced below that required to maintain:
 - a. a climb gradient of 4 percent;
 - b. level flight in the case of a multi-engine airplane with one engine inoperative, whichever thrust is greater.

3. The flight speed must be selected between $V_2 + 10$ knot and $V_2 + 20$ knot, where V_2 is the climbout safety speed. This speed is the lowest flight speed for adequate and safe climbout with one engine inoperative and the live engine(s) developing full takeoff thrust.

For turboprop engines the airworthiness requirements cite: $V_2 \geq 1.2 V_{MS}$ for two-engine and three-engine airplanes and $V_2 \geq 1.15 V_{MS}$ for airplanes with more than three engines. For jet airplanes the requirements quote: $V_2 \geq 1.2 V_{MS}$, irrespective of the number of engines. The speed V_{MS} is now the calibrated minimum stalling speed for the airplane in the takeoff configuration.

The speed V_2 must be maintained throughout the takeoff noise certification test.

4. A constant takeoff configuration must be maintained throughout the takeoff reference procedure except that the landing gear may be retracted after liftoff.

5. The mass of the airplane at the brake release must be the maximum takeoff mass at which the noise certification is requested.

The noise certification reference flight procedures must be calculated under the following reference atmospheric conditions:

- sea-level atmospheric pressure : 1013.25 hPa;
- ambient air temperature : 25°C;
- relative humidity : 70 %;
- zero wind.

The noise evaluation measure is the effective perceived noise level (EPNL) as described in the preceding chapter of this book.

The noise levels at the three reference noise measurement points, when determined according to these Standards, shall not exceed the values indicated in Figure 10.2-2. The noise limits are functions of the maximum certificated takeoff mass of the airplane. At the flyover reference noise measurement point the noise limits are also specified in relation to the number of engines of the airplane.

For comparison, the maximum noise levels according to Annex 16 / Chapter 2 (FAR Part 36 Stage 1) are also given in Figure 10.2-2. The lateral measurement point is at a distance of 650 m from the runway centerline.

Tradeoff provisions for the Annex 16 / Chapter 3 requirements allow that the noise levels go beyond the limits at one or two of the measuring points if:

- a. the sum of the excesses is not greater than 3 EPNdB;
- b. any excess at any single measuring point is not greater than 2 EPNdB;
- c. the excesses are completely offset by reductions at the other measuring points or point.

The noise tests must be carried out under the following atmospheric conditions:

- no precipitation;
- ambient air temperature not above 35°C and not below 2°C over the whole sound path between a point 10 m above the ground and the airplane;
- relative humidity not above 95% and not below 20% over the whole sound path between a point 10 m above the ground and the airplane;
- relative humidity and ambient temperature over the whole sound path between a point 10 m above the ground and the airplane such that the sound attenuation

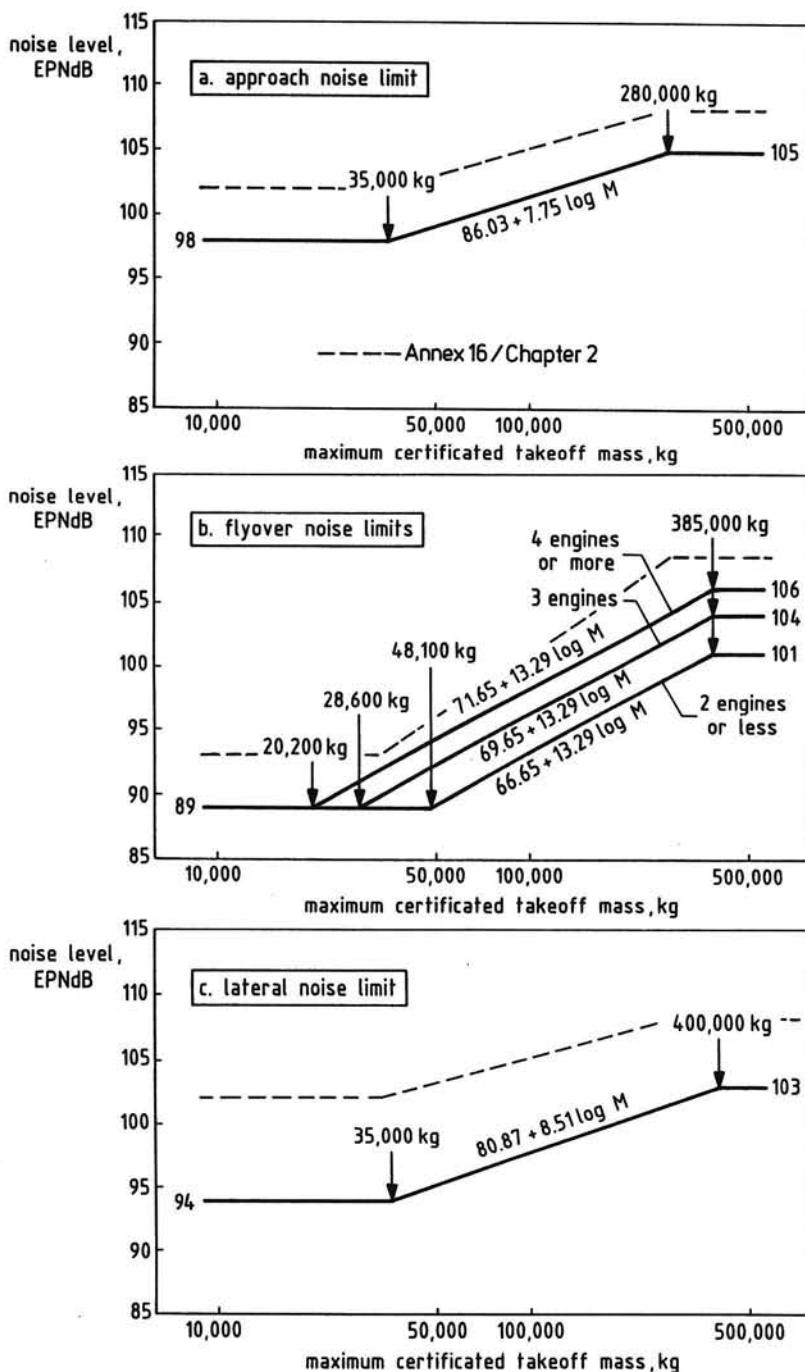


Figure 10.2-2. The allowable noise levels at the three measurement points (M is takeoff mass in 1000 kg)

- in the tertsband centered on 8 kHz is not more than 12 dB/100 m;
- wind velocity not above 12 knot (6.2 m/s) and cross-wind velocity component relative to the flight direction not above 7 knot (3.6 m/s) at 10 m above ground level.

To obtain valid results, the sound pressure levels measured within the 10 dB-down points (see Section 9.5) must exceed the prevailing mean ambient noise levels by at least 3 dB in each tertsband.

The measurement system must consist of a microphone system and a recording system to store the measured noise data for subsequent analysis.

The microphone must be a so-called *pressure type microphone*. The properties of this type of microphone will be discussed in Chapter 11.

The microphone must be mounted with the center of the sensing element at a height of 1.2 m above the ground surface. It must be oriented for grazing incidence, i.e., with the sensing element substantially in the vertical plane defined by the nominal flight path of the airplane and the measuring station as shown in Figure 10.2-3. The microphone must be covered by a *windscreen* when the wind velocity is in excess of 6 knot (3.1 m/s).

Inevitably, actual test conditions and procedures will never be identical to the reference conditions. Consequently, appropriate adjustments are required to obtain from the flight trials the acoustic data that can be used for *noise certification*. The adjustments take account of the effects of:

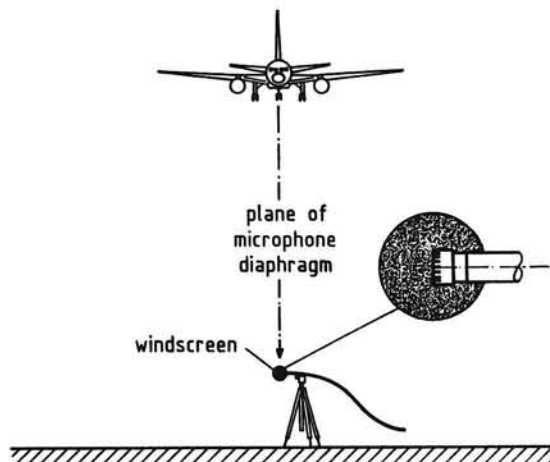


Figure 10.2-3. Microphone orientation

- differences in atmospheric absorption between meteorological test conditions and reference conditions;
- differences between actual and reference slant ranges (affecting atmospheric absorption and spherical spreading);
- differences in measurement time (*10 dB down time*) due to changes in slant range and airspeed;
- atmospheric test conditions concerning noise generation by the source.

The methods for determining these adjustments are described in Appendix 2 of Annex 16 / Volume I.

The demanded EPNL value at each measurement point is given by the arithmetic mean of the adjusted noise levels for all valid test runs.

The minimum sample size acceptable for each of the three measurement stations is six. The samples must be large enough to establish statistically for each of the three average noise certification levels a 90 percent confidence limit not exceeding ± 1.5 EPNdB.

The method for calculating the *confidence interval* will be pointed out in Section 10.6.

Finally, it is worth remarking that the latest U.S. equivalent of Annex 16 / Chapter 3 is known as FAR Part 36 Stage 3, and that a *stage three airplane* means an airplane that has been shown under FAR Part 36 to comply with the newest requirements.

10.3 ANNEX 16 / VOLUME I / CHAPTER 6

The standards of Annex 16 / Chapter 6 are applicable to all propeller-driven small airplanes not exceeding a maximum takeoff mass of 9000 kg, except those airplanes specifically designed for aerobatic purposes or agricultural or fire fighting uses, for which:

- a. the application for the certificate of airworthiness for the prototype was accepted by the certificating authority, on or after 1 January 1975 and before 17 November 1988;
- b. a certificate of airworthiness for the individual airplane was first issued on or after 1 January 1980.

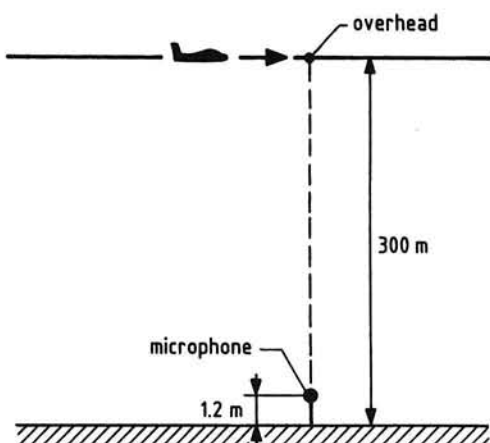


Figure 10.3-1. Reference flight path

When performing noise certification under Annex 16 / Chapter 6, a series of level flyovers at a reference height of 300 m over a measuring station are to be made (Figure 10.3-1).

The pressure type microphone must be placed with the center of the sensing element at a height of 1.2 m above the local ground surface. The microphone must be oriented for grazing incidence, i.e., with the diaphragm in the vertical plane defined by the reference flight path of the airplane and the measurement point, as shown in the previous Figure 10.2-3.

A windscreen must be used with the microphone when the wind velocity is in excess of 6 knot (3.1 m/s).

The noise evaluation measure is the maximum A-weighted noise level (MAL) occurring during flyover, and not EPNL as in Annex 16 / Chapter 3.

The allowable noise limits at the measurement point are shown in Figure 10.3-2 as a function of maximum airplane takeoff mass. These are a 68 dBA constant limit up to an airplane mass of 600 kg, varying linearly with mass from that point to 1500 kg, after which the limit is constant at 80 dBA up to 9000 kg.

The reference procedure must be calculated under the following reference atmospheric conditions:

- sea-level atmospheric pressure of 1013.25 hPa;
- ambient air temperature of 25°C (ISA + 10°C).

Tests to demonstrate compliance with the noise limits of Figure 10.3-2 must include at least four level flights overhead the measurement station at a height of 300 m +10 m/-30 m.

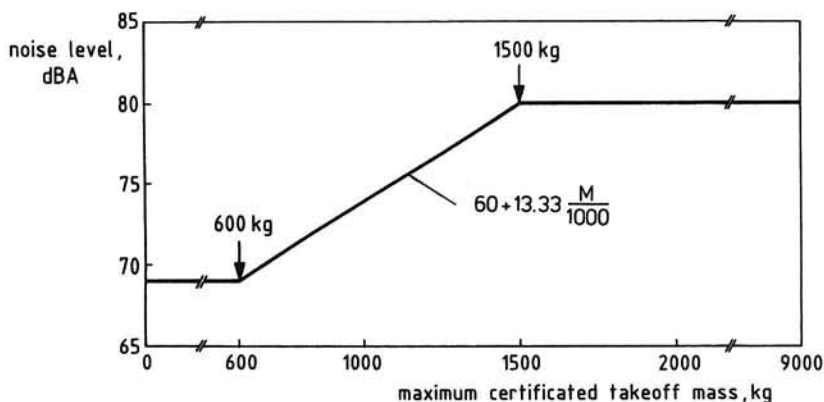


Figure 10.3-2. Noise limits Annex 16 / Chapter 6 (M is mass in kg)

The airplane must pass over the measurement point with a lateral displacement of not more than $\pm 10^\circ$ from the vertical.

Overflight must be executed at stabilized airspeed, with the airplane in the cruise configuration and at the authorized highest power setting in the normal operating range.

The tests must be performed under the following atmospheric conditions:

- there may be no precipitation;
- relative humidity may not be higher than 95 percent or lower than 20 percent

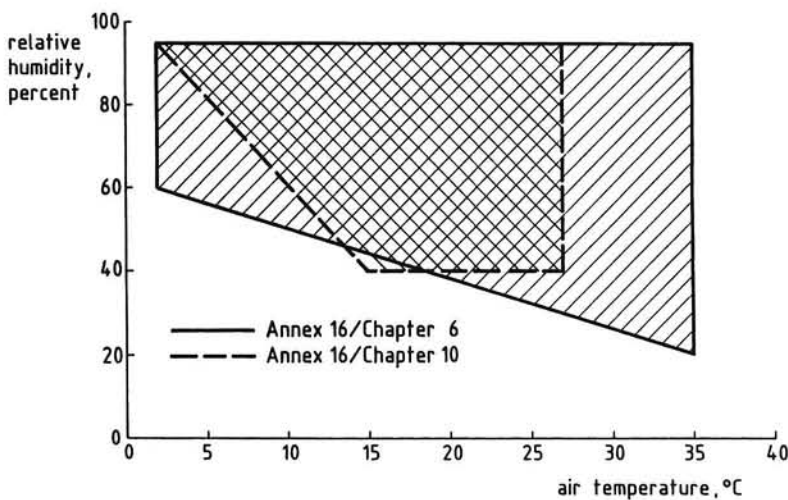


Figure 10.3-3. Measurement window for no absorption correction

and ambient air temperature may not above 35°C or below 2°C at 1.2 m above ground except that on the diagram of Figure 10.3-3 the combinations of temperature and relative humidity which fall below the straight line between 2°C and 60 percent and 35°C and 20 percent must be avoided;

- reported wind may not be above 10 knot (5.1 m/s) at 1.2 m above ground level and cross-wind component may not above 5 knot (2.6 m/s) at 1.2 m above ground. Flights must be made in equal numbers with tail and head wind components;
- there may be no temperature inversions or anomalous wind conditions that would significantly affect the measured noise level.

The *ambient noise level* must be determined in the test area. If airplane noise levels do not exceed the background noise levels by at least 10 dBA, approved corrections for the contribution of background noise to the measured noise levels must be applied.

Corrections for differences between engine power achieved during the tests and the power that would be achieved at settings corresponding to the highest power in the normal operating range must be applied using approved methods.

The noise levels measured when the airplane is at heights different from the reference height must be adjusted to 300 m by the inverse square law (see Chapter 4 of this book).

A performance correction determined for sea-level standard atmospheric conditions (0 m ISA), and limited to a maximum of 5 dBA must be computed using the following formula:

$$\Delta \text{dBA} = 49.6 - 20 \log \left[(3500 - D_{15}) \frac{RC_{\max}}{V_{RC_{\max}}} + 15 \right], \quad (10.3-1)$$

where D_{15} is the takeoff distance to 15 m height at maximum takeoff mass and takeoff power, with the ground run on a dry, hard runway; RC_{\max} is the best rate of climb at maximum takeoff mass and takeoff power; and $V_{RC_{\max}}$ is the airspeed for best rate of climb at maximum takeoff mass and takeoff power in the same units as rate of climb.

When takeoff distance D_{15} is not certificated, the figures of 610 m for single-engine airplanes and 825 m for multi-engine airplanes must be used in Equation (10.3-1). The above performance correction is intended to credit higher performance airplanes based on their ability to climb at a steeper angle and to fly the traffic pattern at a lower power setting. Also, this correction penalizes airplanes with limited performance capability which results in lower rates of climb and higher power

settings in the traffic pattern.

The test results must produce an average $L_{A_{max}}$ value and its 90 percent confidence limit, the noise level being the arithmetic average of the corrected acoustical data for all valid test runs.

The samples must be large enough to establish statistically a 90 percent confidence limit not to exceed ± 1.5 dBA (see Section 10.6).

10.4 ANNEX 16 / VOLUME I / CHAPTER 7

Presently, there are no International Standards and Recommended Practices for propeller-driven STOL airplanes. Pending the development of noise rules, guidelines described in Attachment B to Chapter 7 of Annex 16 / Volume I are used for noise certification of these airplane types.

These guidelines are not applicable to aircraft with vertical takeoff and landing capabilities, but should be applied to all propeller-driven airplanes of over 5700 kg maximum certificated takeoff mass intended for operation in the short takeoff and landing mode, requiring a runway length of not more than 610 m at maximum certificated takeoff mass, and for which a certificate of airworthiness for the individual airplane was first issued on or after 1 January 1976.

Tests to demonstrate compliance with the noise level requirements must consist of a number of approach and takeoff maneuvers and noise levels measurements at the following reference points:

1. On takeoff or landing, at the point on a line parallel to, and 300 m from the runway centerline, or extended centerline, where the noise level is a maximum (*lateral reference noise measurement point*).
2. On takeoff, at the point on the extended centerline of the runway 1500 m from the start of takeoff roll (*flyover reference noise measurement point*).
3. On approach to landing, at the point on the extended centerline of the runway 900 m from the runway threshold (*approach reference noise measurement point*).

The noise evaluation measure should be the effective perceived noise level (EPNL). The maximum noise level at any of the three measurement points should not exceed 96 EPNdB in the case of airplanes with maximum certificated mass of 17000 kg or less. For heavier airplanes the noise level should not exceed a linear variation of the logarithm of the mass at a rate of 2 EPNdB per doubling of mass.

The noise levels specified above may be exceeded at one or two of the

measurement points if:

- a. the sum of any excesses does not exceed 4 EPNdB;
- b. at no measurement point the excess is greater than 3 EPNdB;
- c. the excesses are entirely offset by corresponding reductions at the other measurement points.

The approach and landing procedure should be as follows:

- a. the airplane should be at the maximum landing mass for which the noise certification is requested;
- b. throughout the approach test, the airspeed and engine power setting and airplane configuration should be those specified in the flight manual for STOL landing;
- c. the use of reverse thrust after touch down should be the maximum defined in the flight manual.

The takeoff procedure should be as follows:

- a. the airplane should be at the maximum takeoff mass for which the noise certification is requested;
- b. throughout the takeoff maneuver, the engine power setting, airspeed and airplane configuration should be those specified in the flight manual for takeoff in the STOL mode.

10.5 ANNEX 16 / VOLUME I / CHAPTER 10

The requirements of Chapter 10 are applicable to all propeller-driven small airplanes not exceeding a maximum takeoff mass of 9000 kg, except those airplanes specifically designed for aerobatic purposes and agricultural or fire fighting uses for which application for the certificate of airworthiness for the prototype was accepted by the certificating authority, on or after 17 November 1988.

For airplanes specified above which fail to comply with the Standards of Annex 16 / Chapter 10 and where the application for the certificate of airworthiness for the prototype was accepted by the certificating authority before 17 November 1993, the Standards of Annex 16 / Chapter 6 apply.

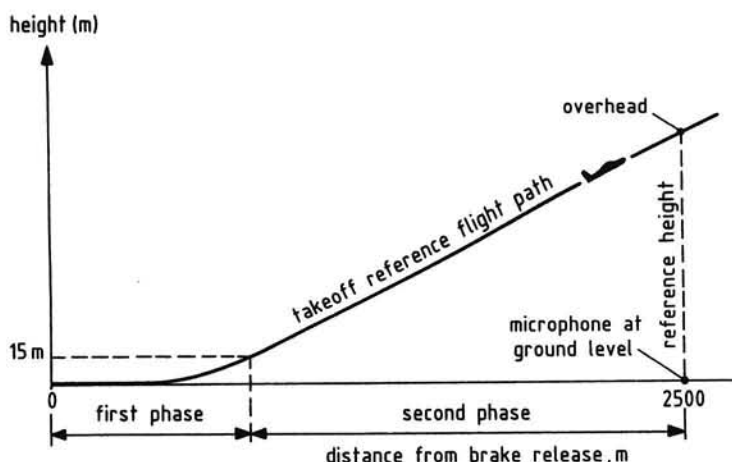


Figure 10.5-1. Takeoff reference profile

When executing noise certification under Annex 16 / Chapter 10, the airplane is to conduct a series of takeoffs over a measurement station (Figure 10.5-1). The reference noise measurement point is the point on the extended centerline of the runway at a distance of 2500 m from the start of takeoff roll.

The microphone must be a 12.7 mm diameter (half inch) pressure type (to be discussed in Chapter 11), with its protective grid, mounted in an inverted position such that the microphone diaphragm is 7 mm above and parallel to a circular metal plate. The plate must be white-painted, 40 cm in diameter and at least 2.5 mm thick. It must be placed horizontally and flush with the surrounding ground surface with no cavities below the plate. The microphone must be located three-quarters

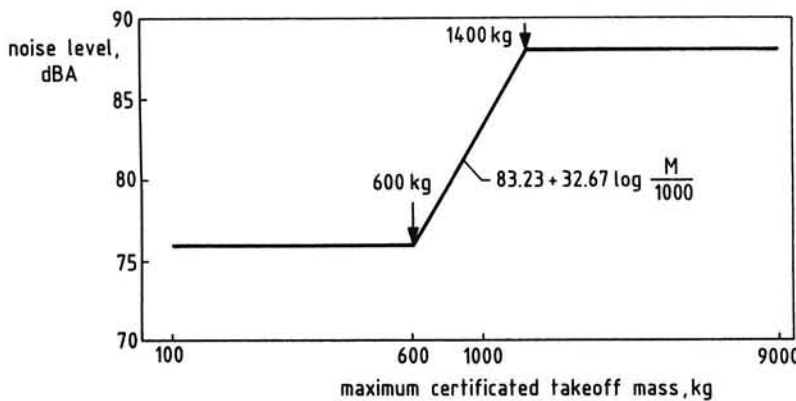


Figure 10.5-2. Noise limits Annex 16 / Chapter 10 (M is mass in kg)

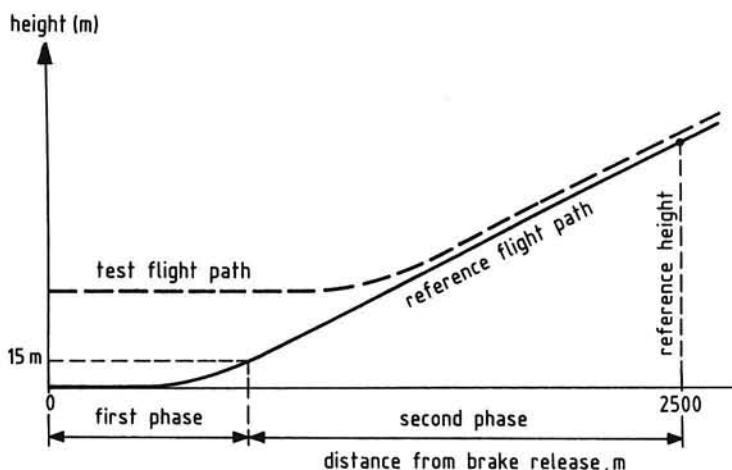


Figure 10.5-3. Typical test and reference profiles

of the distance from the center to the edge along a radius normal to the line of flight of the test airplane (see the previous Figure 8.6-3).

The noise evaluation measure is the maximum A-weighted noise level occurring during overflight, as in Annex 16 / Chapter 6.

The maximum noise levels at the takeoff measurement point must not exceed the following: a 76 dBA constant limit up to an airplane mass of 600 kg varying linearly from that point with the logarithm of airplane mass at a rate of 9.83 dBA per doubling of mass until the limit of 88 dBA is reached after which the limit is constant up to 9000 kg (Figure 10.5-2).

A takeoff reference procedure is used to determine the nominal altitude and airspeed of the airplane when passing over the microphone on a standard day. The takeoff reference flight path must be calculated taking into account the following two phases (Figure 10.5-3):

a. First phase:

- takeoff power must be used from the brake release point to the point at which the height of 15 m (50 ft) above the runway is reached;
- a constant takeoff configuration selected by the applicant must be maintained throughout this phase;
- the mass of the airplane at the brake release must be the maximum takeoff mass at which the noise certification is requested;

- the length of this phase must correspond to the length given in the airworthiness data for a takeoff on a level, paved runway.
- b. Second phase:
 - the beginning of this phase corresponds to the end of the first phase;
 - the airplane must be in the climb configuration with landing gear up, if retractable, and flap setting corresponding to normal climb throughout this phase;
 - the airspeed must be the best rate of climb speed, $V_{RC_{max}}$;
 - the maximum power that can be continuously delivered by the engine(s) in this flight condition must be maintained throughout this phase (unless a lower power is established by the certificating authority).

At sea level and under standard atmospheric conditions, maximum continuous power is normally obtained with full throttle for airplanes with *fixed-pitch propellers*, with full throttle and maximum continuous engine rpm for airplanes equipped with normally aspirated engines and *controllable-pitch* or *constant-speed propellers*, and at maximum continuous manifold pressure and maximum continuous engine rpm for airplanes equipped with supercharged engines and constant speed propellers. For engines with maximum continuous power installed that is less than the installed takeoff power, the airworthiness limitations for maximum continuous power apply during the second phase climb.

The reference procedure must be calculated under the following reference atmospheric conditions:

- sea-level atmospheric pressure of 1013.25 hPa;
- ambient air temperature of 15°C, i.e., ISA sea-level;
- relative humidity of 70 percent;
- zero wind.

The test must be carried out under the following atmospheric conditions:

- no precipitation;

- relative humidity not higher than 95% and not lower than 20% and ambient temperature not above 35°C and not below 2°C at 1.2 m;
- reported wind not above 5.1 m/s (10 kt) and cross wind not above 2.6 m/s (5 kt) at 1.2 m, using a 30 s average;
- no other anomalous meteorological conditions that would significantly affect the noise level of the airplane.

The flight test program must be initiated at the maximum takeoff mass for the airplane, and the mass must be adjusted to maximum takeoff mass after each hour of flight time.

The airplane must conduct a takeoff followed by a continued climb over the microphone. The flight test must be executed at $V_{RC_{max}} \pm 5$ knot indicated airspeed.

The airplane height when directly over the microphone must be measured by an approved technique. The airplane must pass over the microphone within $\pm 10^\circ$ from the vertical and within $\pm 20\%$ of the reference height.

Performance data must be recorded when the airplane is directly over the measurement site.

An independent device accurate to within $\pm 1\%$ must be used for the measurement of propeller rotational speed.

Figure 10.5-3 also illustrates the difference between the test day flight procedure and the standardized takeoff reference profile. Note that the actual flight test path need not include a complete takeoff from standstill on the runway. Rather, it assumes that a flight path intercept technique is used, i.e., the airplane would be flown to intersect the second phase climb path at the right speed and angle of climb when going over the microphone within 20 percent of the reference height.

The ambient noise must be determined in the test area with the system gain set at levels which will be used for airplane noise measurements. If airplane peak noise levels do not exceed the background noise levels by at least 10 dBA, a takeoff measurement point nearer to the start of roll must be used and the measurement results adjusted to the reference measurement point by an approved method.

When certification test conditions differ from the reference conditions adjustments must be made to the measured noise data using approved methods. The adjustments take account of the effects of:

- differences in atmospheric absorption between meteorological test conditions and reference conditions;

- differences in the noise path length between the actual airplane flight path and the reference flight path;
- the change in the helical tip Mach number between test and reference conditions;
- the change in engine power between test and reference conditions.

When the test conditions are within those specified in Figure 10.3-3, no adjustments for differences in atmospheric absorption losses need be applied.

The measuring point must be overflowed at least six times. The test results must produce an average noise level ($L_{A,\text{max}}$) value and its 90 percent confidence limits, the noise level being the arithmetic mean of the corrected acoustical measurements for all valid test runs over the measuring point.

The samples must be large enough to establish statistically a 90 percent confidence limit not exceeding ± 1.5 dBA (see Section 10.6).

10.6 CALCULATING THE CONFIDENCE INTERVAL

The Standards of Annex 16 / Volume I require that the sample size is large enough to establish statistically a 90 percent confidence interval not exceeding ± 1.5 dB. This section is intended to provide some information on the method to determine the confidence interval for the estimate of the mean of a group of measurement data. For a detailed discussion of the subject, the interested reader is referred to the specialized literature on statistical analysis (see, for example, References 55 and 56).

For a number of n values of measured noise levels, acquired under approximately the same conditions, the following statistics can be obtained:

- a. The *sample mean*, being the quotient of the sum of the values of the individual noise levels divided by the number of measurements,

$$\bar{L} = \frac{1}{n} \sum_{i=1}^n L_i , \quad (10.6-1)$$

where the symbol \bar{L} designates the arithmetic average of the individual measurement values L_i , and n is the sample size.

- b. The *sample standard deviation*, denoted by the symbol s . This quantity is found by taking the square root of the sum of the squares of deviations of all individual values divided by the number of measurement values,

$$s = \sqrt{\frac{1}{(n-1)} \sum_{i=1}^n [L_i - \bar{L}]^2} . \quad (10.6-2)$$

This equation shows that the sample standard deviation is obtained by using the number of data in the sample minus one instead of n in the denominator.

An explanation of the use of $(n-1)$ data points rather than n cannot be given within the scope of this text. In so doing, however, the exactness of s for a small sample size is improved.

Clearly, the quantities \bar{L} and s according to Equations (10.6-1) and (10.6-2) will differ from the *true mean*, μ , and the *true standard deviation*, σ , since the latter two quantities are based on the total number of data in the population rather than just the sample size.

This departure from the precise values is known as the *sampling error* which, of course, becomes smaller as the sample size n increases.

In the case of flyover noise measurements, the number of test data within a group will always be relatively small. Nevertheless, the sample standard deviation is approximately equal to the true standard deviation ($s = \sigma$), when the total number of data in the population is normally distributed. Adopting the so-called *Student's t distribution* for the description of the population provides the ability for achieving

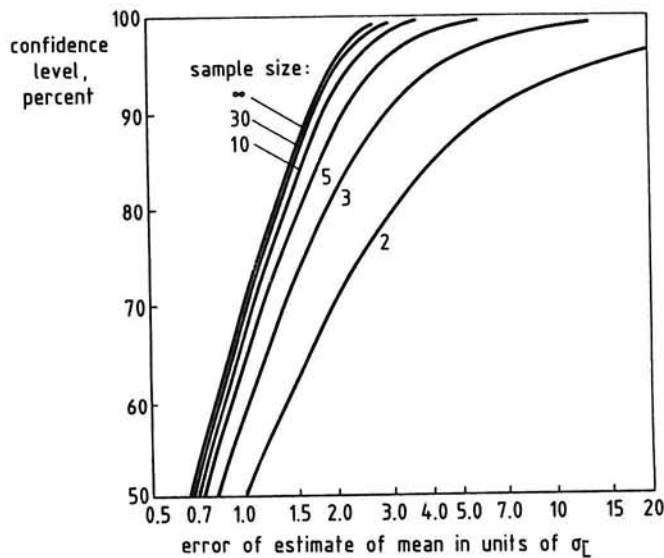


Figure 10.6-1. Relationship between sample size, confidence level, and amount of error in the estimate

*Table 10.6-1. Values of the Student's *t* distribution for a 90 percent confidence level*

<i>n</i>	<i>t</i> ₉₀						
2	6.314	11	1.812	20	1.729	29	1.701
3	2.920	12	1.796	21	1.725	30	1.699
4	2.353	13	1.782	22	1.721	31	1.697
5	2.132	14	1.771	23	1.717	41	1.684
6	2.015	15	1.761	24	1.714	61	1.671
7	1.943	16	1.753	25	1.711	121	1.658
8	1.895	17	1.746	26	1.708	∞	1.645
9	1.860	18	1.740	27	1.706		
10	1.833	19	1.734	28	1.703		

confidence in the estimate of the true mean by relating the sampling error in the estimate to the confidence level.

The relationship between sample size, confidence level in percent, and amount of error as related to the true mean μ is shown in Figure 10.6-1.

The error of the estimate of the true mean, Δ , is given in units of the true standard deviation divided by the square root of the sample size, as

$$t = \frac{\Delta}{\sigma/\sqrt{n}} = \frac{\Delta}{\sigma_L} . \quad (10.6-3)$$

Using the sample standard deviation to estimate σ , we have

$$t = \frac{\Delta}{\sigma_L} = \frac{\Delta}{s/\sqrt{n}} . \quad (10.6-4)$$

In this equation the sample size n is used although $(n-1)$ is employed in calculating the value of s .

Numerical values of the *t*-distribution to give a probability of 90 percent that the true mean is within the interval:

$$\bar{L} - t \frac{s}{\sqrt{n}} \leq \mu \leq \bar{L} + t \frac{s}{\sqrt{n}} \quad (10.6-5)$$

are listed in Table 10.6-1 in terms of the sample size n .

For example, for $n = 6$, there is a 90 percent confidence that the true mean lies within $\pm 2.015 \times s / \sqrt{n}$ of the estimated sample mean.

Both Figure 10.6-1 and Table 10.6-1 show that at a given confidence level an increase in sample size results in a decrease in sampling error since the width of the interval reduces.

11 EFFECTS OF FORWARD MOTION

11.1 INTRODUCTION

When an airplane is in flight its radiation characteristics may be significantly different from those of the airplane at rest on the ground. Therefore, we have to pay some attention to the effects of source motion on ground observed noise levels from aircraft operating in forward flight.

For this aim, in subsequent sections of this chapter analyses will be presented of the sound emission from a moving source which, because of its simplicity, will be assumed to travel uniformly and rectilinearly.

Different types of noise sources radiate differently when in forward motion. However, for brevity's sake, only the radiation by an acoustic point monopole is used here as a reference to demonstrate the derivation and the features of the sound field.

It should be recognized that a major problem in the validation of available theory is that the results from flyover noise measurements always contain the effects of ground reflected sound. These disturbing effects, of course, must be removed from the recordings before the directional pattern of the noise source may become visible.

Ability to extrapolate aircraft noise data gained from measurements taken under static conditions to forward flight conditions is of great importance since perhaps the most reliable noise data are obtained when the airplane is operating statically under well-controlled conditions. On the other hand, in deriving free-field data from inflight measurements one must be able to adjust measured noise data for propagation, ground reflection and forward flight effects.

11.2 GEOMETRIC ACOUSTICS (SUBSONIC SPEEDS)

The geometry of the problem is outlined in Figure 11.2-1, where the sound source moves with constant speed in the x -direction at an altitude h above the ground ($X-Y$ plane).

The instantaneous position of the source is specified by the coordinates $x_s(t)$, $y_s = 0$, and $z_s = h$. The receiver position is given by the coordinates x , y , z . If the source is at $x_s = 0$ at time $t = 0$, we have at time t :

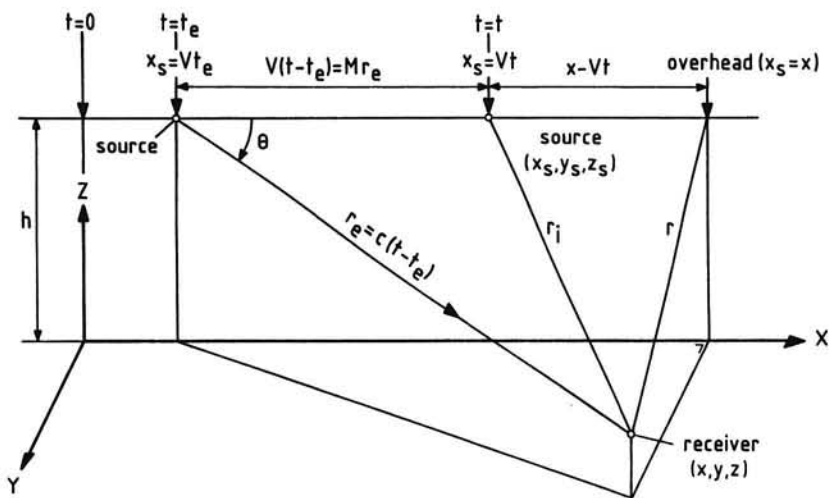


Figure 11.2-1. Source-receiver geometry

$$\left. \begin{aligned} x - x_s &= x - Vt \\ y - y_s &= y \\ z - z_s &= z - h. \end{aligned} \right\} \quad (11.2-1)$$

When the atmosphere is considered to be quiet, isothermal and homogeneous, the sound rays emerging from the source travel along rectilinear paths. Due to the forward motion of the source the sound observed at the time t , the *immission time*, is emitted by the source at an earlier time t_e , the *emission time* (see also Equation (7.5-3)),

$$t_e = t - \frac{r_e}{c}, \quad (11.2-2)$$

where r_e is the distance between the receiver and the source position at the emission time t_e , and c is speed of sound.

The horizontal distance traveled by the source in the time interval $(t - t_e)$ is

$$V(t - t_e) = V \frac{r_e}{c} = M r_e, \quad (11.2-3)$$

where $M = V/c$ may be termed the *convection Mach number*.

The distance r_e follows from the relationship:

$$r_e = [(x - Vt + Mr_e)^2 + y^2 + (z - h)^2]^{1/2}, \quad (11.2-4)$$

Solving this equation for r_e yields

$$r_e = \frac{M(x - Vt) \pm \sqrt{(x - Vt)^2 + (1 - M^2)y^2 + (1 - M^2)(z - h)^2}}{(1 - M^2)} . \quad (11.2-5)$$

When the relationship $y^2 + (z - h)^2 = r^2$ is substituted into Equation (11.2-5), we can write

$$r_e = \frac{M(x - Vt) \pm (x - Vt) \sqrt{1 + (1 - M^2)r^2/(x - Vt)^2}}{(1 - M^2)} . \quad (11.2-6)$$

From Equation (11.2-6) it is evident that when the speed of the source is subsonic ($M < 1$), only the positive sign will give a positive (real) value for r_e .

11.3 GEOMETRIC ACOUSTICS (SUPERSONIC SPEEDS)

When the source travels at a supersonic speed ($M > 1$), both the plus and minus signs in Equation (11.2-6) yield a positive value for the distance r_e provided that $(x - Vt) < 0$. The latter condition requires that the source is beyond the receiver. Then Equation (11.2-6) can be written as

$$r_{e\pm} = \frac{M(Vt - x) \pm (Vt - x) \sqrt{1 - (M^2 - 1)r^2/(Vt - x)^2}}{(M^2 - 1)} . \quad (11.3-1)$$

Introducing $r/(Vt - x) = \tan \delta$ and $\sin \mu = 1/M$, as indicated in Figure 11.3-1, we obtain

$$r_{e\pm} = \frac{M(Vt - x) \pm (Vt - x) \sqrt{1 - (\tan \delta / \tan \mu)^2}}{(M^2 - 1)} . \quad (11.3-2)$$

It appears that the two values of r_e are real only when $\delta < \mu$, indicating that at supersonic speeds the sound is only heard inside the so-called *Mach cone*, of which the semi-apex angle μ is termed *Mach angle*. Accordingly, outside the Mach cone there is complete silence.

Figure 11.3-1 also illustrates the construction of the emission points $x_{s+} = Vt_{e+}$ and $x_{s-} = Vt_{e-}$ as centers of a forward- and backward-moving sound wave.

Apparently, in the case of supersonic motion, two sound waves deliver a contribution to the occurring sound pressure at the receiver position, at least when this point is within the Mach cone.

To explain the development of the Mach cone, let us first consider the pressure disturbances in the air produced by a point source that travels at a low

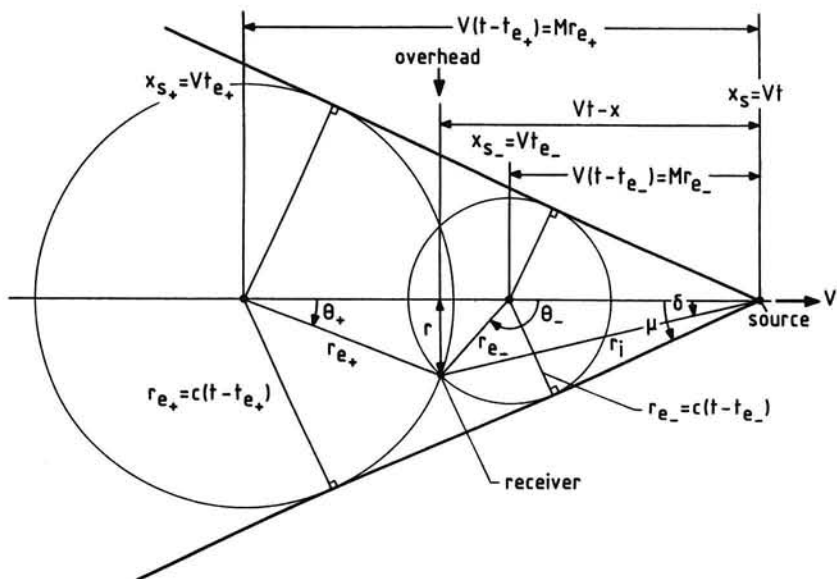


Figure 11.3-1. Wavefront formation from a point source moving at supersonic speed

(subsonic) speed. This situation is illustrated by Figure 11.3-2a, where the circles indicate the locations of the pressure disturbances emitted by the source at equal consecutive time intervals and which are traveling outward from the source at the speed of sound c . It is clear that the whole region around the source is affected and that the disturbances are closer together in the direction of travel of the source. As the speed of the source increases, the pressure disturbances in front of the source are confined to a smaller area. In other words, the air experiences less warning of the approach of the disturbances to flow smoothly around the source.

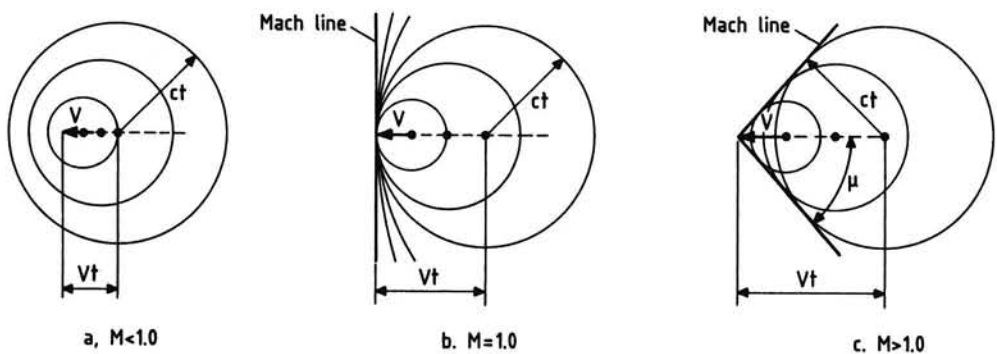


Figure 11.3-2. Pressure perturbations from a moving source

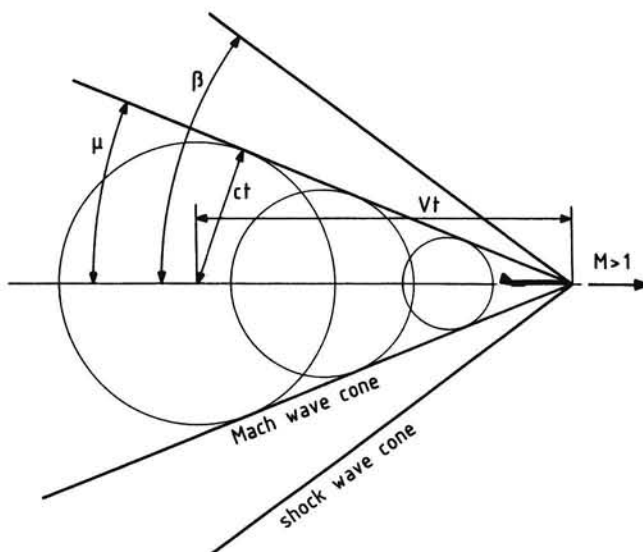


Figure 11.3-3. The conical shock wave at the nose of an airplane flying at supersonic speed

When the forward speed is equal to the speed of sound, the pressure disturbances and the source move at the same speed. Then, as depicted in Figure 11.3-2b, all spheres pass through the source and the wavefronts combine to form a reinforced wavefront, the so-called *Mach line*, directed perpendicular to the forward speed direction.

In Figure 11.3-2c we see the condition in which the speed of the source exceeds the speed of sound ($M > 1$). Now the Mach line is tangent to all the circles of successive disturbances. All Mach lines together form the Mach cone whose vertex is at the source. Clearly, the disturbances radiated by the source never reach the flow outside the Mach cone.

The associated Mach angle, being the semi-apex angle of the cone, is given by

$$\mu = \sin^{-1}\left(\frac{c}{V}\right) = \sin^{-1}\left(\frac{1}{M}\right), \quad (11.3-3)$$

showing that as the Mach number increases, the Mach angle becomes smaller.

As a final point, we note that a Mach line, in fact, is the limiting case of an infinitely weak *shock wave*. This statement is obvious since our linear acoustic theory only links up with the theory of shock waves so far the perturbations in the flow are very small.

From aerodynamics we know that one of the most important effects of a shock

wave is to produce an almost sudden and large increase in the pressure of the air flow behind the shock (References 7 and 58).

As shown in Figure 11.3-3, at the nose of a source with finite dimensions and moving at supersonic speed, a conical shock wave is produced of which the semi-apex angle $\beta > \mu$.

11.4 VELOCITY POTENTIAL

According to Equation (3.1-37) in Chapter 3, the wave equation in terms of the velocity potential for our monopole source moving at subsonic speed at altitude h along a straight line in the x -direction can be written as

$$\nabla^2 \phi_m - \frac{1}{c^2} \frac{\partial^2 \phi_m}{\partial t^2} = \frac{1}{\rho_\infty} Q(t) \delta(x - Vt) \delta(y) \delta(z - h) , \quad (11.4-1)$$

where $Q(t)$ is the mass flow rate out of the source.

The three-dimensional delta function in the right-hand term of Equation (11.4-1) is stipulated to be zero everywhere in the sound field except at the source position where it assumes the value infinite, as discussed earlier in Section 3.1. Assuming a monopole source with harmonic time dependence, Equation (11.4-1) becomes

$$\nabla^2 \phi_m - \frac{1}{c^2} \frac{\partial^2 \phi_m}{\partial t^2} = \frac{1}{\rho_\infty} Q_0 e^{i\omega t} \delta(x - Vt) \delta(y) \delta(z - h) . \quad (11.4-2)$$

In order to find the solution for the velocity potential it is convenient to transform Equation (11.4-2) into a form representing the equivalent radiation from a stationary source. This is obtained by employing the following modified *Lorentz transformation* of coordinates:

$$\left. \begin{aligned} x_L &= (x - Vt)/(1 - M^2) \\ y_L &= y/\sqrt{(1 - M^2)} \\ z_L &= z/\sqrt{(1 - M^2)} \\ h_L &= h/\sqrt{(1 - M^2)} \\ t_L &= (t - \frac{V}{c^2}x)/(1 - M^2) . \end{aligned} \right\} \quad (11.4-3)$$

These coordinate transformations reduce Equation (11.4-2) to

$$\nabla_L^2 \phi_m - \frac{1}{c^2} \frac{\partial^2 \phi_m}{\partial t_L^2} = \frac{1}{(1-M^2)} \frac{Q_0}{\rho_\infty} e^{i\omega t_L} \delta(x_L) \delta(y_L) \delta(z_L - h_L), \quad (11.4-4)$$

where $\nabla_L = \frac{1}{(1-M^2)} \nabla$.

The solution to Equation (11.4-4) was shown previously in Section 3.1 to be

$$\phi_m(r_L, t_L) = \frac{1}{(1-M^2)} \frac{Q_0}{\rho_\infty 4\pi r_L} e^{i\omega(t_L - \frac{r_L}{c})}, \quad (11.4-5)$$

$$\text{where } r_L = \left[x_L^2 + y_L^2 + (z_L - h_L)^2 \right]^{1/2}. \quad (11.4-6)$$

Transforming back to the initial variables in the physical space yields

$$r_L = \frac{1}{(1-M^2)} \left[(x - Vt)^2 + (1-M^2)y^2 + (1-M^2)(z-h)^2 \right]^{1/2}. \quad (11.4-7)$$

This expression may be written in the following alternative form

$$\left. \begin{aligned} r_L &= \frac{1}{(1-M^2)} r_1, && \text{where} \\ r_1 &= \left[(x - Vt)^2 + (1-M^2)y^2 + (1-M^2)(z-h)^2 \right]^{1/2} \end{aligned} \right\} (11.4-8)$$

Using Equation (11.2-5) and denoting the angle between the direction of motion and the direction of r_e by θ , as shown in Figure 11.2-1, we can write

$$\begin{aligned} r_L &= r_e - \frac{M(x - Vt)}{(1-M^2)} = r_e - \frac{M}{(1-M^2)} (r_e \cos \theta - Mr_e) \\ &= r_e \left[1 + \frac{M^2}{(1-M^2)} \right] - \frac{M}{(1-M^2)} r_e \cos \theta \\ &= r_e \frac{1}{(1-M^2)} - \frac{M}{(1-M^2)} r_e \cos \theta \\ &= r_e \frac{1}{(1-M^2)} [1 - M \cos \theta]. \end{aligned} \quad (11.4-9)$$

Note from Equations (11.4-8) and (11.4-9) that the quantities r_1 and r_e are

are related by

$$r_1 = r_e [1 - M \cos \theta] . \quad (11.4-10)$$

The quantity $(t_L - r_L/c)$ in Equation (11.4-5) becomes

$$t_L - \frac{r_L}{c} = \frac{1}{(1 - M^2)} \left(t - \frac{V}{c^2} x \right) - \frac{1}{c} \left[r_e - \frac{M(x - Vt)}{(1 - M^2)} \right] = t - \frac{r_e}{c} . \quad (11.4-11)$$

Inserting Equations (11.4-8) and (11.4-11) into Equation (11.4-5) furnishes the velocity potential for subsonic motion as

$$\phi_m(r_e, t) = - \frac{Q_0 e^{i\omega(t - r_e/c)}}{\rho_\infty 4\pi r_1} . \quad (11.4-12)$$

With Equation (11.4-10), the velocity potential can be expressed as

$$\phi_m(r_e, t) = - \frac{Q_0 e^{i\omega(t - r_e/c)}}{\rho_\infty 4\pi r_e (1 - M \cos \theta)} . \quad (11.4-13)$$

Note from Equation (11.4-13) that for $M = 0$ the velocity potential is identical to that given in Chapter 3 for the stationary source (Equation (3.1-27)).

Turning to supersonic motion, we note that the velocity potential is obtained by including the contributions from the two sound waves emitted at the times t_{e+} and t_{e-} , as discussed in Section 11.3.

Now, from Equation 11.4-12, we have

$$\phi_m(r_e, t) = - \frac{Q_0}{\rho_\infty 4\pi r_1} \left[e^{i\omega(t - r_{e+}/c)} + e^{i\omega(t - r_{e-}/c)} \right] , \quad (11.4-14)$$

where r_1 is given by

$$r_1 = \left[(Vt - x) - (M^2 - 1)r^2 \right]^{1/2} . \quad (11.4-15)$$

With the relations (see the previous Figure 11.3-1)

$$(Vt - x) = Mr_{e\pm} - r_{e\pm} \cos \theta_\pm ,$$

it follows without difficulty that (cf. Equation (11.4-10))

$$r_1 = r_{e+}(M \cos \theta_+ - 1) = -r_{e-}(M \cos \theta_- - 1) , \quad (11.4-16)$$

where θ_+ and θ_- define the directions of $r_{e\pm}$, as depicted in Figure 11.3-1.

11.5 SOUND PRESSURE

The sound pressure observed from a point monopole which moves with constant subsonic speed is obtained from the relationship $p' = -\rho_\infty \partial \phi_m / \partial t$ and Equation (11.4-13) as

$$p'(r_e, t) = \frac{\left(1 - \frac{1}{c} \frac{dr_e}{dt}\right) Q_0 e^{i\omega(t-r_e/c)} i\omega}{4\pi r_e (1 - M\cos\theta)} - \frac{Q_0 e^{i\omega(t-r_e/c)}}{4\pi r_e^2 (1 - M\cos\theta)} \frac{dr_e}{dt}. \quad (11.5-1)$$

Assuming that the observer is in the far-field, we have $1/r_e^2 \ll 1/r_e$. Then the second term of the right-hand side of Equation (11.5-1) is relatively negligible, and the sound pressure is given by

$$p'(r_e, t) = \frac{\left(1 - \frac{1}{c} \frac{dr_e}{dt}\right) Q_0 e^{i\omega(t-r_e/c)} i\omega}{4\pi r_e (1 - M\cos\theta)}. \quad (11.5-2)$$

From Equations (11.2-5) and (11.4-8), we obtain for subsonic motion

$$1 - \frac{1}{c} \frac{dr_e}{dt} = 1 + \frac{1}{1 - M^2} \left[M^2 + \frac{M(x - Vt)}{r_1} \right]. \quad (11.5-3)$$

Substitution of Equation (11.4-10) and using the relationship (see Figure 11.2-1) $x - Vt = r_e \cos\theta - Mr_e$, we readily find

$$1 - \frac{1}{c} \frac{dr_e}{dt} = \frac{1}{1 - M\cos\theta}. \quad (11.5-4)$$

Hence

$$p'(r_e, t) = \frac{Q_0 e^{i\omega(t-r_e/c)} i\omega}{4\pi r_e (1 - M\cos\theta)^2}. \quad (11.5-5)$$

This expression shows that the sound pressure not only decreases with increasing distance from the point of emission, but also that there is an additional directivity factor $(1 - M\cos\theta)^2$.

$$\text{We note from Equation (11.5-5) that the sound pressure has the phase } \varphi(t) = \omega(t - r_e/c), \quad (11.5-6)$$

where ω is the source angular frequency, and r_e is time-dependent.

As the frequency ω_M observed at the receiver position is given by the time derivative of the phase, we get for a moving source

$$\omega_M = \frac{d}{dt} [\omega(t - r_e/c)] = \omega \left[1 - \frac{1}{c} \frac{dr_e}{dt} \right]. \quad (11.5-7)$$

Combining Equations (11.5-4) and (11.5-7), and using $\omega = 2\pi f$ yields the *Doppler formula*, as presented earlier in Chapter 1 (see Equation (1.13-7)),

$$f_M = \frac{f}{(1 - M\cos\theta)}, \quad (11.5-8)$$

where $(1 - M\cos\theta)$ is named the *Doppler factor*.

As has been explained already in Chapter 1, during flyover the observed frequency varies with source position relative to the receiver between the upper limit $f/(1 - M)$ at $\theta = 0^\circ$ (emission point at $x_s = -\infty$) and the lower limit $f/(1 + M)$ at $\theta = 180^\circ$ (emission point at $x_s = +\infty$).

The sound pressure in the case of supersonic motion is obtained from Equations (11.4-14) and (11.4-16):

$$p'(r_e, t) = -\rho_\infty \frac{\partial \phi_m}{\partial t} \\ = -\rho_\infty \frac{\partial}{\partial t} \left[-\frac{Q_0 e^{i\omega(t - r_{e+}/c)}}{\rho_\infty 4\pi r_{e+}(M\cos\theta_+ - 1)} + \frac{Q_0 e^{i\omega(t - r_{e-}/c)}}{\rho_\infty 4\pi r_{e-}(M\cos\theta_- - 1)} \right] \quad (11.5-9)$$

$$\text{or } p'(r_e, t) = \frac{Q_0 i\omega}{4\pi} \left[\frac{(1 - \frac{1}{c} \frac{dr_{e+}}{dt}) e^{i\omega(t - r_{e+}/c)}}{r_{e+}(M\cos\theta_+ - 1)} + \right. \\ \left. - \frac{(1 - \frac{1}{c} \frac{dr_{e-}}{dt}) e^{i\omega(t - r_{e-}/c)}}{r_{e-}(M\cos\theta_- - 1)} \right]. \quad (11.5-10)$$

$$\text{With } 1 - \frac{1}{c} \frac{dr_{e\pm}}{dt} = \frac{1}{(M\cos\theta_\pm - 1)} \quad (11.5-11)$$

the final result reads

$$p'(r_e, t) = \frac{Q_0 i \omega}{4\pi} \left[\frac{e^{i\omega(t - r_{e+}/c)}}{r_{e+}(M \cos \theta_+ - 1)^2} - \frac{e^{i\omega(t - r_{e-}/c)}}{r_{e-}(M \cos \theta_- - 1)^2} \right]. \quad (11.5-12)$$

It is interesting to notice that the two waves contributing to the sound pressure have different frequencies and amplitudes, meaning that the sound pressure amplitude will vary with time.

The results derived so far show that the sound pressure can be expressed in a simple way in terms of emission angle θ and distance r_e as measured with respect to the source position at the emission time t_e .

Returning to the important case of subsonic forward velocity, we see from Equation (11.5-5) that the quotient of the amplitude of the sound pressures radiated by a moving and a stationary point monopole source is given by

$$\frac{(p'_{\max})_M}{(p'_{\max})_{M=0}} = \frac{1}{(1 - M \cos \theta)^2}. \quad (11.5-13)$$

Likewise, we have for the effective pressures

$$\frac{(p_e)_M}{(p_e)_{M=0}} = \frac{1}{(1 - M \cos \theta)^2}. \quad (11.5-14)$$

Apparently, the Mach number of the source is a fundamental parameter in describing the convective effects. Also note that convection effects are absent at 90° to the emission point.

In general, the modification caused by convection to the effective pressure observed from a point multipole is (Reference 57):

$$\frac{(p_e)_M}{(p_e)_{M=0}} = \frac{1}{(1 - M \cos \theta)^{n+1}}. \quad (11.5-15)$$

The factor n in the exponent of the Doppler factor $(1 - M \cos \theta)$ is related to the type of elementary acoustic source. For monopoles and dipoles $n = 1$, and for quadrupoles $n = 2$.

Practical noise sources may be represented by a coalescence of different elementary sources. Therefore, to cover the convective effects, the exponent of the Doppler factor in Equation (11.5-15) may vary between 1.5 and 4.

11.6 SOUND PRESSURE LEVEL

A sound level meter at the receiver position will display the sound pressure level according to

$$\text{SPL}_M = 10 \log \frac{(p_e)_M^2}{p_{e_0}^2}, \quad (11.6-1)$$

where p_{e_0} is the reference pressure of 2.10^{-5} N/m^2 .

Thus, for a monopole or a dipole source the modification caused by convection to the sound pressure level of a stationary source, from Equation (11.5-14), is

$$\begin{aligned} \Delta \text{SPL} &= \text{SPL}_M - \text{SPL}_M = 0 \\ &= 10 \log \frac{1}{(1 - M \cos \theta)^4} \\ &= -40 \log (1 - M \cos \theta). \end{aligned} \quad (11.6-2)$$

Figure 11.6-1 gives a graphic representation of the convective amplification predicted by Equation (11.6-2). The curves show that the effect of forward motion gives a significant contribution to the directivity of the sound field, and that more of the sound energy is radiated forward of the noise source as the Mach number increases.

For example, at a Mach number $M = 0.6$ the sound pressure level varies from

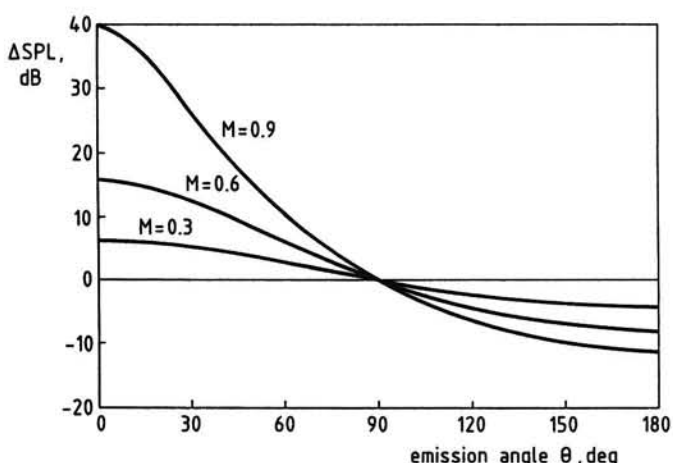


Figure 11.6-1. Convective amplification

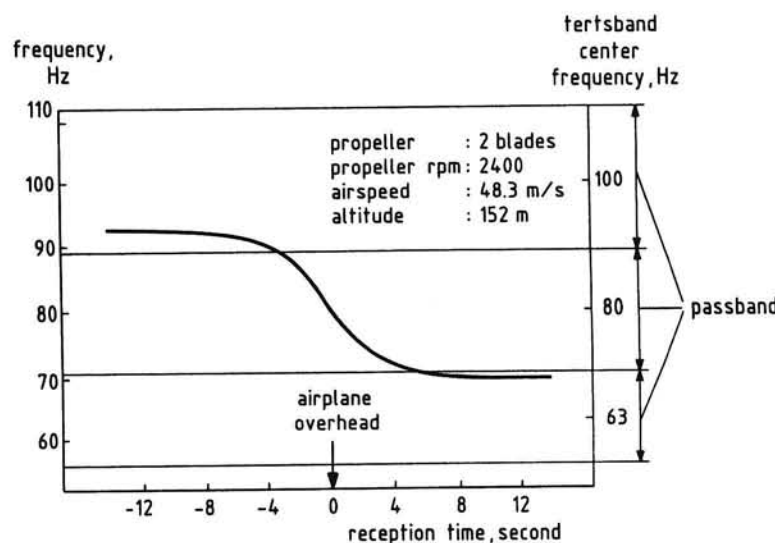


Figure 11.6-2. Frequencies observed from a 80 Hz tone during flyover

a 16 dB rise at $\theta = 0^\circ$ to a 8.2 dB decrease at $\theta = 180^\circ$.

We can further conclude from Figure 11.6-1 that source motion intensifies the unsteadiness of the transient signal as obtained from flyover noise measurements, especially in the neighborhood of overhead.

Finally, as an interesting and important point, we remark that since the observed frequency is increased while a sound source is approaching the receiver and decreased as the source departs from overhead, it is possible for Doppler-shifted tone noises to jump in and out several terstsbands during the flyover.

This phenomenon is illustrated in Figure 11.6-2, where is considered an actual level flyover of a small propeller-driven airplane. Plotted is the observed frequency f_M of the blade passage frequency $f_1 = 80$ Hz as a function of reception time. As can be seen, the curve goes through three adjacent terstsbands, through which the shapes of the measured frequency spectra and thus the corresponding weighted noise levels, can be strongly affected.

11.7 SONIC BOOM

A very special form of ground observed noise is the so-called *sonic boom*. This is an impulsive type of noise, occurring in addition to the noise produced by the propulsion system, and is caused by the shock wave cones formed

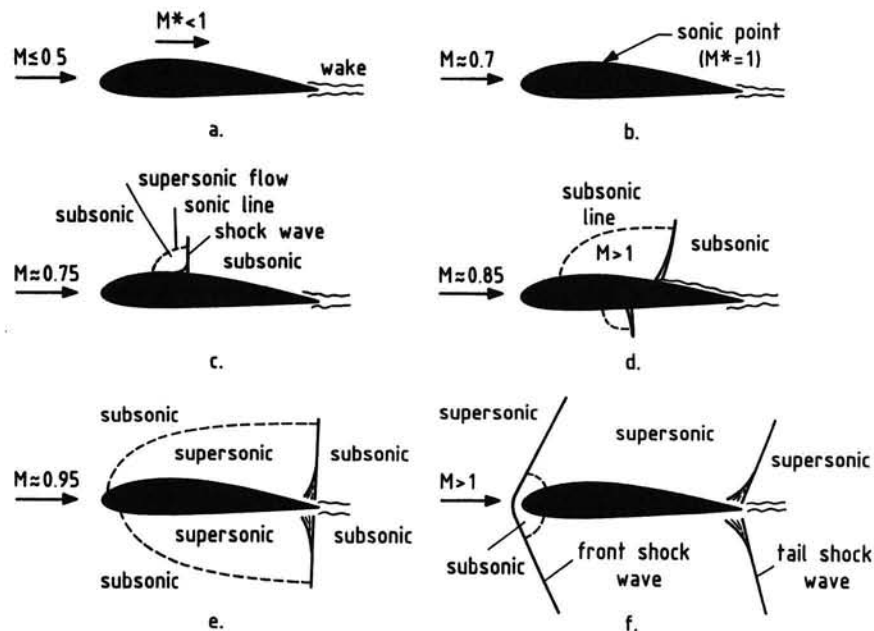


Figure 11.7-1. Shock wave formation

around an airplane when it flies at supersonic speed.

At the ground, the sonic boom is easily observable as two sharp cracks like explosions or thunder.

In order to explain the sonic boom, let us consider the development of the shock waves. To this end, we look at the flow patterns sketched in Figure 11.7-1, where for convenience the airplane is represented by a two-dimensional body having an airfoil shaped cross-section.

Figure 11.7-1a illustrates that up to a flight Mach number of about $M = 0.5$, the flow is subsonic everywhere. Since the maximum local Mach number M^* is always higher than the flight Mach number M , a particular flight Mach number comes about at which locally sonic flow first occurs at a point on the surface of the body (Figure 11.7-1b).

As the flight Mach number increases further, regions of supersonic flow come forth which end through the occurrence of normal shock waves (Figures 11.7-1c and d).

Figure 11.7-1e shows the flow pattern at a flight Mach number just below $M = 1$, where large regions are supersonic.

At supersonic flight speeds, as shown in Figure 11.7-1f, oblique shock waves are present at both the leading edge and the trailing edge of the airfoil section.

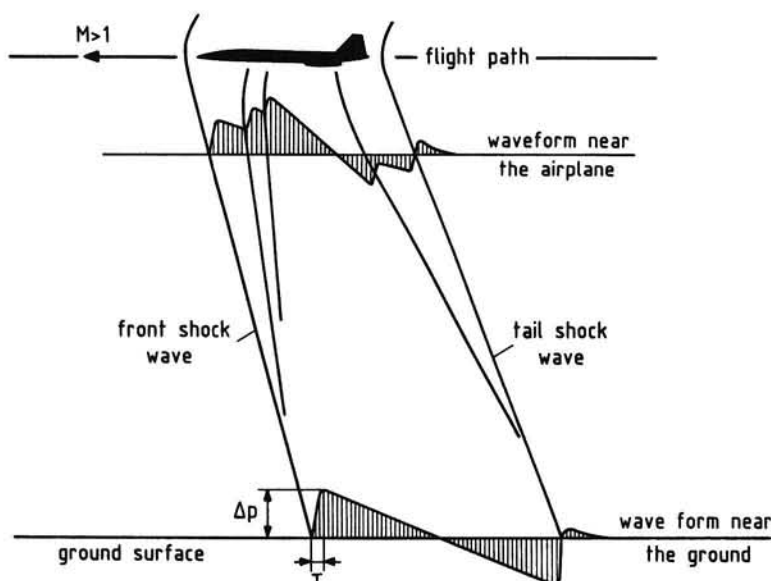


Figure 11.7-2. Pressure distributions resulting from shock waves

The shapes of these shock waves depend on the geometry of the body and the flight Mach number. The bow or front shock wave is detached from the rounded nose and directly behind this shock wave, near the central streamline, a subsonic region is found (Reference 58).

The front shock wave in Figure 11.7-1f produces an increased pressure when the flow passes the shock. As the flow moves along the surface of the curved airfoil section the local pressure falls off continuously to a value less than freestream at the trailing edge. Then there is a sudden pressure rise again due to the tail shock wave, followed by a decline to freestream pressure at some distance behind the body.

As visualized in Figure 11.7-2, in the case of a real airplane with its many shock-generating parts the shock wave pattern is much more compounded than described above.

However, far from the airplane the different shocks will compact so that the observed pressure varies with time in the form of what is called an *N-wave*. When this waveform passes an observer on the ground two sharp reports are heard uncoupled by a time delay of 0.1 to 0.3 second.

The magnitude of the boom overpressure Δp increases somewhat with flight Mach number and diminishes strongly with increasing flight altitude. The highest overpressures, therefore, occur along the ground track and decrease as the lateral distance from the ground track increases.

Measurement data of large supersonic airplanes indicate that the on-track pressure rise ranges from approximately 150 Pa for a flight at an altitude of 9 km to about 25 Pa at 40 km (Reference 5). These numbers indicate that the sonic boom is characterized by high peak sound pressure levels (130 - 120 dB). In this respect, it should be mentioned that the perceived loudness of a short duration sound (impulse noise) is substantially reduced compared with a continuous sound signal of the same sound pressure level. This means that the conventional methods of Chapter 9 are not suitable for computing the loudness of impulse noises. It appears that the loudness of sonic booms is governed by the magnitude of the initial pressure rise, Δp , and the associated rise time τ (see Figure 11.7-2).

However, to abridge this text, a treatment of available procedures for calculating the loudness of sonic booms has been omitted. We suggest reference elsewhere for those readers interested (e.g. Reference 59).

So far we have assumed a homogeneous atmosphere. However, when vertical wind and temperature gradients are present, the individual shock lines which form the shock wave cones, are no longer straight but will be curved in the same way as sound rays are deformed by these atmospheric conditions (see Section 1.4).

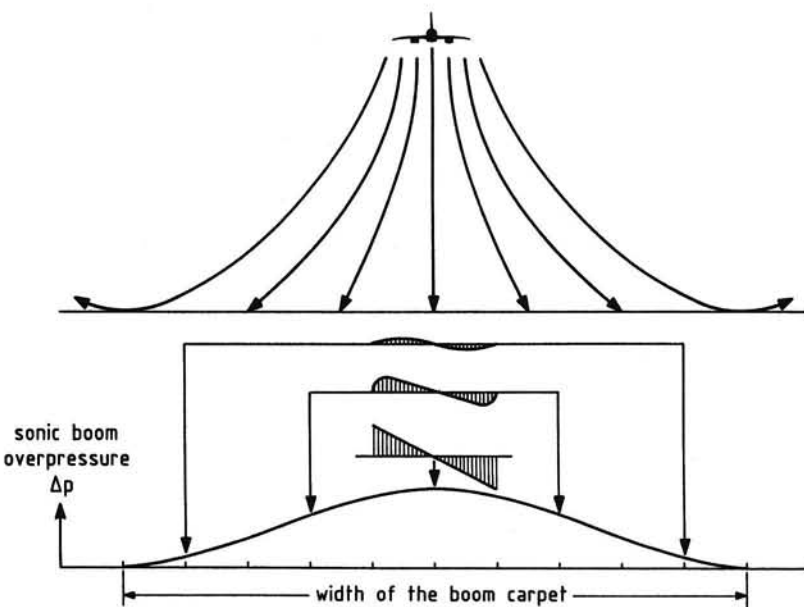


Figure 11.7-3. Bending of shock lines and boom signature shapes

interest, provided that the microphone diaphragm is placed parallel to the direction of propagation of the sound wave, i.e., at grazing incidence (Figure 11.8-1a). As may be understood from the previous Figure 10.2-3, the required grazing incidence condition is fulfilled completely when the noise measurements are taken directly underneath the flight path. In the case of noise measurements made to the side of the flight track, the grazing incidence condition can only be satisfied when level flyovers are performed.

In addition to the above mentioned pressure microphone, two other types are available, namely:

- (1) The *free-field microphone*, having a frequency response which is flat when used in a free field where the direction of the sound wave is perpendicular to the diaphragm of the microphone. In other words, the microphone should point at the noise source (Figure 11.8-1b).
- (2) The *random-incidence microphone* which has a uniform frequency response to sound waves coming at the same time from all directions (Figure 11.8-1c). The latter type of microphone should therefore always be employed when performing sound measurements in a diffuse field.

We complete our discussion on microphone types by remarking that outdoor noise measurements usually are executed in the presence of wind. Then the use of a windscreens with the microphone is recommended to minimize wind-induced noise (see the previous Figure 10.2-3) for wind velocities admissible for airplane noise testing.

The measurement of airplane certification noise levels with the 1.2 m pole microphone, as described in the preceding chapter, therefore, always will require the use of a windscreens.

12 AIRPLANE NOISE SOURCES

12.1 INTRODUCTION

The primary source of noise from an airplane is its propulsion system. Therefore, also from a noise point of view, airplanes may be classified with respect to their engine types. In historical order we can distinguish the following five principal types of airplane powerplants:

- the piston engine with propeller
- the turbojet
- the turboprop } turbo-engines.
- the turbofan
- the propfan

All these engine types produce a propulsive force by accelerating air or gas masses rearwards with respect to the airplane.

The *piston engine* driving a propeller is used today in the small general aviation airplanes only. As shown in Figure 12.1-1, the engines have four or six aircooled cylinders, which are arranged in horizontally opposed pairs.

In the cylinders a mixture of air and gasoline is burned, through which the pistons drive the crankshaft by means of their connecting rods.

The rotating crankshaft, in turn, drives the propeller, which device effects propulsion through the acceleration of atmospheric air. A reduction gear may be present between crankshaft and propeller in order to limit the speed of the propeller blade tips relative to the air. This speed is called the *helical tip speed*, V_{ht} , and is the vector sum of the flight speed V in the direction of the propeller

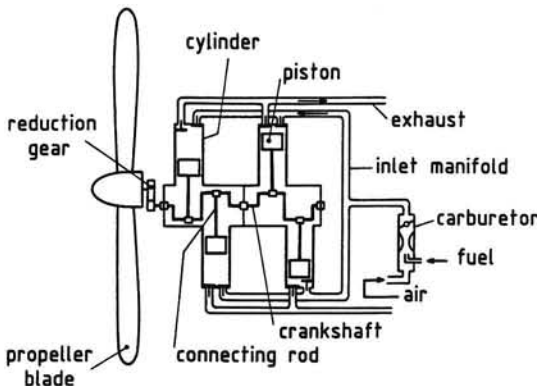


Figure 12.1-1. Piston engine with propeller

axis and the rotational velocity of the blade tip ωR , directed perpendicular to the propeller axis (Figure 12.1-2),

$$V_{ht} = \sqrt{V^2 + (\omega R)^2}, \quad (12.1-1)$$

where ω is the angular velocity of the propeller axis and R is the blade radius. Equation (12.1-1) may be rewritten as

$$V_{ht} = \sqrt{V^2 + (\pi D n_p / 60)^2}, \quad (12.1-2)$$

where $D = 2R$ is the propeller diameter and n_p is the propeller speed in rotations per minute (rpm).

The associated *helical tip Mach number* is

$$M_{ht} = \frac{V_{ht}}{c}. \quad (12.1-3)$$

A feature of propeller performance is a thrust that decreases gradually with increasing airspeed.

The helical blade tip speed, of course, becomes greater as the flight speed increases until at a forward speed of about 700 km/h, V_{ht} approaches the speed of sound and the propeller thrust abruptly falls off. This behavior limits the usefulness of the conventional propeller to lower subsonic airspeeds.

The development of the *turbojet* in the thirties brought a completely new method of propulsion and met an answer to the demand for higher airspeeds. As shown in Figure 12.1-3, the turbojet engine consists of five major parts; air intake, compressor, combustor, turbine, and exhaust nozzle.

The intake sucks in air and decreases the air velocity, after which the air is

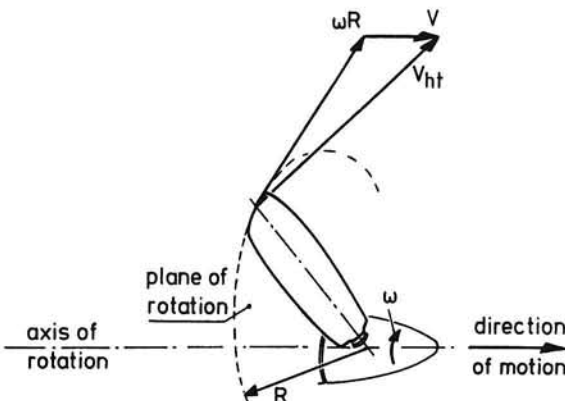


Figure 12.1-2. Propeller helical tip speed

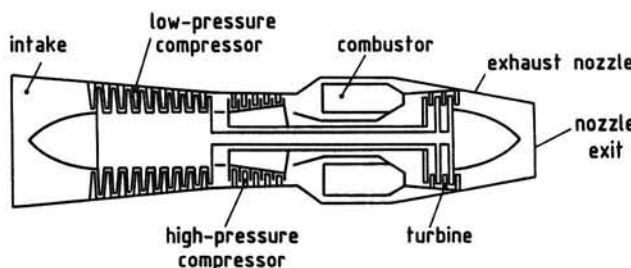


Figure 12.1-3. Two-spool turbojet engine

compressed in the compressor. In the combustor kerosene fuel is sprayed in and burned, providing a high gas temperature. In the turbine just enough energy is extracted from the hot gas flow to drive the compressor. The remaining high-temperature/high-pressure gas flow is accelerated by expansion in the exhaust nozzle and leaves the engine exit as a high-velocity jet.

It is worth noting that the engine shown in Figure 12.1-3 is a *two-spool engine*, i.e., the engine employs two compressors, each driven independently by its own turbine and at different rpm's.

As depicted in the previous Figure 9.9-3, gas turbine engines may be equipped with an *afterburner* where extra fuel is injected. Burning of additional fuel is possible because the gas flow entering the afterburner duct comprises an excess of oxygen. Afterburning increases the temperature of the exhaust gas stream giving an increased jet-velocity and therefore an increased engine thrust. The extra thrust is used for takeoff and climb or for transition from subsonic to supersonic airspeed. Therefore, it is of special significance for military airplanes and supersonic transports.

An essential difference between jet and propeller propulsion is the nature of the rearward mass flow. In the case of the propeller a large mass flow of cold air is transported at a relatively low velocity, whereas the turbojet produces a thrust by accelerating a relative small amount of hot gas to a very high speed. This makes that the turbojet is only economical of fuel at high flight speeds, whereas the propeller is an efficient means of producing thrust at low subsonic airspeeds (Reference 7).

The problem of the inefficiency of the turbojet at low airspeeds can be solved through extracting most of the heat energy from the hot gas flow by means of an enlarged turbine, and then to supply the energy in the form of shaft power to a propeller. This arrangement is called a *turboprop* (Figure 12.1-4). A reduction gear between the compressor and the propeller is always required

In the upper part of Figure 11.7-3 are depicted upward refracted shock lines as seen from ahead of the airplane. Assumed is a quiet atmosphere where the air temperature decreases with increasing height above the ground.

Apparently, due to the negative temperature gradient the travel distance along the shock line to a sideline position increases, through which the strength of the boom is reduced.

The lateral extent of the overpressure is sketched in the lower part of Figure 11.7-3. Also are illustrated the sonic boom signatures at various sideline positions, indicating that the *N*-wave becomes blurred as lateral distance becomes greater.

It is also apparent that a shadow zone may occur where the sonic boom cannot penetrate since the upward bending of the shock line prevents the sonic boom from striking the ground surface. The locations of the lateral cutoff points will depend on flight Mach number, flight altitude, and wind and temperature gradients.

It should be restated that the shock wave cones only occur when the airplane is flying at supersonic speeds. This means that, normally, the sonic boom problem is associated with flight operations above areas well away from the airports of departure and arrival.

Therefore, the sonic boom does not contribute to the noise levels experienced around airports.

We close this section by remarking that the shock waves cannot reach

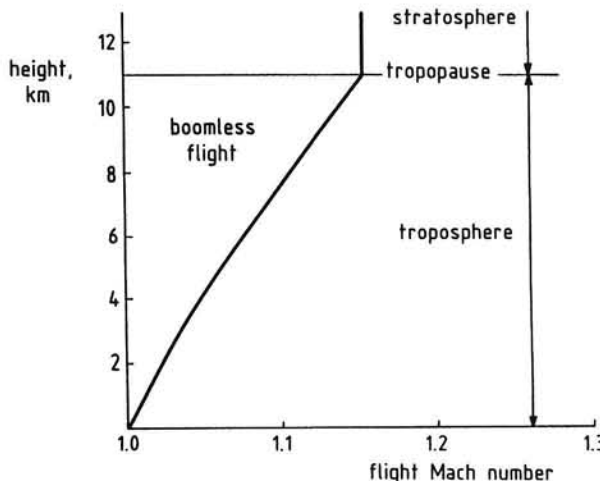


Figure 11.7-4. Area of altitude and Mach number where boomless flight can be performed

the ground if the speed of sound at ground level is greater than the forward speed of the airplane. The circumstance that the shocks, and thus the boom, terminate at some height above the ground occurs in the case of a temperature lapse condition (negative temperature gradient) and at low flight speeds. Consequently, sonic boom annoyance can be avoided by flying at high altitudes and low supersonic speeds.

In Figure 11.7-4 are shown the combinations of flight Mach number and altitude of boomless flight in the International Standard Atmosphere (I.S.A.). It is seen that the range of maximum flight Mach numbers varies from 1.0 at ground level up to about 1.15 in the stratosphere ($11 \text{ km} \leq h \leq 20 \text{ km}$).

11.8 MICROPHONE SELECTION

During flyover noise measurement the sound emitted by the airplane reaches the measuring station at a continuously varying incidence angle. In consequence, the accuracy of the recorded sound signal may be dependent on the position of the airplane relative to the measurement point.

This phenomenon is due to the fact that the frequency response of the microphone is affected by the diffraction and reflections created by its own presence in the sound field, and thus is determined by the orientation of its diaphragm relative to the direction of propagation of the sound wave.

To acquire accurate results from inflight noise measurements a so-called *pressure type microphone* should be used, which has a frequency response for which the sensitivity is independent of frequency over the frequency range of

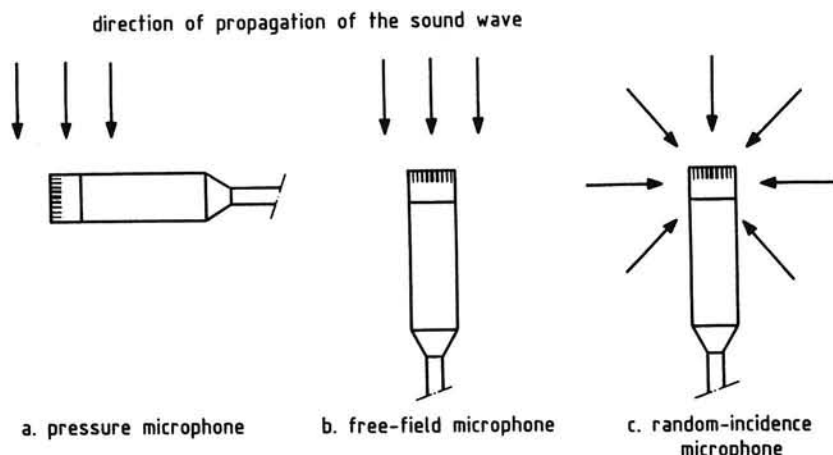


Figure 11.8-1. Types of microphone

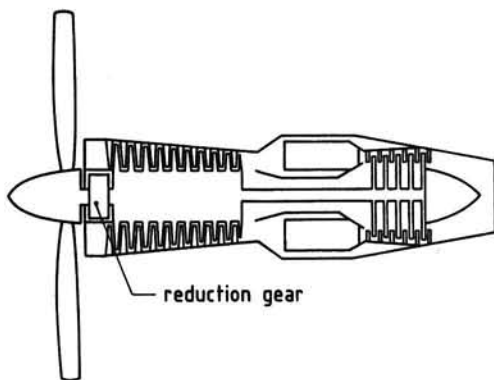


Figure 12.1-4. Turboprop engine *Figure 12.1-5. Two-spool turbofan engine* since the compressor rotates at a very high speed which must be reduced in order to avoid extreme helical propeller blade tip speeds.

Normally there is sufficient residual energy in the gas flow after the turbine to accelerate the gases to a velocity greater than the flight speed, generating an additional jet thrust.

Today many types of small commuter airliners are propelled by turboprop engines.

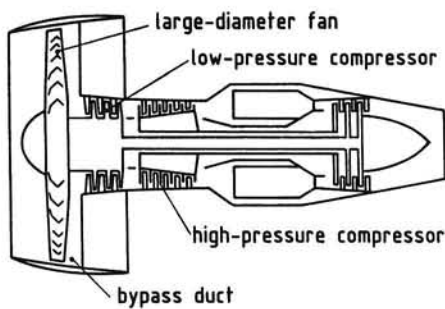
A compromise between the turbojet and the turboprop is the *bypass engine* or *turbofan*. This engine type operates efficiently throughout the entire subsonic airspeed range. As shown in Figure 12.1-5, the propeller is replaced by a thrust-producing ducted fan, which is an integral part of the low-pressure compressor. Part of the air impelled by the fan passes through the bypass duct and is discharged as a cold jet. The rest of the fan flow goes through the high-pressure engine core and forms the hot flow.

The mean velocity at the engine exit is thus lower than for the equivalent turbojet engine, while the mass flow rate is larger.

Due to the reduced exit velocity, the turbofan is not only much more economical but also much quieter than the equivalent turbojet engine.

The characteristics of the turbofan are determined by its *bypass ratio*, BPR, being the ratio of the mass flow rate of the cold flow to the mass flow rate of the hot flow. Early bypass engines had a bypass ratio of about one, whereas today's turbofans have a bypass ratio between 4 and 6.

To accelerate the cold flow, a large percentage of the energy available from the hot gas flow is supplied as shaft power to the fan. Therefore, in principle, the turbofan is similar to the turboprop except that its bypass ratio is much lower. Nevertheless, in addition to the thrust produced by the hot jet, the fan also accelerates such a large mass of cold air that it supplies a generous contribution to the thrust.



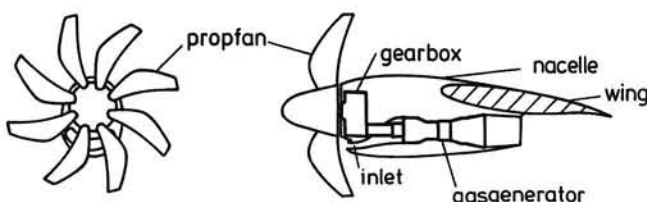


Figure 12.1-6. Propfan

Because of the need to conserve fuel, the propeller is again considered as a propulsor for large commercial airplanes. The concepts that are currently under development are called *propfans* (Figure 12.1-6). These engines incorporate one or two multibladed, small-diameter, propellers, which have very thin blade sections. The blades are swept back at the tips in order to retain good efficiency up to high-subsonic airspeeds.

In considering the noise produced by airplanes, it should be noted that in addition to powerplant noise, the so-called *airframe noise* is of significance. This source is common to all airplanes in flight and concerns the aerodynamic noise in the boundary layers surrounding the moving airplane. Some remarks on this noise source will be made in Section 12.7. The intermediate text of this concluding chapter, i.e., Sections 12.2 to 12.6 will be devoted to a review of the noise radiation characteristics of propeller and jet propulsion. Finally, interior noise will be discussed briefly in Section 12.8.

12.2 PISTON ENGINE NOISE CHARACTERISTICS

The piston engines used in airplanes operate on the four-stroke cycle principle. As portrayed in Figure 12.2-1, the working cycle, i.e., the complete sequence of operations returning to the original state, requires two revolutions of the crankshaft; two strokes toward the crankshaft and two strokes toward the cylinder head.

The conversion of the chemical energy in the fuel into shaft power may be analyzed on the basis of the graph on the right-hand side of Figure 12.2-1, which shows a plot of pressure versus volume of space in the cylinder above the piston. In successive order we have the following events:

- (1) The intake stroke. The piston travels from the cylinder head to the bottom of the cylinder. A mixture of vaporized fuel and air is sucked into the cylinder through the open inlet valve at almost constant pressure ($p_2 \approx p_1$).

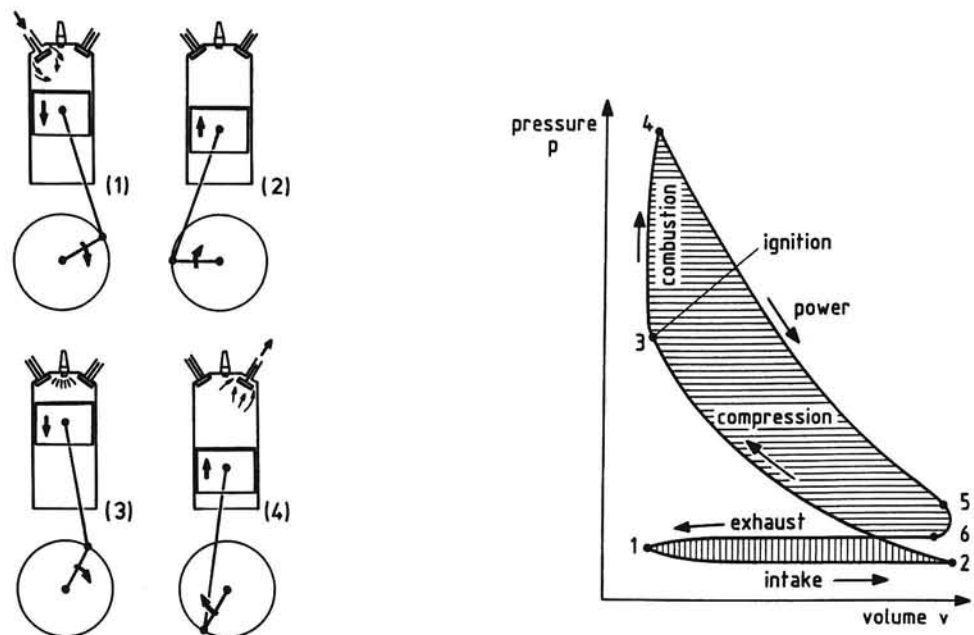


Figure 12.2-1. The working cycle of a four-stroke piston engine

- (2) The compression stroke. The piston moves upward to the top of the cylinder. The mass of gas confined in the cylinder is compressed from the inlet-manifold pressure p_2 to a pressure p_3 . When the piston approaches the top of the stroke, the charge is ignited by the ignition system. Between points 3 and 4, combustion takes place at approximately constant volume and the gas pressure increases to p_4 .
- (3) The power stroke. The high gas pressure pushes the piston downward and the burning gas expands to a pressure p_5 , doing work on the piston. Just before the piston reaches the bottom of the stroke the exhaust valve opens and the pressure inside the cylinder drops to the value $p_6 \approx p_1$.
- (4) The exhaust stroke. The piston again moves upward and the burned gas in the cylinder is forced out through the exhaust valve to the engine exhaust system.

The above described events form the so-called *Otto-cycle*, named after Nicholas A. Otto, who constructed the first successful piston engine in 1876.

The net work per cylinder done during one cycle, W_i , is the force acting on the piston times its displacement and is proportional to the net area of the pv -diagram in Figure 12.2-1. Notice that the horizontal-hatched area represents

positive work, i.e., work done by the gas on the piston, and that from this work must be subtracted the negative work, represented by the vertical-hatched area. In mathematical form

$$W_i = \oint p \, dv = \frac{\pi}{4} D^2 \oint p \, dS , \quad (12.2-1)$$

where D is the cylinder diameter or bore and S is the stroke, the largest distance that the piston travels.

The work W_i is fully determined by the design of the engine and the fuel/air ratio.

At an engine rotational speed n in rpm, the number of strokes in one second is $n/120$. Hence, the power delivered by the pistons to the crankshaft is given by

$$P_{br} = \frac{NW_i n}{120} , \quad (12.2-2)$$

where N is the number of cylinders and P_{br} is the shaft power.

The piston engine produces noise at a series of discrete frequencies. These frequencies are integer multiples of the *cylinder firing frequency*,

$$f_c = \frac{n}{120} , \quad (12.2-3)$$

where n is again the engine rotational speed in rpm.

The most intense noise levels, however, are found at the *exhaust firing frequency*, f_e , and its harmonics, where

$$f_e = \frac{Nn}{120} . \quad (12.2-4)$$

In Figure 12.2-2 is shown the typical shape of an exhaust noise spectrum from a piston engine without muffler, where a number of harmonics of the cylinder firing frequency can be discerned (Reference 60).

According to Reference 61, the overall A-weighted level of the exhaust noise of an unmuffled piston engine at 150 m (500 ft) sideline can be estimated by the

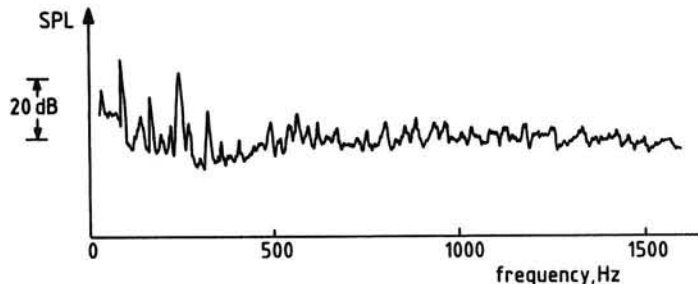


Figure 12.2-2. Piston engine exhaust noise spectrum

following expression,

$$L_A = 8 + 14 \log P_{br} , \quad (12.2-5)$$

where P_{br} is shaft power in watt.

Before leaving the characteristics of piston engine noise, it is worth mentioning that the exhaust of the engine produces more noise than that of an equally rated turboprop engine. The latter engine type is only an appreciable contributor to the high-frequency broadband noise of the spectrum. However, when overall noise level reductions of propeller-driven airplanes powered by piston engines require reduction of the exhaust noise, an exhaust muffler on the engine can be used to great advantage (References 60 and 61).

12.3 PROPELLER-DRIVEN AIRPLANE NOISE

As illustrated in Figure 12.3-1, the propeller blades convert the shaft power of the engine into a thrust by accelerating air backward with respect to the airplane. The useful power available for propulsion is given by the product of thrust T and airspeed V . This quantity is called power available and denoted by the symbol P_a . The ratio of power available to engine shaft power is the *propulsive efficiency* of the propeller,

$$\eta_j = \frac{TV}{P_{br}} . \quad (12.3-1)$$

A discussion of propulsive efficiency is beyond the scope of this text. It is suffice to say that at low airspeeds the propulsive efficiency is virtually constant but when the helical tip Mach number of the blades of a conventional propeller approaches unity, η_j collapses through which the propeller thrust is dramatically impaired.

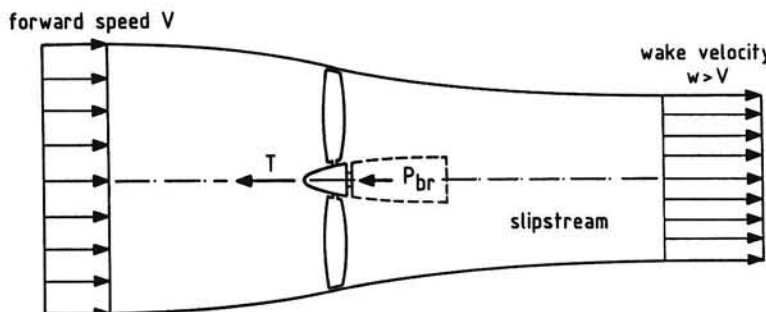


Figure 12.3-1. Propulsive action of propeller

In this book, naturally, the emphasis is on powerplant noise which originates from the engine and the propeller, and of which the propeller is nearly always the most significant component.

The noise generated by the propeller is composed of the so-called *rotational noise* and the *vortex noise*.

Rotational noise originates from the fact that the rotating blades periodically excite the air in the propeller disc. The effect of receiving periodic bumps by the air is twofold. The first effect is termed *loading noise* and is connected with a concentrated force due to the circulation flow around the blades. This means that loading noise is associated with the production of thrust.

The fluctuating forces exerted on the air by the rotational motion of the blades radiate acoustic energy in the way of an array of dipoles with their axes normal to the propeller plane.

The second contribution to the rotational noise is named *thickness noise* and is caused by the symmetrical volume displacements of the air in the propeller disc owing to the finite thickness of the blades. The resulting noise radiation can be described by a distribution of acoustic monopoles.

Both loading noise and thickness noise are characterized by a discrete frequency spectrum that is harmonically related to the fundamental or blade passage frequency f_1 (see also Equation (7.1-1)),

$$f_1 = \frac{B n_p}{60} , \quad (12.3-2)$$

where B is the number of blades and n_p is the propeller rpm.

The vortex noise arises from unsteady random disturbances initiated at the blades. Because of the turbulent regions in the wakes generated behind the propeller, the noise radiation may be represented by quadrupoles. This broadband noise has a continuous spectrum over a wide range of frequencies above 1000 Hz. It is, however, nearly always of less importance compared to the rotational noise.

Therefore, *propeller noise spectra* exhibit peaks at frequencies which are integer multiples of the blade passing frequency.

Under static conditions, the blade passage frequency is the most important frequency, while the contributions to the total noise level decrease with increasing harmonic number.

Since, as stated above, rotational noise is usually the predominant source of propeller noise, we may explain these characteristics of the frequency spectrum by considering an element of air in the propeller plane.

In Figure 12.3-2a is sketched a simplified picture of the fluctuating pressure, as produced by a two-bladed propeller. As depicted in Figure 12.3-2b, the

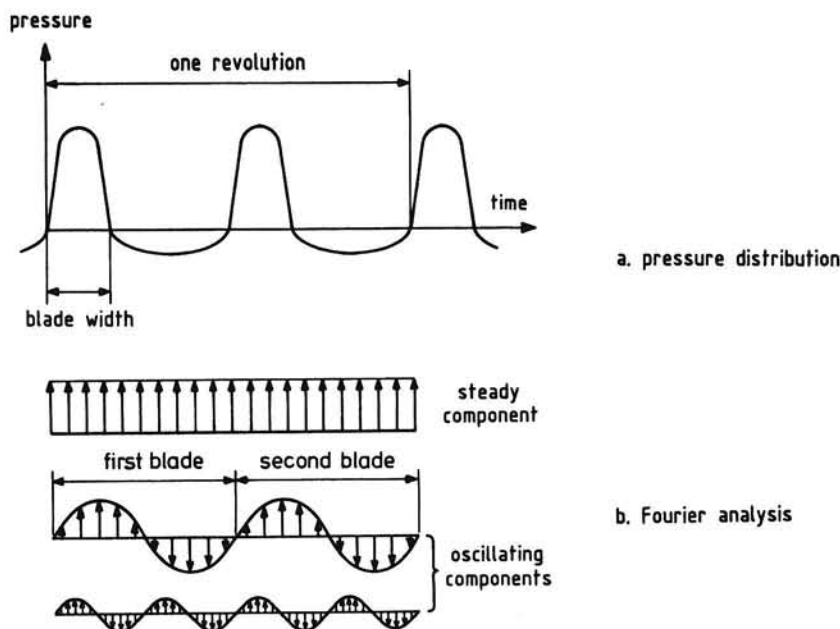


Figure 12.3-2. Steady and periodic components of disturbances created in the air by two-bladed propeller

periodic pressure variation can be Fourier analyzed, yielding a steady component which is the useful thrust of the blade element, and a series of oscillating components whose frequencies are integral multiples of the fundamental frequency. Their sound pressure levels represent the propeller noise spectrum due to the regular motion of the blades through the air.

From the foregoing discussions it may be clear that the frequency spectrum of propeller noise is of the same type as that of piston-engine exhaust noise, i.e., both sources produce a series of tone noises harmonically related to their fundamental frequencies.

In Figure 12.3-3 is shown the variation of the sound pressure level of the harmonic components of the noise measured of a small propeller-driven airplane, operating statically on the ground.

The airplane has an ungeared, two-bladed propeller, driven by a four-cylinder piston engine. This implies that $f_l = f_e$ through which propeller and engine exhaust components cannot be separated.

The noise spectrum in Figure 12.3-3 is typical for the noise production at static conditions, showing a harmonic decay rate of 3 to 4 dB at the important frequencies below 1000 Hz. The propeller diameter is 1.88 m and the rotational

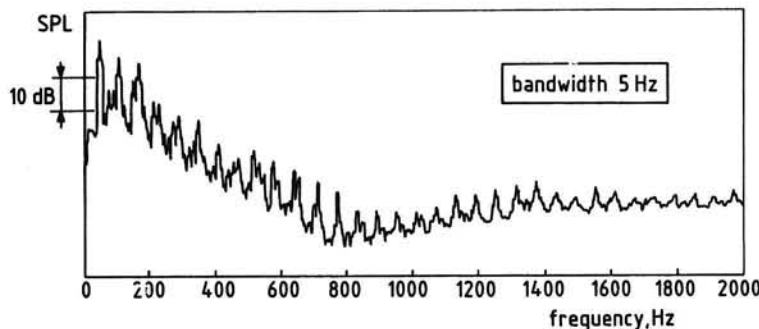


Figure 12.3-3. Frequency spectrum (Piper Cherokee Arrow PA-28R-200)

speed is 1800 rpm. Using $c = 340$ m/s, the helical tip Mach number, from Equations (12.1-2) and (12.1-3), is

$$M_{ht} = M_t = \frac{\pi \times 1.88 \times 1800 / 60}{340} = 0.52 .$$

It is known from experiments that with increasing M_{ht} the higher frequency components become more significant. At transonic and supersonic blade tip velocities, higher harmonics may even exceed the contribution from the blade passage frequency due to shock waves in the flow around the blades. Consequently, there are additional quadrupole noise sources at higher frequencies which make this so-called *supersonic propeller* a source of intense noise.

In Figure 12.3-4 is indicated schematically how the noise is distributed in space. The harmonic levels of the engine exhaust noise are only slightly

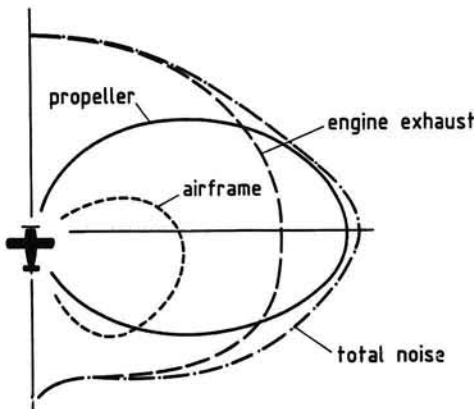


Figure 12.3-4. Typical noise directivity patterns of small propeller-driven airplane noise sources

directional. Propeller noise has its maximum at angles between 0° and 30° behind the plane of rotation, and decreases near the propeller axis. The airframe noise shows a similar dipole directivity which is oriented normal to the flight direction.

We conclude this section with recalling that airplane noise signatures differ for static and in-flight operation. Essentially, the characteristics of the noise observed on the ground are changed for three reasons: (1) the effect of forward motion on the directional pattern of the noise field; (2) the effects of ground reflection and noise shielding; and (3) the aerodynamic noise generation in the boundary layers over the outer surface of the airplane.

12.4 PROPELLER NOISE PREDICTION

As reviewed in Reference 62, over the years a large number of theoretically based methods have been developed to predict propeller noise. All such methods need detailed knowledge of the propeller configuration and consequently require great effort to estimate the noise levels. Therefore, also several empirical methods have been developed, which show relative simplicity and ease of use. A widely used procedure of the latter type is presented in Reference 63, which consists of generalized curves indicating the influence of a number of factors on the noise characteristics of propellers. The procedure enables the calculation of the perceived noise level (PNL) as functions of emission angle and distance from the source.

Since details of blade shape are not considered, the method provides a suitable tool for preliminary design studies on propeller geometrics. The input is limited to the following design and operational parameters:

- propeller diameter, D
- number of blades per propeller, B
- propeller rotational speed, n_p
- engine shaft power, P_{br}
- speed of sound in air, c
- distance from propeller, r
- angular position of observer, θ
- number of propellers, N
- airspeed, V .

For the prediction of far-field propeller noise, the following expression for the maximum sound pressure level can be constructed from the various graphs given in Reference 63 (see also Reference 31):

$$\text{SPL}_{\max}(r) = 83.4 + 15.3 \log P_{br} - 20 \log D + 38.5 M_t + \\ - 3(B - 2) + 10 \log N - 20 \log r , \quad (12.4-1)$$

where both D and r are expressed in meter, P_{br} is shaft power in watt, and M_t is the rotational tip Mach number (cf. Equation (12.1-1)),

$$M_t = \frac{\pi D n_p}{60 c} . \quad (12.4-2)$$

Note from Equation (12.4-1) that atmospheric attenuation and forward speed are ignored in calculating the sound pressure level, although a subsequent adjustment is made to M_t . The value of SPL_{\max} predicted by Equation (12.4-1) occurs at an emission angle θ of approximately 105° , according to the assumed directivity which is plotted in Figure 12.4-1. Examining the curve in this figure, we see that the maximum sound pressure level is about 2 dB higher than its space average. The method assumes the directivity pattern to be independent of airplane type and the airplane's flight and engine conditions.

By means of a correction, based on helical tip Mach number and number of blades, the sound pressure level obtained from Equation (12.4-1) can be converted into perceived noise level.

The A-weighted noise level may then be determined by subtracting 14 dB from the PNL-value (see Equation (9.3-1) of Chapter 9).

Similar empirical methods are available, of which the use is restricted to the prediction of small propeller-driven airplane noise (References 64 to 66). It may be noticed that the method according to Reference 66 includes also the

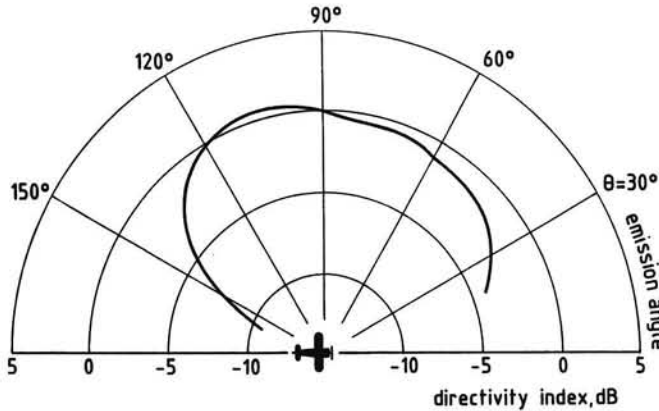


Figure 12.4-1. Directivity index

propeller tip thickness and twist which are supposed to contribute to the noise generation.

Comparisons between predicted and measured noise levels are made in Reference 67, where it is shown that both measurements and predictions are essentially linear in the helical tip Mach number. From this observation the conclusion may be drawn that M_{ht} is the most important noise generating parameter. Therefore, from acoustic as well as aerodynamic considerations there is a strong need to limit the helical tip Mach number. Consequently, modern propellers are tending to run more slowly and to have a smaller diameter. To maintain thrust they employ an increased number of blades. The effect of adding more blades to the propeller, however, is to increase the frequencies at which the harmonics occur so that the favorable effect on perceived loudness gained from this measure may be reduced.

12.5 TURBO-ENGINE NOISE

The noise sources involved in the operation of turbojet and turbofan propulsion engines are the fan, compressor, combustor, turbine and exhaust jet.

As visualized by Figure 12.5-1, these noise components show typical directivity patterns. The noise levels depend on the type of engine, but are always maximum at about 45° to the direction of motion.

Fan, compressor, combustor and turbine noise is generated inside the engine, while the exhaust jet noise, caused by the turbulent mixing of the hot gas flow with the ambient air, occurs outside the engine. The fan radiates its noise more or less equally forward through the air inlet and aft through the fan discharge duct. The turbofan compressor noise is emitted to the front, whereas the noise of the combustor and turbine contributes to the exhaust noise behind the engine. The noise levels from turbojets and low-bypass ratio turbofans with and without afterburner, when operating under full-power conditions, are almost entirely due to exhaust jet noise. Only at low engine ratings, as applied during landing approach, the compressor becomes the predominant noise source.

High-bypass ratio turbofan engines, where a significant portion of the thrust is derived from the bypass flow produce lower exhaust-jet velocities than turbojet engines and show therefore reduced exhaust jet noise.

During a flyover of a turbofan-powered airplane the ground observed noise level varies with time (Figure 12.5-2). Because the various engine noise components reach their maximum values at different instants, the observer, normally, can hear two noise peaks: one when the airplane is approaching overhead, and the fan noise is peaking; and the other when the airplane is receding, and exhaust noise is ruling.

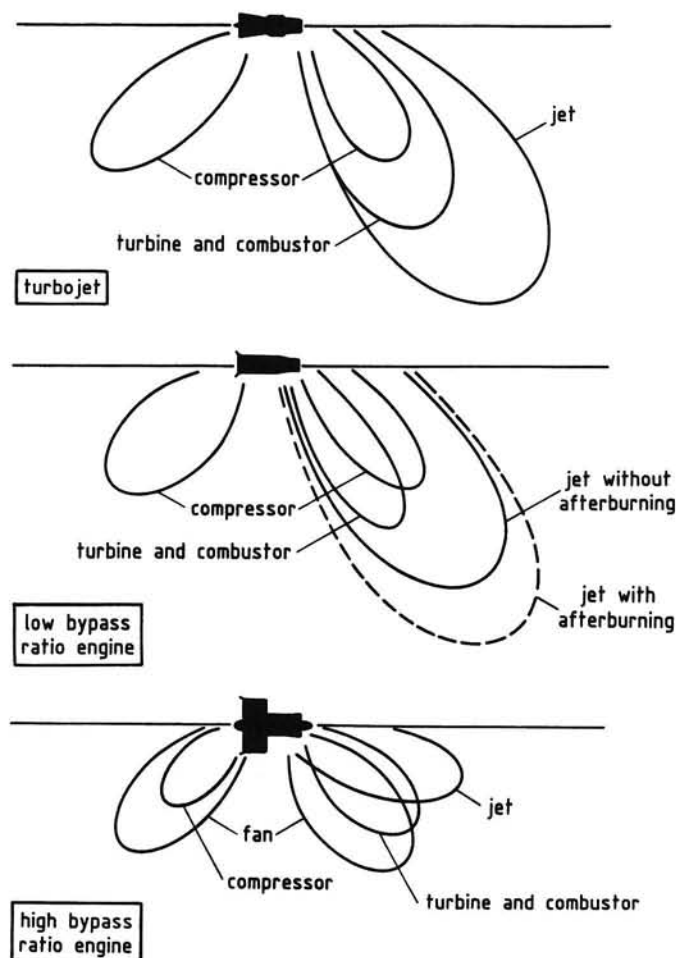


Figure 12.5-1. Directivity of turbo-engine noise components

Figure 12.5-3 shows that the effect of bypassing the core engine is to lower the exhaust jet noise and to increase the fan (compressor) noise due to the increase in fan size. The curves in Figure 12.5-3 have been normalized to the same takeoff thrust and position relative to the engine.

The very noisy engines of the first generation commercial jet-powered airplanes used nearly all modified jet nozzles to suppress their exhaust jet noise.

Two main types of noise-suppressors were employed, one being the so-called *multitube type*, as sketched in Figure 12.5-4a. The other type of noise-suppressor is the *corrugated nozzle*, that is, a nozzle with a corrugated cross-section (Figure 12.5-4b).

These devices break up the exhaust jet into smaller parts by increasing the total

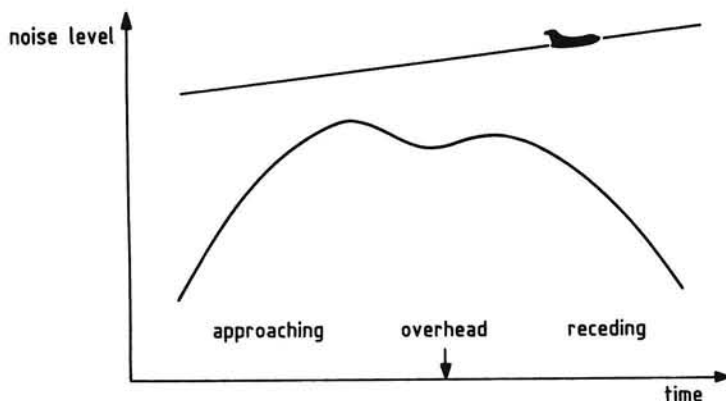


Figure 12.5-2. Time-history of flyover noise

perimeter of the nozzle area. The result is a reduction of the magnitude of the turbulence in the mixing region of the exhaust flow, shifting the spectrum to higher frequencies. Since high frequencies are highly weakened when traveling through the atmosphere, the ground observed noise levels are less at any given distance from the source. The amount of attenuation is 10 to 12 dB, which corresponds to a reduction in perceived noisiness of about one-half.

Attenuation of fan noise is obtained by elimination of the inlet guide vanes as used in early turbofan engines.

The wakes trailing behind these vanes were main sources of fluctuations in the pressure field around the downstream rotor and stator vanes, and so the cause of significant tone noise.

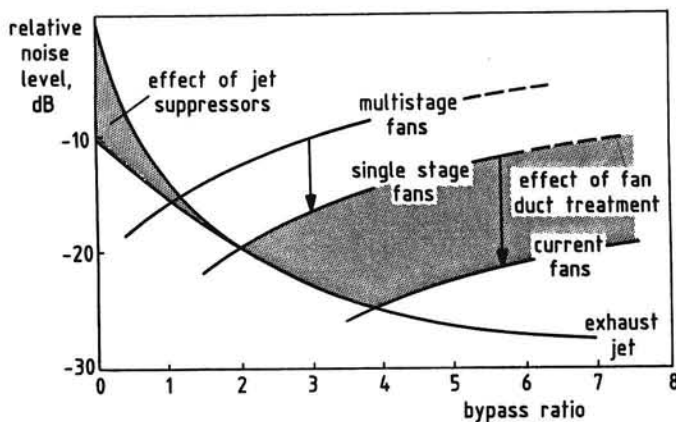


Figure 12.5-3. Effect of bypass ratio on fan and exhaust noise

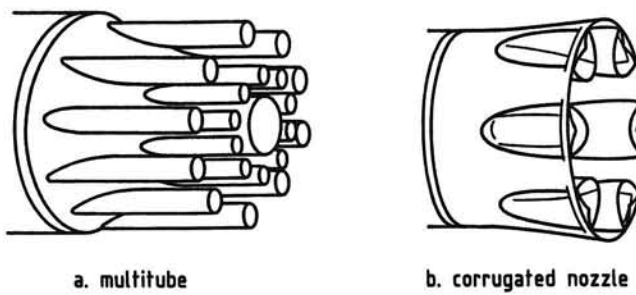


Figure 12.5-4. suppressor nozzle types

Application of a single-stage-low-pressure fan (single rotor and stator) instead of a two-stage fan further has reduced the fan noise because in the latter fan type the flow around the blades of the second stage is disturbed by the first one, causing intensified pressure fluctuations and thus extra noise generation by the second stage.

In addition, improved fan design and acoustic treatment of the fan duct by acoustic lining are quite effective measures to reduce fan noise.

Further, the use of mixers on low-bypass ratio engines is an adequate way of lowering the maximum exhaust-jet velocity and therefore the exhaust jet noise (Figure 12.5-5). This device mixes the hot and cold flows ahead of the nozzle exit, and expels the lower velocity exhaust jet through a single nozzle. The more uniform velocity profile at the engine exit leads to a reduced noise production.

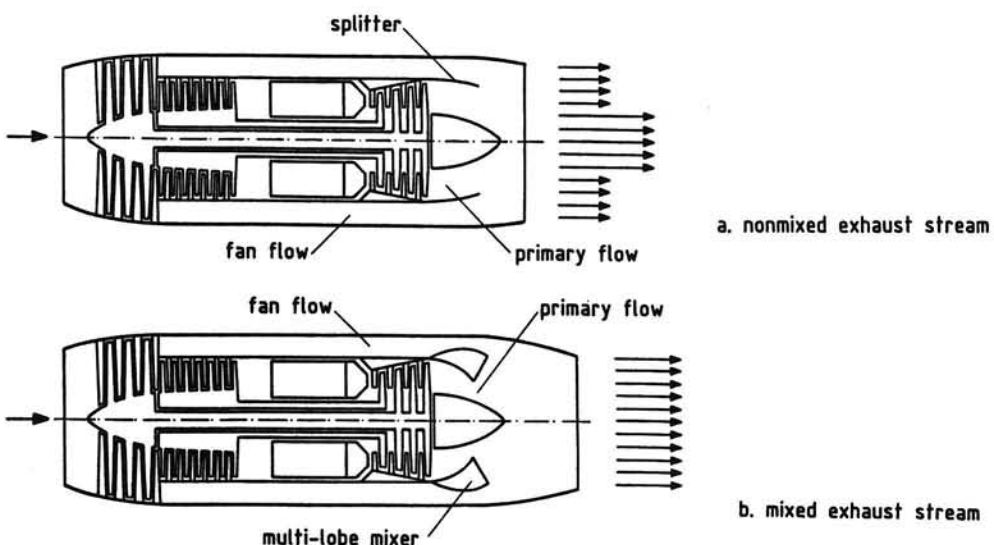


Figure 12.5-5. Reduction of maximum jet velocity by internal exhaust mixers

Returning to Figure 12.5-3, we see that when the bypass ratio is about four, the exhaust jet noise and fan noise are of equal importance. In regard to this observation, in the next section a short description will be given of the noise-generation mechanisms of these two governing noise components.

12.6 FAN AND EXHAUST JET NOISE

Figure 12.6-1 shows two typical frequency spectra of fan noise radiated in forward direction by a single-stage fan running at subsonic and supersonic tip speeds. Supersonic tip speeds, normally, occur at high thrust settings, as used during takeoff.

The fan noise of Figure 12.6-1a is composed of discrete frequency noise and broadband noise. Apparently, the noise of a subsonic fan is dominated by discrete frequency noise or tone noise. This noise component occurs at the fan blade fundamental frequency and its higher harmonics and is heard as fan whine. The remainder of the spectrum is predominantly broadband in nature and

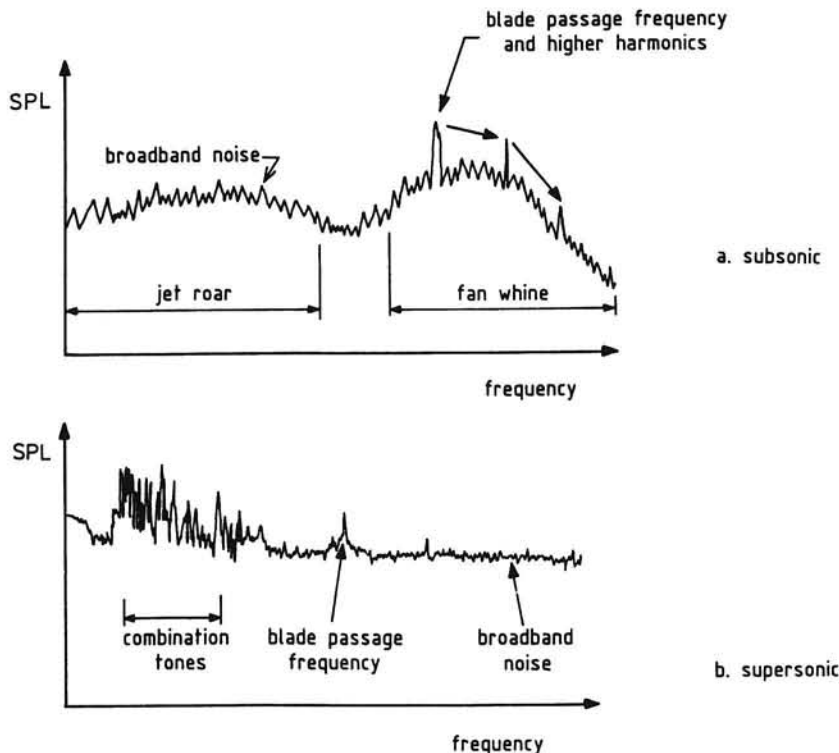


Figure 12.6-1. Typical narrow band fan spectra

extends over a wide range of frequencies.

In addition, the supersonic spectrum in Figure 12.6-1b shows closely spaced discrete frequencies at multiples of the frequency associated with the engine rpm. These tones are known as *multiple pure tones* or *combination tones*.

As this noise component has a sound characteristic very similar to that of a buzz-saw, it is often called *buzzsaw noise*.

The occurrence of combination tones in the noise spectrum of a supersonic fan is the result of shock waves generated by supersonic flow over the fan blades. The tone and broadband noise is attributable to small fluctuations in the pressure field around the rotor blades and stator vanes. These pressure fluctuations can be distinguished according to their periodic and nonperiodic nature, where the tone noise is caused by the periodics and the broadband noise arises from the nonperiodic pressure disturbances.

The latter pressure fluctuations are due to the random turbulence generated in the boundary layer over the surface of the inlet duct and the wakes shed by the fan blades. Broadband noise is also produced by irregular pressure fluctuations caused by initial turbulence in the airflow into the inlet.

The cyclic part of the pressure field is caused by the regular interaction of wakes from rotating blades with downstream stationary vanes.

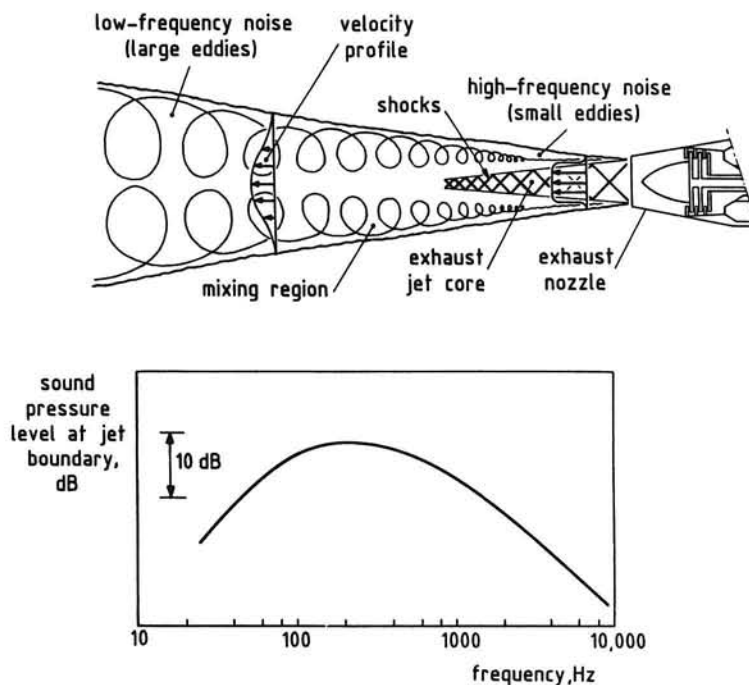


Figure 12.6-2. Generation of exhaust jet noise

As noted earlier, inlet guide vanes in older engine types were responsible for high levels of tone noise due to the interaction processes between their wakes with the downstream rotor.

In modern turbofan-engines without inlet guide vanes, the wake intensity is strongly dependent on the distance between rotor and stator rows. If the distance is too small then there are intense periodic pressure fluctuations resulting in high tone noise levels, which can be reduced by an increased spacing between blades and vanes.

Also by proper fan design and selection of blade and vane numbers, it is possible to produce a further decrease of level in the discrete frequency noise component (References 5 and 8).

The application of these advances in noise reduction technology to the high-bypass ratio turbofan has made this engine type to the obvious powerplant for modern commercial jet airplanes.

As mentioned already, exhaust jet noise is generated by the turbulent mixing of the high-velocity exhaust jet with the ambient air. The mixing process causes pressure fluctuations in the exhaust jet which travel as sound waves through the surrounding atmosphere.

In the vicinity of the nozzle exit the jet velocity is high, and little mixing occurs. There, only small eddies are created causing high frequency noise (Figure 12.6-2). Farther downstream of the nozzle exit the mixing action intensifies and the turbulence is of a coarser type. In this region, noise at lower frequencies is produced. Finally, large turbulent swirls are formed which convert a greater portion of the kinetic energy into low-frequency noise.

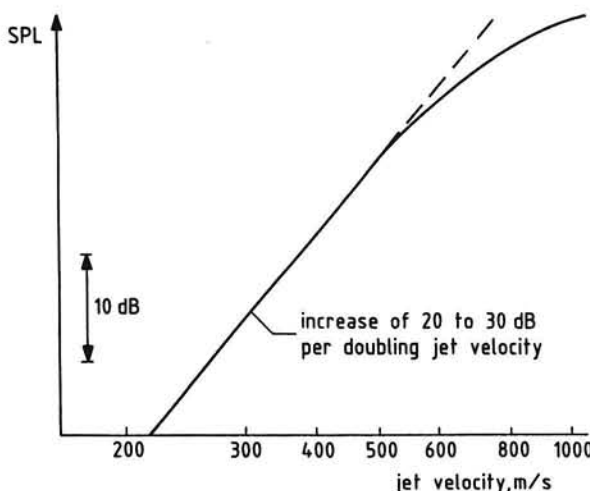


Figure 12.6-3. Sensitivity of exhaust jet noise to jet velocity

Therefore, as shown in the lower part of Figure 12.6-2, the jet exhaust noise is distributed through all frequencies within the audible range.

Additionally, when the jet velocity is supersonic relative to the local conditions, a regular shock pattern is formed within the exhaust jet core, giving an enlargement of the mixing noise.

Obviously, the intensity of the turbulence determines the noise generation by the exhaust jet, where the intensity decreases with decreasing jet velocity. The manner in which the exhaust jet noise level varies with jet velocity is illustrated in Figure 12.6-3. The decrease in sound pressure level when the velocity is halved is of the order of 20 to 30 dB. This is in agreement with the previous Equation (3.3-14). The graph also manifests that the underlying eight power law for the sound intensity as derived in Chapter 3 does not hold for high Mach number exhaust flow (Reference 6).

12.7 AIRFRAME NOISE

Airframe noise is defined as the far-field noise observed from an airplane when it travels through the atmosphere with the propulsion system inoperative. It is a form of aerodynamic noise, as this noise is generated by the turbulence in the airflow over the outer surface of the airplane.

The turbulent part of the boundary layer radiates sound directly, but especially causes substantial sound radiation upon passing by trailing edges, high-lift devices, landing gear wheel wells, and other airframe cavities and abrupt structural discontinuities. Also panel vibrations, caused by unsteady airflow on

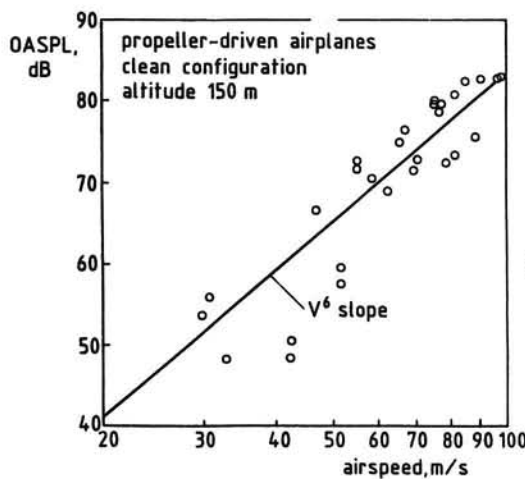


Figure 12.7-1. Airframe noise levels

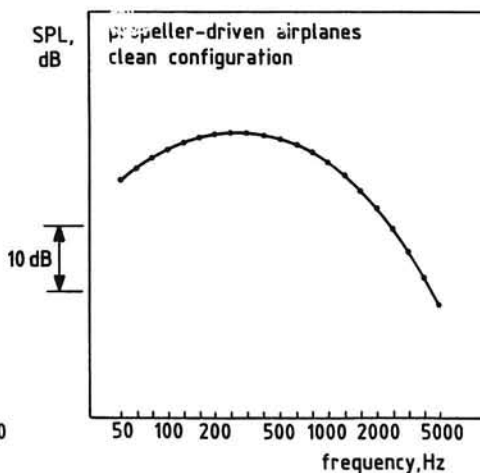


Figure 12.7-2. Frequency spectrum

the airplane structure, may be an important source of non-propulsive noise (References 68 and 69).

Airframe noise contributes the most to overall airplane noise levels during landing approaches, when landing gear and aerodynamic devices are deployed. Measurements have shown that during this phase of flight, where the power setting is relatively low, the noise produced by the airframe causes levels that are about 10 dB below the sound pressure levels produced by the airplane with power on. Therefore, it is an important source of noise that may impose a lower bound on the noise produced by the airplane, below which further engine noise reduction will not significantly lower the ground observed noise levels.

Available airframe noise data mainly are coming from systematic outdoor full scale flight experiments made on several airplane types during low-altitude flyovers with engines off or with engines rated at flight idle power setting.

In Figure 12.7-1 are plotted airframe noise levels as a function of airspeed for a glider and a number of small propeller-driven airplanes in the so-called *clean configuration* (Reference 70). The term configuration indicates the description of the external shape of the airplane when flying in a particular phase of flight. Clean configuration means an airplane condition with the landing gear and aerodynamic devices such as leading-edge slats, trailing-edge flaps, and spoilers retracted.

The data in Figure 12.7-1 concern peak airframe noise levels, which are normalized to an altitude of 150 m (500 ft) by accounting for spherical spreading and atmospheric absorption.

From the straight line in the figure, it can be seen that the measurements exhibit approximately a sixth power dependence on forward speed.

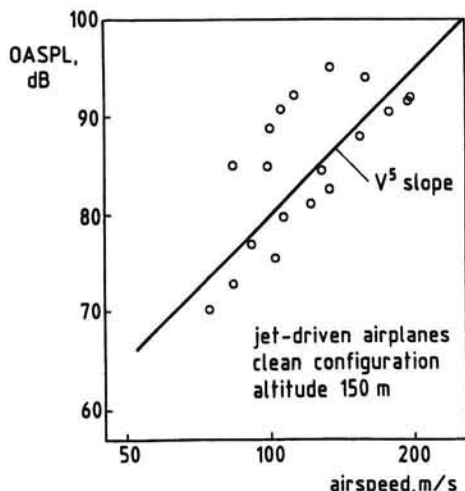


Figure 12.7-3. Airframe noise levels

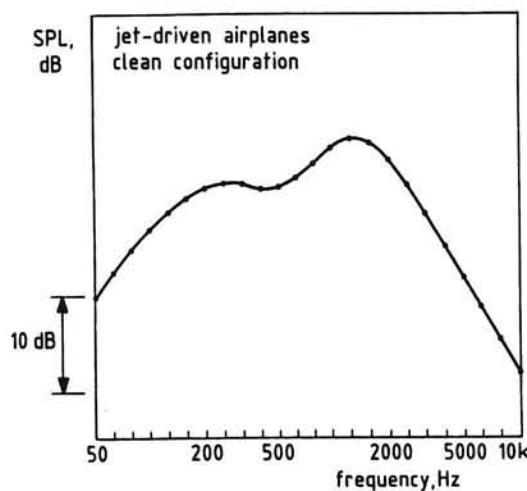


Figure 12.7-4. Frequency spectrum

A sketch of the typical shape of the tertsband spectrum obtained from frequency analysis of the above noise recordings is given in Figure 12.7-2. The graph indicates that the spectrum is broadband throughout the entire frequency range with a peak frequency at about 200 Hz.

Similar data of clean configuration airframe noise measured for four jet-driven airplanes are presented in Figure 12.7-3 (References 71 and 72). These data, which also are adjusted to a distance of 150 m, show that the velocity dependence is now the fifth power, being a lower value than that established for propeller-driven airplanes. It is of importance to note that the noise levels in the two Figures 12.7-1 and 12.7-3 cover a range of airplane masses from 590 kg (1300 lb) to 227,000 kg (500,000 lb). Figure 12.7-4 displays the typical shape of the one-third octave band spectra for these clean configured jet-driven airplanes. Note that the spectrum manifests two peaks, a lower one in the vicinity of 200 Hz and a higher one near 1250 Hz.

Measurements made on takeoff and landing configured jet-driven airplanes have made clear that the deployment of landing gear and aerodynamic devices causes additional noise generation by the flow around these components and over the associated cavities.

Figure 12.7-5 illustrates the influence on peak overall sound pressure levels of the landing gear and the complete *dirty configuration*, that is, the condition of the airplane with its aerodynamic devices and landing gear deployed.

In combination with theoretical methods, the complete airplane airframe noise data have been used to develop semi-empirical models for estimating

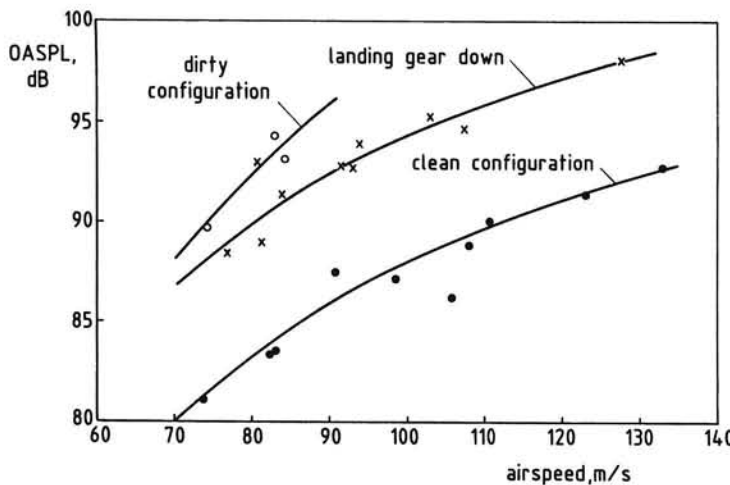


Figure 12.7-5. Effect of configuration on airframe noise levels at 150 m altitude

airframe noise produced by each airplane component individually (References 73 and 74).

Reference 69 reports that noise assessments made by using the component method of Reference 73 reveal that for an envisioned advanced technology transport on approach, the airframe noise in terms of EPNL is comparable to the largest contributor to the total airplane noise, the fan. This means that further reductions in fan noise result in airframe noise becoming the dominant source during approach to landing. Therefore, future airplane noise reduction activities should also include airframe noise reduction efforts.

12.8 NOISE INSIDE AIRCRAFT

Interior noise levels are of direct importance to passenger comfort, and influence crew fatigue, hearing impairment and flight safety.

Noise inside aircraft arises from such sources as propellers, exhausts from reciprocating engines, exhaust streams behind turbojet and turbofan engines, and turbulent airflow over the outer surface of the aircraft. Noise from internal sources, such as air-conditioning systems, may also contribute to the interior noise levels.

It is important to note that most turbofan and turbojet transports have sufficient attenuating structure to cut interior noise significantly. Also, many of these airplanes have rear fuselage-mounted engines, providing further reductions of cockpit noise. Consequently, the noise entering the fuselage interior often is mainly due to the turbulent boundary layer. Cabin windows, especially, can generate considerable boundary layer noise. This contribution can be effectively reduced by application of double windows. Therefore jet-powered airplanes, producing more external noise, are less of a problem from a noise standpoint than propeller-driven aircraft.

Moreover, investigations on passenger response to interior noise have shown that the pure-tone characteristics of propellers are more annoying than the broadband noise from jet-propulsion devices when the A-weighted noise levels are the same. For that reason, the study of interior noise control is of special significance for propeller-driven aircraft.

The present interest is directed to both general aviation airplanes and future large high-subsonic transports powered by propfans.

Noise emitted by the various external sources is transmitted to the interior of the fuselage along airborne paths and structureborne paths. The term *airborne* is applied to those paths in which sound energy is incident on the fuselage shell, with subsequent transmission through the fuselage sidewalls into

the cockpit and passenger cabin. Transmission of engine vibration through the engine mounts with subsequent acoustic radiation into the interior of the fuselage is an example of a *structureborne* path.

Obviously, the ability to predict and identify noise transmission paths is essential in order that appropriate treatments for noise reduction can be effected for the least added weight.

An extensive review of research related to propeller-driven airplane interior noise control is given in Reference 75. It appears that the most dominant source for interior noise is the noise transmitted from the propeller blades along the direct airborne path to the fuselage.

An important measure of reducing the noise inside a multi-engined airplane is the use of a *synchrophaser*, which is the name of the system that controls propeller rpm's and prevents angular drift of the propeller blade positions relative to a reference propeller. This control unit improves the acoustic environment inside the airplane by eliminating the *beats*, i.e., the periodic variations in cabin noise level that result from the superposition of pure tones of different frequencies due to operation of the propellers at slightly different rotational speeds (Reference 76).

To explain this phenomenon we consider two simple-harmonic waves, which are observed simultaneously.

We assume, for simplicity, that at the observation point the waves have the same amplitude and phase, but only nearly the same frequency.

Then the sound pressure at the given point can be expressed as

$$p'(t) = A [\cos 2\pi ft + \cos [2\pi(f + \Delta f)t]] , \quad (12.8-1)$$

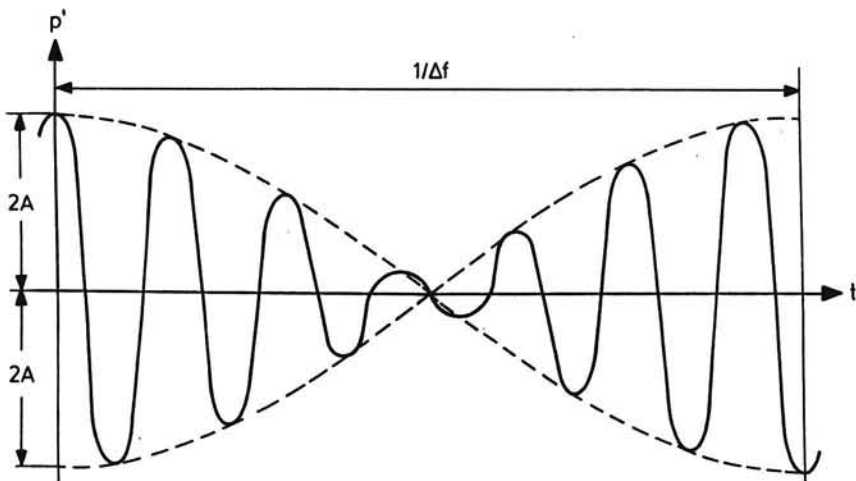


Figure 12.8-1. Beat representation

where A is the amplitude and Δf the frequency difference which is small compared with f .

Using the trigonometric relationship $\cos x \cos y = 2 \cos [0.5(x+y)] \cos [0.5(x-y)]$, we find the sound pressure given by

$$p'(t) = 2A \cos[2\pi(f + \frac{\Delta f}{2})t] \cos[2\pi \frac{\Delta f}{2}t]. \quad (12.8-2)$$

Equation (12.8-2) represents a periodic pressure variation of frequency $(f + \Delta f/2)$ having a time-varying amplitude $2A \cos[2\pi \Delta f/2 t]$ (Figure 12.8-1).

Thus the two sounds are heard as having the same frequency. However, the amplitude of the sound varies with a frequency which is equal to the difference between the two original frequencies. These fluctuations in amplitude are the cause of the beats as mentioned above.

Clearly, tuning of the propellers, i.e., adjusting their rpm's to equal values, is required for obtaining equal thrust per engine and avoiding the extra annoyance due to the periodic increase and decrease of the amplitude at the beat frequency. The use of synchrophasing in combination with *blade-matching* also may reduce structural vibration significantly. The term *blade-matching* indicates that the blades of the propellers are positioned in a fixed and optimum order relative to each other, through which the propeller blade noise signals strike the fuselage in a predetermined sequence.

Tertband sound pressure levels measured at two powersettings in the cockpit of a DHC-2 "Beaver" airplane are presented in Figure 12.8-2 (Reference 77). The Beaver is a single-engined airplane driven by a nine-cylinder radial air-

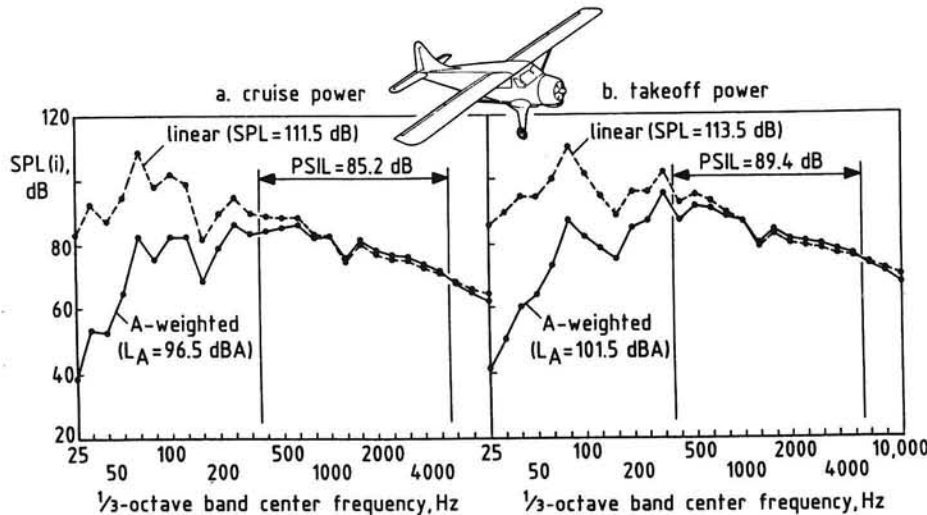


Figure 12.8-2. Cockpit noise levels in flight

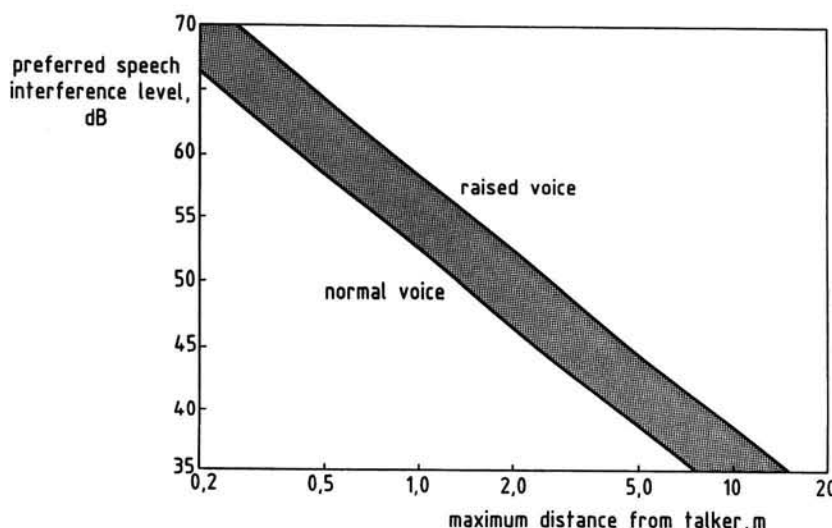


Figure 12.8-3. Ambient noise level limits for acceptable speech communication
cooled piston engine with two-bladed constant-speed propeller. The loaded mass
of the airplane is 22700 lb.

The recordings were made at ear height between the pilot's and copilot's positions. The spectra in Figure 12.8-2 show that the noise signals are characterized by peaks at the harmonics of engine exhaust and propeller fundamentals. When the spectra are A-weighted, the lower harmonics are considerably reduced but still control the resulting A-weighted noise level.

For hearing conservation purposes, according to the procedure described previously in Section 9.9, the A-weighted noise level (AL) in combination with the exposure time yields the noise dose and so the composite noise exposure index (CNEI).

In addition to AL, the *preferred speech interference level* (PSIL) is employed to assess the speech intelligibility. PSIL is obtained by averaging measured 1/1-octave band levels centered at 500, 1000, 2000, and 4000 Hz. The frequencies in this range are most likely to interfere with speech communication. This implies, as depicted in Figure 12.8-2, that higher harmonics of the propulsion noise are the most relevant in establishing the PSIL.

For guidance on intelligibility of speech, we may use Figure 12.8-3, where are plotted acceptable PSIL values as a function of distance between speaker and receiver (Reference 3). We see, for example, that at a distance of 0.5 m maximum preferred speech interference levels up to 64 dB are tolerable in order that face-to-face conversion remains possible.

REFERENCES

1. A. Wilson, *Noise - Final Report Committee on the Problem of Noise*, Comnd. 2056, Her Majesty's Stationery Office (HMSO), London, 1963.
2. E.G. Richardson, *Sound*, a physical text-book, Edward Arnold, London, 1961.
3. J.R. Hassall and K. Zaveri, *Acoustic Noise Measurements*, Brüel & Kjær, 1979.
4. G. Porges, *Applied Acoustics*, Edward Arnold, London, 1977.
5. M.J.T. Smith, *Aircraft Noise*, Cambridge University Press, Cambridge, 1989.
6. A.P. Dowling and J.E. Ffowcs Williams, *Sound and Sources of Sound*, Ellis Harwood Limited, Chichester, 1983.
7. G.J.J. Ruijgrok, *Elements of Airplane Performance*, Delft University Press, 1990.
8. E.J. Richards and D.J. Mead, *Noise and Acoustic Fatigue in Aeronautics*, John Wiley, London, 1968.
9. A.M. Kuethe and J.D. Schetzer, *Foundations of Aerodynamics*, John Wiley, London, 1959.
10. P.M. Morse and K.U. Ingard, *Theoretical Acoustics*, McGraw-Hill, New York, 1968.
11. M.J. Lighthill, *On Sound Generated Aerodynamically, I - General Theory*, Proc. Roy. Soc. London, Ser. A, Vol. 211, No. 1107, March 20, 1952.
12. C.M. Harris (editor), *Handbook of Acoustical Measurements and Noise Control*, McGraw-Hill, New York, 1991.
13. O.V. Rudenko and S.I. Soluyan, *Theoretical Foundations of Nonlinear Acoustics*, (translated from Russian by R.T. Beyer), Consultants Bureau, New York, 1977.
14. C.L. Morfey and G.P. Howell, *Nonlinear Propagation of Aircraft Noise in the Atmosphere*, American Institute of Aeronautics and Astronautics (AIAA), Paper 80-1041, 1980.
15. M.E. Goldstein, *Aeroacoustics*, McGraw-Hill, New York, 1976.
16. M.R. Spiegel, *Advanced Mathematics for Engineers and Scientists*, McGraw-Hill, New York, 1971.
17. Anon., *Standard Values of Atmospheric Absorption as a Function of Temperature and Humidity for Use in Evaluating Aircraft Flyover Noise*, Society of Automotive Engineers (SAE), ARP 866, 1964.
18. Anon., *International Standards and Recommended Practices, Environmental Protection*, Annex 16 to the Convention on International Civil Aviation, Volume I, *Aircraft Noise*, Appendix I, Section 8, Second

- Edition, International Civil Aviation Organization (ICAO), Montreal, 1988.
19. F.M. Wiener and D.N. Keast, *Experimental Study of the Propagation of Sound over Ground*, Journal of the Acoustical Society of America, Vol. 31, No. 6, 1959.
20. T.F.W. Embleton, G.J. Thiessen and J.E. Piercy, *Propagation in an Inversion and Reflections at the Ground*, Journal of the Acoustical Society of America, Vol. 59, No. 2, 1976.
21. P.J. Dickinson, *Temperature Inversion Effects on Aircraft Noise Propagation*, Journal of Sound and Vibration (47), 1976.
22. A.R. Kriebel, *Refraction and Attenuation of Sound by Wind and Thermal Profiles over a Ground Plane*, Journal of the Acoustical Society of America, Vol. 51, No. 1, 1972.
23. C.I. Chessel, *Meteorological and Ground Effects on the Propagation of Aircraft Noise close to the Earth's Surface*, Journal of Sound and Vibration (60), 1978.
24. F.W. Cole, *Introduction to Meteorology*, John Wiley, New York, 1980.
25. S. Gade, *Sound Intensity (Theory, Instrumentation and Applications)*, Brüel & Kjær Technical Reviews, Nos. 3 and 4, 1982.
26. D.D. Davis, G.M. Stokes, D. Moore and G.L. Stevens, *Theoretical and Experimental Investigation of Mufflers with Comments on Engine-Exhaust Muffler Design*, United States (U.S.) National Advisory Committee for Aeronautics (NACA), Report 1192, 1954.
27. R.B. Randall, *Application of B&K Equipment to Frequency Analysis*, Brüel & Kjær, 1977.
28. Anon., *Preferred Frequencies for Acoustical Measurements*, International Organization for Standardization (ISO), Recommendation R 266, 1962.
29. Anon., *International Standards and Recommended Practices Environmental Protection*; Annex 16 to the Convention on International Civil Aviation, Volume I, *Aircraft Noise*, Second Edition, ICAO, Montreal, 1988.
30. H. Heller, *Aircraft Exterior Noise Measurement and Analysis Techniques*, North Atlantic Treaty Organization (NATO), Advisory Group for Aerospace Research and Development (AGARD), AGARD-AG-300, Vol. 9, 1991.
31. F.W.J. van Deventer and G.J.J. Ruijgrok, *External Noise of Light Propeller-driven Aircraft*, International Council of the Aeronautical Sciences (ICAS), Paper No. 76-48, 1976.
32. D.W. Andrews and D.W. Durenberger, *Description of Noise Measurement and Analysis Procedures Developed for Light General Aviation Aircraft*, Delft University of Technology, Faculty of Aerospace

- Engineering, Report LR-246, 1977.
33. W.L. Howes, *Ground Reflection of Jet Noise*, U.S. National Aeronautics and Space Administration (NASA), Technical Report R-35, 1959.
34. R. Hoch and P. Thomas, *The Influence of Reflection on the Sound-Pressure Spectra of Jets*, NASA, TTF-12, 246, 1969.
35. T.F.W. Embleton, J.E. Piercy and N. Olsen, *Outdoor Sound Propagation over Ground of Finite Impedance*, Journal of the Acoustical Society of America, Vol. 59, No. 2, 1976.
36. P.J. Dickinson and P.E. Doak, *Measurements of the Normal Acoustic Impedance of Ground Surfaces*, Journal of Sound and Vibration (13), 1970.
37. C.I. Chessell, *Propagation of Noise Along a Finite Impedance Boundary*, Journal of the Acoustical Society of America, Vol. 62, No. 4, 1977.
38. M.E. Delany and E.N. Bazley, *Acoustical Properties of Fibrous Absorbent Materials*, Applied Acoustics (3), 1970.
39. K. Attenborough, *Predicted Ground Effect for Highway Noise*, Journal of Sound and Vibration, 81(3), 1982.
40. C.A. Yoerke and R. Larson, *Prediction of Free-Field Noise Levels from Pole Microphone Measurements*, AIAA, Paper 80-1058, 1980.
41. W.L. Willshire, Jr., *Assessment of Ground Effects on the Propagation of Aircraft Noise*, The T-38 Flight Experiment, NASA, TP-1747, 1980.
42. S.P. Pao, A.R. Wenzel and P.B. Oncley, *Prediction of Ground Effects on Aircraft Noise*, NASA, TP-1104, 1978.
43. W.L. Willshire, Jr. and P.A. Nystrom, *Investigation of Effects of Microphone Position and Orientation on Near-Ground Noise Measurements*, NASA, TP-2004, 1982.
44. Anon., *Ground-Plane Microphone Configuration for Propeller-Driven Light-Aircraft Noise Measurement*, SAE, ARP 4055, 1988.
45. W.L. Willshire, Jr., *Lateral Attenuation of High-By-Pass Ratio Engined Aircraft Noise*, NASA, TM-81968, 1981.
46. Anon., *Normal Equal-Loudness Contours for Pure Tones and Normal Threshold of Hearing Under Free Field Listening Conditions*, ISO, Recommendation R 226, 1961.
47. K.D. Kryter, *Possible Modifications to Procedures for the Calculation of Perceived Noisiness*, NASA, CR-1635, 1969.
48. G. Hellström, *Noise Shielding Aircraft Configurations. A Comparison between Predicted and Experimental Results*, ICAS, Paper No. 76-58, 1976.
49. Anon., *Prediction Method for Lateral Attenuation of Airplane Noise During Takeoff and Landing*, SAE, AIR 1751, 1980.
50. G.J.J. Ruijgrok, *Lateral Attenuation of Aircraft Noise*, Journal of Aircraft,

- Vol. 20, No. 11, November 1983.
51. SAE A-21 Committee on Aircraft Noise, *Procedure for the Calculation of Airplane Noise in the Vicinity of Airports*, SAE, AIR 1845, 1986.
52. K.S. Persons and R.L. Bennett, *Handbook of Noise Ratings*, NASA, CR-2376, 1974.
53. F.W.J. van Deventer, *Propeller Aircraft Noise Around General Aviation Airports*, SAE, Paper 790594, 1979.
54. B. Griefahn, *Präventivmedizinische Vorschläge für den nächtlichen Schallschutz*, Zeitschrift für Lärmbekämpfung, 37, 1990.
55. B.L. Amstadter, *Reliability Mathematics*, McGraw-Hill, New York, 1971.
56. A.H.-S. Ang and W.H. Tang, *Probability Concepts in Engineering Planning and Design*, Vol. I - Basic Principles, John Wiley, New York, 1975.
57. D.G. Crighton, J.E. Ffowcs Williams and I.C. Cheeseman, *The Outlook for Simulation of Forward Flight Effects on Aircraft Noise*, AIAA, Paper 76-530, 1976.
58. H.W. Liepmann and A. Roshko, *Elements of Gasdynamics*, John Wiley, New York, 1957.
59. K.P. Shepherd and B.M. Sullivan, *A Loudness Calculation Procedure Applied to Shaped Sonic Booms*, NASA, TP-3134, 1991.
60. D.J. Maglieri and H.H. Hubbard, *Factors Affecting the Noise from Small Propeller-Driven Aircraft*, SAE, Paper 750516, 1975.
61. D.B. Thurston, *Design for Flying*, McGraw-Hill, New York, 1978.
62. F.B. Metzger and B. Magliozi, *New Directions in Aircraft Propulsor Noise Research*, SAE, Paper 750515, 1975.
63. Anon., *Prediction Procedure for Near Field and Far Field Propeller Noise*, SAE, AIR 1407, 1977.
64. G. Dübener, *Fluglärmbekämpfung bei Propeller-Flugzeugen*, Aero-Revue 12, 1973.
65. S.K. Rathgeber, *The Development of a Flyover Noise Prediction Technique Using Multiple Linear Regression Analysis*, SAE, Paper 810588, 1981.
66. M.H. Smith, *A Prediction Procedure for Propeller Aircraft Flyover Noise Based on Empirical Data*, SAE, Paper 810604, 1981.
67. D.F. Wilford and H. Bonneau, *Flyover Noise Measurements for Turbo-Prop Aircraft*, AIAA, Paper 83-0746, 1983.
68. J.C. Hardin, *Airframe Self-Noise - Four Years of Research*, NATO, AGARD Lecture Series 80 on Aerodynamic Noise, 1977.
69. W.L. Willshire, Jr. and M.B. Tracy, *Non-Propulsive Aerodynamic Noise*, NATO, AGARD Conference Preprint 512, 1991.
70. G.J. Healy, *Measurements and Analysis of Aircraft Far-Field Aerody-*

- namic Noise*, NASA, CR-2377, 1974.
- 71. T.W. Putnam and P.L. Lasagna, *Measurements and Analysis of Aircraft Airframe Noise*, AIAA, Paper 75-510, 1975.
 - 72. P. Fethney, *An Experimental Study of Airframe Self-Noise*, AIAA, Paper 75-511, 1975.
 - 73. M.R. Fink, *Airframe Noise Prediction Method*, U.S. Federal Aviation Administration (FAA), RD-77-29, (AD-A039 664), 1977.
 - 74. J.D. Revell, *Induced Drag Effect on Airframe Noise*, AIAA, Paper 75-487, 1975.
 - 75. J.S. Mixson and C.A. Powell, *Review of Recent Research on Interior Noise of Propeller Aircraft*, Journal of Aircraft, Vol. 22, No. 11, 1985.
 - 76. F.B. Metzger, *Strategies for Aircraft Interior Noise Reduction in Existing and Future Propeller Aircraft*, SAE, Paper 810560, 1981.
 - 77. D.M. van Paassen, *Noise Inside a DHC-2 "Beaver" Airplane*, Delft University of Technology, Faculty of Aerospace Engineering, Memorandum M-493, 1983 (in Dutch).
 - 78. Anon., *Engineering Sciences Data; Data Sheets; Noise Sub-series*, Vol. 1-5, Engineering Sciences Data Unit (ESDU) International Ltd, London.

APPENDIX A

NOY VALUES

SPL, dB	one-third octave band center frequency, Hz											
	50	63	80	100	125	160	200	250	315	400	500	630
29												
30												
31												
32												
33												
34												
35												
36												
37												
38												
39												
40										1.00	1.00	1.00
41										1.07	1.07	1.07
42										1.15	1.15	1.15
43										1.23	1.23	1.23
44										1.32	1.32	1.32
45								1.08	1.24	1.41	1.41	1.41
46								1.00	1.16	1.52	1.52	1.52
47								1.08	1.25	1.62	1.62	1.62
48								1.00	1.34	1.74	1.74	1.74
49								1.08	1.45	1.87	1.87	1.87
50							1.17	1.36	1.56	1.76	2.00	2.00
51							1.00	1.26	1.47	1.68	2.14	2.14
52							1.08	1.36	1.58	1.80	2.30	2.30
53							1.00	1.18	1.47	1.71	2.46	2.46
54							1.09	1.28	1.58	1.85	2.64	2.64
55						1.18	1.38	1.71	2.00	2.25	2.50	2.83
56						1.00	1.29	1.50	1.85	2.15	2.42	3.03
57						1.09	1.40	1.63	2.00	2.33	2.61	3.25
58						1.18	1.53	1.77	2.15	2.51	2.81	3.48
59						1.29	1.66	1.92	2.33	2.71	3.03	3.73
60			1.00	1.40	1.81	2.08	2.51	2.93	3.26	3.57	4.00	4.00
61			1.10	1.53	1.97	2.26	2.71	3.16	3.51	3.83	4.29	4.29
62			1.21	1.66	2.15	2.45	2.93	3.41	3.78	4.11	4.59	4.59
63			1.32	1.81	2.34	2.65	3.16	3.69	4.06	4.41	4.92	4.92
64		1.00	1.45	1.97	2.54	2.88	3.41	3.98	4.38	4.73	5.28	5.28
65	1.11	1.60	2.15	2.77	3.12	3.69	4.30	4.71	5.08	5.66	5.66	5.66
66	1.22	1.75	2.34	3.01	3.39	3.98	4.64	5.07	5.45	6.06	6.06	6.06
67	1.35	1.92	2.54	3.28	3.68	4.30	5.01	5.46	5.85	6.50	6.50	6.50
68	1.49	2.11	2.77	3.57	3.99	4.64	5.41	5.88	6.27	6.96	6.96	6.96
69	1.65	2.32	3.01	3.88	4.33	5.01	5.84	6.33	6.73	7.46	7.46	7.46

SPL, dB	one-third octave band center frequency, Hz											
	800	1000	1250	1600	2000	2500	3150	4000	5000	6300	8000	10000
29							1.00	1.00				
30						1.00	1.07	1.07	1.00			
31					1.00	1.07	1.15	1.15	1.07	1.00		
32					1.07	1.15	1.23	1.23	1.15	1.07		
33				1.00	1.07	1.23	1.32	1.32	1.23	1.15		
34				1.00	1.15	1.32	1.41	1.41	1.32	1.23		
35			1.07	1.23	1.41	1.51	1.51	1.41	1.32			
36			1.15	1.32	1.51	1.62	1.62	1.51	1.41			
37			1.23	1.41	1.62	1.74	1.74	1.62	1.51	1.00		
38		1.00	1.32	1.51	1.74	1.86	1.86	1.74	1.62	1.10		
39		1.07	1.41	1.62	1.86	1.99	1.99	1.86	1.74	1.21		
40	1.00	1.00	1.15	1.51	1.74	1.99	2.14	2.14	1.99	1.86	1.34	
41	1.07	1.07	1.23	1.62	1.86	2.14	2.29	2.29	2.14	1.99	1.48	1.00
42	1.15	1.15	1.32	1.74	1.99	2.29	2.45	2.45	2.29	2.14	1.63	1.10
43	1.23	1.23	1.41	1.86	2.14	2.45	2.63	2.63	2.45	2.29	1.79	1.21
44	1.32	1.32	1.52	1.99	2.29	2.63	2.81	2.81	2.63	2.45	1.99	1.34
45	1.41	1.41	1.62	2.14	2.45	2.81	3.02	3.02	2.81	2.63	2.14	1.48
46	1.52	1.52	1.74	2.29	2.63	3.02	3.23	3.23	3.02	2.81	2.29	1.63
47	1.62	1.62	1.87	2.45	2.81	3.23	3.46	3.46	3.23	3.02	2.45	1.79
48	1.74	1.74	2.00	2.63	3.02	3.46	3.71	3.71	3.46	3.23	2.63	1.98
49	1.87	1.87	2.14	2.81	3.23	3.71	3.97	3.97	3.71	3.46	2.81	2.15
50	2.00	2.00	2.30	3.02	3.46	3.97	4.26	4.26	3.97	3.71	3.02	2.40
51	2.14	2.14	2.46	3.23	3.71	4.26	4.56	4.56	4.26	3.97	3.23	2.63
52	2.30	2.30	2.64	3.46	3.97	4.56	4.89	4.89	4.56	4.26	3.46	2.81
53	2.46	2.46	2.83	3.71	4.26	4.89	5.24	5.24	4.89	4.56	3.71	3.02
54	2.64	2.64	3.03	3.97	4.56	5.24	5.61	5.61	5.24	4.89	3.97	3.23
55	2.83	2.83	3.25	4.26	4.89	5.61	6.01	6.01	5.61	5.24	4.26	3.46
56	3.03	3.03	3.48	4.56	5.24	6.01	6.44	6.44	6.01	5.61	4.56	3.71
57	3.25	3.25	3.73	4.89	5.61	6.44	6.90	6.90	6.44	6.01	4.89	3.97
58	3.48	3.48	4.00	5.24	6.01	6.90	7.39	7.39	6.90	6.44	5.24	4.26
59	3.73	3.73	4.29	5.61	6.44	7.39	7.92	7.92	7.39	6.90	5.61	4.56
60	4.00	4.00	4.59	6.01	6.90	7.92	8.49	8.49	7.92	7.39	6.01	4.89
61	4.29	4.29	4.92	6.44	7.39	8.49	9.09	9.09	8.49	7.92	6.44	5.24
62	4.59	4.59	5.28	6.90	7.92	9.09	9.74	9.74	9.09	8.49	6.90	5.61
63	4.92	4.92	5.66	7.39	8.49	9.74	10.4	10.4	9.74	9.09	7.39	6.01
64	5.28	5.28	6.06	7.92	9.09	10.4	11.2	11.2	10.4	9.74	7.92	6.44
65	5.66	5.66	6.50	8.49	9.74	11.2	12.0	12.0	11.2	10.4	8.49	6.90
66	6.06	6.06	6.96	9.09	10.4	12.0	12.8	12.8	12.0	11.2	9.09	7.39
67	6.50	6.50	7.46	9.74	11.2	12.8	13.8	13.8	12.8	12.0	9.74	7.92
68	6.96	6.96	8.00	10.4	12.0	13.8	14.7	14.7	13.8	12.8	10.4	8.49
69	7.46	7.46	8.57	11.2	12.8	14.7	15.8	15.8	14.7	13.8	11.2	9.09

SPL, dB	one-third octave band center frequency, Hz											
	50	63	80	100	125	160	200	250	315	400	500	630
70	1.82	2.55	3.28	4.23	4.69	5.41	6.31	6.81	7.23	8.00	8.00	8.00
71	2.02	2.79	3.57	4.60	5.09	5.84	6.81	7.33	7.75	8.57	8.57	8.57
72	2.23	3.07	3.88	5.01	5.52	6.31	7.36	7.90	8.32	9.19	9.19	9.19
73	2.46	3.37	4.23	5.45	5.99	6.81	7.94	8.50	8.93	9.85	9.85	9.85
74	2.72	3.70	4.66	5.94	6.50	7.36	8.57	9.15	9.59	10.6	10.6	10.6
75	3.01	4.06	5.01	6.46	7.05	7.94	9.19	9.85	10.3	11.3	11.3	11.3
76	3.32	4.46	5.45	7.03	7.65	8.57	9.85	10.6	11.0	12.1	12.1	12.1
77	3.67	4.89	5.94	7.66	8.29	9.19	10.6	11.3	11.8	13.0	13.0	13.0
78	4.06	5.37	6.46	8.33	9.00	9.85	11.3	12.1	12.7	13.9	13.9	13.9
79	4.49	5.90	7.03	9.07	9.76	10.6	12.1	13.0	13.6	14.9	14.9	14.9
80	4.96	6.48	7.66	9.85	10.6	11.3	13.0	13.9	14.6	16.0	16.0	16.0
81	5.48	7.11	8.33	10.6	11.3	12.1	13.9	14.9	15.7	17.1	17.1	17.1
82	6.06	7.81	9.07	11.3	12.1	13.0	14.9	16.0	16.9	18.4	18.4	18.4
83	6.70	8.57	9.87	12.1	13.0	13.9	16.0	17.1	18.1	19.7	19.7	19.7
84	7.41	9.41	10.7	13.0	13.9	14.9	17.1	18.4	19.4	21.1	21.1	21.1
85	8.19	10.3	11.7	13.9	14.9	16.0	18.4	19.7	20.8	22.6	22.6	22.6
86	9.05	11.3	12.7	14.9	16.0	17.1	19.7	21.1	22.4	24.3	24.3	24.3
87	10.0	12.1	13.9	16.0	17.1	18.4	21.1	22.6	24.0	26.0	26.0	26.0
88	11.1	13.0	14.9	17.1	18.4	19.7	22.6	24.3	25.8	27.9	27.9	27.9
89	12.2	13.9	16.0	18.4	19.7	21.1	24.3	26.0	27.7	29.9	29.9	29.9
90	13.5	14.9	17.1	19.7	21.1	22.6	26.0	27.9	29.7	32.0	32.0	32.0
91	14.9	16.0	18.4	21.1	22.6	24.3	27.9	29.9	31.8	34.3	34.3	34.3
92	16.0	17.1	19.7	22.6	24.3	26.0	29.9	32.0	34.2	36.8	36.8	36.8
93	17.1	18.4	21.1	24.3	26.0	27.9	32.0	34.3	36.7	39.4	39.4	39.4
94	18.4	19.7	22.6	26.0	27.9	29.9	34.3	36.8	39.4	42.2	42.2	42.2
95	19.7	21.1	24.3	27.9	29.9	32.0	36.8	39.4	42.2	45.3	45.3	45.3
96	21.1	22.6	26.0	29.9	32.0	34.3	39.4	42.2	45.3	48.5	48.5	48.5
97	22.6	24.3	27.9	32.0	34.3	36.8	42.2	45.3	48.5	52.0	52.0	52.0
98	24.3	26.0	29.9	34.3	36.8	39.4	45.3	48.5	52.0	55.7	55.7	55.7
99	26.0	27.9	32.0	36.8	39.4	42.2	48.5	52.0	55.7	59.7	59.7	59.7
100	27.9	29.9	34.3	39.4	42.2	45.3	52.0	55.7	59.7	64.0	64.0	64.0
101	29.9	32.0	36.8	42.2	45.3	48.5	55.7	59.7	64.0	68.6	68.6	68.6
102	32.0	34.3	39.4	45.3	48.5	52.0	59.7	64.0	68.6	73.5	73.5	73.5
103	34.3	36.8	42.2	48.5	52.0	55.7	64.0	68.6	73.5	78.8	78.8	78.8
104	36.8	39.4	45.3	52.0	55.7	59.7	68.6	73.5	78.8	84.4	84.4	84.4
105	39.4	42.2	48.5	55.7	59.7	64.0	73.5	78.8	84.4	90.5	90.5	90.5
106	42.2	45.3	52.0	59.7	64.0	68.6	78.8	84.4	90.5	97.0	97.0	97.0
107	45.3	48.5	55.7	64.0	68.6	73.5	84.4	90.5	97.0	104	104	104
108	48.5	52.0	59.7	68.6	73.5	78.8	90.5	97.0	104	111	111	111
109	52.0	55.7	64.0	73.5	78.8	84.4	97.0	104	111	119	119	119

SPL, dB	one-third octave band center frequency, Hz											
	800	1000	1250	1600	2000	2500	3150	4000	5000	6300	8000	10000
70	8.00	8.00	9.19	12.0	13.8	15.8	16.9	16.9	15.8	14.7	12.0	9.74
71	8.57	8.57	9.85	12.8	14.7	16.9	18.1	18.1	16.9	15.8	12.8	10.4
72	9.19	9.19	10.6	13.8	15.8	18.1	19.4	19.4	18.1	16.9	13.8	11.2
73	9.85	9.85	11.3	14.7	16.9	19.4	20.8	20.8	19.4	18.1	14.7	12.0
74	10.6	10.6	12.1	15.8	18.1	20.8	22.3	22.3	20.8	19.4	15.8	12.8
75	11.3	11.3	13.0	16.9	19.4	22.3	23.9	23.9	22.3	20.8	16.9	13.8
76	12.1	12.1	13.9	18.1	20.8	23.9	25.6	25.6	23.9	22.3	18.1	14.7
77	13.0	13.0	14.9	19.4	22.3	25.6	27.4	27.4	25.6	23.9	19.4	15.8
78	13.9	13.9	16.0	20.8	23.9	27.4	29.4	29.4	27.4	25.6	20.8	16.9
79	14.9	14.9	17.1	22.3	25.6	29.4	31.5	31.5	29.4	27.4	22.3	18.1
80	16.0	16.0	18.4	23.9	27.4	31.5	33.7	33.7	31.5	29.4	23.9	19.4
81	17.1	17.1	19.7	25.6	29.4	33.7	36.1	36.1	33.7	31.5	25.6	20.8
82	18.4	18.4	21.1	27.4	31.5	36.1	38.7	38.7	36.1	33.7	27.4	22.3
83	19.7	19.7	22.6	29.4	33.7	38.7	41.5	41.5	38.7	36.1	29.4	23.9
84	21.1	21.1	24.3	31.5	36.1	41.5	44.4	44.4	41.5	38.7	31.5	25.6
85	22.6	22.6	26.0	33.7	38.7	44.4	47.6	47.6	44.4	41.5	33.7	27.4
86	24.3	24.3	27.9	36.1	41.5	47.6	51.0	51.0	47.6	44.4	36.1	29.4
87	26.0	26.0	29.9	38.7	44.4	51.0	54.7	54.7	51.0	47.6	38.7	31.5
88	27.9	27.9	32.0	41.5	47.6	54.7	58.6	58.6	54.7	51.0	41.5	33.7
89	29.9	29.9	34.3	44.4	51.0	58.6	62.7	62.7	58.6	54.7	44.4	36.1
90	32.0	32.0	36.8	47.6	54.7	62.7	67.2	67.2	62.7	58.6	47.6	38.7
91	34.3	34.3	39.4	51.0	58.6	67.2	72.0	72.0	67.2	62.7	51.0	41.5
92	36.8	36.8	42.2	54.7	62.7	72.0	77.2	77.2	72.0	67.2	54.7	44.4
93	39.4	39.4	45.3	58.6	67.2	77.2	82.7	82.7	77.2	72.0	58.6	47.6
94	42.2	42.2	48.5	62.7	72.0	82.7	88.6	88.6	82.7	77.2	62.7	51.0
95	45.3	45.3	52.0	67.2	77.2	88.6	94.9	94.9	88.6	82.7	67.2	54.7
96	48.5	48.5	55.7	72.0	82.7	94.9	102	102	94.9	88.6	72.0	58.6
97	52.0	52.0	59.7	77.2	88.6	102	109	109	102	94.9	77.2	62.7
98	55.7	55.7	64.0	82.7	94.9	109	117	117	109	102	82.7	67.2
99	59.7	59.7	68.6	88.6	102	117	125	125	117	109	88.6	72.0
100	64.0	64.0	73.5	94.9	109	125	134	134	125	117	94.9	77.2
101	68.6	68.6	78.8	102	117	134	144	144	134	125	102	82.7
102	73.5	73.5	84.4	109	125	144	154	154	144	134	109	88.6
103	78.8	78.8	90.5	117	134	154	165	165	154	144	117	94.9
104	84.4	84.4	97.0	125	144	165	177	177	165	154	125	102
105	90.5	90.5	104	134	154	177	189	189	177	165	134	109
106	97.0	97.0	111	144	165	189	203	203	189	177	144	117
107	104	104	119	154	177	203	217	217	203	189	154	125
108	111	111	128	165	189	217	233	233	217	203	165	134
109	119	119	137	177	203	233	249	249	233	217	177	144

SPL, dB	one-third octave band center frequency, Hz											
	50	63	80	100	125	160	200	250	315	400	500	630
110	55.7	59.7	68.6	78.8	84.4	90.5	104	111	119	128	128	128
111	59.7	64.0	73.5	84.4	90.5	97.0	111	119	128	137	137	137
112	64.0	68.6	78.8	90.5	97.0	104	119	128	137	147	147	147
113	68.6	73.5	84.4	97.0	104	111	128	137	147	158	158	158
114	73.5	78.8	90.5	104	111	119	137	147	158	169	169	169
115	78.8	84.4	97.0	111	119	128	147	158	169	181	181	181
116	84.4	90.5	104	119	128	137	158	169	181	194	194	194
117	90.5	97.0	111	128	137	147	169	181	194	208	208	208
118	97.0	104	119	137	147	158	181	194	208	223	223	223
119	104	111	128	147	158	169	194	208	223	239	239	239
120	111	119	137	158	169	181	208	223	239	256	256	256
121	119	128	147	169	181	194	223	239	256	274	274	274
122	128	137	158	181	194	208	239	256	274	294	294	294
123	137	147	169	194	208	223	256	274	294	315	315	315
124	147	158	181	208	223	239	274	294	315	338	338	338
125	158	169	194	223	239	256	294	315	338	362	362	362
126	169	181	208	239	256	274	315	338	362	388	388	388
127	181	194	223	256	274	294	338	362	388	416	416	416
128	194	208	239	274	294	315	362	388	416	446	446	446
129	208	223	256	294	315	338	388	416	446	478	478	478
130	223	239	274	315	338	362	416	446	478	512	512	512
131	239	256	294	338	362	388	446	478	512	549	549	549
132	256	274	315	362	388	416	478	512	549	588	588	588
133	274	294	338	388	416	446	512	549	588	630	630	630
134	294	315	362	416	446	478	549	588	630	676	676	676
135	315	338	388	446	478	512	588	630	676	724	724	724
136	338	362	416	478	512	549	630	676	724	776	776	776
137	362	388	446	512	549	588	676	724	776	832	832	832
138	388	416	478	549	588	630	724	776	832	891	891	891
139	416	446	512	588	630	676	776	832	891	955	955	955
140	446	478	549	630	676	724	832	891	955	1024	1024	1024
141	478	512	588	676	724	776	891	955	1024	1098	1098	1098
142	512	549	630	724	776	832	995	1024	1098	1176	1176	1176
143	549	588	676	776	832	891	1024	1098	1176	1261	1261	1261
144	588	630	724	832	891	955	1098	1176	1261	1351	1351	1351
145	630	676	776	891	955	1024	1176	1261	1351	1448	1448	1448
146	676	724	832	955	1024	1098	1261	1351	1448	1552	1552	1552
147	724	776	891	1024	1098	1176	1351	1448	1552	1664	1664	1664
148	776	832	955	1098	1176	1261	1448	1552	1664	1783	1783	1783
149	832	891	1024	1176	1261	1351	1552	1664	1783	1911	1911	1911
150	891	955	1098	1261	1351	1448	1664	1783	1911	2048	2048	2048

APPENDIX B

SI-UNITS

The International System of Units consists of seven basic units, which are listed in Table B-1.

From these basic metric units, the units of a wide range of quantities can be derived, whereby the product and/or quotient of any number of basic units forms the resultant unit of the derived quantity.

The units of some of the more common quantities are presented in Table B-2. Finally, in Table B-3 are tabulated a number of factors to convert English engineering units into metric units.

Table B-1. Basic SI-units

QUANTITY	NAME OF UNIT	UNIT
length	meter	m
mass	kilogram	kg
time	second	s
temperature	kelvin	K
electric current	ampère	A
luminous intensity	candela	cd
amount of substance	mole	mol

Table B-2. Derived SI-units

QUANTITY	NAME OF UNIT	SYMBOL	UNIT
force	newton	N	kg m/s^2
pressure	pascal	Pa	N/m^2
work (energy)	joule	J	$\text{J} = \text{N m}$
power	watt	W	J/s
velocity	meter per second	V	m/s
acceleration	meter per second squared	a	m/s^2
moment of force	newton meter	M	N m
density	kilogram per unit cubic meter	ρ	kg/m^3

Table B-3. Conversion factors

QUANTITY	UNIT	SI-EQUIVALENT
length	1 foot (ft) 1 mile (statute) 1 nautical 1 inch (in)	= 0.3048 m = 1.60934 km = 1.852 km = 0.0254 m
area	1 ft ²	= 0.092903 m ²
volume	1 imperial gallon 1 U.S. gallon 1 pint (pt) 1 quart (qt)	= 4.54609 dm ³ = 3.78541 dm ³ = 0.568261 dm ³ = 1.13652 dm ³
velocity	1 ft/min 1 ft/s 1 mile/h (m.p.h.) 1 nautical/h (knot)	= 0.00508 m/s = 0.3048 m/s = 1.60934 km/h = 1.852 km/h
acceleration	1 ft/s ²	= 0.3048 m/s ²
mass	1 pound (lb)	= 0.453592 kg
mass rate of flow	1 lb/s	= 0.453592 kg/s
volume rate of flow	1 gal/h 1 ft ³ /s	= 4.54609 dm ³ /h = 0.0283168 m ³ /s
density	1 lb/ft ³	= 16.0185 kg/m ³
moment of inertia	1 lb ft ²	= 0.0421401 kg m ²
dynamic viscosity	1 lb/ft s	= 1.48816 kg/m s
kinematic viscosity	1 ft ² /s	= 0.092903 m ² /s
temperature	T°C (celsius;centigrade) T°F (fahrenheit) T°R (rankine)	= (T°C + 273.15)K = 5/9(T°F + 459.67)K = 5/9(T°R)K

APPENDIX C

GLOSSARY

Absorption coefficient – The fraction of the incident sound energy that is absorbed by a unit area of acoustical absorbent material when sound waves are falling on it equally from all directions.

Acoustic absorption – The absorption of sound energy by a wall material into which air can penetrate.

Acoustic center – The point from which the sound waves observable at remote points, appear to diverge.

Acoustic power – The total sound energy emitted by the source per unit time.

Acoustics – The science of sound, encompassing its generation, transmission, control, and effects on man.

Acoustic scattering – Irregular and diffuse reflection of a sound in many directions.

Active component of the particle velocity – The component of the particle velocity that is in phase with the sound pressure.

Adiabatic process – A thermodynamic change of state of a system in which there is no transfer of heat across the boundaries of the system.

Aeronautics – The science of design, construction and operation of aircraft.

Afterburner – An apparatus for augmenting the thrust of a turbojet, consisting of a duct placed aft the turbine, into which additional fuel is injected and burned.

Air-breathing engine – Engine that takes in atmospheric air for the purpose of combustion.

Aircraft – All air-supported vehicles.

Airfoil – A body so shaped as to produce an aerodynamic reaction force normal to its motion through the air without excessive drag.

Airframe – The complete assembly of the airplane without its engines and

removable items such as furnishings.

Airframe noise – Noise generated by an airplane during forward flight in the absence of engine noise.

Airplane – A power-driven heavier-than-air aircraft, obtaining its lift from aerodynamic reaction forces on surfaces which remain fixed under given flight conditions.

Airplane configuration – The description of the external shape of the airplane when flying in a particular phase of flight.

Airspeed – The speed of the center of gravity of an aircraft relative to the air.

Algorithm – A method of computation either numerical or algebraic.

Ambient noise – The all-encompassing noise as associated with a given environment.

Amplitude – The peak value of a periodic quantity.

Anechoic chamber – A room in which essentially free-field conditions prevail.

Antinodes – The points in a standing-wave system where the amplitude of the sound pressure has its maximum value.

Approach – The maneuver by which the airplane is brought into the right position relative to the landing area for landing.

Atmospheric attenuation – The natural attenuation of sound when it propagates through the atmosphere.

Aviation – The operation of heavier-than-air aircraft.

Background noise – The total noise in a given situation, independent of the presence of the desired signal.

Beats – Periodic pressure perturbations that result from the superposition of sound waves having slightly different frequencies.

Broadband sound – See random sound.

Boundary layer — The region adjacent to the outer surface of the airplane where the air is moving slower than further out due to the effect of skin friction.

Bypass ratio (BPR) — The ratio of the air mass flow through the bypass duct of a gas turbine engine to the air mass flow through the combustion chambers calculated at maximum thrust when the engine is stationary at sea level in I.S.A.

Center frequency — The geometric mean (midpoint on a logarithmic scale) of a constant percentage bandwidth, or the arithmetic mean of a constant bandwidth.

Characteristic acoustic impedance — The complex ratio of the sound pressure to the particle velocity at a point in a medium.

Characteristic acoustic reactance — The imaginary component of the characteristic acoustic impedance.

Characteristic acoustic resistance — The real component of the characteristic acoustic impedance.

Coefficient of dynamic viscosity — A state variable which determines the shear stress between air layers moving adjacent to each other at different velocities.

Compactness ratio — The ratio of a typical dimension of a sound source to the wavelength of the sound.

Complex sound — A sound produced by the combination of pure tones of different frequencies and amplitudes.

Constant bandwidth — A frequency interval having a fixed value, regardless of center frequency.

Constant percentage bandwidth — A frequency interval that is a fixed percentage of its center frequency.

Constant-speed propeller — A propeller, the pitch of which varies automatically to maintain a desired constant rotational speed.

Continuous (stationary) sound signal — A sound signal whose sound pressure level remains almost constant over a long time period.

Continuous spectrum — The spectrum of a sound, whose components are continuously distributed over the frequency range.

Controllable-pitch propeller — A propeller whose blades are so mounted that their pitch may be changed while the propeller is rotating.

Crest factor — The ratio of the sound pressure amplitude of a signal to its root-mean-square value measured over a specified time interval.

Cycle — The complete sequence of values of a periodic quantity which occur during a period.

Dead room — A room which is characterized by a large amount of wall absorption.

Decibel (dB) — A measure, on a logarithmic scale, of the magnitude of a particular quantity with respect to a standardized reference quantity of the same kind.

Diffraction — The bending of sound waves round obstacles.

Diffuse field — A sound field in which the effective pressure is the same everywhere and the sound intensity is zero throughout the entire region.

Directivity index — The difference between the sound pressure level at a specified distance and direction from a sound source and the sound pressure level at the same distance from a non-directional source which radiates the same acoustic power.

Direct sound field — Region in an enclosure where the occurring sound pressure is caused by the source without any contribution from reflections.

Direct sound wave — A sound wave emitted from the source prior to the

time it has undergone its first reflection from a boundary of an enclosure.

Doppler effect — The change in observed frequency of a moving source caused by the time rate of change in the distance between source and receiver.

Effective (sound) pressure — The root-mean-square value of the instantaneous sound pressures over a time interval at the point under consideration. In the case of a periodic sound, the interval must be an integral number of periods or an interval that is long compared with the period.

In the case of a random sound, the interval must be long enough to make the resulting effective pressure essentially independent of the length of the interval.

Energy density — The sound energy in a given part of a sound field divided by the volume of that part.

Far field — That part of the sound field where the sound wave is spreading spherically. Characterized by a sound pressure that is inversely proportional to distance.

Fixed-pitch propeller — A propeller having no provision for changing the pitch setting.

Fourier transform — The mathematical operation for decomposing a time function into its frequency components.

Free field — A sound field free from reflective surfaces.

Free progressive waves — Sound waves traveling in a free field.

Frequency — The number of cycles per second of a periodic sound signal.

Frequency analysis — Procedure of determining the contributions to the total sound pressure level by the individual frequencies.

Frequency weighting — A prescribed frequency response provided in a sound level meter to reflect the human

interpretation of the loudness of sounds at different frequencies.

Fundamental frequency — The reciprocal of the shortest period during which a periodic sound reproduces itself.

Harmonic — A sinusoidal component whose frequency is an integral multiple of the fundamental (lowest) frequency of the periodic sound to which it is related.

Helical blade tip speed — The velocity of the blade tip relative to the air.

Hertz — The unit of frequency, representing cycles per second.

Impulse noise — A sound of a transient nature having a high sound pressure level existing for only a very short time. Impulse noise has the characteristics of a gun shot.

Infrasound — Sound at frequencies below the audible range.

Interior noise — The noise inside an aircraft.

I.S.A. — The performance of aircraft depends on the atmospheric conditions. Since there are large variations of temperature and pressure in the actual atmosphere, a reference atmosphere is commonly used which is based on conditions in the mid-latitudes of the Northern Hemisphere. This is called the *International Standard Atmosphere* or I.S.A.

Kármán vortex street — A double trail of vortices formed alternately on each side of a cylinder moving at right angles to its long axis through the air.

Lapse rate — The rate at which the air temperature decreases with height.

Level — The level, in decibel, of an acoustic quantity is ten times the logarithm to the base ten of the ratio of that quantity to a reference quantity of the same kind.

Line spectrum — The spectrum of a sound, whose components are confined to a number of discrete frequencies.

Longitudinal wave – A wave in which the direction of displacement is normal to the wavefront.

Loudness – The way in which a listener reacts to a sound in terms of how quiet, or how loud a hearing sensation seems to be.

Mach angle – The semi-apex angle of a Mach cone.

Mach cone – Cone-shaped Mach waves emanating from a nondirectional point source moving at supersonic speed.

Mach line – A line representing a Mach wave.

Mach number – The ratio of the local flow velocity or airspeed to the speed of sound.

Mach wave – A shock wave occurring along a common line of intersection of all pressure perturbations emanating from a nondirectional point source moving at supersonic speed.

Manifold pressure – The pressure existing in the inlet of a piston engine when the engine is in operation.

Masking – The process by which the threshold of audibility of a sound or tone is raised by the presence of other tones of the same sound or of another sound.

Maximum continuous engine rating – Rating which has no time limit on engine usage.

Metric sabin – A measure of the acoustic absorption of a wall surface. One metric sabin is the equivalent of one square meter of a perfectly absorptive surface.

Molecular velocity – The root-mean-square value of the speed of the molecules in a gas.

Near field – That part of the sound field near the source where there is no simple relationship between sound pressure and distance.

Nodes – The points in a standing-wave system where the amplitude of the

sound pressure is zero, independent of time.

Octave band – A frequency interval whose upper limiting frequency is two times its lower limiting frequency.

Particle velocity – The velocity of air molecules about their rest position in a sound wave.

Period – The time required to complete one cycle.

Pink noise – Broadband noise whose pressure band level is constant, e.g., the spectrum band level is inversely proportional to frequency.

Planetary boundary layer – The atmospheric region adjacent to the Earth's surface where surface friction affects the magnitude of wind speed.

Plane wave – A wave in which the wavefronts are parallel planes normal to the direction of propagation.

Point source – A source that radiates sound as if it were radiated from a single point.

Power spectral density – The sound intensity per unit frequency interval.

Presbyacousias – The age-related increase in the threshold of audibility.

Pressure band level – The sound pressure level of a sound within a specified frequency interval.

Propfan – A propulsion unit comprising a gas turbine engine driving one or two multibladed propellers designed to give efficient performance up to high-subsonic airspeeds.

Pure tone – A sound wave, the instantaneous sound pressure of which is a sinusoidal function of time.

Random sound – A sound that is characterized by a continuous varying frequency distribution over a wide range of frequencies.

Rate of climb – Time rate of change of flight altitude. The vertical component of airspeed.

Reactive sound field – A sound field

- where the sound pressure and particle velocity are (partly) out of phase.
- Reactivity index** — The difference between the sound intensity level and the sound pressure level, in a reactive sound field.
- Reflection factor** — The ratio of the sound pressure of a wave incident upon a boundary to the sound pressure of the wave reflected from it.
- Refraction** — Bending of sound rays due to the occurrence of wind and temperature gradients in the atmosphere.
- Relative humidity** — The ratio of the actual water vapor pressure in the air to the saturation vapor pressure at that temperature. Relative humidity is expressed in percent.
- Reverberant field** — The region in enclosures in which the reflected sound dominates.
- Reverberation** — The persistence of sound pressure level in an enclosure after a sound source has been stopped.
- Reverberation chamber** — An enclosure in which all the inner surfaces have been made as sound-reflective as possible.
- Room absorption** — The product of the mean absorption coefficient for a given room and its entire inner wall-surface area.
- Shadow zone** — Region in a sound field into which no direct sound can penetrate.
- Shock wave** — The narrow region crossing the streamlines in which the velocity of the air changes suddenly and in which an increase of entropy occurs.
- Simple harmonic motion** — A periodic motion whose displacement varies as a sinusoidal function of time.
- Slat** — Movable part of wing leading edge which can be moved forward or downward mechanically to form a slot with the wing surface to delay airflow breakaway.
- Sonic boom** — An impulsive type of noise produced at an observing point by the shock wave cones formed around an airplane when it flies at supersonic speed.
- Sound field** — Region in which sound waves are present.
- Sound intensity** — The energy per unit time transmitted by a sound wave per unit area in a specified direction.
- Sound pressure** — The instantaneous value of the fluctuating pressure disturbance on the static pressure.
- Sound ray** — Imaginary curve directed normally to the wavefronts.
- Spectrum** — The distribution in frequency of the magnitudes of the components of a sound wave.
- Spectrum pressure level** — The sound pressure level of a sound at a particular frequency for the sound intensity per unit frequency interval.
- Speed of sound** — The rate at which a sound wave propagates through a medium.
- Spherical sound wave** — A wave in which the wavefronts are concentric spheres.
- Spoiler** — A device which changes the airflow round an airfoil with the object of reducing lift and/or increasing drag.
- Stable atmosphere** — The condition that in the atmosphere every mass of air that ascends or descends as a result of local instability tends to return to its origin.
- Standing sound wave** — Periodic wave having a fixed distribution in space which is the result of interference of two progressive waves of the same frequency and amplitude which are traveling along the same line in opposite directions. They are characterized by the existence of maximum and minimum amplitudes that are fixed in space.

Static pressure – The air pressure at a point in the sound field that would exist without the presence of sound waves.

Supercharging – Increasing the inlet manifold pressure of a piston engine by means of a compressor driven by the engine.

Supersonic airplane – An airplane capable of sustaining level flight at speeds faster than the speed of sound.

Surface impedance – The complex ratio of the sound pressure at a point on the surface of a ground medium to the corresponding air particle velocity at the surface.

Surface wind – The wind velocity up to about 10 meters above the ground.

Takeoff engine rating – The maximum rating which can be used for a short time.

Temperature gradient – Variation of air temperature with height.

Temperature inversion – An increase in air temperature with height (negative lapse rate).

Tertsband (1/3-octave band) – A frequency interval of which the ratio of the upper limiting frequency to the lower limiting frequency is $2^{1/3}$.

Threshold of audibility (hearing) – The minimum sound pressure level that is needed to produce an audible sound.

Transient sound signal – A sound signal whose sound pressure level varies with time.

Transmission coefficient – The ratio of the intensities in transmitted and incident waves when sound passes a partition.

Transmission factor – The ratio of the effective pressure of the sound incident upon a boundary to the effective pressure of the sound transmitted through it.

Transmission loss – The difference between the sound pressure levels of in-

cident and transmitted waves when sound is transmitted through a partition.

Troposphere – The atmospheric layer nearest the Earth's surface, having a more or less uniform decrease of temperature with height. On the Equator, this layer extends to a height of approximately 18 km and 8 km over the Poles.

The troposphere is the domain of the atmospheric phenomena collectively called *weather*, due to the presence of considerable moisture in the lower levels, and the occurrence of horizontal wind velocities and vertical air movements.

Turbulent flow – The chaotic mixing of adjacent streamlines.

Ultrasound – Sound at frequencies beyond the audible range.

Wavefront – Imaginary surface around the source which is the locus of points having the same particle displacement at a given instant.

Wavelength – The perpendicular distance between two wavefronts which are separated by one complete period.

Wave number – The ratio of circular frequency of a periodic sound signal to the speed of sound.

White noise – A random noise having constant energy per unit frequency bandwidth over a specified frequency range.

Wind gradient – Variation in horizontal wind speed with height.

Wing flap – Any surface adjusted in flight, the primary function of which is to modify the lift.

INDEX

1/3-octave band 301
10 dB down-time 195, 224

A

A-weighted
equivalent – sound level 194
sound level 190
A-weighting 190
absorbent lining 126
absorption
acoustic – 100, 296
coefficient 100, 296
of the room 101
room – 102, 300
acoustic
absorption 100, 296
center 11, 21, 296
characteristic – impedance 48,
297
characteristic – reactance 49,
297
characteristic – resistance 15,
43, 49, 297
energy 2
foam 126
impedance of the surface 168
lining 132
monopole 22, 51
power 11, 296
scattering 296
sources 38
acoustics 296
linear – 30
active component of the particle
velocity 296
actual total noise dose 213
adiabatic process 296
aeronautics 296
afterburner 296
afterburning 191, 258
air-breathing engine 296
airborne path 279
aircraft 296
airfoil 296

airframe 296
noise 260, 276, 296
airplane 296
configuration 296
supersonic – 301
airspeed 296
algorithm 296
ambient noise 156, 296
level 227
amplitude 4, 296
analyzers 145
anechoic chamber 7, 105, 296
angle of incidence 163
angular frequency 4
Annex 16 215
antinodes 114, 296
approach 296
atmosphere
International Standard – 298
stable – 300
atmospheric absorption 71
atmospheric attenuation 71, 296
attenuator
reactive – 120
resistive – 126, 132
audible range 17
aviation 296

B

background noise 156, 296
band
number 146
pressure – level 146
bandpass filter 145
band
1/12-octave – 149
1/3-octave – 148
half-octave – 148
octave – 145
bandwidth 145
constant percentage – 297
constant – 167, 297
beats 280, 296
bel 12

Bell, Alexander Graham 12
 blade passage frequency 138
 blade-matching 281
 boundary layer 297
 broadband sound 24, 296
 buzzsaw noise 274
 bypass engine 259
 bypass ratio 259, 297

C

CAEP 215
 CAN 215
 center frequency 145, 297
 chamber
 anechoic – 105, 296
 double-expansion – 122
 reverberation – 105, 300
 single-expansion – 121
 characteristic acoustic
 impedance 48, 297
 reactance 49, 297
 resistance 15, 43, 49, 297
 clean configuration 277
 coefficient
 absorption – 100, 296
 Fourier – 139
 of dynamic viscosity 73, 297
 sound attenuation – 71
 sound transmission – 108
 transmission – 301
 coincidence effect 112
 combination tones 274
 compactness ratio 55, 297
 complex sound 297
 composite noise exposure index 213
 condensation 32
 condenser microphone 16
 confidence interval 224, 234
 configuration 277
 clean – 277
 dirty – 278
 conical shock wave 242
 constant bandwidth 167, 297
 constant percentage bandwidth 297
 constant-speed propeller 232, 282,
 297

continuity equation 32
 continuous sound signal 26, 297
 continuous spectrum 25, 297
 controllable-pitch propeller 297
 convection 247
 Mach number 238
 convective amplification 248
 convective effects 247
 convergence effects 92
 convex sound rays 85
 crest factor 5, 297
 cumulative perceived noise level
 196
 cumulative sound exposure level
 195
 cutoff frequency 135, 167
 cycle 297
 cylinder firing frequency 139, 262

D

day-night average level 206
 dB 12, 297
 dead room 7, 297
 decibel 12, 297
 delta function 57, 242
 diffraction 7, 297
 diffractive wave 7
 diffuse field 98, 297
 dipole 22
 source 58
 direct sound
 field 297
 pressure level 97
 sound wave 297
 directionality 21, 66, 71
 directivity
 factor 245
 index 21, 71, 297
 patterns 269
 dirty configuration 278
 discrete sound 24
 divergence effects 92
 divergence theorem 56
 Doppler
 effect 27, 298
 factor 246

- formula 246
- shift 27
- double-expansion chamber 122

- E**
- effective perceived noise level 195
- effective (sound) pressure 5, 50, 247, 298
- effects of source motion 237
- elementary sources of sound 22
- emission angle 162
- emission time 156, 160, 238
- energy density 44, 98, 298
- engine rating
 - maximum continuous – 299
 - takeoff – 301
- enthalpy 35
- equation
 - Helmholtz – 50
 - Laplace's – 56
 - of continuity 30, 31
 - of state 36
- equivalent
 - A-weighted sound level 194
 - cumulative perceived noise level 196
 - sound pressure level 193
- Euler's equations of motion 34
- excess ground attenuation 182, 204
- exhaust firing frequency 138, 262
- exhaust noise 63
- expansion ratio 122

- F**
- FAA 217
- factor
 - plane wave reflection – 176
 - reflection – 78, 161
 - transmission – 78
- FAR 217
- far field 11, 52, 70, 298
- Federal Aviation Administration 217
- Federal Aviation Regulations 217
- field
 - diffuse – 98, 297
- direct sound – 297
- free – 3, 97, 298
- near – 97, 299
- reactive sound – 299
- reverberant – 98, 300
- first law of thermodynamics 35
- fixed-pitch propeller 232, 298
- focusing effects 91
- footprint 203
- forward flight effects 237
- Fourier
 - coefficients 139
 - inverse – transform 142
 - series 139
 - theorem 51, 139
 - transform 139, 142, 298
 - transform pair 142
- free progressive wave 3, 298
- free field 3, 97, 298
 - chamber 7
 - condition 6, 11
 - microphone 255
- frequency 3, 298
 - analysis 139, 298
 - center – 145, 297
 - cutoff – 135, 167
 - cylinder firing – 139, 262
 - engine exhaust firing – 138, 262
 - fundamental – 140, 298
 - propeller blade passage – 138
 - resonant – 129
 - weighting 298
- fundamental frequency 140, 298

- G**
- gradient
 - of speed of sound 81
 - temperature – 8, 301
 - wind – 8, 301
- grazing incidence 176
- Green's theorem in space 56
- ground
 - effect 162
 - excess – attenuation 204
 - interference effects 163

reflection 162
wave 176

H

half-octave bands 148
harmonic 298
functions 41
motion 4
harmonics 140
hearing
conservation 282
loss 212
range 29
helical blade tip speed 256, 298
helical tip Mach number 257
Helmholtz equation 50
Helmholtz resonator 126
Hertz 3, 298
higher order modes 133
hold facility 27

I

I.S.A. 298
ICAO 215
immission time 156, 161, 238
impedance
normal surface – 170
of the plate 113
specific – 170
surface – 168, 301
tube 172
impulse noise 26, 198
impulse characteristic 26
impulsive noise 26
incident intensity 99
infrasound 4, 298
inhomogeneous wave equation 58
instantaneous sound pressure 5
interference effects 167
interior noise 279, 298
International Civil Aviation Organization 215
International Standard Atmosphere 81, 298
inverse
Fourier transform 142

distance law 69, 157
square law 69
inverted microphone 181

J

jet-engine 63

K

Kármán vortex street 298

L

Laplace's equation 56
Laplacian operator 38
lapse rate 81, 84, 298
lateral noise attenuation 205
level 298
of speech 104
Lighthill 63
line spectrum 25, 298
linear acoustics 30, 32
linear liner 132
liner
linear – 132
perforated – 132
loading noise 264
locally reacting 170
longitudinal wave 299
Lorentz transformation 242
loudness 4, 185, 299
level 186

M

Mach
angle 239, 299
cone 239, 299
convection – number 238
helical tip – number 257
line 241, 299
number 299
wave 299
manifold pressure 299
masking 187, 299
metric sabin 101, 299
microphone
condenser – 16

free-field – 255
 inverted – 181
 pressure type – 223, 254
 random-incidence – 255
 molecular velocity 43, 299
 monopole
 acoustic – 22, 51
 point – 55
 source 52
 moving source 237
 muffler 132
 multiple pure tones 274
 musical tone 24

N

N-wave 251
 narrow-band resonator 132
 near field 11, 70, 97, 299
 nerve deafness 212
 nodes 114, 299
 noise
 suppressor 270
 actual total – dose 213
 airframe – 260, 276, 296
 ambient – level 227
 ambient – 156, 296
 and number index 207
 background – 156, 296
 buzzsaw – 274
 certification standards 215
 certification 223
 composite – exposure index
 213
 contours 205
 dose 213
 exhaust – 63
 exposure zones 210
 inside aircraft 279
 impulse – 26, 298
 indices 205
 interior – 279, 298
 lateral – attenuation 205
 limits 217
 load 208
 loading – 264
 non-propulsive – 277

pink – 148, 299
 propeller – spectra 264
 propeller – 266
 rotational – 264
 single-event – exposure level
 194
 single-event – contours 203
 suppressor 270
 thickness – 264
 vortex – 264
 white – 25, 147, 301
 non-propulsive noise 277
 non-stationary signals 26
 normal surface impedance 170
 noy 187

O

observed frequency 27
 octave band 145, 299
 one-third octave band 148
 one-twelfth octave band 149
 open window area 101
 Otto-cycle 261
 overall sound pressure level 26

P

particle velocity 41, 43, 48, 299
 passband 145
 perceived noise
 cumulative – 196
 deciBel 187
 effective – 195
 equivalent cumulative – 196
 level 187
 tone corrected – level 189, 198
 weighted equivalent continuous
 – level 206
 perforated liner 132
 performance correction 227
 period 3, 257, 299
 phase change on reflection 163
 phon 185
 pink noise 148, 299
 piston engine 256
 plane wave 40, 299
 reflection factor 176

planetary boundary layer 88, 299
 point monopole 55
 point source 70, 299
 Poisson's relations 35, 37
 power spectral density 145, 299
 power watt level 12
 preferred speech interference level 282
 presbyacousias 212, 299
 pressure
 band level 146, 299
 effective – 50, 66, 247
 manifold – 299
 microphone 116
 sound – 3
 spectrum – level 147, 300
 static – 30, 301
 type microphone 223, 254
 principle of Huygens 7
 propagation constant 169
 propeller
 constant-speed – 215, 232, 282, 297
 controllable pitch – 232, 282, 297
 fixed-pitch – 232, 298
 noise 266
 noise spectra 264
 supersonic – 266
 propfan 260, 299
 propulsive efficiency 263
 pure tone 19, 24, 42, 299

Q

quadrupole 23, 64

R

radius of curvature 90
 random sound 24, 299
 random-incidence microphone 255
 rate of climb 299
 ratio
 bypass – 259, 297
 compactness – 55, 297
 expansion – 122
 of specific heats 5, 37

standing wave – 115
 ray
 path 76
 sound – 300
 tube 93
 reactive
 attenuation 118
 attenuator 120
 sound field 18, 299
 reactivity index 18, 300
 reference duration 213
 reflected rays 84
 reflected sound 76
 reflection
 factor 78, 119, 161, 300
 ground – 162
 surface – 87
 refraction 9, 300
 of sound rays 96
 Snell's law of – 78, 91
 relative humidity 73, 300
 resistive attenuator 126, 132
 resonance frequency 113
 resonant cavities 126
 resonant frequency 129
 resonator
 Helmholtz – 126
 narrow-band – 132
 reverberant field 98, 300
 reverberant level 104
 reverberation 105, 300
 chamber 105, 300
 distance 103
 time 105
 Reynolds number 72
 room absorption 102, 300
 root-mean-square value 5
 rotational noise 264

S

Sabine formula 106
 sample mean 234
 sample standard deviation 234
 sampling error 235
 shadow zone 6, 8, 82, 91, 300
 shock wave 241, 250, 300

simple harmonic motion 4, 300
single
event noise exposure level 194
event noise contours 203
expansion chamber 121
stage fan 273
slat 300
sleep disturbance 210
slope of the ray path 89
Snell's law of refraction 78, 91
Sommerfeld's radiation condition 48
sone 186
sonic boom 249, 300
sound
A-weighted - level 190
attenuation coefficient 71
broadband - 24, 296
complex - 297
continuous - signal 26, 297
cumulative - exposure level 195
direct - field 297
direct - pressure level 97, 98
direct - wave 297
discrete - 24
effective - pressure 298
equivalent - pressure level 193
equivalent A-weighted - level 194
exposure level 194
field 3, 4, 300
infra - 4, 298
intensity 13, 44, 50, 117, 300
intensity level 15
level meter 16
non-stationary - signals 26
power 12
pressure 3, 245, 300
pressure level 16, 248
random - 24, 299
ray 5, 300
reactive - field 299
reflected - 76
source 2
speed of - 5, 41, 300
spherical - wave 300

standing - wave 300
stationary - signal 26
transient - signal 26, 301
transmission coefficient 108
transmitted - 77
ultra - 4, 301
sound rays
convex - 85
refraction of - 96
specific
gas constant 5, 36
heat at constant pressure 36
heat at constant volume 36
impedance 170
volume 35
spectrum 25, 300
continuous - 25, 297
line - 25, 298
pressure level 300
speed of sound 5, 41, 300
spherical sound wave 300
spherical spreading 70
spoiler 300
stable atmosphere 300
standard deviation
sample - 234
true - 235
standing wave 114, 300
apparatus 172
ratio 115
static pressure 30, 301
stationary sound signals 26
Strouhal number 67
structureborne path 280
student's t distribution 235
supercharging 301
supersonic
airplane 301
motion 239
propeller 266
surface
friction 88
reflections 87
impedance 168, 301
wave 177
wind 301
synchrophaser 280

T

temperature
 gradient 8, 301
 inversion 10, 84, 301
 lapse 9
 lapse condition 91
 negative - gradient 9
 tertsband 148, 187, 301
 theorem
 divergence - 56
 Fourier's - 51, 139
 Green's - in space 56
 thickness noise 264
 threshold of
 audibility 29, 301
 hearing 29
 pain 14, 29
 thrust cutback procedure 203
 time
 emission - 156
 immission - 156
 tone
 corrected perceived noise level
 198
 correction 189
 correction factor 198
 pure - 299
 trace wavelength 109
 transient sound signal 26, 301
 transmission
 factor 78, 119, 301
 loss 109, 120, 301
 coefficient 301
 transmitted sound 77
 troposphere 301
 true standard deviation 235
 turbofan 259
 turbojet 257
 turboprop 258
 turbulence 68
 turbulent flow 301

U

ultrasound 4, 301

V

velocity
 active component of the particle
 - 296
 gradient 88
 molecular - 43, 299
 particle - 43, 48, 299
 potential 39, 45, 65, 242, 244
 viscosity 71
 von Kármán 64
 vortex noise 264

W

wave
 -fronts 5, 301
 -length 5, 301
 conical shock - 242
 direct sound - 297
 equation 38
 free progressive - 3, 298
 ground - 176
 inhomogeneous - equation 58
 longitudinal - 299
 Mach - 299
 N - 251
 number 301
 plane - 40, 299
 scalar - equation 40
 shock - 300
 standing - 114
 surface - 177
 weighting
 frequency - 298
 filters 189
 white noise 25, 147, 301
 wind
 direction 91
 down- 10, 91
 gradient 8, 10, 88, 91, 301
 profile 10, 96
 surface - 301
 up- 10, 91
 windscreen 223, 255
 wing flap 301







7267978

The purpose of this book is to provide insight into those elements of acoustics and aeronautics that are connected directly with the problem of aviation noise. It is intended as a textbook for a university course on aviation acoustics at an undergraduate level. The simplicity of presentation also lends itself to the book's use as an instrument of self-study for the practicing engineer. The contents of the book are a reflection of an annual course on aviation noise presented by the author to senior undergraduate students of aerospace engineering at Delft University of Technology.

The author, Gerrit J.J. Ruijgrok, is a Professor of Aerospace Engineering at the University of Gent, Belgium, and at the Delft University of Technology, The Netherlands. He is also the author of the book *Elements of Airplane Performance*. His educational and research tasks are concentrated on performance, propulsion and noise of aircraft. He was graduated from Delft University with a degree in aeronautical engineering.